PAPER P-741

IMAGE QUALITY IN SAMPLED DATA SYSTEMS

Lucien M. Biberman
Richard Legault
A. Fenner Milton
Frederick A. Rosell
Otto H. Schade, Sr.
Alvin D. Schnitzler
Harry L. Snyder

August 1971

INSTITUTE FOR DEFENSE ANALYSES
SCIENCE AND TECHNOLOGY DIVISION

The work reported in this document was conducted under contract DAHC15 67 C 0011 for the Department of Defense. The publication of this Paper does not indicate endorsement by the Department of Defense, nor should the contents be construed as reflecting the official position of that agency.

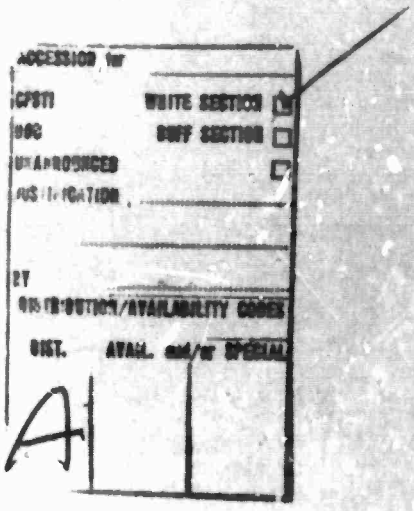

DISCLAIMER NOTICE

THIS DOCUMENT IS THE BEST QUALITY AVAILABLE.

COPY FURNISHED CONTAINED A SIGNIFICANT NUMBER OF PAGES WHICH DO NOT REPRODUCE LEGIBLY.

MISSING PAGE
NUMBERS ARE BLANK
AND WERE NOT
FILMED

UNCLASSIFIED

Security Classification

DOCUMENT CONTROL DATA - R & D

(Security classification of title, body of abstract and indexing annotation must be entered when the overall report is classified)

1 ORIGINATING ACTIVITY (Corporate author)

INSTITUTE FOR DEFENSE ANALYSES
400 Army-Navy Drive
Arlington, Virginia 22202

2a. REPORT SECURITY CLASSIFICATION: UNCLASSIFIED

2b. GROUP: --

3 REPORT TITLE

Image Quality in Sampled Data Systems

4 DESCRIPTIVE NOTES (Type of report and inclusive dates)

Paper P-741--August 1971

5 AUTHOR(S) (First name, middle initial, last name)

Lucien M. Biberman, Richard Legault, A. Fenner Milton, Frederick A. Rosell, Otto H. Schade, Sr., Alvin D. Schnitzler, Harry L. Snyder

6 REPORT DATE: August 1971

7a. TOTAL NO OF PAGES: 232

7b. NO OF REFS: 52

8a. CONTRACT OR GRANT NO: DAHC15 67 C 0011

8b. PROJECT NO: Task T-36

8c.

8d.

9a. ORIGINATOR'S REPORT NUMBER(S): P-741

9b. OTHER REPORT NO.(S) (Any other numbers that may be assigned this report): None

10 DISTRIBUTION STATEMENT

Approved for public release; distribution unlimited.

11 SUPPLEMENTARY NOTES: NA

12 SPONSORING MILITARY ACTIVITY: Advanced Research Projects Agency
Arlington, Virginia 22209

13 ABSTRACT

This paper deals with "aliasing," an important effect of one- and two-dimensional sampling on image quality. Aliasing changes the normal criteria of utility of the modulation transfer function (MTF) as a measure of system quality. Aliasing can be eliminated by letting the MTF fall to zero at one-half the sampling frequency. This, of course, markedly reduces the signal-to-noise ratio at the display (SNR_D) near cutoff and thus reduces operator performance. False imagery occurs if aliasing is not eliminated, and this reduces operator performance also.

Several factors control the amount of information an observer extracts from an image and the rate at which he extracts it. Of great importance is the signal-to-noise ratio (SNR) as a function of spatial frequency. This paper presents the results of a series of experimental programs relating observer performance to the modulation transfer function area (MTFA) and to the SNR_D and derives the relationship between MTFA and SNR_D.

This paper discusses the tradeoffs as they are presently understood.

DD FORM 1473

UNCLASSIFIED

Security Classification

14 KEY WORDS	LINK A		LINK B		LINK C	
	ROLE	WT	ROLE	WT	ROLE	WT
aliasing						
display signal-to-noise ratio						
image quality						
low-light-level devices						
low-light-level television						
modulation transfer function						
raster effects						
real-time sensors						
reconnaissance systems						
sampled data systems						
sensors						
television camera tubes						
television displays						
vision						
visual systems						

PAPER P-741

IMAGE QUALITY IN SAMPLED DATA SYSTEMS

Lucien M. Biberman
Institute for Defense Analyses

Richard Legault
University of Michigan

A. Fenner Milton
Institute for Defense Analyses

Frederick A. Rosell
Westinghouse Defense and Space Center

Otto H. Schade, Sr.
Consultant

Alvin D. Schnitzler
Institute for Defense Analyses

Harry L. Snyder
Virginia Polytechnic Institute and State University

August 1971

IDA

INSTITUTE FOR DEFENSE ANALYSES
SCIENCE AND TECHNOLOGY DIVISION
400 Army-Navy Drive, Arlington, Virginia 22202
Contract DAHC15 67 C 0011
Task T-36

FOREWORD

Periodically a need arises for sampled data systems to transmit photographs, maps, or other images. Each time, the problem gives rise to questions such as: "What does sampling do to picture quality?" and "What must the sampling frequency and format be to minimize image deterioration?"

Most recently, the problem was referred to IDA with a request for a "ten-day review" to meet an urgent decision date. Thus, it was possible only to assemble what was already known and at hand, not to do any new independent research on the problem. The material in this paper was largely in the minds and files of the contributors. Richard Legault of the University of Michigan, Otto H. Schade, Sr., Frederick A. Rosell of Westinghouse Aerospace, and Alvin D. Schnitzler and Lucien M. Biberman of IDA attempted to collect pertinent documentation and write only that new material that time and understanding would permit.*

The use of sampled data systems affects the signal-to-noise ratio of the imagery and, in addition, introduces spurious signals caused by a heterodyne-like process. The need to maintain desirably large (near unity) modulation transfer function (MTF) values over the entire spatial frequency of interest must be weighed against the need for prefiltering before sampling so as to minimize aliasing. This is the dominant tradeoff.

---

* A. Fenner Milton and Robert Sendall reviewed this paper and contributed appreciably to its completion. Further, A. Fenner Milton made substantial contributions to the rewriting of the Summary.

The aliasing problem is not new, and the literature contains the work of O. H. Schade, Sr., who analyzed this problem beginning in 1951 in a now classical series of articles (Ref. 1). Part III of this series is especially important in considering the interaction of the raster and the lens MTF on vertical resolution. The importance of this paper led us to reproduce it with care as part of our documentation.

The use of sampled data systems and the aliasing problem have been studied and reported by W. Duane Montgomery in IDA Research Papers P-543, Some Consequences of Sampling in Image Transmission Systems, and P-677, An Analysis of Aliasing for Sampling on Composite Lattices (Refs. 2, 3). These two papers were stimulated by the work of Helmut Weiss of Aerojet in his early FLIR analysis for the FLIR Specification Committee sponsored by the Office of the Director of Defense Research and Engineering (ODDR&E) and IDA.

The entire problem of image quality in electrooptical image-forming systems has been a major concern in IDA for some years. Our efforts have resulted in a two-volume work, Photoelectronic Image Forming Devices (Ref. 4). A supplement to that work is IDA Report R-169, Low-Light-Level Devices (Ref. 5). By and large, this paper is a compilation of material from the book, the report, the publications of O. H. Schade, Sr., and several short new writings of Biberman, Legault, Snyder, Rosell, Schade, and Schnitzler. The material is thus a collection of remarks, small papers, and fragments of published and unpublished work rather than an integrated, finished and edited report.

This paper was produced as part of a contract program on infrared and night vision carried on under the sponsorship of ODDR&E, Office of Information and Communications, and monitored by E. N. Myers.

Finally, it should be noted that in Section VII the rectangular array of detectors for two-dimensional mosaic sampling systems is not the optimum means for arranging an array of detectors. A significant saving in the number of detectors is possible through a more judicious choice.

FOREWORD REFERENCES

1. O.H. Schade, Sr., "Image Gradation, Graininess and Sharpness in Television and Motion Picture Systems," J. Soc. Motion Picture Television Engrs.:

   Part I, "Image Structure and Transfer Characteristics," pp. 137-171, February 1951;

   Part II, "The Grain Structure of Motion Picture Images--An Analysis of Deviations and Fluctuations of the Sample Number," Vol. 58, pp. 181-222, March 1952;

   Part III, "The Grain Structure of Television Images," Vol. 61, pp. 97-164, August 1953;

   Part IV, A and B, "Image Analysis in Photographic and Television Systems (Definition and Sharpness)," Vol. 64, pp. 593-617, November 1955.

2. Institute for Defense Analyses, Some Consequences of Sampling in Image Transmission Systems, IDA Research Paper P-543, W.D. Montgomery, December 1969.

3. Institute for Defense Analyses, An Analysis of Aliasing for Sampling on Composite Lattices, IDA Paper P-677, W.D. Montgomery, November 1970.

4. L.M. Biberman and S. Nudelman, eds., Photoelectronic Imaging Devices, Vol. I, Physical Processes and Methods of Analysis, Vol. II, Devices and Their Evaluation, Plenum Press, New York, 1971.

5. Institute for Defense Analyses, Low-Light-Level Devices: A Designers' Manual, IDA Report R-169, L.M. Biberman, F.A. Rosell, O.H. Schade, Sr., A.D. Schnitzler, and H.L. Snyder, August 1971.

ABSTRACT

This paper deals with "aliasing," an important effect of one- and two-dimensional sampling on image quality. Aliasing changes the normal criteria of utility of the modulation transfer function (MTF) as a measure of system quality. Aliasing can be eliminated by letting the MTF fall to zero at one-half the sampling frequency. This, of course, markedly reduces the signal-to-noise ratio at the display (SNR_D) near cutoff and thus reduces operator performance. False imagery occurs if aliasing is not eliminated, and this reduces operator performance also.

Several factors control the amount of information an observer extracts from an image and the rate at which he extracts it. Of great importance is the signal-to-noise ratio (SNR) as a function of spatial frequency. This paper presents the results of a series of experimental programs relating observer performance to the modulation transfer function area (MTFA) and to the SNR_D and derives the relationship between MTFA and SNR_D.

This paper discusses the tradeoffs as they are presently understood.

CONTENTS

SUMMARY

by Lucien M. Biberman and A. Fenner Milton

In photographic imagery the actual detectors are silver halide grains. A fairly large number of grains usually define the image. Since more than a planar layer of grains is involved because of the combination of depth of focus and the third dimension (depth) of the emulsion, a significant number of grains are involved in the reproduction of even a point image.

The spread function of the optics used is usually large compared to the dimensions of an individual grain, so that in photography the problems involved in sampling the imagery with a finite number of detectors become insignificant in relation to other considerations.

In the case of image formation by a matrix of detectors with electrical outputs, the problems associated with fabrication, cost, interconnections of wiring, number of amplifiers, and so forth serve to constrain the number of detectors used. Thus, there tend to be many fewer detector elements per image in such a matrix than in film, and the limitations associated with sampling the imagery must be considered.

It is important to estimate accurately how few individual detectors one can use in the matrix without significantly degrading the image.

Basically, there are three factors affecting this problem of finite sampling and image quality:

1. The number of samples per image.
2. The signal-to-noise ratio per sample.
3. The generation of spurious signals by the sampling process.

In Section I, Fig. I-1, we show the number of resolvable lines on an output display necessary per linear "critical" dimension of a target image for various visual tasks, such as detection or recognition. In Section II we discuss the number of errors of a photointerpreter versus a quantity known as modulation transfer function area (MTFA). It is clearly shown that a high value of modulation transfer function (MTF) is desirable relative to the modulation threshold of the observer to ensure few interpreter errors.

Unfortunately, it is true that a spatial frequency passband larger than half the sampling frequency permits the transmission of spurious "sideband" frequencies that are reflected back into the passband. That is, with a sampling system it is possible for image transformation effects to occur that cannot be simply described by an MTF. These effects are called aliasing, and they occur because, although the sampling process can be linear, it is not translationally invariant. If aliasing occurs, an input of one spatial frequency can cause a spurious output at another spatial frequency. Under such circumstances an analysis of sampling theory (Section VII) is required to understand the output. The central result of sampling theory (Nyquist's theorem) demonstrates that it is quite impossible to obtain useful, unambiguous information from a sampled system concerning input spatial frequencies that are greater than 1/2L, where L is the appropriate detector or sample spacing. Higher spatial frequencies could be observed in the output, but these would be impossible to interpret, i.e., they would be effectively spurious. In the absence of other constraints the sampling process can thus set the resolution of the system at 1/2L. If a space-filling detector configuration (abutting detectors) is used, this of course does not mean that bright target images which at the detector plane have a dimension smaller than L cannot be seen, but rather that these target images cannot be localized any better than ± 1/2L.

Besides imposing a resolution limit on the system, the sampling process can cause higher spatial frequencies to be translated back into the useful passband of the system. For the most obvious situation where detector and spot sizes just fill the plane (the detector

part of this is necessary for efficient detection), aliasing can convert spatially periodic images with frequencies between 1/2L and 1/L back into the 0 - 1/2L frequency passband. When dealing with periodic inputs, this could cause a false signal. However, as Schade shows in Section VI, if a lens system is designed so that its MTF is zero for frequencies greater than 1/2L, no frequencies greater than 1/2L will fall on the detector plane and no aliasing problem will occur; i.e., no outside frequencies will be translated into the operational passband of the system.

The only problem here is that any realizable lens filter that has an MTF of zero for frequencies greater than 1/2L is likely to have an MTF much less than unity for frequencies approaching 1/2L. Thus, there is a tradeoff between the desire to eliminate aliasing and a desire not to degrade the MTF for spatial frequencies less than 1/2L. Schade suggests for commercial TV situations that the use of a lens MTF that drops to 35 percent at a spatial frequency of 1/2L is tolerable.

Where the prefiltering tradeoff should fall depends critically on the type of images being viewed. When dealing with periodic inputs, aliasing can cause a false signal. Without prefiltering, when counting a row of small objects where the fundamental frequency of the row is higher than 1/2L, it would be possible to count a smaller number than is actually present. If there were no post-sampling filtering, another aliasing effect would be present, and a naive photointerpreter might neglect the sampling process and count a larger number of objects than is actually present. However, if the overlap of the output display were adjusted to give a flat picture for a uniform input, the necessary post-filtering to eliminate transformations to higher spatial frequencies would be automatically provided. Since no amount of post-filtering can eliminate the downconversion of spatial frequencies caused by aliasing, this is the principal design consideration. It should be remembered that in real space the effects of aliasing are sharply localized.

When one is dealing with localized signals, one must consider both frequency and phase relations. The physical situation of the sampling process is such that a signal derived from an x to x + L sampling interval cannot be translated by the sampling process out of that interval. This means that the high-frequency part of a sharp edge cannot produce a ghost at a distance more than the detector spacing L away from that edge. Thus, for an ordinary aperiodic scene, no false signals can be produced, and prefiltering is not an important design goal. The sampling process may produce some structure near sharp edges, but unless several edges are close together, no effects will occur that cannot be explained by the loss of information concerning input frequencies greater than 1/2L.

If periodic images are likely to be viewed, it would be prudent to experimentally investigate the photointerpretation problem caused by aliasing (clutter formation) in order to help the system designer make the necessary tradeoff. If a low-frequency target were to be viewed against a high-frequency periodic background, aliasing could only cause a significant clutter problem if the amplitude difference between the target signal and the high-frequency part of the background were less than a factor of three..

At a minimum, photointerpreters should be made aware of the aliasing phenomenon when using sampled systems.

I. INTRODUCTION

by Lucien M. Biberman

It is a truism that a good picture is better than a bad picture, but it has not been abundantly clear, especially to the designers of most imaging systems, what criteria must be used to decide whether a picture is good or bad.

Designers of optical lenses and airborne cameras have given much thought to the question of how to predict whether their equipment designs will permit their clients to capture and see specified graphic detail. The need to meet contractual specifications for camera and lens performance has promoted a sharper understanding of the lens quality required to produce recognizable pictures of terrain from aircraft or earth satellites. Although questions of image quality, signal, and noise are still argued, the parameters are now so well known that a definite range of performance can be expected from photointerpreters working with imagery produced by lenses and cameras built to a given set of hard specifications.

Two main sets of factors govern the performance of man and his low-light-level viewing aids. The first set is well understood and includes the physics of light, optics, solid-state materials, and engineering approaches to the design of photoelectronic devices. The second set is related to the less well-known factors of psychophysics and vision and the interrelation between visual tasks, the quality of the image, the time available, and other subjective matters affecting the observer and his task.

Part V of IDA Report R-169 (Ref. 1) introduces television camera tubes and develops the concepts leading to SNR_D, Rosell's signal-to-noise

ratio at the display. It is SNR_D, the authors believe, that is the most powerful means of evaluating "resolution," a term usually used loosely and incorrectly. In SNR_D one has a meaningful parameter by which to judge television camera tube performance. If one chooses to specify a value of SNR_D that implies a 50 percent probability of seeing, the spatial frequency corresponding to that value of SNR_D at 100 percent input modulation is what is now loosely called "limiting resolution," that (specific value of) resolution usually listed in the commercial literature.

Images of rectangular objects parallel to the raster lines tend to loose their horizontal boundaries (but not their vertical boundaries) because they blend with the raster lines. Ohmart (Ref. 2) has shown that this effect increases the required search time for such objects by a very significant amount. Schade, in Section VI of this paper, considers in detail the factors involved.

The problem of image size has long been understood. Steedman and Baker (Ref. 3) analyzed it long ago, but their work has been ignored because their data complicate the problem of systems design. More of the early airborne systems were deficient because of inadequate display size than for almost any other reason.

John Johnson, of the Night Vision Laboratories, did research on image quality and published his findings in a 1958 report (Ref. 4) that is used as the present-day Bible on the subject. Unfortunately, the important diagrams and tables in Johnson's report are separated from the explanatory text. Thus, where the text states that "for a target to be recognizable, there must be system 'resolution' sufficient to place 4.0 ± 0.8 line pairs across the critical dimension of that target," the related table and diagram show "resolution across minimum dimension" and make no reference to "line pairs," which is the universal standard of resolution terminology EXCEPT in the television industry, which talks about "TV lines." Further, Johnson assumes a knowledgeable readership and so does not explain the implicit relationships between resolution and contrast.

As a result, designers commonly misuse Johnson's data, referring to "lines on target" instead of line pairs in the minimum dimension at a contrast considerably above liminal. This confusion of "line pairs" with "TV lines" often results in systems that are underdesigned or underspecified by a factor of 2. Confusion of "lines on target" with "line pairs per minimum dimension" leads not only to the line-pair error but also to neglect of the length-to-width ratio of typical targets. These two errors result in a typical underdesign factor of 4.

The relationship between an observer's performance and the performance of the image-forming system he is using is expressed by the difference between the modulation transfer function (MTF) of the equipment and the demand modulation function (DMF) of the observer, as mentioned earlier. The DMF* is not very well known, except in a few isolated tasks such as recognition of standard USAF three-bar test target patterns.

Tests in which targets are immersed in varying degrees of clutter indicate that the search function takes so long that the observer has closed to such a short range before he detects the target that he detects it and recognizes it simultaneously. In fact, under some conditions, detection, recognition, and identification occur almost simultaneously.

The proper design of devices starts, therefore, with an understanding of the difficulty of the visual task and thus with an understanding of the form of the DMF. The MTF of the system or, more important, the signal-to-noise ratio versus spatial frequency must then be matched to that demand curve to ensure, at least theoretically, before detailed design begins, that a real and useful device can be produced. Had this process been carried out in the past, it is quite probable that the vast majority of low-light-level systems designed to meet specific requirements would have been recognized as inadequate before they became hardware. As it is, although there are some good

*Sometimes called the aerial image modulation (AIM) curve.

data on the DMF, to the best of our knowledge these data relate to the detection of the USAF three-bar chart.

The form and performance of imaging devices are closely related to the application--to the character of the scene, its spectral composition, contrast and radiance, and to the difficulty and degree of detail in the visual task to be performed and the speed of its performance. The amount of time the observer has to make his observation, together with the detail required in his observation, is usually a factor overlooked in discussing the capability of these sensors.

Figure I-1 gives the resolution, in line pairs per minimum target dimension, required to detect, determine the orientation of, recognize, and identify various typical military targets broadside. Figure I-2 is a print of noise-free line-scan imagery of military vehicles, taken obliquely at 30 scans per vehicle. Figure I-3 is a sampling in the presence of noise at 32 scans per vehicle. A comparison of Figs. I-2 and I-3 illustrates how seriously noise can degrade image quality, even if the number of scans is increased.

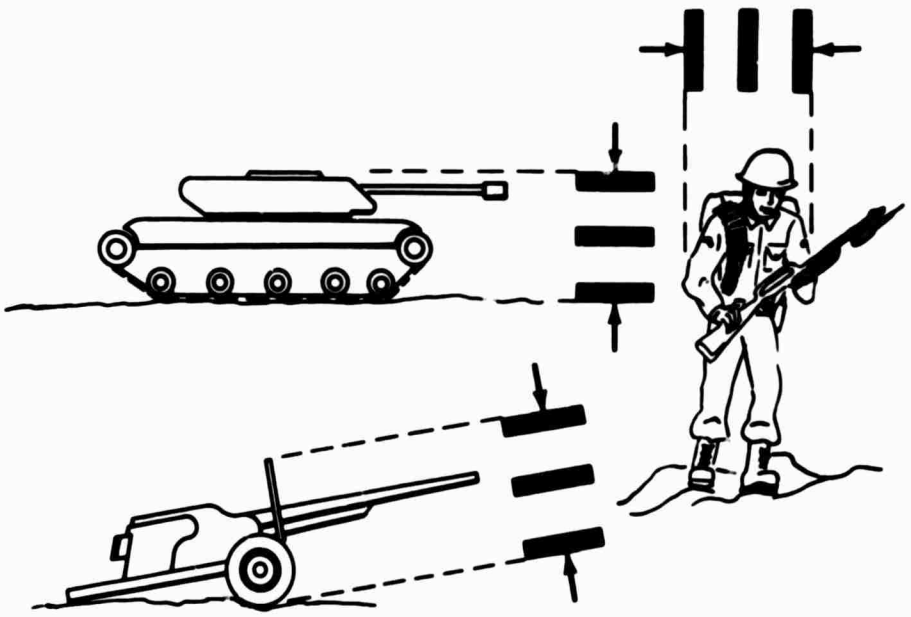

METHOD OF OPTICAL IMAGE TRANSFORMATION

TARGET	RESOLUTION IN LINE PAIRS PER MINIMUM DIMENSION			
BROADSIDE VIEW	DETECTION	ORIENTATION	RECOGNITION	IDENTIFICATION
TRUCK	0.90	1.25	4.5	8.0
M-48 TANK	0.75	1.20	3.5	7.0
STALIN TANK	0.75	1.20	3.3	6.0
CENTURION TANK	0.75	1.20	3.5	6.0
HALF-TRACK	1.00	1.50	4.0	5.0
JEEP	1.20	1.50	4.5	5.5
COMMAND CAR	1.20	1.50	4.3	5.5
SOLDIER (STANDING)	1.50	1.80	3.8	8.0
105 HOWITZER	1.00	1.50	4.8	6.0
AVERAGE	1.0 ± 0.25	1.4 ± 0.35	4.0 ± 0.8	6.4 ± 1.5

FIGURE i-1. Required Resolution for Detection, Orientation, Recognition, and Identification

FIGURE I-2. Noise-Free Line-Scan Imagery. Print of Oblique Line-Scan Images; 30 Scans Per Vehicle (Courtesy of Perkin-Elmer Corp.).

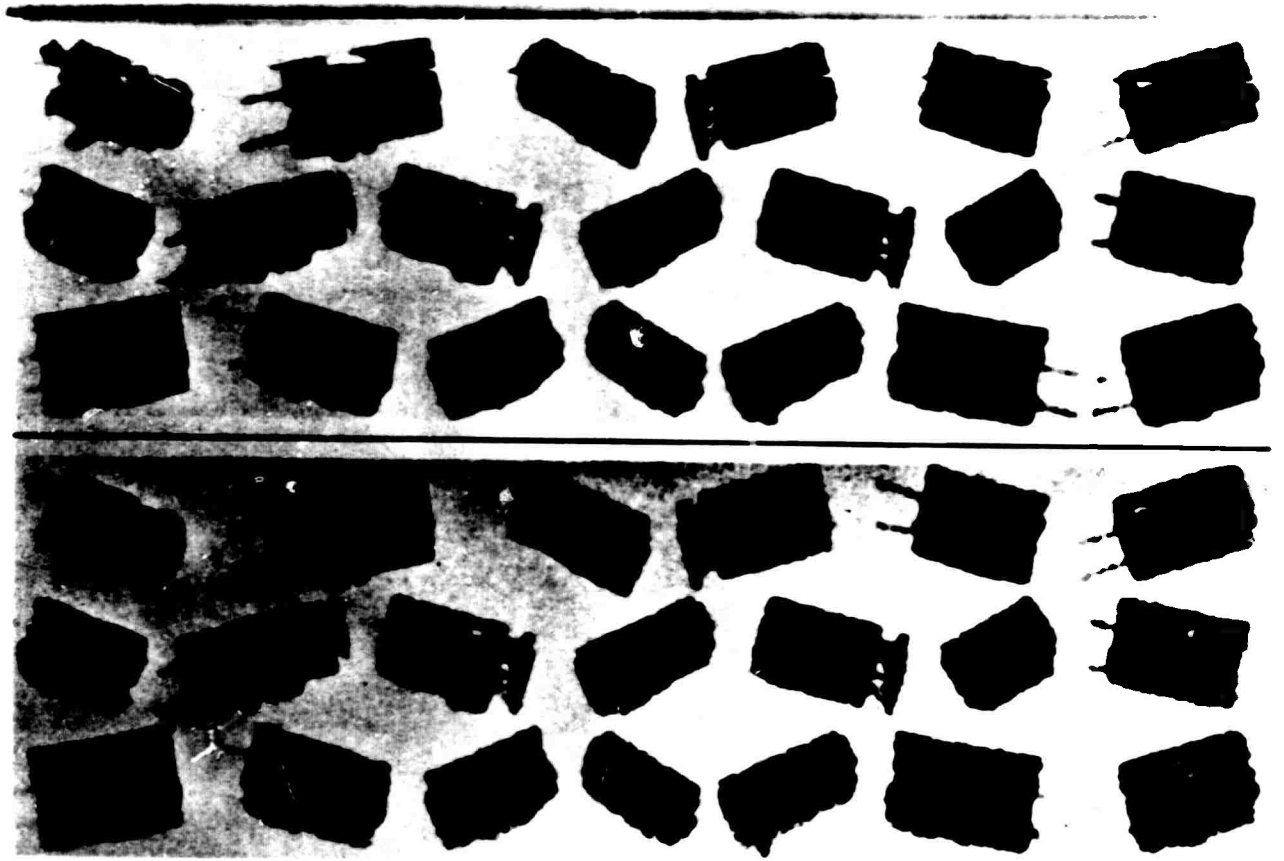

FIGURE I-3. Two-Dimensional Sampling with Noise: 32 Scans Per Vehicle. Signal-to-Noise Ratios: 4 (Top), 3 (Bottom) (Courtesy of Perkin-Elmer Corp.).

SECTION I. REFERENCES

1. Institute for Defense Analyses, Low-Light-Level Devices: A Designers' Manual, IDA Report R-169, L.M. Biberman, F.A. Rosell, O.H. Schade, Sr., A.D. Schnitzler, and H.L. Snyder, August 1971.

2. Martin Marietta Corporation, Orlando, Fla., Target Acquisition Studies: Fixed Television Fields of View, Report No. OR 9656, James G. Ohmart et al., October 1968.

3. Wright Air Development Division, Wright-Patterson Air Force Base, Target Size and Visual Perception, Technical Report 60-93, W.C. Steedman and C.A. Baker, February 1960.

4. John Johnson, in Proc. Image Intensifier Symposium, Ft. Belvoir, Virginia, October 6-7, 1958. (No report number.)

II. IMAGE QUALITY AND OPERATOR PERFORMANCE*

by Harry L. Snyder, Frederick A. Rosell, and Lucien M. Biberman

A. CORRELATION BETWEEN MTFA AND OPERATOR PERFORMANCE

1. Introduction

The purpose of this section is to describe the present state of knowledge about the ability of a trained observer to obtain target-relevant information from an imaging system display, and to relate this information-extraction performance to design characteristics of the imaging system. Unfortunately, as shall be noted below, the research pertaining to this relationship for low-light-level systems is somewhat ambiguous, and one must rely upon the related definitive data from the imagery developed by hard-copy photographic systems and then develop an analytical generalization to raster-scan systems.

During the past two decades, over 300 laboratory and analytical studies have been performed to assess the relationship between variation in line-scan display image parameters and observer performance. Conclusions drawn from critical reviews of these studies (e.g., Refs. 1-4) have indicated that cross-study comparisons are virtually impossible. Variation in specific system design parameters, or in the manner by which display image quality is synthetically manipulated, is often incompletely controlled, so that concomitant variation in the several contributing sources of image quality results. Table II-1 lists some of the experimental variables which have been shown to have a significant effect upon operator information-extraction (e.g., target-acquisition) performance. It should be noted that individual

---

*Adapted from IDA Report R-169.

experiments have tended to examine the effects of one, two, and sometimes three such variables. However, due to the inherent interaction (nonindependence) among these variables in their effects upon operator performance, quantitative combination of the results is hazardous even in the presence of good experimental control and measurement. In the absence of such control, any a posteriori attempt to combine the results is merely foolish.

TABLE II-1. SOME OF THE VARIABLES AFFECTING INFORMATION EXTRACTION PERFORMANCE

Atmosphere	Scene
Aerosol Content	Target Characteristics
Cloud Cover	Background Characteristics
Illumination Level	Terrain Masking
	Clutter Level
Sensor	**Display**
Bandwidth	Luminance
Number of Scan Lines	Size
Field of View	Number of Scan Lines
Field/Frame Rate	Contrast
Aspect Ratio	Scene Movement
S/N Level	Dynamic Range
Integration Time	Gamma
Image Processing	S/N Level
	Aspect Ratio
Edge Enhancement	
Gamma	
Spatial Filtering	

Because of these gross conflicts and inconsistencies in the experimental literature dealing with the effects of individual system parameters, recent efforts have been oriented toward the development of (1) analytical expressions of overall image quality, such as those discussed in Part V of IDA Report R-169, and (2) experimental evaluations of logically derived summary measures of image quality. The remainder of this section will discuss the present content and limitations of data pertaining to summary measures of image quality and operator performance.

2. Modulation Transfer Function Area (MTFA)

Any summary measure of image quality, to be useful, must be (1) easily measured for existing imaging systems, (2) quantitatively predictable, analytically, for future imaging systems at the paper design stage, and (3) highly correlated with (or validated by) empirically determined operator performance under the operational conditions of interest for the specified mission. To date, the summary measure of image quality which shows the greatest promise for meeting these criteria is the modulation transfer function area (MTFA).

Originally proposed by Charman and Olin (Ref. 5), who termed it the threshold quality factor, and renamed by Borough et al. (Ref. 6), the MTFA concept has been evaluated in two experimental situations and demonstrated to relate strongly to the ability of image interpreters to obtain critical information from reconnaissance photographic imagery. In its original form, the MTFA was proposed as a unitary measure of photographic image quality which contains "the cumulative effect of the various stages of the atmosphere-camera-emulsion-development-observation process, the 'noise' introduced in the perceived image by photographic grain, and the limitations imposed by the physiological and psychological systems of the observer" (Ref. 5, p. 385). While this measure was originally developed for direct photographic systems, its generalization to electrooptical systems is analytically straightforward.

The MTFA is derived in such a manner as to make use of the modulation transfer function (MTF) of the imaging system, thereby retaining the analytical convenience of component analysis based upon sine-wave response characteristics. In addition, it attempts to take into account other variables critical to the imaging and interpreting problem, such as exposure, the characteristic curve, granularity, the human observer capabilities and limitations, and the nature of the interpretation task. For the electrooptical system, the first three of these variables can be considered analogous to detector irradiance level, gamma (typically unity), and noise, respectively.

Figure II-1 shows that the MTFA is the area bounded by the imaging system MTF curve and the detection threshold curve of the total system, including the eye. The MTF curve for the imaging system is obtained in the conventional manner, while the detection threshold curve requires several assumptions regarding the human operator. Specifically, it is assumed that the viewing conditions are optimum, and that threshold detection of any target in the imaged display is a function of the target image contrast modulation, the noise in the observer visual system, and the noise in the imaging system exclusive of the observer. It should be noted that the crossover of the two curves in Fig. II-1 represents the limiting resolution of the system for a sine-wave target.

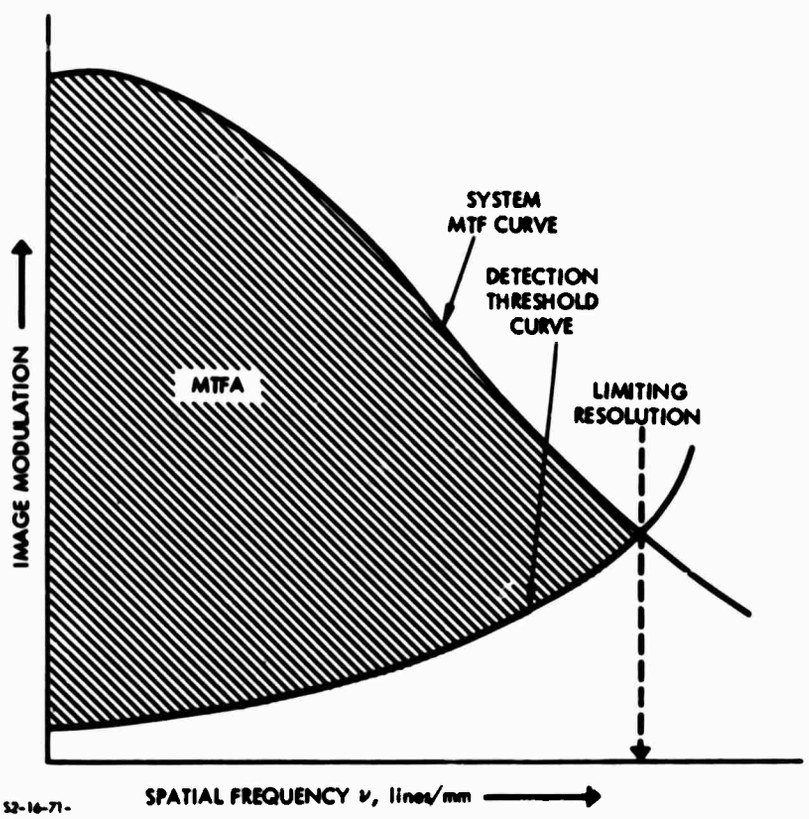

FIGURE II-1. Modulation Transfer Function Area (MTFA)

At low spatial frequencies, the threshold detection curve is dependent upon the properties of the human visual system, as shown in Fig. II-2. At higher spatial frequencies, the effect of imaging system noise becomes important. For the photographic case, this imaging system noise is equivalent to granularity. It is assumed further that the eye's contrast threshold is 0.04, so that this target image contrast modulation must be realized at the display for the target to be detected, regardless of the contrast modulation of the target object.

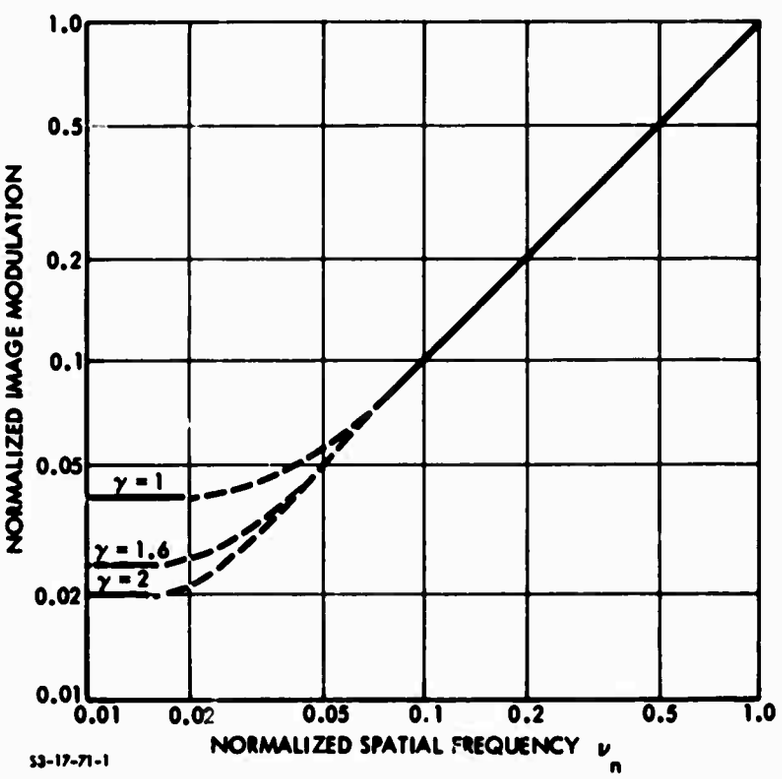

FIGURE II-2. Generalized Detection Threshold

Figure II-2 illustrates the normalized detection threshold curve, which must be adjusted both vertically and horizontally for a specific set of conditions. First, the curve is positioned vertically by increasing the normalized ordinate scale by $\frac{M_t(\nu)}{M_o}$, where $M_t(\nu)$ is the normalized value as shown in Fig. II-2 and M_o is the object contrast

modulation. Note that the lower portion of the threshold curve (at the lower spatial frequencies) is also adjusted by the system gamma, which, if greater than unity, enhances the modulation recorded at the display (e.g., the film) so that the minimum detectable threshold modulation decreases by $\frac{0.04}{\gamma}$.

Next, the detection threshold curve is positioned horizontally by multiplying the scale of the abscissa in Fig. II-2 by $\frac{2}{C\sigma(D)}$, where C is an empirically derived constant [0.03 for fine-grained films and 0.04 for coarser grained films (Ref. 7)] and $\sigma(D)$ is equal to the rms granularity measured with a 24-micron scanning aperture, as used in the Kodak handbooks.

Algebraically, the detection threshold curve for a photographic system is therefore (Ref. 5):

$$M_t(\nu) = 0.034 \left[\frac{dD}{d(\log_{10}E)}\right]^{-1} \left[0.033 + \sigma(D)^2\nu^2S^2\right]^{1/2}$$

in which

ν = any spatial frequency, in lines per millimeter

0.034 = an empirically derived constant*

D = mean film density

E = exposure

0.033 = an empirically derived constant*

$\sigma(D)$ = rms granularity for a 24 μ scanning aperture

S = signal-to-noise ratio necessary for threshold viewing, assumed to be about 4.5 (Ref. 14).

$\frac{dD}{d(\log_{10}E)}$ = film characteristic slope, including effects of development

*For derivation, see Charman and Olin (Ref. 5). Generation of these values is considered unimportant in the present context.

When the MTF curve and the detection threshold curve are plotted on log-log coordinates (Ref. 6), the expression for the MTFA becomes:

$$\text{MTFA (log-log)} = \int_{\log \nu_o}^{\log \nu_1} \left(\log T_\nu\right) d \log \nu - \int_{\log \nu_o}^{\log \nu_1} \left(\log \frac{M_t(\nu)}{M_o}\right) d \log \nu$$

$$= \int_{\log \nu_o}^{\log \nu_1} \left(\log \frac{M_o T_\nu}{M_t(\nu)}\right) d \log \nu$$

where

ν_o = the low spatial frequency limit, in lines/millimeter

ν_1 = the spatial frequency at which the MTF curve crosses the detection threshold curve (limiting resolution)

T_ν = the MTF value at spatial frequency ν

M_o = the object contrast modulation

$M_t(\nu)$ = the normalized detection threshold curve value, as taken from Fig. II-2.

When the MTF curve and the detection threshold curve are plotted on linear coordinates, the area of interest is given by (Ref. 6):

$$\text{MTFA (linear)} = \int_o^{\nu_1} \left(T_\nu - \frac{M_t(\nu)}{M_o}\right) d\nu.$$

The linear form computation utilizes no lower frequency cutoff, whereas the log-log formulation employs an arbitrary cutoff at, say, 10 lines/millimeter. The reason for this difference is simply that the log-log plot integration would place an inappropriately large weight upon integration over the lower spatial frequencies were this cutoff eliminated. The nature of the linear plot avoids the need for such an arbitrary cutoff.

It might also be noted, parenthetically, that the detection threshold curve, as described here, is akin to such concepts as contrast sensitivity (Ref. 8), sine-wave response (Refs. 9-11), and demand modulation function (DMF).

3. Evaluation of the MTFA

To date, two empirical evaluations of the MTFA concept have been conducted, both using photographic imagery. In the first study (Ref. 6), an attempt was made to relate MTFA to subjective estimates of image quality obtained from a large number of trained image interpreters. In the second of these experiments, actual information-extraction performance data were obtained, as well as subjective estimates of image quality, and both measures were compared with the MTFA values of the imagery. Schematically, these relationships can be thought of as those depicted in Fig. II-3. While it is desirable from an operational viewpoint to have a quick judgment of subjective image quality to serve as an indicant of the quality of any source of imagery for, say, rapid screening purposes, the critical measure of goodness of any imaging system is the ability of the observer to perform the required information-extraction tasks.

In the first study to evaluate MTFA, the purpose was to determine whether a strong relationship existed between MTFA and subjective image quality. This limited evaluation was imposed simply to reduce data collection costs in the event that the MTFA measure proved fruitless. In this experiment performed by Borough et al. (Ref. 6), nine photographic reconnaissance negatives were used as the basis for laboratory-controlled manipulation of image quality. Each of the scenes was printed in 32 different MTFA variants, determined by four different MTF's, three levels of granularity, and three levels of contrast, as illustrated in Fig. II-4. Four cells of the matrix were deleted because their MTFA values corresponded to others in the 32-cell matrix. The MTF curves are illustrated in Fig. II-5.

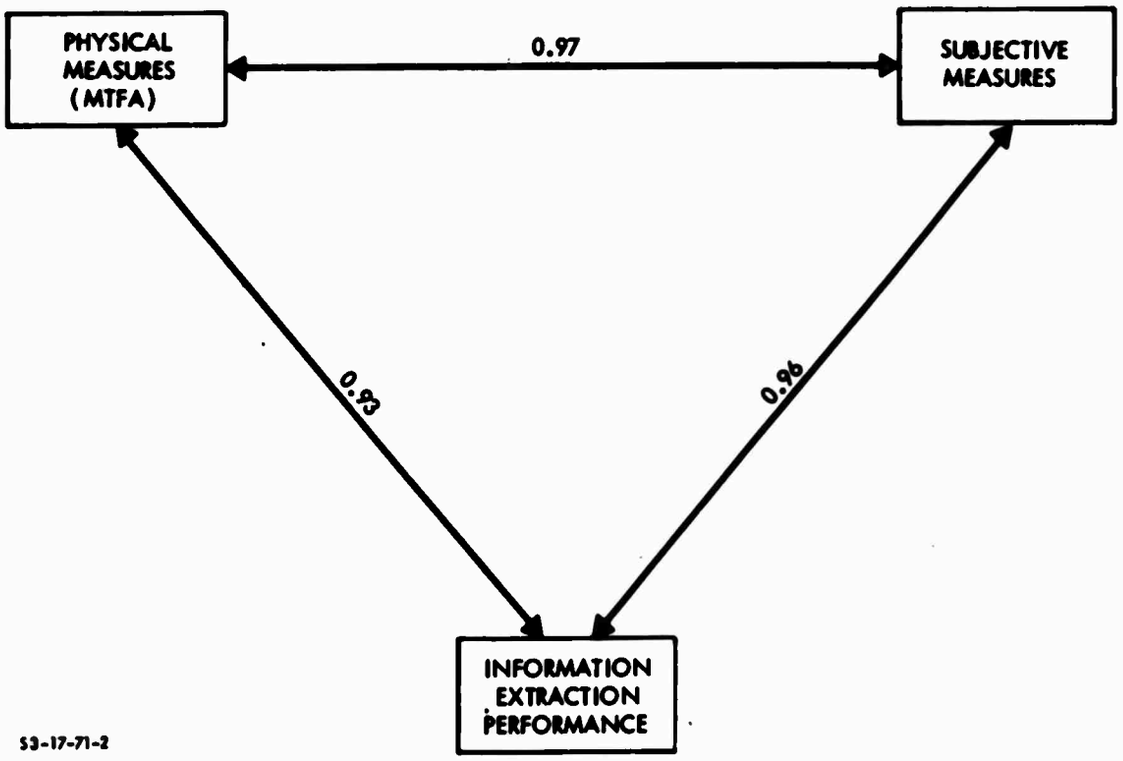

FIGURE II-3. Indices of Image Quality

The resulting 288 transparencies (9 scenes by 32 variants/scene) were used in a partial paired-comparison evaluation by 36 experienced photointerpreters. The subjects were asked to select the photo of each pair that had the best quality for extraction of intelligence information. All pairs were composed of two variants of the same scene; each subject made a total of 256 comparisons, for a grand total for all subjects of 36 x 256 = 9216 judgments.

Correlations were obtained between the subjective image quality rating (derived from the paired comparisons) for each of the 32 variants and several physical measures of image quality. Table II-2 shows the results. Most important to this discussion is the mean correlation of 0.92 between MTFA (linear) and subjective image quality, which

indicates that MTFA is strongly related to subjective estimates of image quality.

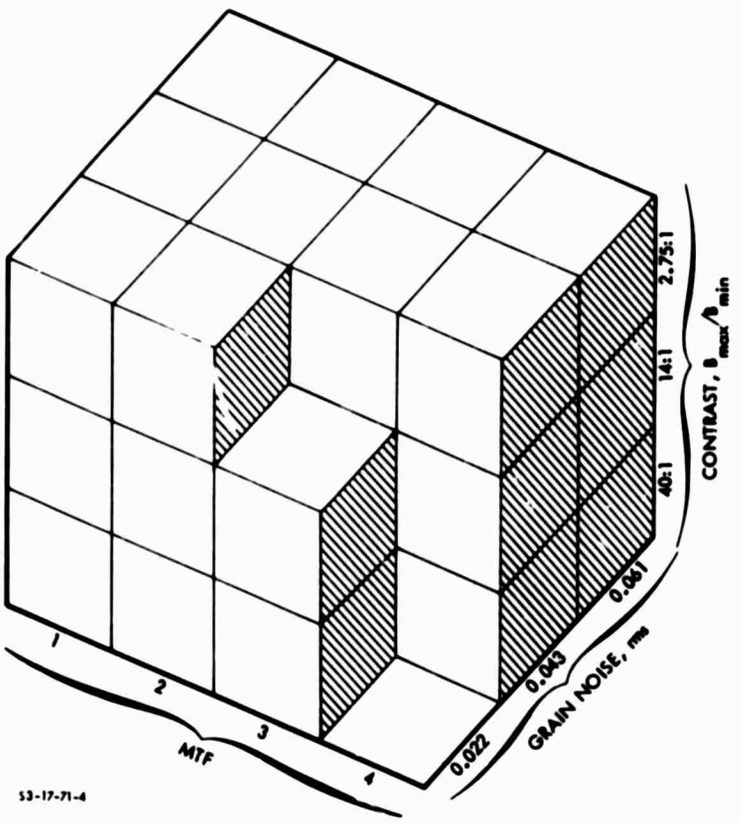

FIGURE II-4. Production of MTFA Values

The next experiment, by Klingberg, Elworth, and Filleau (Ref. 12), examined the relationship between objectively measured information-extraction performance and the MTFA values. As a check on the results of Borough et al., Klingberg et al. also obtained subjective estimates of image quality, so that all three correlations suggested by Fig. II-3 were evaluated.

The imagery used for this experiment was the same as that used by Borough et al. (Ref. 6). A group of 384 trained military photointerpreters served as subjects. Each subject was given one variant of each of the nine scenes and asked to (1) rank the image on a nine-point

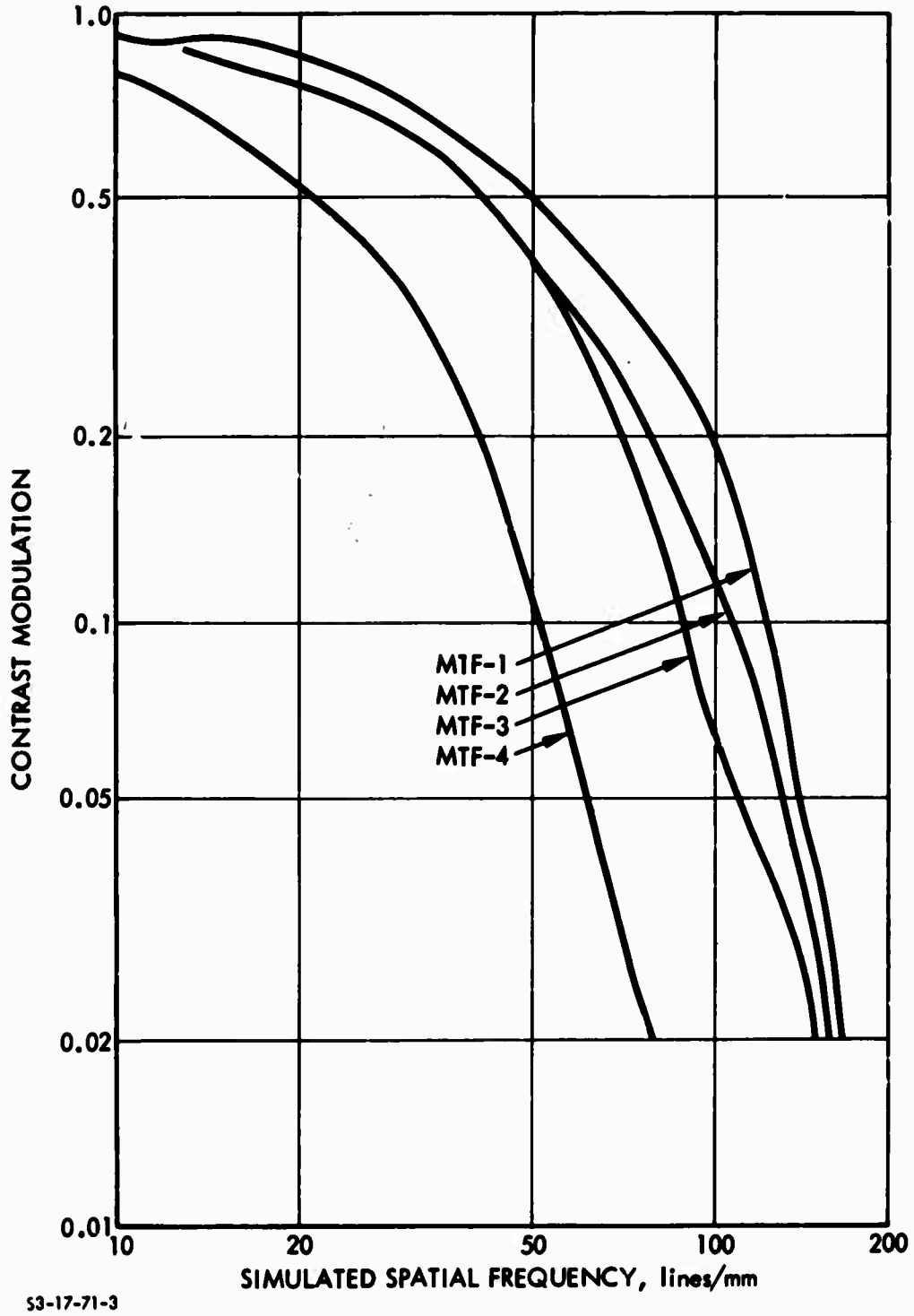

FIGURE II-5. Average Modulation Transfer Functions Measured by Edge-Response Method

interpretability scale, using utility of image quality for information extraction as the criterion, and (2) answer each of eight multiple-choice questions dealing with the content of the scene. The interpretability scale values were used to develop a subjective image quality measure for the 288 images, while scores on the multiple-choice interpretation questions were used to measure information-extraction performance.

TABLE II-2. CORRELATIONS OF PHYSICAL VARIABLES WITH SUBJECTIVE IMAGE QUALITY SCALE VALUE

Physical Variables	Scene Number									Mean r*
	1	2	3	4	5	6	7	8	9	
MTFA (Linear)	0.921	0.927	0.900	0.925	0.935	0.919	0.919	0.920	0.913	0.920**
Modulation	0.220	0.641	0.511	0.618	0.680	0.699	0.497	0.698	0.632	0.576
MTF	0.698	0.529	0.580	0.660	0.579	0.608	0.697	0.469	0.542	0.601
Granularity	-0.543	-0.632	-0.618	-0.450	-0.516	-0.428	-0.505	-0.589	-0.577	-0.543
MTFA (Log-Log--2 Cycle)	0.666	0.863	0.866	0.821	0.874	0.890	0.749	0.902	0.876	0.846
MTFA (Log-Log--10 Cycle)	0.768	0.923	0.923	0.867	0.920	0.921	0.824	0.941	0.920	0.900
Acutance	0.599	0.448	0.526	0.568	0.564	0.599	0.625	0.440	0.602	0.555

*These mean values were determined by transforming the correlations to Fisher's Z values. Such a transformation is necessary when correlations are being combined to obtain a mean correlation.

**This mean value was significantly greater ($p < 0.01$) than all of the other mean correlation values except the value for MTFA (Log-Log--10 Cycle). This latter value was still significantly less than the MTFA linear value at the 0.05 level of significance.

Figure II-6 shows the scattergram between information-extraction performance and MTFA for the 32 MTFA values. The resulting correlation, averaged across the nine scenes, is -0.93. (The minus value is due to the use of number of errors, which is inversely related to MTFA, as a measure.)

Individual correlations among performance, MTFA, and subjective quality (rank) are shown in Table II-3. It is apparent that the relationship between MTFA and performance is not as high for some scenes

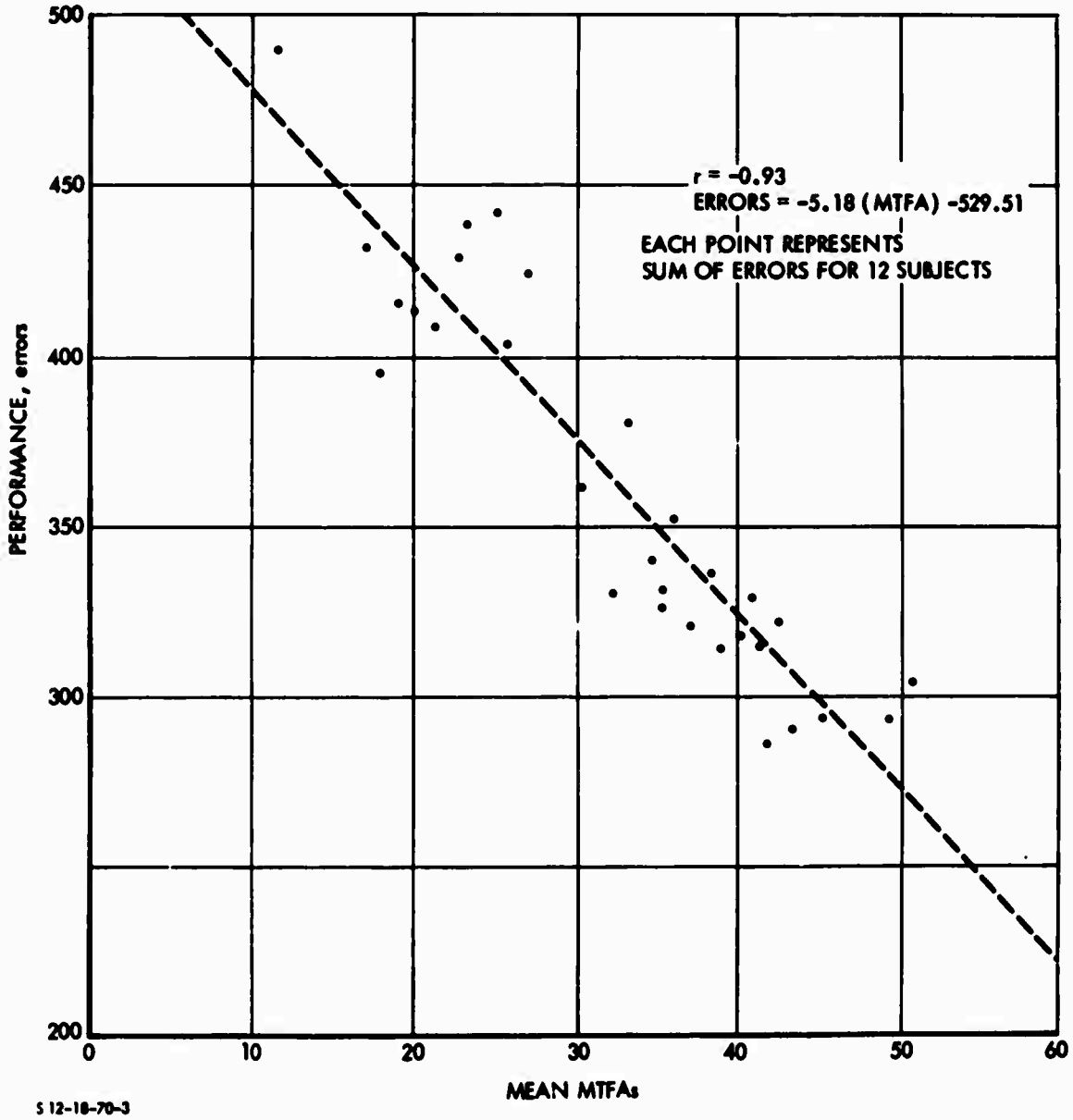

FIGURE II-6. Scattergram of Information Extraction Performance Versus MTFA

(e.g., 6 and 9) as for others, but that the mean correlation $\bar{r}$ across scenes (0.72) is quite high. Further, if one disregards scene content and places all scenes on a common performance continuum, the correlation of -0.93 accounts for over 86 percent of the variance in information-extraction performance. Further, the 0.97 correlation of MTFA with subjective quality (rank) agrees quite well with the correlation of 0.92 obtained by Borough et al

TABLE II-3. CORRELATIONS (PEARSON r's) BETWEEN IMAGE QUALITY, INTERPRETER PERFORMANCE AND SUBJECTIVE JUDGMENTS

Scene	1	2	3	4	5	6	7	8	9	$\bar{r}^*$	r_m^{**}
Performance/MTFA	0.69	0.66	0.80	0.65	0.78	0.55	0.84	0.86	0.46	0.72	0.93
Performance/Rank	0.71	0.67	0.89	0.60	0.80	0.42	0.78	0.76	0.42	0.70	0.96
MTFA/Rank	0.90	0.87	0.90	0.93	0.94	0.87	0.92	0.86	0.83	0.90	0.97

N = 32 image quality levels (MTFA)

$^*\bar{r}$ = Average of r's using Z scores.

$^{**}r_m$ = Values averaged across scenes before computing correlation.

A further comparison among these measures is given in Table II-4, which compares the paired-comparison subjective quality values V of Borough et al. with the other measures obtained by Klingberg et al. both for individual scenes and all nine scenes combined. As the summary matrix indicates, information-extraction performance, MTFA, and subjectively scaled image quality (obtained by either absolute judgments or paired comparisons) intercorrelate highly. These resulting values are shown on the appropriate lines in Fig. II-3.

TABLE II-4. INTERCORRELATIONS OF ALL MEASURES BY SCENE

SCENE 1

	R	M	V
Performance (P)	0.71	0.69	0.68
Ranks (R)		0.90	0.92
MTFA (M)			0.92
Paired-Comparison Values (V)			

SCENE 2

	R	M	V
	0.67	0.66	0.67
		0.87	0.87
			0.93

SCENE 3

	R	M	V
	0.89	0.80	0.83
		0.90	0.91
			0.88

SCENE 4

	R	M	V
Performance (P)	0.60	0.65	0.64
Ranks (R)		0.93	0.92
MTFA (M)			0.92
Paired-Comparison Values (V)			

SCENE 5

	R	M	V
	0.80	0.78	0.76
		0.94	0.92
			0.93

SCENE 6

	R	M	V
	0.42	0.55	0.70
		0.87	0.83
			0.92

SCENE 7

	R	M	V
Performance (P)	0.78	0.84	0.82
Ranks (R)		0.92	0.90
MTFA (M)			0.92
Paired-Comparison Values (V)			

SCENE 8

	R	M	V
	0.76	0.86	0.82
		0.86	0.87
			0.92

SCENE 9

	R	M	V
	0.42	0.46	0.43
		0.83	0.77
			0.91

ALL SCENES COMBINED

	R	M	V
Performance (P)	0.97	0.93	0.93
Ranks (R)		0.96	0.97
MTFA (M)			0.97
Paired-Comparison Values (V)			

B. CORRELATION BETWEEN MTFA AND SNR_D

In the material above, Snyder showed the correlation between MTFA and viewer error, while in Part V of IDA Report R-169, Rosell has derived the concept of SNR_D, the display signal-to-noise ratio. If these

two concepts could be related, the missing link between the physical properties of electrooptical devices and operator performance would be established. As will be shown, there is a one-to-one correspondence between MTFA and the area under the SNR_D curves, provided that sine-wave patterns are used as test inputs in calculating or measuring SNR_D.

The beginning point of Snyder's analysis is Eq. II-1, which states that the eye's threshold detection requirements for a sine-wave pattern of frequency k is

$$M_t(k) = 0.034\ [dD/d(\log_{10} E)]^{-1}\ [0.033 + \sigma_D^2\ k^2\ S^2]^{\frac{1}{2}} \qquad \text{(II-1)}$$

where $[dD/d(\log_{10} E)]$ is a sensor gamma, σ_D^2 is noise, and S is a threshold signal-to-noise ratio. $M_t(k)$ should not be confused with the sensor's MTF. It has no relation to it. $M_t(k)$ is the signal modulation needed by the eye to detect the pattern in the presence of noise. The constant term in the root bracket pertains to low spatial frequencies wherein the eye is limited by spatial image extent, its dc response, or other factors. To a first approximation, one can ignore it. Then, for sensor $\gamma = 1$,

$$M_t(k) = 0.034\ \sigma\ k\ S \qquad \text{(II-2)}$$

To convert Eq. II-2 to Rosell's terminology, one lets σ equal the rms video noise, k be expressed in N_{TV} lines/picture height, S be SNR_{DT}, the display signal-to-noise ratio required for 50 percent probability of pattern detection, and the constant 0.034 be changed to β to reflect the change in nomenclature and units. Now,

$$M_t\ (N_{TV}) = \beta \cdot i_n \cdot N_{TV} \cdot SNR_{DT} \qquad \text{(II-3)}$$

or

$$SNR_{DT} = \frac{1}{\beta} \frac{M_t\,(N_{TV})}{N_{TV}} \cdot \frac{1}{i_n} \qquad \text{(II-4)}$$

If next one lets $M_t\,(N_{TV})$ be equal to

$$M_t\,(N_{TV}) = \Delta i_{ST} \qquad \text{(II-5)}$$

where Δi_{ST} is the threshold video signal, then

$$SNR_{DT} = \frac{1}{\beta} \cdot \frac{1}{N_{TV}} \cdot \frac{\Delta i_{ST}}{i_n} \qquad \text{(II-6)}$$

but $\Delta i_{ST}/i_n$ is the threshold video signal-to-noise ratio $SNR_{V,O,T}$ required, so that:

$$SNR_{DT} = \frac{(1/\beta) \cdot SNR_{VT}}{N_{TV}} \qquad \text{(II-7)}$$

which is the relationship between threshold display signal-to-noise and threshold video signal-to-noise ratio as used by Rosell throughout his analysis.

Next, one turns to the concept of MTFA, which Snyder defines as

$$MTFA = \int_0^{k_o} \left[T(k) - \frac{M_t(k)}{M_o} \right] dk \qquad \text{(II-8)}$$

where T(k) is the sensor's MTF, M_o is an object modulacion, and k_o is a specific spatial frequency to be defined. In our terminology $T(k) = R_W(N)$, the sine-wave response.

If one uses Eqs. II-5 and II-6 in Eq. II-8 and lets $M_o = C\Delta i_s$, the product of input image contrast and highlight signal current, Eq. II-8 becomes

$$MTFA = \int_0^{N_o} R_W(N_{TV}) - \left[\frac{\beta\ SNR_{DT} \cdot N_{TV} \cdot i_n}{C i_s}\right] dN \qquad \text{(II-9)}$$

where N_o is the frequency corresponding to k_o but now expressed in terms of TV lines per picture height. Note that $C\ i_s/i_n$ is the broad-area video signal-to-noise ratio that the sensor can produce, i.e.,

$$SNR_{V,0,C} = C\ i_s/i_n \qquad \text{(II-10)}$$

and

$$MTFA = \int_0^{N_o} \left[R_W(N_{TV}) - \frac{\beta\ SNR_{DT} \cdot N_{TV}}{SNR_{V,0,C}}\right] dN$$

$$= \int_0^{N_o} \left[\frac{R_W(N_{TV}) \cdot SNR_{V,0,C} - \beta\ SNR_{DT} \cdot N_{TV}}{SNR_{V,0,C}}\right] dN \qquad \text{(II-11)}$$

Now, using Eq. II-7

$$MTFA = \int_0^{N_o} \frac{[R_W(N_{TV}) \cdot SNR_{V,0,C} - SNR_{VT}]}{SNR_{V,0,C}}\ dN \qquad \text{(II-12)}$$

and then noting that the actual video signal-to-noise ratio at line number N_{TV} is equal to

$$SNR_{V,N,C} = R_W(N_{TV}) \cdot SNR_{V,0,C} \qquad \text{(II-13)}$$

one sees that Eq. II-12 becomes

$$MTFA = \int_{o}^{N_o} \left[\frac{SNR_{V,N,C} - SNR_{VT}}{SNR_{V,0,C}} \right] dN \qquad \text{(II-14)}$$

and the interpretation of MTFA becomes quite clear--it is the integral of the difference between the video SNR that the sensor can provide less that required by the observer normalized to that which the sensor can provide at zero spatial frequency. The limits of integration are to the line number where $SNR_{V,N,C}$ intersects $SNR_{V,T}$, as shown in Fig. II-7.

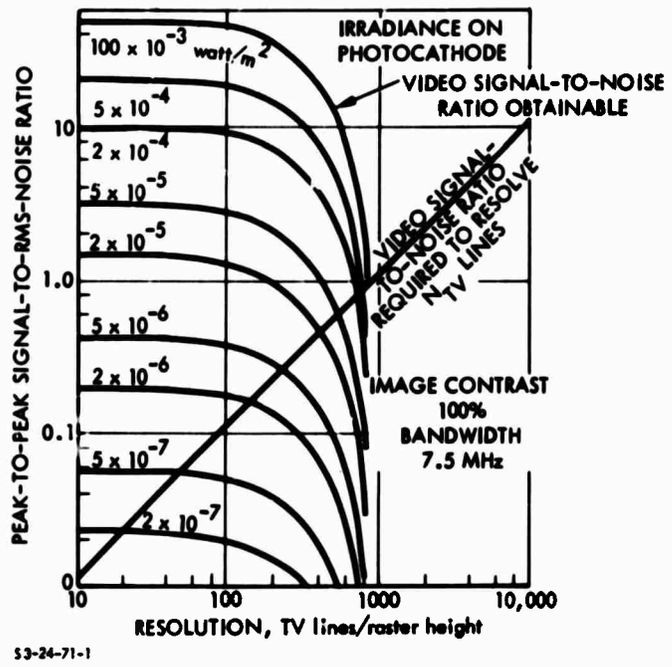

FIGURE II-7. Peak-to-Peak Video Signal-to-Noise Ratio Required Versus that Obtainable as a Function of Resolving Power for the I-SEC

In an alternate derivation, one reverts to Eq. II-11 and divides numerator and denominator by $1/\beta\ N_{TV}$. Then,

$$MTFA = \int_0^{N_o} \left[\frac{(SNR_{V,0,C} \cdot R_W(N_{TV})/\beta N_{TV}) - SNR_{DT}}{SNR_{V,0,C}/\beta N_{TV}} \right] dN$$

$$= \int_0^{N_o} \left[\frac{SNR_D - SNR_{DT}}{SNR_{DO}} \right] dN \qquad \text{(II-15)}$$

where SNR_D is the display SNR obtainable from the sensor, SNR_{DT} is that needed by the eye, and SNR_{DO} is that obtainable at zero spatial frequency.

The relationship between the two methods is shown by comparing areas A and B in Fig. II-8. The shaded areas are equal, i.e.,

$$\text{Area A} = \text{Area B}$$

$$MTFA = \text{Area A} = \text{Area B}$$

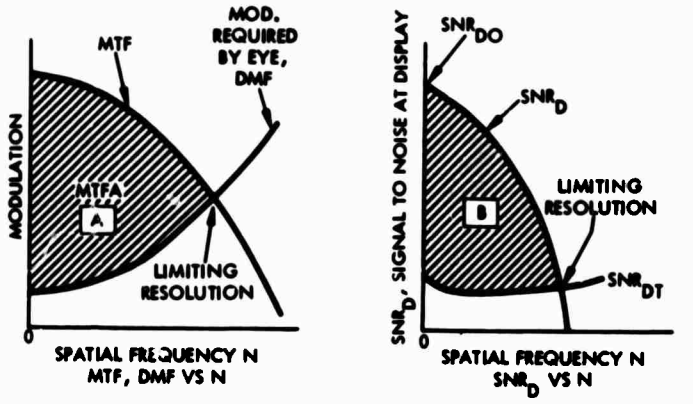

A = B

MTF	- MODULATION TRANSFER FUNCTION
MTFA	- MODULATION TRANSFER FUNCTION AREA
DMF	- DEMAND MODULATION FUNCTION
N	- SPATIAL FREQUENCY, TV LINES/PICTURE HEIGHT
SNR_D	- DISPLAY SIGNAL-TO-NOISE RATIO
SNR_{DT}	- DISPLAY SIGNAL-TO-NOISE RATIO, THRESHOLD
SNR_{DO}	- DISPLAY SIGNAL-TO-NOISE RATIO AT ZERO SPATIAL FREQUENCY

S8-27-70-2

FIGURE II-8. Comparison of MTFA and SNR_D

C. CONCLUSIONS AND CAUTIONS

These data show unequivocally that a measure of image quality based upon the excess of MTF over the threshold detection level correlates highly with the ability of observers to obtain critical operational information from the imagery. As is shown in Part V of IDA Report R-169, there are other ways to define the same (or a very similar) quantity. For example, Rosell's display signal-to-noise ratio (SNR_D)* is essentially the same quantity as MTFA when appropriate alterations are made in the calculations to account for the differences between photographic imaging system variables and electrooptical line-scan system variables. In both cases, the general value of interest is the excess of signal over noise as a function of spatial frequency. Viewed in that context, the data reported here demonstrate that MTFA (or SNR_D) is an extremely useful and valid measure of the figure of merit of an imaging system. At the same time, however, some cautions must be noted.

First, the specification of the detection threshold curve (or Rosell's 50 percent probability-of-detection S/N level) implies that optimum viewing conditions are obtained. In the studies reported here, the observer was ground based, supplied with an ample nonglare display luminance, and was not time-restricted in his responses. Similarly, in the data used to develop the concept of SNR_D, observers were not severely hampered by operational constraints. In both cases, therefore, the detection threshold curves represent the best performance of which the well-trained observer is capable. If, for the sake of argument, this threshold were to be uniformly elevated by adverse operational circumstances for all spatial frequencies of the display, no changes in the relationships presented here would occur--the relative magnitudes of MTFA would remain unchanged. If, on the other hand, operational requirements caused a nonuniform elevation of the detection

---

*Discussed in Section V-A-2 of IDA Report R-169.

threshold curve across all usable spatial frequencies, then inversions could occur in the MTFA values for systems having different MTFs.

This is not a minor consideration when it is realized that the eye's contrast threshold varies not only with spatial frequency but also with display signal-to-noise, overall image luminance, adaptation level (mean surround luminance), and such environmental parameters as glare, vibration, glint, and time stress. As the MTFA concept is applied to electrooptical systems, it is particularly important to note that the MTF is defined specifically in the absence of noise, so that at low detector irradiance (and hence low S/N) levels, a display may have a considerable amount of "snow" and thereby produce poor target acquisition performance, even though the system MTF remains unchanged. For this reason, it is vital that the display S/N level be included as a determinant of the detection threshold curve used in MTFA calculation, and that other conditions under which the MTFA is defined (e.g., display luminance and operating environment) also be specified to avoid ambiguity. Otherwise, the MTFA obviously cannot be used to predict observer performance over a wide range of electrooptical system operating conditions.

Secondly, it is likely that, upon further analysis, we must learn how to weigh the excess signal over the noise at various spatial frequencies, rather than integrate uniformly as in the current MTFA or SNR_D concepts, for the following reason. It has been shown that noise of a spatial frequency similar to the spatial frequency of the target of interest has the most deleterious effect upon threshold detection performance (Ref. 13). Thus, because various missions might require acquisition of targets of predominantly specific spatial frequencies, and because various imaging system designs might produce noise power at certain spatial frequency bands, one cannot simply conclude that the excess of signal above noise can be assumed to be of equal importance at all spatial frequencies. That is, there are undoubtedly spatial frequency bands which are more important for some missions than others, and appropriate weighting of these bands should be considered when evaluating a particular system (by MTFA or SNR_D) for that

mission, and that uniform integration across all spatial frequencies from zero to limiting resolution might produce nonrepresentative results.

Finally, although the writer is convinced that the MTFA approach (or, equivalently, the SNR_D discussed in Part V of IDA Report R-169) presents the most valid figure of merit for present and near-future imaging systems, cautions must be noted as to the representativeness of the data which lead to this conclusion. The data of Borough et al. (Ref. 6) and Klingberg et al. (Ref. 12) were obtained for non-time-limited, nonstressed viewing conditions; the display of the imagery was nearly optimal; and the imagery itself was continuous-image photographic negative material, not line-scanned, cathode-ray-tube presentations under dynamic conditions. Clearly, verification of these results is indicated for conditions more representative of the operational mission in which the typical line-scan system is employed.

Interdependence of Sensitivity and Resolution

Sensitivity and resolution must not be quoted as two independent parameters. Rather, one should specify SNR_D as a function of spatial frequency for a number of light levels. The actual data required are data of the form of Fig. II-9. For more limited appraisals one can use an approximation to SNR_D, i.e., $I_S R_\omega(N)$, where I_S includes the cathode response and tube gain factors while $R_\omega(N)$ is the spatial frequency response of the tube. One may well compare tubes on the basis of this factor of merit as long as comparison is made at the same specific value of input illumination and the same specific value of resolution.

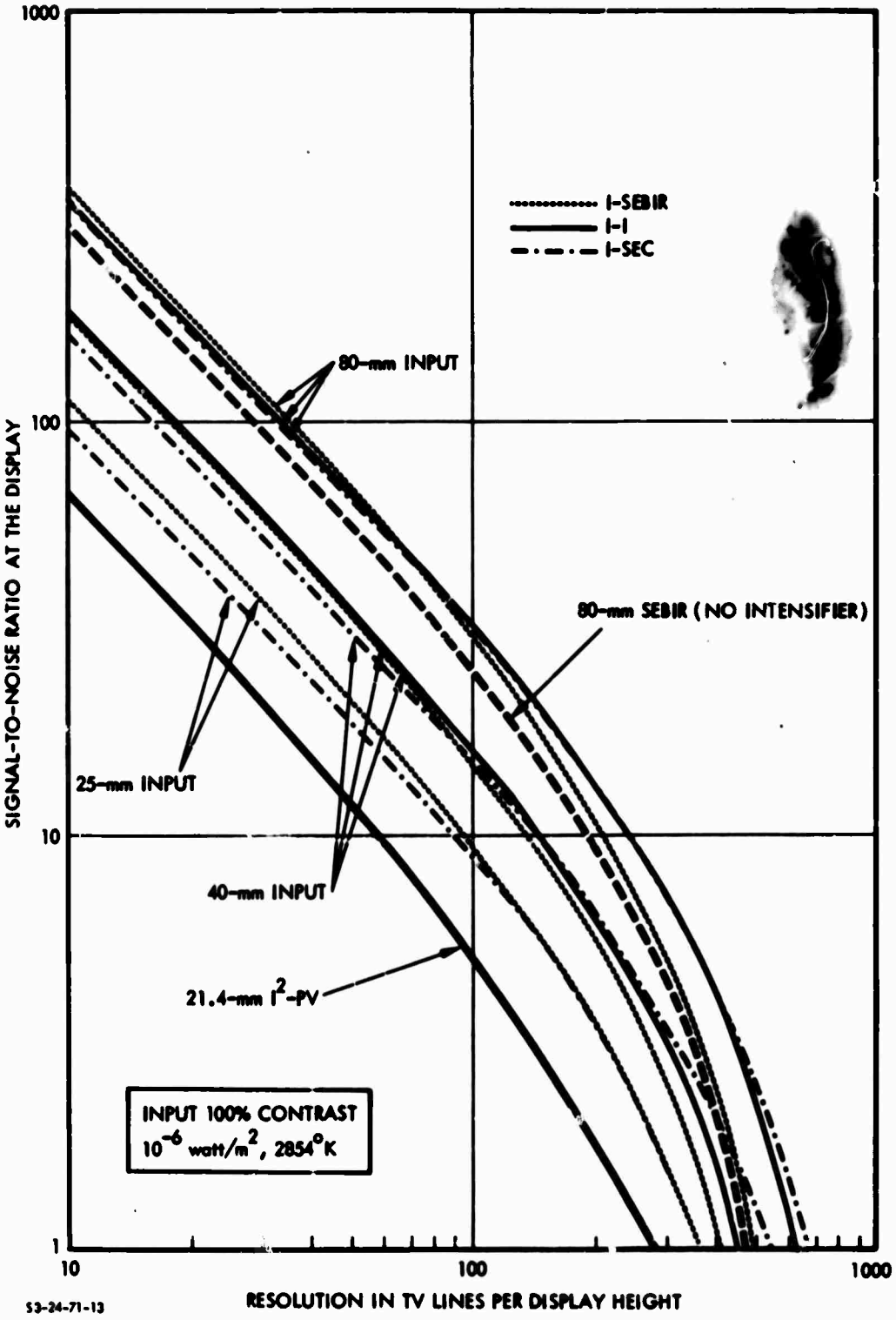

FIGURE II-9. The Performance of Some Tube-Intensifier Combinations

SECTION II. REFERENCES

1. Air Force Avionics Laboratory, Low Light Level TV Viewfinder Simulation Program. Phase A: State-of-the-Art Review, Report AFAL-TR-67-293, H.L. Snyder et al., November 1967.

2. B. Hillman, "Human Factor Considerations in Real-Time Airborne Target Acquisition," in Air-to-Surface Missile Technology, 1975-1980, IDA Report R-133, December 1967.

3. The Boeing Company, Night and All-Weather Target Acquisition: State-of-the-Art Review. Part III: Television and Low-Light-Level Television Systems, Boeing Company Report D162-10116-3, H.W. Hairfield, May 1970.

4. The Boeing Company, Night and All-Weather Target Acquisition: State-of-the-Art Review. Part II: Infrared and Laser Systems, Boeing Company Report D162-10116-2, C.R. Filleau, April 1970.

5. W.N. Charman and A. Olin, "Image Quality Criteria for Aerial Camera Systems," Phot. Sci. and Eng., Vol. 9, pp. 385-397, December 1965.

6. The Boeing Company, Quantitative Determination of Image Quality, Boeing Company Report D2-114058-1, H.C. Borough, R.F. Fallis, T.H. Warnock and J.H. Britt, May 1967.

7. F. Scott, in Image Evaluation for Reconnaissance, Proceedings of a Symposium, Itek 9048-6, April 9-17, 1963.

8. F.W. Campbell and D.G. Green, "Optical and Retinal Factors Affecting Visual Resolution," J. Physiol., Vol. 181, pp. 576-593, 1965.

9. J.J. DePalma and E.M. Lowry, "Sine-Wave Response of the Visual System. II. Sine-Wave and Square-Wave Contrast Sensitivity," J. Opt. Soc. Am., Vol. 52, pp. 328-335, 1962.

10. E.M. Lowry and J.J. DePalma, "Sine-Wave Response of the Visual System. I. The Mach Phenomenon," J. Opt. Soc. Am., Vol. 51, pp. 740-746, 1961.

11. C. Bryngdahl, "Characteristics of the Visual System: Psychophysical Measurements of the Response to Spatial Sine-Wave Stimuli in the Photopic Region," J. Opt. Soc. Am., Vol. 56, pp. 811-821, 1966.

12. The Boeing Company, Image Quality and Detection Performance of Military Interpreters, Final Report, Air Force Office of Scientific Research Contract F44620-69-C-0128, C.L. Klingberg, C.L. Elworth, and C.R. Filleau, April 1970.

13. B.H. Eckhardt, "Application of Spatial Frequency Data to the Prediction of Imaging System Effectiveness," in CIRADS: Supplementary Proceedings, Human Factors Conference, Advanced Research Projects Agency, January 12, 1967.

14. P.D. Carman and W.N. Charman, "Detection, Recognition, and Resolution in Photographic Systems," J. Opt. Soc. Am., Vol. 54, pp. 1121-1130, 1964.

III. THE PERFORMANCE OF RECONNAISSANCE SYSTEMS*

by Alvin D. Schnitzler

The purpose of a reconnaissance system** is to increase the acquisition and flow of visual information from a scene to an interpreter over what would be possible if the interpreter were forced to rely on his eyes alone. Hence, a reconnaissance system is a component in a communication system, and the analysis of a reconnaissance system may be considered as a communication problem.

A communication system consists of the five basic components: (1) an information source, (2) a transmitter or power source, (3) a transmissive medium, (4) a receiver, and (5) a user. In reconnaissance, the information source is the scene, the transmitter or power source is the irradiance of the scene by the sun, moon, airglow, and stars, the transmissive medium is the atmosphere, the receiver is the reconnaissance system itself, and the user is the image interpreter.

The transmission of information from the scene arises from the spatial modulation of the reflected irradiation by spatial variations in the reflectivity.

The display of information from the scene by a reconnaissance system depends on the fidelity of reproduction in the output image of the spatial variations in reflectivity and on the magnitude of the noise, which is equivalent to random spatial fluctuations in the

---

* Paper given before the IRIS Image Forming Specialty Group, Dallas, Texas, 7 January 1971.

** For the purposes of this analysis, systems operating in the visible or near-visible regions are considered, but the analysis generally applies more broadly across the specifications.

reflectivity of the scene. The fidelity of reproduction in the output image is generally determined by either the spatial impulse response (point spread function) or, equivalently, by the spatial frequency response (modulation transfer function). However, if the reconnaissance system incorporated a static array of detectors, which sample small areas of the input image irradiance at fixed points, fidelity would be degraded and information lost, even if the frequency response of all other components were unity. The effect of static sampling is (1) to distort contrast boundaries, reducing information concerning the shape of an object and (2) to introduce spurious periodic components in the output image. The reduction in shape information obviously increases as the size of the input image of an object decreases relative to a detector size. If the input image of an object falls on a single detector, all shape information is lost. The presence of spurious periodic components in an output image is completely analogous to ripple in the vertical deflection of a horizontal oscilloscope trace. If the amplitude and period of the ripple are comparable to the amplitude and duration of a signal pulse (contrast and extent of an object in the output image), respectively, the signal pulse shape is distorted, and the probability of detecting or identifying the pulse is reduced. If the signal is not a pulse but, rather, is periodic, beat frequencies between the harmonics of the signal and the ripple will arise with varying phase relative to the signal, further distorting the signal. In a system with a static array of detectors, spatial beat frequencies can arise seriously when viewing periodic test patterns of frequency greater than the reciprocal of the sampling spatial interval, as shown in Fig. 72 of Section VI. Thus, it is advisable to utilize a lowpass filter to limit the input spatial frequencies to a sampling system.

The probability of detecting a signal in the presence of noise is a monotonic function of the signal-to-noise ratio. It has been amply demonstrated that the probability of detecting the presence of an object on a uniform background depends on the signal-to-noise ratio of the output image formed by the reconnaissance system (Section IV). The output signal is the spatial variation in the luminance of the output

image. The output noise is measured by the rms fluctuation in the spatial variation of the luminance.

If identification of an object is required rather than mere detection, then a higher signal-to-noise ratio is required. Furthermore, shape information is then vital. If the reconnaissance system incorporates a static detector array, a sufficient number of samples per object are required to provide the required shape information.

The probability of identifying an object with either a continuous two-dimensional sampling of the input image (i.e., convolution of the point spread function with the input image) or a static array of detectors of sufficient density to provide many samples per object is determined by the output image signal-to-noise ratio alone. The probability of identifying an object with a static array of detectors at high output image signal-to-noise ratio depends only on the number of samples per object. A more complicated regime than either of the above exists, in which the probability of identification depends on both the signal-to-noise ratio and the number of samples per object. The number of samples and the signal-to-noise ratio required to detect or identify any particular object such as a truck or tank on various terrains can only be determined empirically (Section I, Fig. I-1).

However, the quality of a reconnaissance system (useful to compare the expected performance of one system with another) can be measured under controlled conditions in the laboratory and, in some cases, is subject to analysis. For example, the quality of an infrared system and of a photoelectronic imaging (PEI) system, such as an image intensifier or low-light-level television system, can be predicted by employing the modulation transfer function and a calculated expression for the noise equivalent modulation to determine the resolution as a function of system parameters and operating conditions.

In measurement and analysis of the performance of PEI systems, it has become customary to utilize both sine-wave and square-wave (bar) test patterns. Although sine-wave functions are the basic functions

in frequency response analysis, they are difficult to generate experimentally. However, the results of measurements using either sine-wave or square-wave test patterns and analysis based on sine-wave functions are easily related (Ref. 1) by the simple Fourier series expansion of a periodic square-wave function. The following discussion is based on analysis of a simple sine-wave test pattern. To a good approximation, it has been demonstrated (Ref. 2) that in the vicinity of the threshold of visual perception of the image of test objects or patterns on a display, detection probability is independent of the distribution of luminance within an image element. Thus, for a sine-wave test pattern, it is necessary to calculate the difference and the fluctuations of the difference in luminance of adjacent image elements considered somewhat arbitrarily to be the positive and negative half cycles of the sine-wave modulation. The calculation yields the explicit dependence of the output signal-to-noise ratio on the basic parameters of a PEI system. The result is given by

$$(S/N)_D = (2\epsilon\bar{\eta}\,\bar{n}_h t)^{\frac{1}{2}}\, M_D/\pi\nu_{os} \qquad \text{(III-1)}$$

where ϵ is the length-to-width ratio of a half period of the sine-wave test pattern, $\bar{\eta}$ is the spectrally weighted (over the spectrum of the input irradiance) quantum efficiency of the sensor (photocathode), $\bar{n}_h$ is the irradiance of the sensor averaged over the sensor area, t is the integration time of the eye, M_D is the output modulation of the test pattern determined by the frequency response or modulation transfer function $T(\nu_{os})$ and the input modulation M_s (i.e., $M_o = T(\nu_{os})\, M_s$), and ν_{os} is the frequency of the test pattern image on the sensor in cycles per millimeter.

According to Eq. III-1, at a given input irradiance, as the frequency of the test pattern increases the output modulation required for a specified output signal-to-noise ratio increases. It has been determined (Ref. 3) that if the $(S/N)_D$ is approximately 3.8, then the modulation (equal to 3.8 times the noise-equivalent modulation) prescribed

by Eq. III-1 approximates the modulation M_t required by the eye for 50 percent probability of detection of the image of a sine-wave test pattern. Thus, from Eq. III-1, the modulation required by the eye at the output of a PEI system is given by

$$M_t = 3.8\pi\nu_{os}/(2\epsilon\bar{\eta}\,\bar{n}_h t)^{\frac{1}{2}} \qquad \text{(III-2)}$$

Higher values of M_t would be required if higher detection probability, shorter detection time, or detection under more difficult conditions were required. Note the dependence of M_t on the length-to-width ratio ϵ. As ϵ increases, M_t decreases.

In the notation usually employed in the analysis of television systems, the output modulation required by the eye is given by

$$M_t = 3.8\pi N/[G\epsilon(I_s/e)t]^{\frac{1}{2}} \qquad \text{(III-3)}$$

where N is the number of television lines per raster height, I_s is the total photocathode current, and the camera tube raster width-to-height ratio is 4/3. Eq. III-3 applies to low-light-level television systems with sufficient intensifier gain that the output signal-to-noise ratio is independent of video preamplifier noise.

An expression analogous to Eqs. III-2 and III-3 that is applicable to photographic systems has been developed by W. N. Charman and A. Olin (Ref. 4). Their expression for the required modulation of the image of a test pattern is given by

$$M_t(\nu_{od}) = 0.034 \cdot \left[\frac{dD}{d(\log_{10}E)}\right]^{-1} [0.33 + G^2\nu_{od}^{\,2}\,S^2]^{\frac{1}{2}} \qquad \text{(III-4)}$$

where $M_t(\nu_{od})$ is the modulation in effective exposure, ν_{od} is the frequency of the sine-wave test pattern on the photograph, D is the mean density, E is the exposure, G is the rms granularity of the

photographic emulsion measured with a 24-μm diameter scanning aperture at the mean density D, and S is the required signal-to-noise ratio. The authors referenced empirical data that "suggests a value of 4.5 is reasonable for the required signal-to-noise ratio, S." The first term in the square root factor of Eq. III-4 was introduced in an attempt to take into account noise in the visual system. At the higher spatial frequencies, noise due to the granularity of the film is dominant.

It is interesting to note that in all of the above three systems for which Eqs. III-2 through III-4, respectively, are applicable, the required modulation, except in the vicinity of zero frequency, increases linearly with spatial frequency.

The overall quality of reconnaissance systems can now be illustrated as in Fig. III-1 and the optimum sampling rate (samples per unit length) of a sampling system can be estimated. Shown in Fig. III-1 are the following curves:

- The output modulation $M_D(N)$ on the screen of the kinescope in a good low-light-level television system used for night vision. The modulation M_s of the test pattern is assumed to be unity. Hence, $M_D(N) = T(N)$, the frequency response or modulation transfer function of the system.
- The required output modulation $M_t(N)$ predicted by Eq. III-3 for values of total photocathode current I_s equal to 10^{-13}, 10^{-12}, and 10^{-11} amp, respectively. In night-vision systems, the effect on $M_t(N)$ of decreasing the photocathode current while increasing the brightness gain to maintain the same output luminance is equivalent to the effect on $M_t(N)$ in photographic systems of increasing the rms granularity of a photographic emulsion.
- The minimum required output modulation for viewing distances equal to eight and four times the raster height H, i.e., 8H and 4H, respectively. These curves were deduced from data determined by A. van Meeteren (Ref. 5) with sine-wave test patterns at an average luminance of 7.7 cd/m^2. The experimental

conditions were such that no significant granularity or noise occurred in the illuminated test pattern except that due to the fundamental photon nature of light. For the given value of output luminance the curve labeled 8H represents the minimum possible values of $M_t(N)$ when viewing a picture (photographic or television) from eight times the picture height. In general, the minimum required output modulations at viewing distances KH and 8H, respectively, are related by $M_{t,KH}(N) = M_{t,8H}(KN/8)$, where K is a positive number. Small effective values of KH can be realized, if desired, by the employment of magnification.

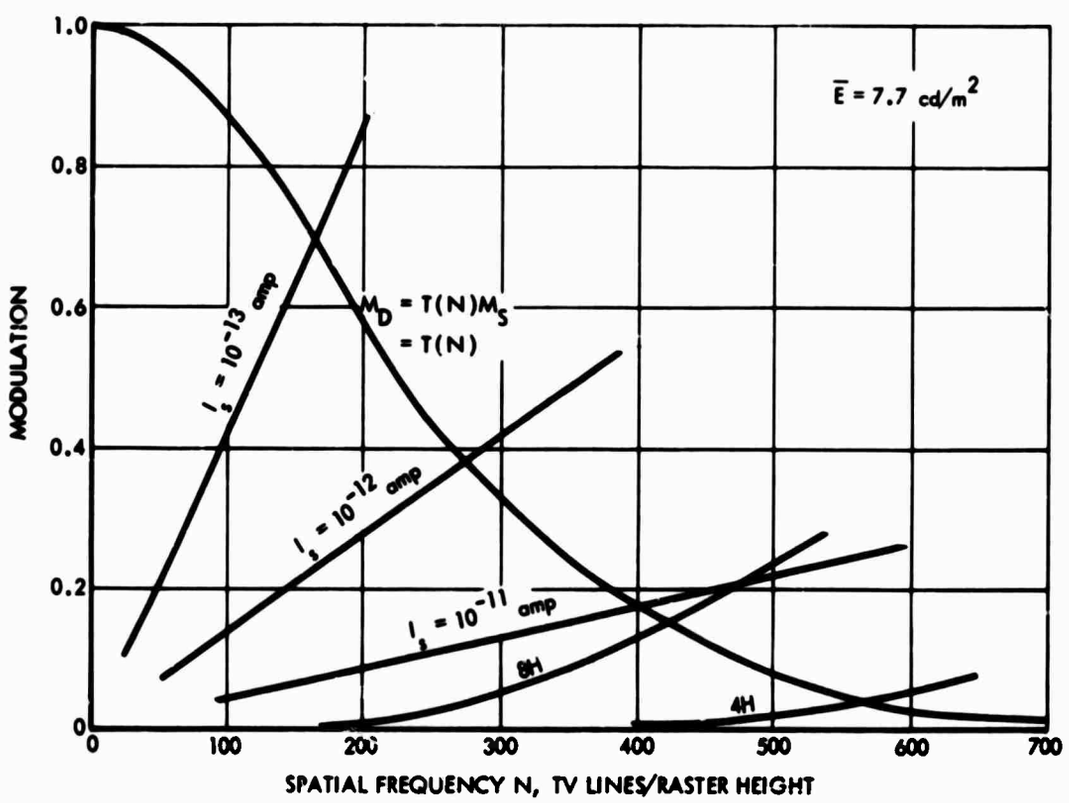

FIGURE III-1. Output Modulation $M_D(N)$ for M_s of Unity; Required Modulation $M_t(N)$ for $I_s = 10^{-13}$, 10^{-12}, and 10^{-11} amp; and Minimum Required Output Modulation for Viewing Distances of 8H and 4H

At low values of photocathode current I_s, the required output modulation $M_t(N)$ is quite insensitive to viewing distance, but, as I_s increases, $M_t(N)$ approaches a particular minimum required output modulation curve $M_{t,KH}(N)$, depending on both the viewing distance and output luminance.

The intersection of a required output modulation curve $M_t(N)$ for a particular value of photocathode current and the output modulation curve $M_D(N)$ determines the resolution of the low-light-level television with a 100 percent modulated sine-wave test pattern. Likewise, the intersection of a minimum required output modulation curve $M_{t,KH}(N)$ and the output modulation curve determines the limiting resolution under the most favorable conditions when viewed from a distance KH at an output luminance of 7.72 cd/m^2. The ratio of the output modulation to the required modulation is the output signal-to-noise ratio divided by the required signal-to-noise ratio (3.8) for 50 percent detection probability.

The dependence of the quality of a reconnaissance system on output modulation $M_D(N)$, required output modulation $M_t(N)$, and resolution is made clear by considering the spatial frequency spectral density of the input irradiance of a simple target such as a narrow rectangle. The spectral density found by Fourier transformation is given by

$$F_s(\nu_s) = F_o A_s \sin \pi \nu_s W_s / \pi \nu_s W_s \qquad \text{(III-5)}$$

where ν_s is the frequency in cycles per unit length on the sensor, F_o is the irradiance of the target image on the sensor, A_s is the area of the target image, and W_s is the width of the target image. On the display, the spectral density of the luminance $E_D(\nu_D)$ is given by

$$E_D(\nu_D) = E_o A_D T(\nu_D) \sin \pi \nu_D W_D / \pi \nu_D W_D \qquad \text{(III-6)}$$

where $T(\nu_D)$ is the modulation transfer function of the system and the subscript D refers to the display.

The input function $\sin \pi \nu_s W_s / \pi \nu_s W_s$ decreases from unity at $\nu_s = 0$ to zero at $\nu_s = 1/W_s$ and then undergoes damped oscillations about the frequency axis. It is clear that the fidelity of reproduction and the realization of high signal-to-noise ratio requires high frequency response over the target frequency range from zero to $\nu_s = 1/W_s$.

The number of scan lines will have a very strong influence on the MTF of the system. In the direction perpendicular to the scan, the MTF will be effectively zero for frequencies greater than half the inverse sampling distance. If, under the conditions of operation (a given light level), the resolution turns out to be much lower than this, a smaller number of scans can be used without degrading the system. Systems which are to be used under lower light level conditions will require fewer scan lines.

The number of resolution lines or optimum scan lines required for detection, recognition, and identification of military targets is presented in the table in Section I, Fig. T-1. Note that the units of this table are in cycles per target, equal to one-half the number of lines per target.

The resolution given in Fig. III-1 and the data of the table may be combined to predict range. For example, if the irradiance and quantum efficiency of the photocathode yield a current of 10^{-11} amp, the resolution is approximately 400 lines per raster height. If we consider recognition of a vehicle, we see from the table that eight lines are required. Thus, the vehicle must subtend 8/400 or 0.02 of the field of view. If the field of view were 10 deg, the vehicle must subtend 0.2 deg. If the height of the vehicle were 10 ft, the range would be approximately 1000 yd.

SECTION III. REFERENCES

1. J.W. Coltman, "The Specification of Imaging Properties by Response to a Sine Wave Input," J. Opt. Soc. Am., Vol. 44, No. 6, p. 468, June 1954.

2. A. Rose, "The Sensitivity Performance of the Human Eye on an Absolute Scale," J. Opt. Soc. Am., Vol. 38, No. 2, p. 196, February 1948; "Television Pickup Tubes and the Problem of Vision," Advances in Electronics. Vol. 1, p. 131, 1948.

3. O.H. Schade, Sr., "Optical and Photoelectric Analog of the Eye," J. Opt. Soc. Am., Vol. 46, No. 9, pp. 721-739, September 1956; "The Resolving-Power Functions and Quantum Processes of Television Cameras," RCA Review, Vol. 28, p. 460, September 1967.

4. W.N. Charman and A. Olin, "Image Quality Criteria for Aerial Camera Systems," Phot. Sci. and Eng., Vol. 9, p. 385, December 1965.

5. A. van Meeteren, Modulation Sensitivity and Spatial Bandwidth of the Eye at Low Luminances, paper presented at Optical Society of America meeting, Chicago, Ill., October 21-24, 1969.

IV. THE CALCULATION OF THE SIGNAL-TO-NOISE RATIO IN THE DETECTION AND RECOGNITION OF APERIODIC IMAGES*

by Frederick A. Rosell

In viewing a scene indirectly on the display of an electrooptical sensor, the lens and photosurface of the sensor replace the lens and retina of the eye as the primary phototransducer. The purpose of replacing the eye in this manner is to provide the observer with capability he does not ordinarily have. For example, the sensor can have greater aperture and longer focal length to increase light gathering capability and resolution of scene detail. Photocathodes of greater quantum efficiency than the eye can be obtained in the visible region, and, if desired, imaging at wavelengths far beyond the visible can be provided. Even without these attributes, the sensor may be of some use, since it can be remotely located.

The essentials of an electrooptical imaging sensor are shown in Fig. IV-1. The scene, consisting of a small area a in this case, is imaged on the photosurface by the lens. The photosurface converts the scene photon image to a photoelectron image that is amplified and magnified by a signal processor and focused on a phosphor that creates a visible light image. Finally, photons from the displayed image are collected by the observer's lens and projected onto his retina, which converts the image to sensory impulses for subsequent processing and interpretation by the brain.

In the following discussion, the degree to which the sensor can aid the observer will be determined. The main emphasis will be on the overall sensor sensitivity and resolving power. The observer will be

*From IDA Report R-169.

as an integral part of the overall system. We will show that the capability of the sensor-augmented observer can be analytically predicted for simple scene test patterns such as disks, rectangles, and bar patterns and that these predictions correlate closely with measured results. However, sensory system performance prediction must still be regarded as an art needing considerable development to achieve greater precision and to extend the results to more complicated (and more realistic) imaging situations. To the extent that the analysis applies at all, it applies equally well to any electrooptical sensor, including low-light level television and real-time forward-looking infrared scanners.

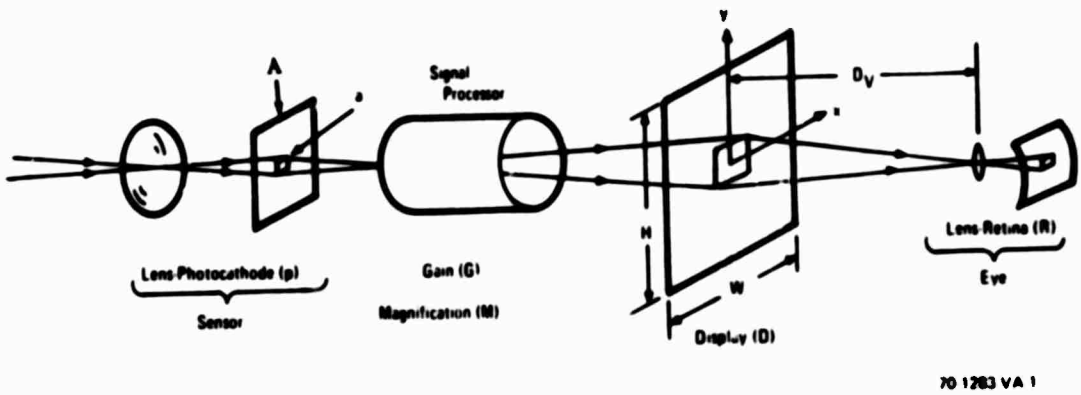

FIGURE IV-1. Electrooptical Image Process

In most electrooptical sensory systems, the designer has some latitude in selecting the sensor objective lens and input photodetector type. For present purposes, both the lens and phototransducer can be considered to be design parameters. Then, the beginning point of the analysis is the output of the photosurface, which may be considered to be the source of a photoelectron image. System elements, including the observer, will be generally unaware of the source of this image. We do observe, however, that the photon-to-electron

conversion process is noisy and that there is a signal-to-noise ratio associated with the primary photoprocess that inherently limits its information content.

The function of the signal processor is to amplify the signal and magnify it as necessary to preclude the possibility that the eye will be acuity-limited by either image size or luminance. Were the sensor ideal, the signal and noises generated by the input photosurface would be equally amplified so that the signal-to-noise ratio generated by the input photosurface would be identical to that at the phosphored screen and, in turn, would be identical to that generated by the eye retina. In real sensors, the signals may be distorted or smeared by the signal-processor finite apertures and display elements, and noises may be added.

A. DETECTION OF ISOLATED RECTANGULAR IMAGES

In the beginning of this analysis, it will be assumed that the image is large relative to the sensor point image spread function, so that the finite sensor apertures can be neglected and the signal processor is noise free. The eye viewing the display also has limitations, depending on the display brightness, video gain, image size, and viewing distance. Fluctuation noises are associated with the conversion of display photons to sensory impulses, and both the eye and the retina have finite apertures. However, we shall assume that the display luminance is sufficient and that the image is large enough, relative to the viewing distance, to preclude either retinal fluctuation noise or acuity limitations on image detection. On the other hand, the image will not be so large as to exceed the spatial integration capability of the eye. With these assumptions, the signal-to-noise ratio at the output of the photosurface display and at the retina will be equal. Linearity of all processes is assumed in the following.

The elementary model describing the effect of photoconversion-fluctuation noise is ordinarily attributed to Rose (Ref. 1), who, in

turn, attributes it to de Vries (Ref. 2). The basic model assumes that the photon-to-photoelectron conversion process is random in space and time and that the randomness can be characterized by the Poisson probability distribution law. According to Poisson statistics, if the photosurface generates $\dot{n}_{xy}$ photoelectrons per unit area and time, then the average or mean number $\bar{n}_o$ generated in time t by an area a will be

$$\bar{n}_o = \dot{n}_{xy}\,(at) \qquad \text{(IV-1)}$$

Also, the standard deviation or rms fluctuation noise associated with $\bar{n}$ is equal to $(\bar{n})^{\frac{1}{2}}$, so that the signal-to-noise ratio becomes $\bar{n}/(\bar{n})^{\frac{1}{2}}$, provided that there is no background flux. With background, the Rose model assumes that the incremental signal becomes $\bar{n}_o - \bar{n}_b$ and that the signal-to-noise ratio becomes

$$SNR_D = \left(\bar{n}_o - \bar{n}_b\right) \Big/ \left(\bar{n}_b\right)^{\frac{1}{2}} \qquad \text{(IV-2)}$$

Note that the symbol D is added to the signal-to-noise ratio SNR to indicate that the calculations are referenced to an idealized, hypothetical display without line structure and an MTF of 1. This is convenient when the effects of observer viewing distance are to be taken into account.

In a later model, Coltman and Anderson (Ref. 3) assumed that the noises from the background and the object should be quadratically summed, so that Eq. IV-2 becomes

$$SNR_D = \left(\bar{n}_o - \bar{n}_b\right) \Big/ \left(\bar{n}_o + \bar{n}_b\right)^{\frac{1}{2}} \qquad \text{(IV-3)}$$

This model appears to be more consistent with the statistical detection model discussed below. In both models, the inference is that the eye compares the area with signal to some other area of equal size in which the signal is absent. Before proceeding, we define contast as

$$C = \left(\bar{\dot{n}}_{xy\ max} - \bar{\dot{n}}_{xy\ min}\right) \Big/ \bar{\dot{n}}_{xy\ max} \qquad \text{(IV-4)}$$

So that contrast is always positive and varies only from 0 to 1. Further, we will assume that signals are always positive, so that combining Eqs. IV-1, IV-3, and IV-4 yields

$$SNR_D = C\left(\bar{\dot{n}}_{xy\ max} \cdot at\right) \Big/ \left[(2-C)\bar{\dot{n}}_{xy\ max} \cdot at\right]^{\frac{1}{2}} \qquad \text{(IV-5)}$$

In the above, we have set t equal to the integration time of the eye t_e.

As the next step, we note that the photoelectron rate can be written in terms of the photocurrent i_s, as

$$\bar{\dot{n}} = i_s/(eA) \qquad \text{(IV-6)}$$

where e is the charge of an electron and A is the effective area of the photocathode. Now, Eq. IV-5 may be written as

$$SNR_D = \left[ta/A\right]^{\frac{1}{2}} \cdot C\, i_{s\ max} \Big/ \left[(2-C)\, e\, i_{s\ max}\right]^{\frac{1}{2}} \qquad \text{(IV-7)}$$

Now, we multiply the numerator and denominator of Eq. V-A-7 by Δf, the video bandwidth, with the result that

$$SNR_D = \left[t\ \Delta f\ a/A\right]^{\frac{1}{2}} \cdot \left[C\, i_{s\ max} \Big/ \left[(2-C)\, e\ \Delta f\, i_{s\ max}\right]^{\frac{1}{2}}\right] \qquad \text{(IV-8)}$$

The second term in the above can be recognized by those familiar with television signal-to-noise analysis as the broad-area video signal-to-noise ratio $SNR_{V,O,C}$. "Broad-area" means that the image used to make the measurement is large compared to the point spread or impulse response of the sensor.

The original formulation of fluctuation noise limitations to imaging, as formulated by de Vries in 1943, gave the image signal-to-noise ratio (or SNR_D, as we define it here) as

$$SNR_D = \frac{\Delta n}{(n_o + n_b)^{1/2}}$$

while Schade prefers

$$SNR_D = \frac{\Delta n}{[(n_o + n_b)/2]^{1/2}} .$$

When an independent source of noise n_s is added, the de Vries formulation leads to

$$SNR_D = \frac{\Delta n}{(n_o + n_b + 2n_s)^{1/2}} ,$$

while Schade's formulation led to

$$SNR_D = \frac{\Delta n}{[(n_o + n_b)/2 + n_s]^{1/2}} .$$

Written in terms of a photocurrent, the de Vries model gives

$$SNR_D = \frac{\Delta i \cdot (at)^{1/2}}{[e\,(i_o + i_b) + 2\,ei_s]}$$

$$= \frac{\Delta i\,(at)^{1/2}}{[2\,e\bar{I} + 2\,ei_s]} ,$$

whereas the Schade model gives

$$SNR_D = \frac{\Delta i\ (at)^{1/2}}{(e\bar{i} + ei_s)^{1/2}}$$

In order to convert the de Vries model to a form recognizable in terms of a video signal-to-noise ratio as used in this document, the numerator and denominator were multiplied by Δf, the video bandwidth, whereas, to achieve the same result with the Schade model, the numerator and denominator are multiplied by $2\Delta f$. With this understanding, both models are similar in the noise expression but differ by the $\sqrt{2}$ in the signal expression. However, in the analysis reported herein, we have used a value of 0.2 sec (following Rose) for the eye's integration time, while Schade prefers a value of approximately 0.1 sec for the usual range of display luminances (0.2 to 1 ft-L). With this adjustment both the de Vries model and the Schade model give the same numerical result. In future work Schade's model will be used and 0.1 sec used as the eye integration time.

In passing, it should be observed that in using $\bar{i}$, the average current, the apparent dependence of noise on image contrast is eliminated, since

$$(2 - C)\ i_{max} = 2\ \bar{i}$$

The only purpose of the use of i_{max} is that it converts directly to highlight irradiance, which is the quantity usually plotted in resolution-versus-irradiance characteristics.

With these observations, Eq. IV-7 is written as

$$SNR_D = [t\ \Delta f\ a/A]^{\frac{1}{2}} \cdot SNR_{V,O,C} \qquad \text{(IV-9)}$$

If our premise is correct, and if Eq. IV-9 is correct, then we should be able to demonstrate that for a series of image sizes a constant level of probability of detection will require larger video signal-to-noise ratios (SNR_V) for small images than for large images. Further, we should be able to show that a given value of SNR_D is associated with a given value of probability of detection--over a very broad range of image sizes.

These predictions were well borne out in the experiment described below, wherein a rectangular image is electronically generated, mixed with band-limited white noise,* and displayed on a television monitor (Fig. IV-2). A selector was devised so that the image could appear in any one of four quadrants.

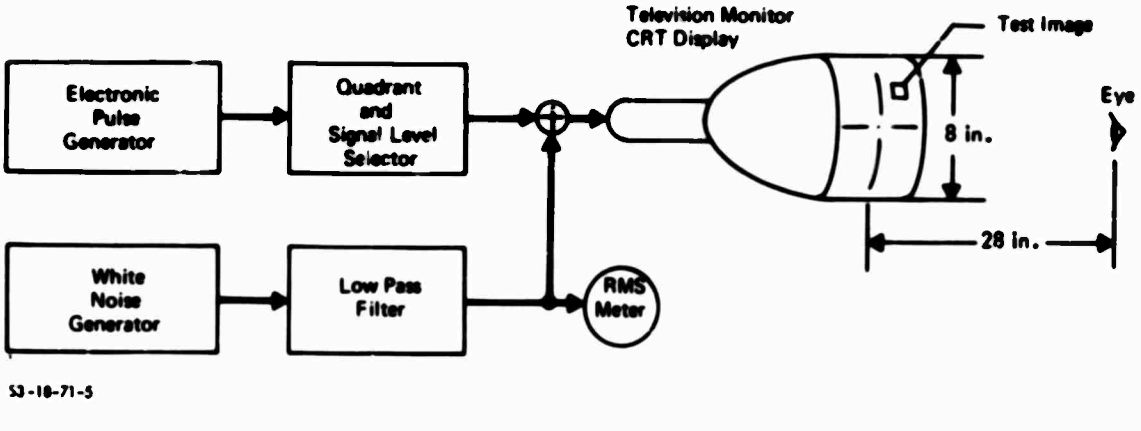

FIGURE IV-2. Equipment for Display Signal-to-Noise Ratio Experiment

*In the experiments reported herein, the noise was Gaussian rather than Poisson distribution. In the Coltman and Anderson experiment (Ref. 3), however, the results obtained using noise of either Gaussian or Poisson distribution appear to correlate closely.

Response was forced (i.e., the observer had to pick a quadrant whether he saw an image or not). The probability of detection obtained in this way was then corrected for chance. The ratio of viewing distance to display height was $D_V/H = 3.5$, with the displayed scene being 8 in. high and 28 in. distant. In the first experiment, the image was a series of rectangles of different sizes. Their dimensions were expressed in terms of scan line widths, and a 525-line total vertical scan with 490 active lines was assumed. Thus, the image size in terms of scan lines became

$$n_x n_y = (490)^2 \cdot \alpha(a/A) \qquad \text{(IV-10)}$$

where α is the width-to-height aspect ratio of the CRT display, 4:3 in this case. The image chosen was 4 scan lines high and from 4 to 180 scan lines wide. Next, the probability of detecting the image was determined as a function of the video signal-to-noise ratio at a video bandwidth of 7.1 MHz. The result is shown in Fig. IV-3a. Observe that the larger the rectangle, the smaller the SNR_V needed.

The display signal-to-noise ratio required was computed from Fig. IV-3a and the equation

$$SNR_D = (1/490)\,(n_x n_y\, t\, \Delta f/\alpha)^{\frac{1}{2}} \cdot SNR_V \qquad \text{(IV-11)}$$

which was derived using Eqs. IV-8 and IV-9 and is plotted in Fig. IV-4 for $t = 0.2$ sec. As can be seen, the display signal-to-noise ratio required for a given probability of detection is a constant independent of image size over a wide range of image aspect ratios. It should be noted that the angular extent of the image relative to the observer's eye varied from 0.13 x 0.13 deg for the rectangle of 1:1 length-to-width ratio to 0.13 x 6.2 deg for the 45:1 ratio. The eye-and-brain combination can apparently integrate over large areas in space.

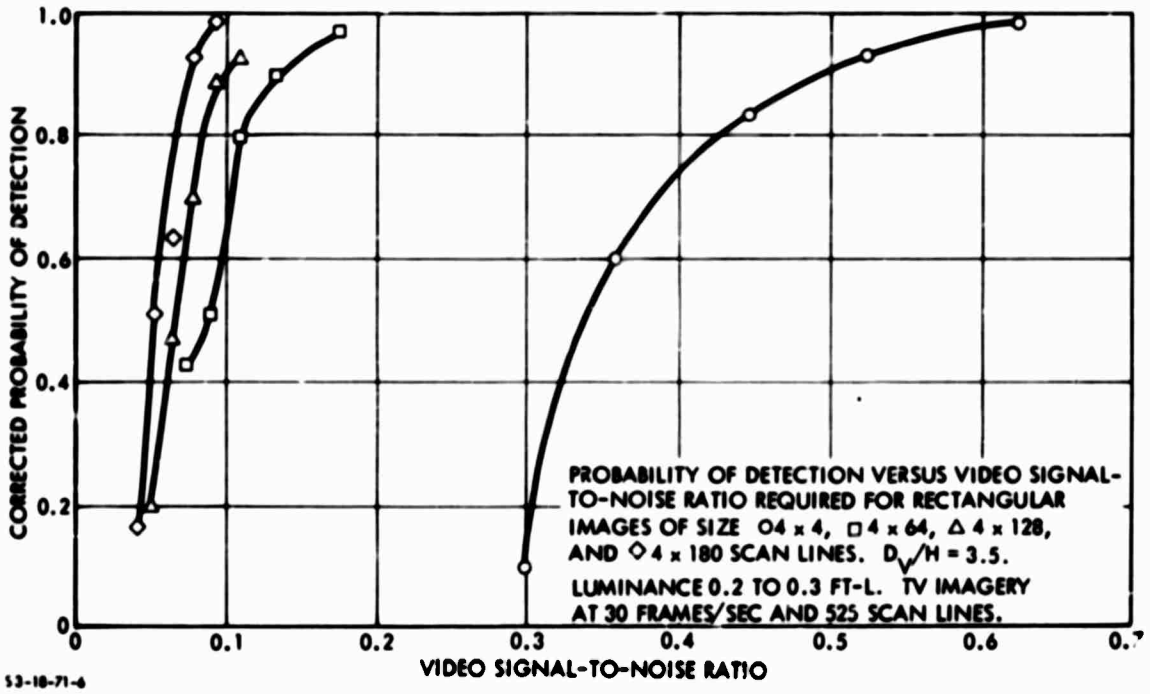

FIGURE IV-3a. Corrected Probability of Detection Versus Video Signal-to-Noise Ratio for Rectangular Images

It has been observed that the long, thin rectangles in Fig. IV-3a are nearly "all edge" and that the eye is more sensitive to edges than to areas. As a preliminary test of this concept, various squares were used as test images. These squares were 2 x 2, 4 x 4, 8 x 8, 16 x 16, 32 x 32, and 64 x 64 scan lines in size and varied in angular subtense at the eye from 0.06 x 0.06 deg to 2 x 2 deg. The result is shown in Fig. IV-3b. As can be seen, the SNR_D required to detect the images 2 x 2 to 16 x 16 scan lines in size (angular subtense from 0.06 to 0.5 deg) is approximately constant. However, the SNR_D required to detect the squares of larger angular extent (1 and 2 deg) increases. This lends some support to the "edge" theory. Since the large areas are of less importance to the user of a system, it is felt that the notion of a constant SNR_D based on image area is appropriate for most system prediction purposes.

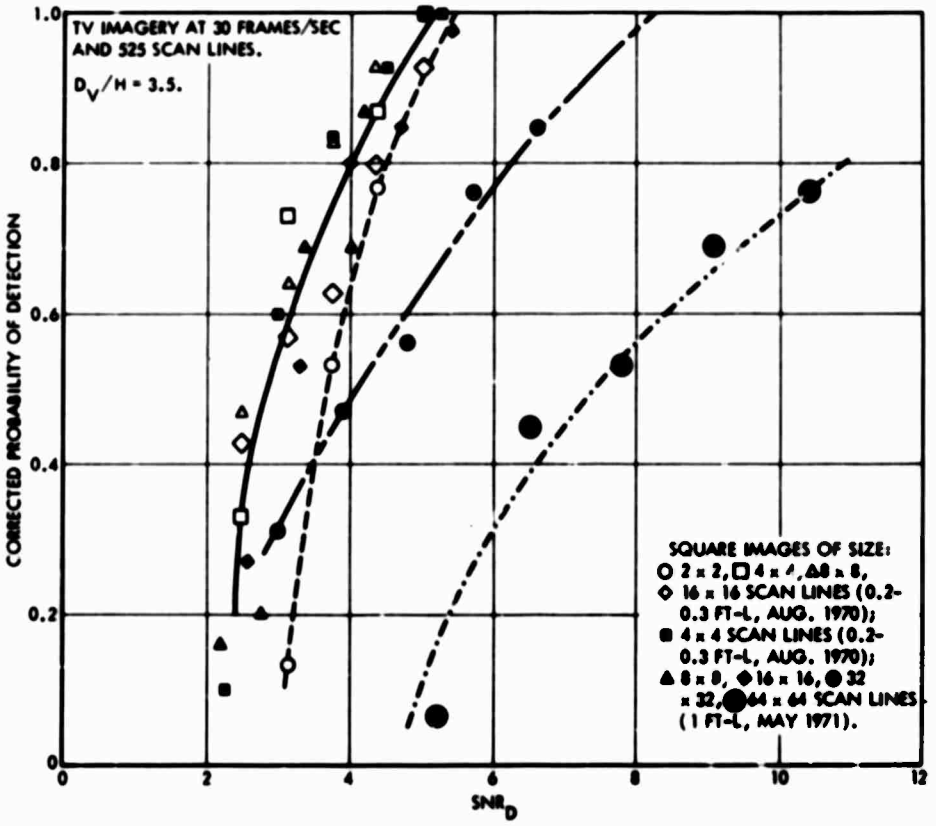

FIGURE IV-3b. Corrected Probability of Detection Versus Display Signal-to-Noise Ratio for Square Images

We have also observed that the detectability of a displayed image is almost entirely a function of its SNR_D, not of its displayed contrast, unless the contrast becomes so low that the eye becomes acuity-limited by the fluctuations generated in the retina by the display background luminance. However, this only means that the noise generated in the retinal photoprocess should have been included in the analysis. Had it been, detectability would probably have been independent of the displayed contrast, as before. The SNR_D is, of course, a strong function of the image contrast at the input photocathode, which can be far different from the displayed image contrast.

The curve used to fit the experimental points is based on a probability model originally suggested by Legault (Ref. 4). In this model, which is derived in the Appendix, it is assumed that the mean number of photoelectrons within the sampling interval has become

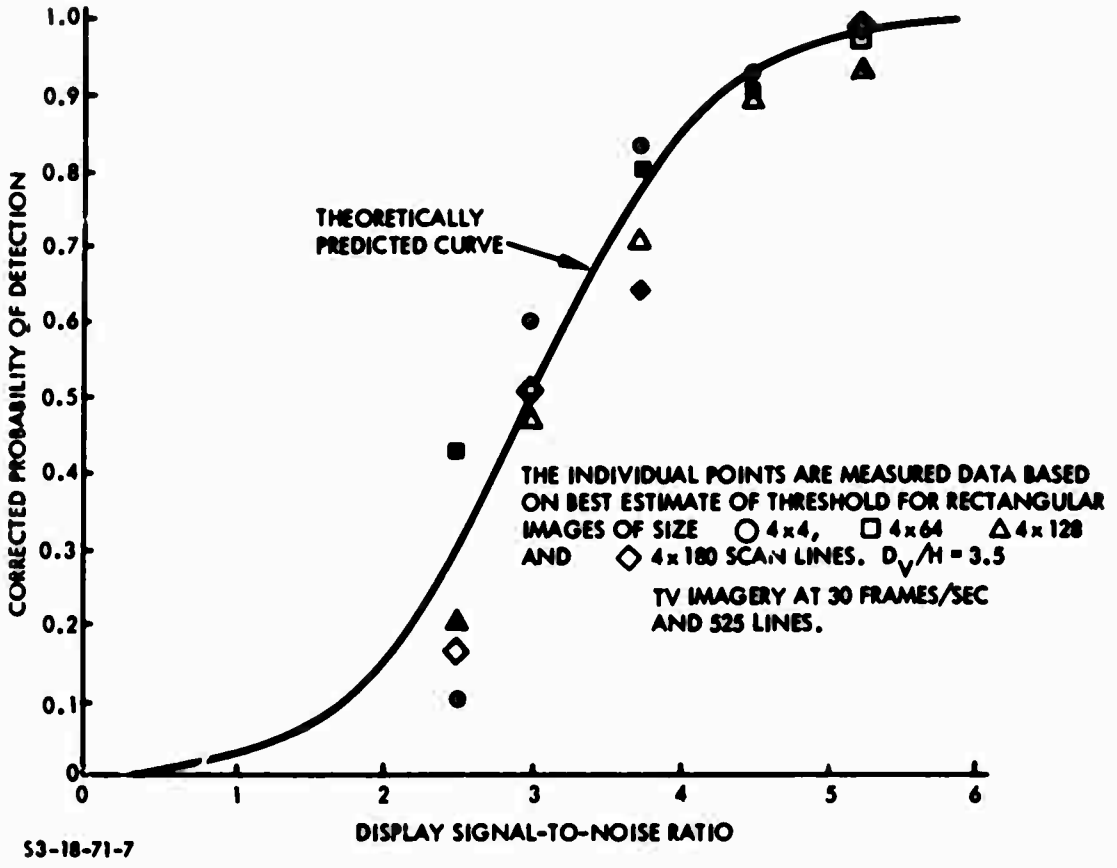

FIGURE IV-4. Measured and Predicted Probability of Detection

sufficiently large that the Gaussian or normal probability distribution given by

$$f_Z(z) = \exp\,[-z^2/2]/(2\pi)^{\frac{1}{2}} \qquad \text{(IV-12)}$$

becomes a good approximation of the Poisson distribution law, which actually represents the signal and noise processes. In the above, Z is a random variable shown to be numerically equal to

$$Z = SNR_D - SNR_{D,T} \qquad \text{(IV-13)}$$

where $SNR_{D,T}$ is the display signal-to-noise ratio needed to obtain a detection probability of 0.5, which is generally considered to be the

threshold of detection as indicated by the subscript T. Other values of SNR_D are obtained from the formula

$$Pd\ (-\infty < Z < z_2) = \frac{1}{(2\pi)^{\frac{1}{2}}} \int_{-\infty}^{z_2} \exp\left[-z^2/_2\right] dz \qquad \text{(IV-14)}$$

which cannot be integrated in closed form, but is widely available in standard mathematical tables.

In the foregoing, a model was developed for the SNR developed at the output of the input photocathode in a perfect system in which the image's spatial fidelity is preserved at each reimaging step, and the only noise is that generated in the primary photoprocess. In this case, the SNR developed by the photocathode is identical to that at the display and the observer's retina. In psychophysical experiments that approximate the perfect sensor case, it was shown that the SNR_D required to detect rectangular targets is relatively a constant over a wide range of image sizes and that probabilities of detection can be associated with the display signal-to-noise ratios developed.

B. EFFECT OF FINITE APERTURES ON APERIODIC IMAGE DETECTION

The rectangular images discussed in the previous section were aperiodic images. However, it was assumed that they were reproduced at the retina and converted to sensory impulses with perfect spatial fidelity. In real sensors, the images at the display may be distorted in amplitude, shape, position (phase), or all three. These distortions are due to finite imaging apertures such as the objective lens, any fiber-optic coupling plates, electron lenses, electron scanning beams, finite phosphor particles, and the like. The effect of these apertures is to smear image detail in a manner directly analogous to that of electrical filter networks, except that the sensor apertures can result in both one- and two-dimensional filtering effects, as shown in Fig. IV-5. This analogy can be put to good use.

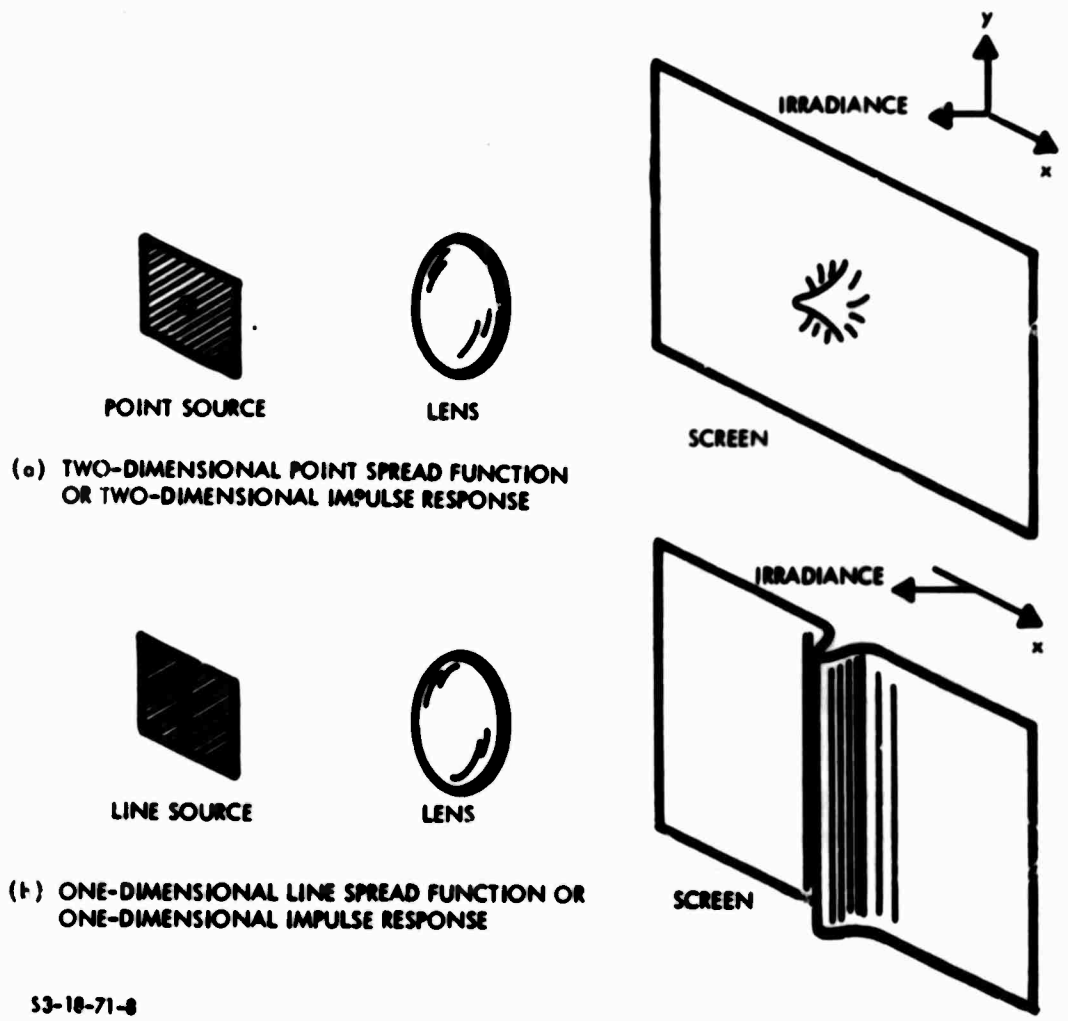

FIGURE IV-5. Impulse Responses

In the discussion that follows, all of the various system elements, including the observer, are considered to be linear and amenable to Fourier analysis, wherein complicated input signals are decomposed into simpler signals for which the system response is known, and then the total response is found by summing the individual responses in linear combination. The requirements and properties of linearity are well known (Ref. 5) and will not be belabored further here, except to note that, without the mathematical simplifications

made possible by assuming linearity, analysis becomes all but impossible in many cases. Also, in the interest of focusing on fundamental principles, it will be assumed that, where two-dimensional apertures are involved, the two dimensions are independent and separable. With this assumption, complicated two-dimensional problems can be reduced to the more familiar one-dimensional problems.

In the Fourier analysis of sensors, it is convenient to employ a certain set of input test signals known as the singularity test signals. The most useful singularity test signal is the unit volume impulse $\delta_o(x,y)$, which is of zero amplitude everywhere except at one point, where its amplitude is infinite. However, its volume (or its area, in the one-dimensional case) is always unity. The sensor response with an impulse input is designated as $r_o(x,y)$ and is known either as the impulse response or the point spread function. The Fourier transform of the impulse response is designated as $R_o(\omega_x,\omega_y)$ and is known as either the complex steady-state frequency response or the optical transfer function. If either $r_o(x,y)$ or $R_o(\omega_x,\omega_y)$ are known for the sensor, the response to any other input can be determined. $R_o(\omega_x,\omega_y)$ may be written as

$$R_o(\omega_x,\omega_y) = \mathfrak{F}\left[r_o(x,y)\right] = \left|R_o(\omega_x,\omega_y)\right| \exp\left[j\phi(\omega_x) + j\phi(\omega_y)\right] \tag{IV-15}$$

where $\mathfrak{F}$ implies "the Fourier transform of." $R_o(\omega_x,\omega_y)$ is known as either the sine-wave response or the modulation transfer function (MTF), while $\phi(\omega_x)$ and $\phi(\omega_y)$ are the phase transfer functions. By the use of the separability assumption (Ref. 6),

$$R_o(\omega_x,\omega_y) = \mathfrak{F}\left\{r_o(x) \cdot r_o(y)\right\} = \mathfrak{F}_x\left[r_o(x)\right] \cdot \mathfrak{F}_y\left[r_o(y)\right] \tag{IV-16}$$

A typical one-dimensional MTF curve is shown in Fig. IV-6. This curve happens to be a Gaussian or error curve filter, which closely approximates the MTF of many sensors and is given quantitatively by

$$\left|R_o(\omega)\right| = \exp\left[-\frac{\omega^2\alpha^2}{2}\right] \qquad \text{(IV-17)}$$

If phase shift is zero, then $|R_o(\omega)| = R_o(\omega)$, and we can find the filter's response to any input signal. Suppose the input signals to be rectangular pulses, as shown by the dashed curves of Fig. IV-7. It is seen that, as the input pulse is made progressively narrower, the output pulse becomes progressively wider relative to the input pulse width, and its amplitude eventually drops to well below that of the input pulse. Nevertheless, the area under the output pulse curve is identical to that under the input pulse. This is the nature of the error curve filter and of many optical apertures encountered in nature. Apertures of this type are dissipationless. Suppose that the eye is viewing an image that has first passed through a dissipationless filter. The effect of the filter would be expected to be that of smoothing the noise and smearing the signal. In the rectangle experiment, it was shown that, as images get larger, the eye expands the distance over which it integrates. If this is so, and there is every reason to believe that it is, then it could be inferred th , since the integrated signal in the filtered signal is the same and the noise is reduced, the image detectability is enhanced by the filtering, or, as a minimum, the detectability remains unchanged.

We find this result unpleasing. While it is possible to improve a signal-to-noise ratio by filtering, this seems unlikely when the signal and noise occupy the same spatial area and frequency band, as is the case here. Also, it is a common experience that finite apertures degrade images; they do not enhance them. The following solution to this dilemma is proposed. As the output pulse is smeared, the amplitude of the signal in the tails of the pulse becomes small.

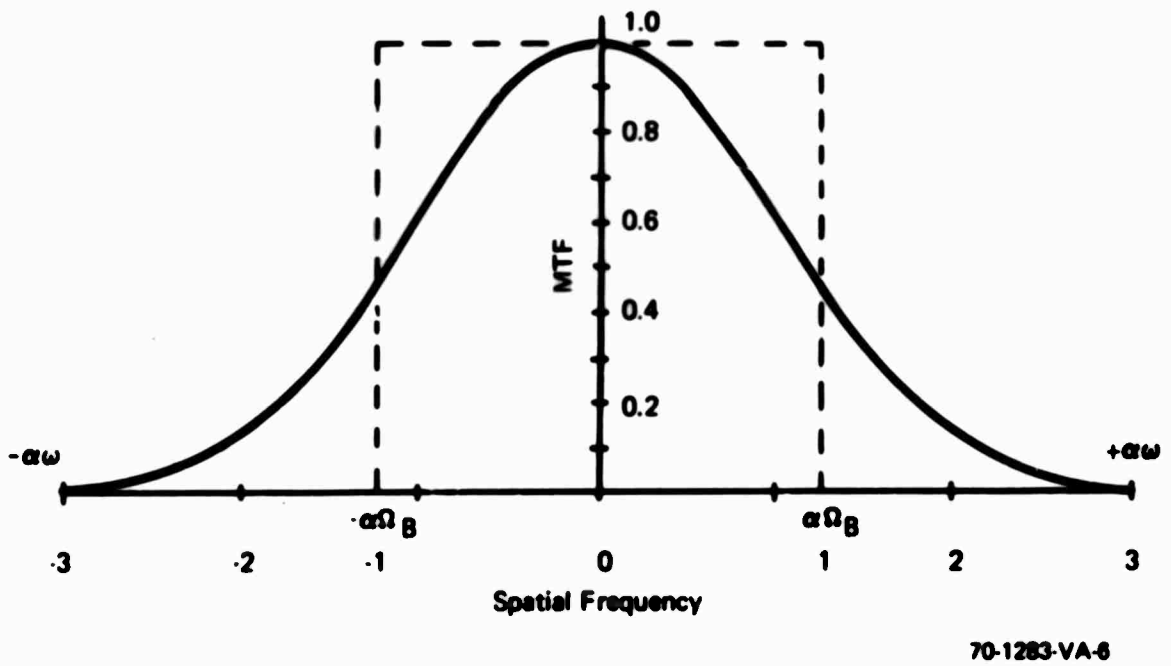

FIGURE IV-6. Modulation Transfer Function and Effective Bandwidth for Error Curve Filter in Dimensionless Coordinates

We presume these small signals to be less effective than the higher amplitudes near the peak of the pulse. Thus, an analytical model that weights the higher amplitudes in favor of the lower amplitudes would seem to be desired. This can be obtained by viewing the eye as an energy detector and by applying the Fourier energy integral, which represents the equivalence between energy in the space and the spatial frequency domains. In two dimensions, the Fourier energy integral is equal to

$$\int_{-\infty}^{\infty}\int f^2(x,y)dxdy = \frac{1}{\pi^2}\int_{0}^{\infty}\int |F(\omega_x,\omega_y)|^2 \, d\omega_x d\omega_y \qquad \text{(IV-18)}$$

By using this formulation, which is also known as Parseval's relation and Plancherel's theorem (Ref. 7), the SNR_D of Eq. IV-5 is modified to read

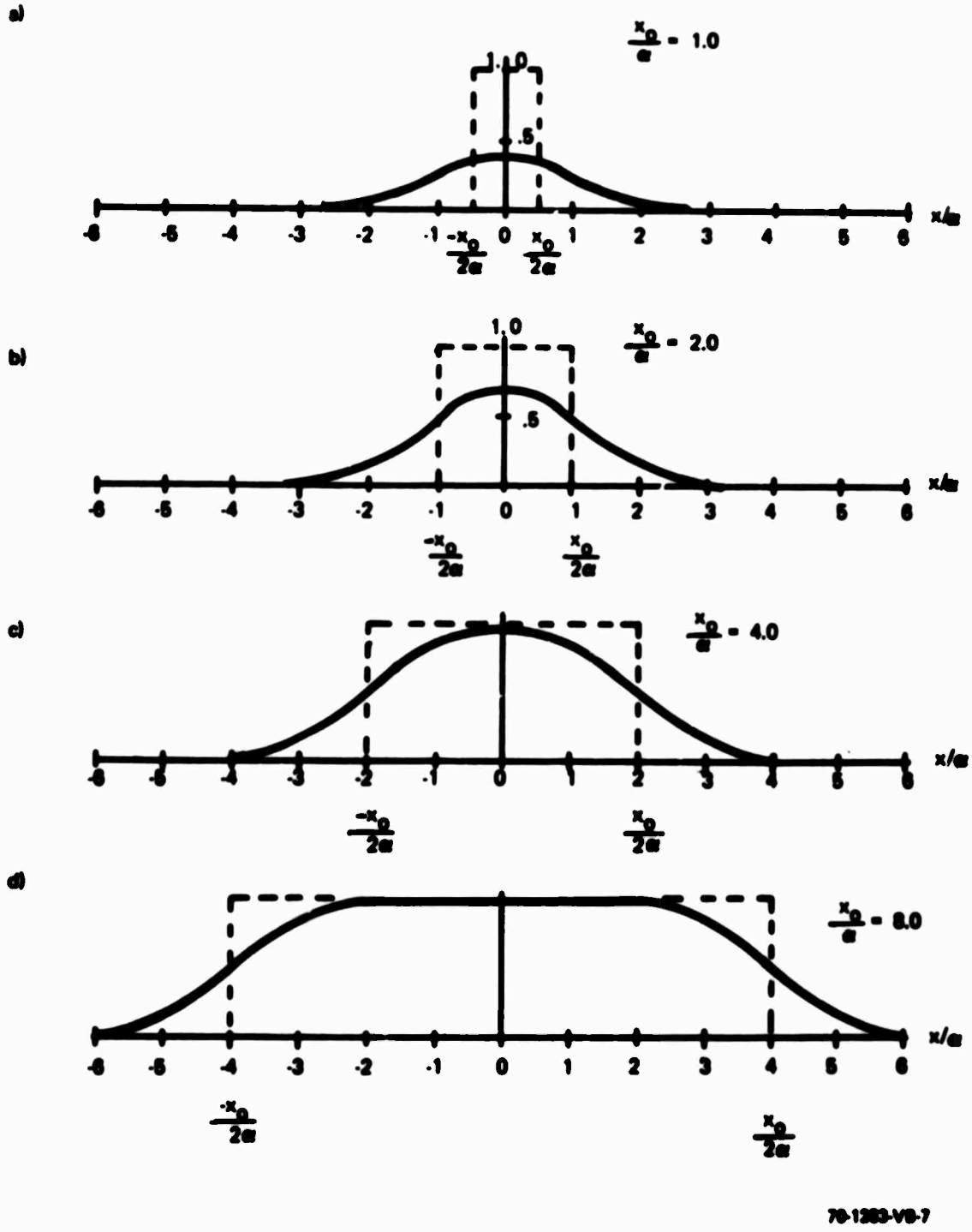

FIGURE IV-7. Output Pulse (-) for an Error Curve Filter as the Width of a Unit Amplitude Rectangular Input Pulse (---) Is Varied

$$SNR_D = \frac{C\left(\bar{\dot{n}}_{xy}t\right)^{\frac{1}{2}} \iint_{-\infty}^{\infty} g^2(x,y)\,dxdy}{\left[(2-C)\iint_{-\infty}^{\infty} g^2(x,y)\,dxdy\right]^{\frac{1}{2}}} \qquad \text{(IV-19)}$$

In the above, $\left[\bar{\dot{n}}_{xy}t\ g(x,y)\right]$ represents the signal envelope at the output of the filter. Alternatively, the result of Eq. IV-19 can be expressed in the spatial frequency domain or

$$SNR_D = \frac{C}{\pi}\frac{\left(\bar{\dot{n}}_{xy}\ t\right)^{\frac{1}{2}} \iint_{-\infty}^{\infty} |G(\omega_x,\omega_y)|^2\,d\omega_x d\omega_y}{\left[(2-C)\iint_{-\infty}^{\infty} |G(\omega_x,\omega_y)|^2\,d\omega_x d\omega_y\right]^{\frac{1}{2}}} \qquad \text{(IV-20)}$$

In general,

$$\iint_{-\infty}^{\infty} g^2(x,y)\,dx\,dy \leq \iint_{-\infty}^{\infty} g(x,y)\,dx\,dy \qquad \text{(IV-21)}$$

for positive signals, and

$$\iint_{0}^{\infty} |G(\omega_x,\omega_y)|^2\,d\omega_w d\omega_y \leq \iint_{0}^{\infty} |G(\omega_x,\omega_y)|\,d\omega_x d\omega_y \qquad \text{(IV-22)}$$

The result, in the new formulation, is that a photoelectron image passed through an aperture will be less detectable than one that is not.

To illustrate the effect of the new proposed model, we will calculate the minimum detectable power P_{min} and the minimum detectable highlight irradiance E_{min} for a sensor-augmented observer when the input image is a square of unit contrast. First, suppose the sensor MTF to be unity. The photoelectron current $i_{s\ max}$ may be written as

$$i_{s\ max} = \sigma A E \qquad \text{(IV-23)}$$

where σ is the photocathode's sensitivity (in amp/watt) to a given source such as a tungsten lamp operated at 2854°K, and E is the photocathode's highlight irradiance (in watt/m^2) due to the same given source. Using Eq. IV-23 in Eq. IV-7, we obtain

$$SNR_D = \left[\frac{\sigma a E t}{e}\right]^{\frac{1}{2}} \qquad \text{(IV-24)}$$

For threshold detection (50 percent probability of detection), SNR_{DT} = 2.8. With this value for $SNR_{D,T}$, E becomes E_{min}, and thus, for the perfect sensor with unit MTF,

$$E_{min} = (2.8)^2\ e/(\sigma a t) \qquad \text{(IV-25)}$$

and

$$P_{min} = (2.8)^2\ e/(\sigma t) \qquad \text{(IV-26)}$$

These equations are plotted in Figs. IV-8 and IV-9 for $\sigma = 4.10^{-3}$ amp/watt and t = 0.2 sec. We include the effect of the apertures, assuming that the apertures in x and y are independent and separable, so that Eq. IV-16 holds. The impulse response in x (or y) is given by

$$r_o(x) = \exp\left[-x^2/2\alpha^2\right] \Big/ \left(2\pi\alpha^2\right)^{\frac{1}{2}} \qquad \text{(IV-27)}$$

and α is taken to be 2.31×10^{-2} mm. For a square image, g(x) or g(y) is given by

$$g(x) = \frac{1}{2} \operatorname{erf} \left[\frac{x + x_o/2}{\left(2\alpha^2\right)^{\frac{1}{2}}} \right] - \frac{1}{2} \operatorname{erf} \left[\frac{x - x_o/2}{\left(2\alpha^2\right)^{\frac{1}{2}}} \right] \qquad \text{(IV-28)}$$

where erf is the error function and x_o is the input pulse width. Now,

$$E_{min} = \frac{(2.8)^2}{e\sigma t_e} \frac{\left[\int_{-\infty}^{\infty} g^2(x)\, dx \int_{-\infty}^{\infty} g^2(y)\, dy \right]^2}{\int_{-\infty}^{\infty} g^2(x)\, dx \int_{-\infty}^{\infty} g^2(y)\, dy} \qquad \text{(IV-29)}$$

where g(x) is given by Eq. IV-28 and g(x) = g(y). P_{min} is found from Eq. IV-29, and

$$P_{min} = E_{min} \cdot a \qquad \text{(IV-30)}$$

where a is the input image area. The impact of the assumed apertures can be observed from the curves shown in Figs. IV-8 and IV-9. It is seen that, with unity MTF, E_{min} is proportional to 1/a, while P_{min} is constant. With the assumed MTF, E_{min} increases at a much faster rate as image size is diminished, while P_{min} is no longer a constant but increases as image size decreases.

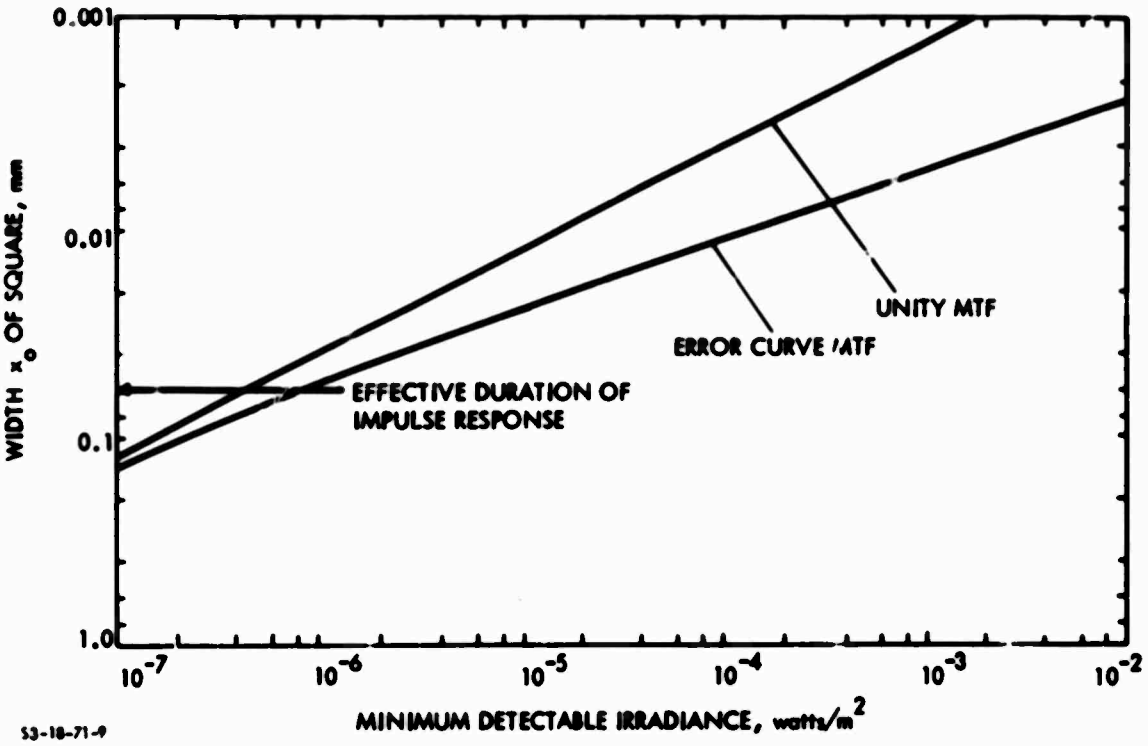

FIGURE IV-8. Minimum Detectable Irradiance

C. DETECTION OF PERIODIC SIGNALS

Rectangular images are not ordinarily used in measuring and specifying image-forming sensors. Instead, it is more usual to employ periodic images of various forms and types, including sine waves, bars, bursts of bars, and circular sector or wedges. A typical bar-burst pattern (Ref. 8) is shown in Fig. IV-10. Whatever the pattern form, the thought is to project patterns of various spatial frequencies onto the sensor photocathode and to measure sensor response both electrically and psychophysically. The electrical tests are mainly to obtain the MTF and the signal current transfer characteristics. In psychophysical tests, an observer is requested to determine the pattern of highest spatial frequency that can be just barely detected as the highlight irradiance of the pattern image is varied. The highest spatial frequency that can be just barely detected at a given irradiance is designated as the limiting

resolution, and its plot as a function of irradiance is called its limiting resolution versus photocathode irradiance level characteristic.

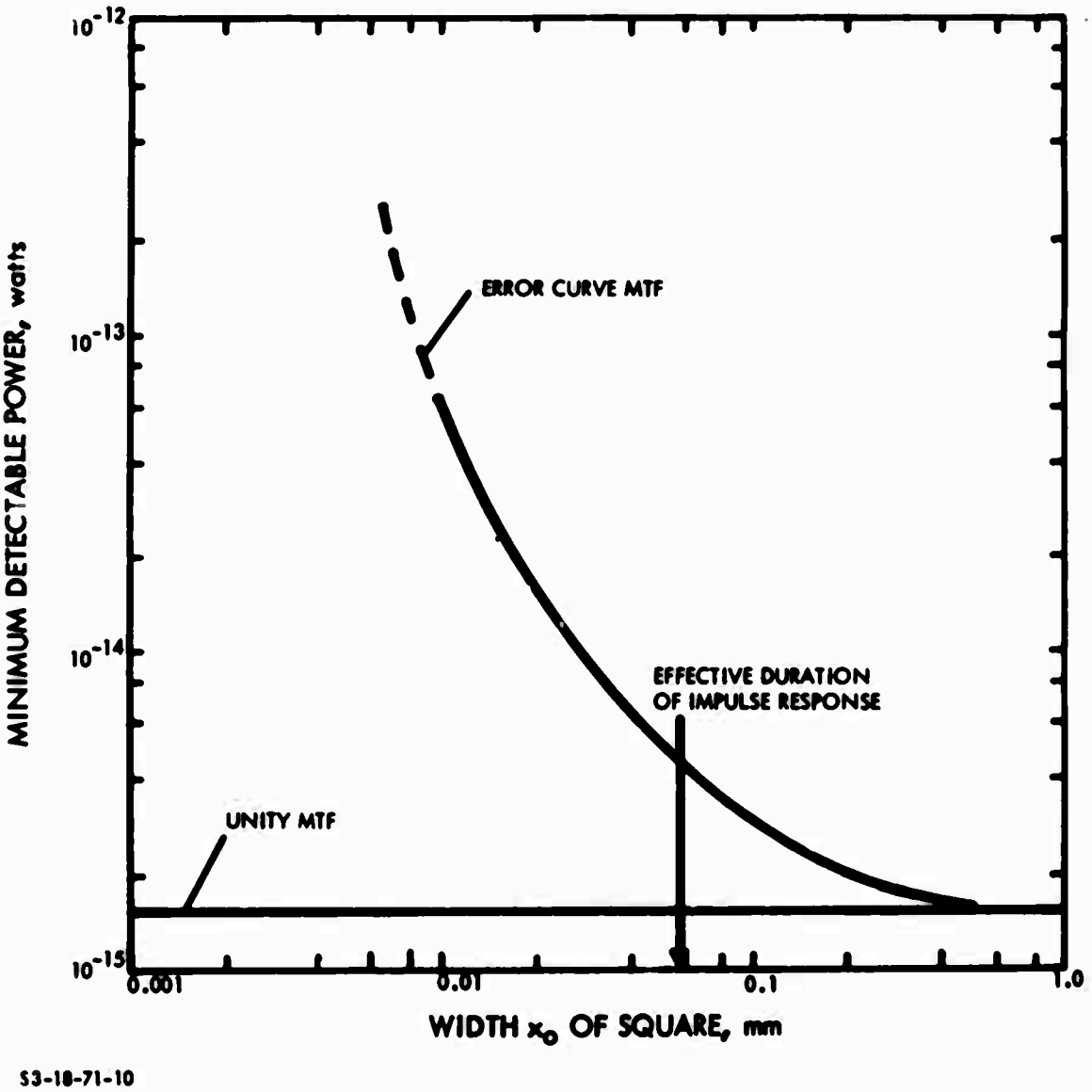

FIGURE IV-9. Minimum Detectable Power

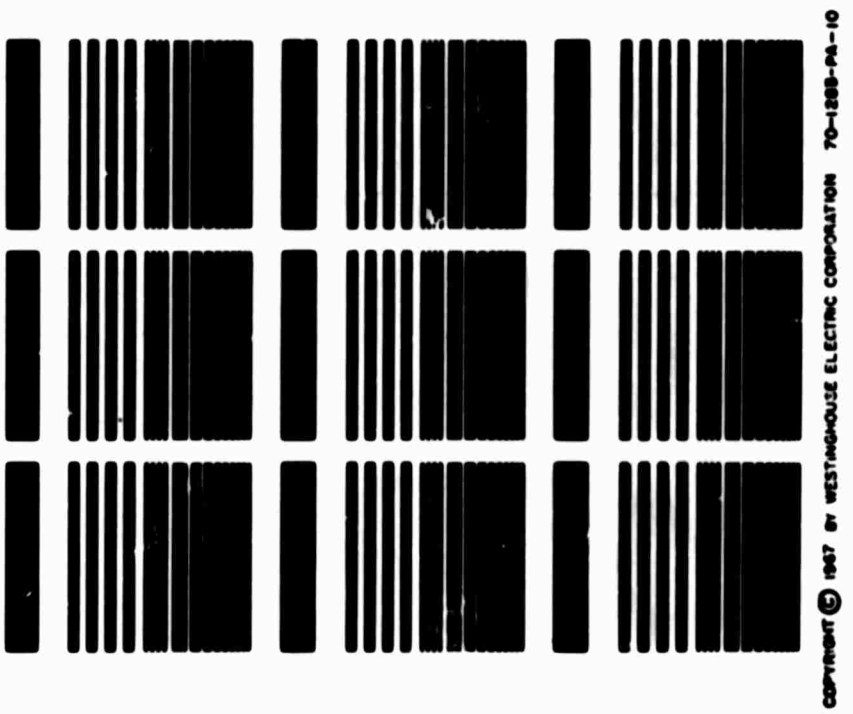

FIGURE IV-10. Resolution Test Chart

This characteristic is widely used by all sensor manufacturers to specify and compare the performance of their products with others, even though the patterns and methods of measurement have not been standardized in any form, and widely different techniques are used. Surprisingly, fairly close correlations have been experienced between various manufacturers and laboratories, but, as we shall see, this result is mainly fortuitous. As sensors improve, substantial errors can be encountered unless standards are adopted.

The original experimentations and analyses relating to the detectability of sine-wave and bar patterns displayed on a CRT were performed by Coltman and Anderson (Ref. 3) using an electronic setup similar to that in Fig. IV-2. The main difference is that vertically oriented sine-wave patterns that filled the entire screen were used instead of squares and rectangles. However, the early analysis proceeds along the lines followed in the previous section. The bar-pattern

image being viewed is divided into square elements of size Δy, where Δy is numerically equal to the bar spacing (which is also equal to the bar width). Then, SNR_D is calculated for this single square element, which eventually results in Eq. IV-9. Next, we note that if we define bar spacing Δy in terms of the number N_{TV} of squares that can be fitted into a picture height, then

$$N_{TV} = \frac{Y}{\Delta y} \qquad \text{(IV-31)}$$

Also, if X is the picture width, which is equal to α Y, and α is the picture aspect ratio, then $A = \alpha Y^2 = \Delta y^2 \times N_{TV}^2$. Note further that $a = \Delta y^2$, so that Eq. IV-9 becomes

$$SNR_{D/L} = \frac{[t\ \Delta f/\alpha]^{\frac{1}{2}}}{N_{TV}} \cdot SNR_{V,O,C} \qquad \text{(IV-32)}$$

This equation, which is designated the per-element display signal-to-noise ratio, was derived fro the photoelectron-noise-limited case, where the noise is white and the sensor MTF is unity. This situation was simulated in the laboratory by Coltman and Anderson (Ref. 3). Their formulation was somewhat different, in that they set up the equation in the form

$$N_{TVP/W} = k[\Delta f']^{\frac{1}{2}} \cdot SNR_{V,RMS} \qquad \text{(IV-33)}$$

and then they evaluated k experimentally for threshold identification of the pattern. Their value was found to be equal to 615 when $\Delta f'$ was given in MHz, $N_{TVP/W}$ was given in line pairs/picture width, and the $SNR_{V,RMS}$ was in terms of rms signal to rms noise. Converting the Coltman and Anderson nomenclature to that used here, we have

$$N_{TV} = \frac{2 \times N_{TVP/W}}{4/3} \frac{\text{lines}}{\text{picture height}}, \qquad \text{(IV-34a)}$$

$$SNR_{V,0,C} = 2.82\ SNR_{V,RMS}\ \frac{\text{peak signal}}{\text{rms noise}}\ , \qquad \text{(IV-34b)}$$

and

$$\Delta f = 10^{-6}\ \Delta f'\ (E_z). \qquad \text{(IV-34c)}$$

Inserting these results, along with the constant k = 615, into Eq. IV-33, we find

$$N_{TV} = 3.27\ (\Delta f)^{\frac{1}{2}}\ \cdot\ SNR_{V,0,C} \qquad \text{(IV-35)}$$

Next, we solve Eq. IV-33 for N_{TV}:

$$N_{TV} = \frac{[t/\alpha]^{\frac{1}{2}}}{SNR_{D/E}}\ (\Delta f)^{\frac{1}{2}}\ \cdot\ SNR_{V,0,C} \qquad \text{(IV-36)}$$

By comparison of Eqs. IV-35 and IV-36, we find that equality would result if

$$\frac{[t/\alpha]^{\frac{1}{2}}}{SNR_{D/E}} = 3.27 \qquad \text{(IV-37)}$$

If t = 0.2 sec and α = 4/3, then

$$SNR_{D/E,T} = 1.18 \qquad \text{(IV-38)}$$

The inference is that threshold display signal-to-noise ratio $SNR_{D/E,T}$ is a constant and is equal to about 1.18. Actually, the constant k = 615 was determined for sine-wave patterns. In an earlier experiment, Coltman (Ref. 9) found k to be 640 for square waves, which would

make $SNR_{D/E,T} = 1.23$. However, in the earlier experiment the bars were of limited extent, which will be found to make a difference.

Somewhat later, Parton and Moody (Ref. 10) gave an equation that is rewritten in the nomenclature used in this paper and rearranged as follows:

$$SNR_{D/E} = \left[\frac{t}{\alpha}\right]^{\frac{1}{2}} \frac{C}{N_{TV}} \left[\frac{\sigma AE}{e}\right]^{\frac{1}{2}} \qquad \text{(IV-39)}$$

by multiplying numerator and denominator by Δf and noting that $[\sigma AE/e\Delta f]^{\frac{1}{2}} = SNR_{V,O}$, we find that

$$SNR_D = \frac{[t\ \Delta f/\alpha]^{\frac{1}{2}}}{N_{TV}} C \cdot SNR_{V,O} \qquad \text{(IV-40)}$$

which is essentially Eq. IV-32. Parton and Moody gave a value of 1.2 for threshold $SNR_{D/E,T}$. This number has been used since that time, although, we believe, incorrectly.

Coltman and Anderson also suggested that the effect of the sensor MTF could be taken into account by simply modifying the SNR_V obtainable from the photocathode by the MTF. In the nomenclature of this report, this modification becomes

$$SNR_D = \frac{[t\ \Delta f/\alpha]^{\frac{1}{2}}}{N_{TV}} \cdot |R_O(N_{TV})| \cdot SNR_{V,O,C} \qquad \text{(IV-41)}$$

where $|R_O(N_{TV})|$ is the sensor sine-wave response or MTF. This equation has been used extensively to calculate the limiting resolution of sensors, and the results so computed are in very good agreement with measured results. We believe that this is so not because the equation is right, but because it is not too far wrong and because of compensating errors.

That Eq. IV-41 holds so well is surprising for several reasons. First, the SNRD derived is for a single element of size $1/N_{TV} \cdot 1/N_{TV}$, where N_{TV} is the width of a single bar, and the results are reputed to hold for the detection of the entire bar pattern. The height of the bar pattern is stipulated to be large with respect to the bar spacing, but otherwise to account is taken of it. The threshold $SNR_{D/E,T}$ is supposedly a constant independent of the height. That would infer that the height is of no moment. A bar pattern is presumably a one-dimensional pattern if the bars are very long compared to their spacing; yet, the derivation assumes a two-dimensional element. This assumption does not seem physically reasonable.

To show the impact of reducing the number of bars available to the observer, Coltman and Anderson devised the experiment shown in Fig. IV-11. The displayed pattern was left fixed, and a series of cardboard apertures were employed to vary the number of lines seen by the observer (Ref. 2, p. 862). The mask was of square aspect ratio. The results as shown in Fig. IV-11 "show that the observer probably uses no more than seven line pairs in making an identification. As the number which he is permitted to see is decreased, the signal required rises rapidly, being greater by a factor of four when only one line pair is presented" (Ref. 2, p. 862).

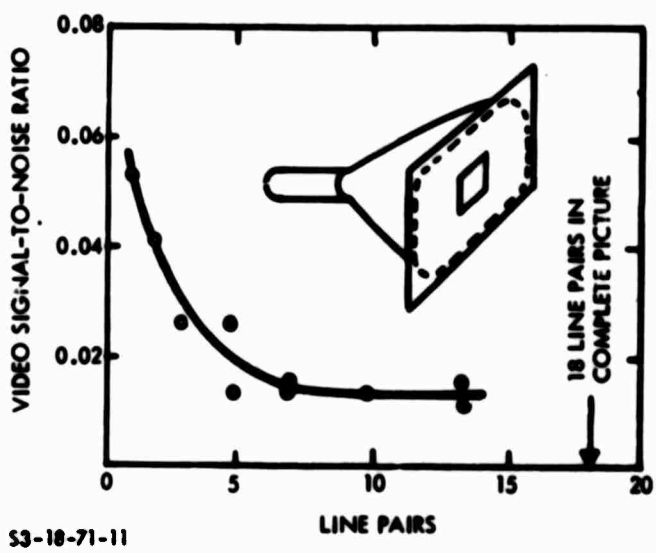

FIGURE IV-11. Number of Line Pairs Seen Through Mask (Adapted from Ref. 3)

Schade (Ref. 11, p. 731) also notes that "the sampling aperture of the eye for lines and edges is its line image, limited in length to fourteen equivalent point image diameters." These two observations give a possible explanation for the use of the elemental image of size $1/N_{TV} \cdot 1/N_{TV}$. However, if this is to hold over a wide range of spatial frequencies, it is necessary to conclude that, as the pattern spacing changes, the eye's ability to integrate along the line changes in direct proportion, or else it reaches some limit. This is at considerable variance with the results obtained in the rectangle experiment, where, in Fig. IV-4, it was shown that the eye could integrate a line of length-to-width aspect ratio from 1:1 to at least 45:1 and perhaps even more, since no end point was determined.

Since the notion of using an elemental image to describe a one-dimensional bar pattern conflicts with physical intuition, and since the notion of a limited but variable integrating capability, or even of a fixed integrating capability, for the eye conflicts with measured data on a television display (Fig. IV-3a, p. 66), it was decided to take a new approach. First, we will define detection. By detection, it is implied that the observer must be able to determine that a bar pattern is actually present. We will further stipulate that the observer makes this determination on the basis of a single line pair. Thus, the problem reduces to the two-dimensional rectangle detection problem discussed earlier, except that we feel that a higher signal-to-noise ratio is needed because the identification of a bar must be positive. For this reason, and because the result will be found to fit well, we will assume that the bar must be detected with nearly 100 percent probability. From Fig. IV-4 this will be seen to require an SNR_{DT} of 5.3. Let the dimensions of the bar be given in terms of the reciprocal distances $N_v \cdot N_h$, where

$$N_h = \frac{Y}{\Delta y} \qquad \text{(IV-42a)}$$

$$N_v = \frac{Y}{n_v \cdot \Delta y} \qquad \text{(IV-42b)}$$

in which Y is the picture height, Δy is the linear dimension of the bar width, and n_v is the height of the bar measured in terms of a number of bar widths. The image area relative to the total effective photocathode area is then

$$\frac{a}{A} = \frac{n_v \Delta y^2}{\alpha_Y 2} \qquad \text{(IV-43a)}$$

$$= \frac{1}{\alpha N_v \cdot N_h} \qquad \text{(IV-43b)}$$

$$= \frac{n_v}{N_{TV}^2} \qquad \text{(IV-43c)}$$

where $N_{TV} = Y/\Delta y$ lines per picture height. The result is that Eq. IV-41 becomes either

$$SNR_{D/A} = \frac{[t\ \Delta f/\alpha]^{\frac{1}{2}}}{[N_v \cdot N_h]^{\frac{1}{2}}} \cdot SNR_{V,0,C} \qquad \text{(IV-44)}$$

or

$$SNR_{D/A} = [t\ \Delta f/\alpha]^{\frac{1}{2}} \cdot \frac{n_v^{\frac{1}{2}}}{N_{TV}} \cdot SNR_{V,0,C} \qquad \text{(IV-45)}$$

These equations become the new trial models for the recognition of bar patterns. They are called the area models. The $SNR_{D/A,T}$ required is taken to be 5.3, as previously discussed.

Next, we focus our attention on Eq. IV-45, which is very similar to Eq. IV-32, which was previously used for bar-pattern detection.

The right sides of the two equations would, in fact, be identical if Eq. IV-45 were divided by $(n_v)^{\frac{1}{2}}$, which would result in the formula

$$\frac{SNR_{D/A}}{(n_v)^{\frac{1}{2}}} = \frac{[t\ \Delta f/\alpha]^{\frac{1}{2}}}{N_{TV}} \cdot SNR_{V,O,C} \qquad \text{(IV-46)}$$

Consider $SNR_{D/A}/(n_v)^{\frac{1}{2}}$ to be a new display signal-to-noise ratio that has a threshold value for bar patterns of frequency N_{TV} and of

$$SNR_{D/E,T} = (SNR_{D/A,T})/(n_v)^{\frac{1}{2}} \qquad \text{(IV-47)}$$

This equation is plotted as the solid line in Fig. IV-12. We note that the per-element $SNR_{D/E,T}$ drops quickly to a value of about 1.2 at a bar height-to-width ratio of about 20 lines (or 10 line pairs) and decreases slowly thereafter. This appears to be the origin of the value of $SNR_{D/E,T} = 1.2$ for bar or sine-wave patterns. It is not 1.2 but is nearly so over a fairly broad range of bar heights. When other effects are taken into account, it will probably be found that the apparent range of validity of $SNR_{D/E,T} = 1.2$ will be even larger.

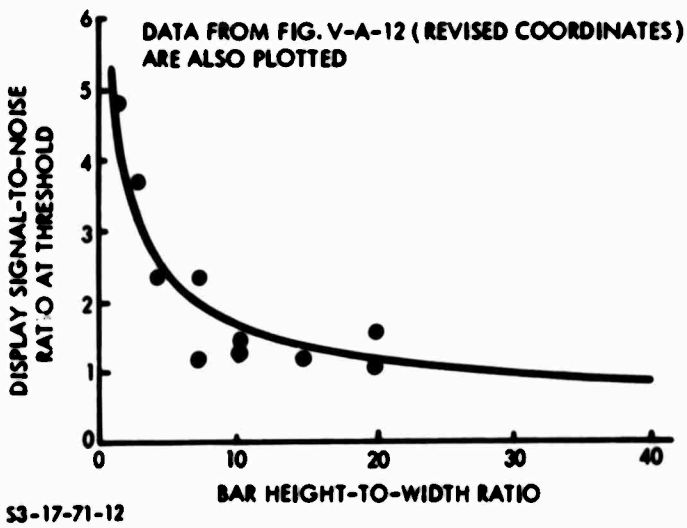

FIGURE IV-12. Threshold Display Signal-to-Noise Ratio Required to Identify Bar Pattern as a Function of Bar Height-to-Width Ratio

It is of considerable interest to replot the Coltman and Anderson data in Fig. IV-11 on Fig. IV-12, using the relation

$$SNR_{D/E,T} = \frac{[0.15\ \Delta f]^{\frac{1}{2}}}{N_{TV}} \cdot SNR_{VM,T} \qquad \text{(IV-48)}$$

where $SNR_{VM,T}$ is now the measured value of threshold video signal-to-noise ratio after the conversion factors of Eq. IV-34 are applied to the data. The fit of the Coltman and Anderson data to the predicted curve, using Eq. IV-46, is seen to be well within the experimental measurement errors. It is concluded that the effect of the cardboard apertures was mainly to decrease the bar height over which the eye can integrate. Attempts to show that the eye uses only seven line pairs in making an identification have proved unfruitful. Similarly, the premise that the eye can integrate over a small portion of the bar length is not borne out.

In a preliminary experiment, the SNR_D required to identify a bar pattern was determined for three bar length-to-width ratios with the result shown in Fig. IV-13. The SNR_D was calculated on the basis of the area of a single bar in the pattern. As can be seen, the probability of detection is the same for all three patterns when plotted versus $SNR_{D/A}$.

We next turn to the formulation of a model that, though it will require considerable modification and verification, represents the most accurate representation of the fundamentals of imaging as we know them and is felt to be the best point of departure for further model development. In the beginning of this model development, it is assumed that the input test pattern is a sine wave and that the sensor MTF is unity.

Recall that we have hypothesized that the eye uses only a single line, or line pair, in identifying a bar pattern. For this analysis, the displayed pattern is taken to be an infinitely long train of cosine waves in the x direction and a rectangle in the y direction,

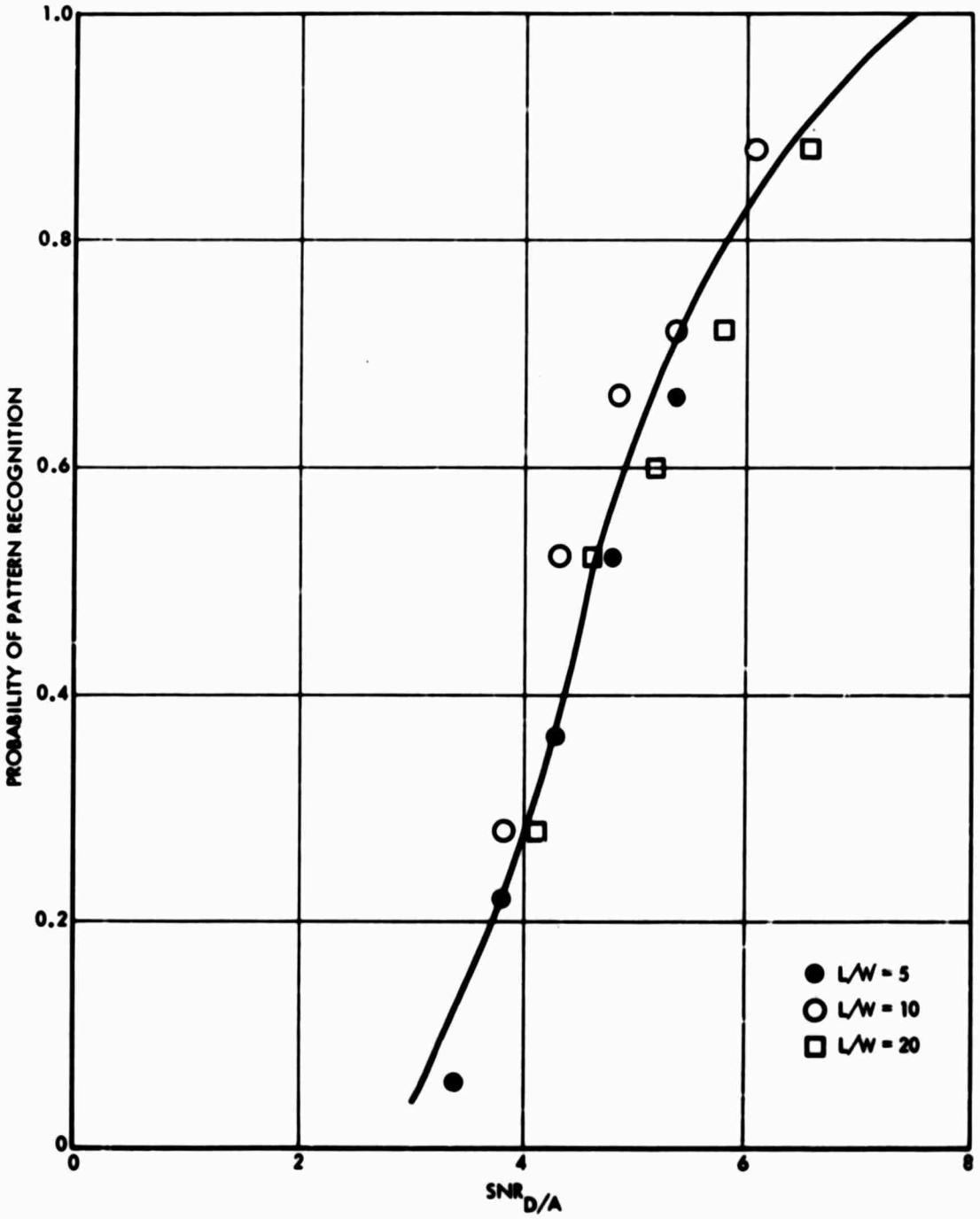

FIGURE IV-13. Probability of Pattern Recognition Versus $SNR_{D/A}$ for 372-Line Bar Pattern for Three Length-to-Width Ratios (L/W)

but only the single cycle shown in Fig. IV-14 used for the pattern identification. Quantitatively, the wave form used by the eye will be assumed to be

$$g(x) = \begin{cases} 0 & -\infty < x < -x_o \\ \frac{1}{2}\,(1 + \cos \pi\, x/x_o) & -x_o \le x \le x_o \\ 0 & x_o < x < \infty \end{cases} \qquad \text{(IV-49)}$$

$$g(y) = \begin{cases} 0 & -\infty < y < -y_o/2 \\ 1 & -y_o/2 \le y \le y_o/2 \\ 0 & y_o/2 < y < \infty \end{cases} \qquad \text{(IV-50)}$$

and

$$g(x,y) = g(x) \cdot g(y) \qquad \text{(IV-51)}$$

The basic $SNR_{D/A}$ expression to be used will be Eq. IV-7, rearranged to read:

$$SNR_{D/A} = \left[\frac{t}{A}\right]^{\frac{1}{2}} \frac{C\, i_{s\ max}\, a}{\left[(2-C)\, i_{s\ max}\, a\right]^{\frac{1}{2}}}$$

$$= \left[\frac{t/\alpha}{y^2}\right]^{\frac{1}{2}} \frac{C\, i_{s\ max}\, a}{\left[(2-C)\, i_{s\ max}\, a\right]^{\frac{1}{2}}} \qquad \text{(IV-52)}$$

where A, the effective photocathode area, is equal to αY^2, as previously noted. The area a in Eq. IV-52 will be treated according to the Fourier energy integral of Eq. IV-18. Thus,

$$a = \iint_{-\infty}^{\infty} g^2 (x,y)\, dxdy \qquad \text{(IV-53)}$$

and, because of the independence and separability assumption,

$$a = \int_{-\infty}^{\infty} g^2 (x)\, dx \int_{-\infty}^{\infty} g^2 (y)\, dy \qquad \text{(IV-54)}$$

The appeal of this formulation is that it is identical to that used for the aperiodic rectangle detection problem, that it eliminates the problem of deciding what to do about images that have both positive and negative components, that it treats signals and noise alike, that integration limits become fairly well defined, that it gives results that are in good agreement with those obtained by other investigators, and that the results predicted using this concept correlate well with measured results.

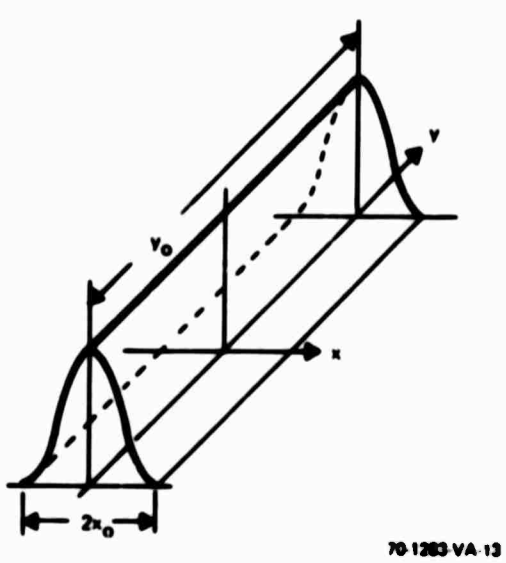

FIGURE IV-14. Portion of Wave Train Assumed Used by the Eye to Recognize Wave Pattern

The result of applying Eq. IV-54 to Eqs. IV-49 and IV-50 is that

$$a = 3\, y_o\, x_o/4 \qquad \text{(IV-55)}$$

and Eq. IV-52 becomes

$$SNR_{D/A} = \left[\frac{t/\alpha}{y^2/x_o y_o}\right]^{\frac{1}{2}} \frac{0.75\, C\, i_{s\,max}}{\left[0.75\,(2-C)e\, i_{s\,max}\right]^{\frac{1}{2}}} \qquad \text{(IV-56)}$$

Also, since $N_v = Y/y_o$ and $N_h = Y/x_o$, where N_v and N_h are expressed in TV lines per picture height,

$$SNR_{D/A} = \left[\frac{t/\alpha}{N_v \cdot N_h}\right]^{\frac{1}{2}} \frac{0.75\, C\, i_{s\,max}}{\left[0.75\,(2-C)e\, i_{s\,max}\right]^{\frac{1}{2}}} \qquad \text{(IV-57)}$$

which is very similar to the trial model postulated in Eq. IV-44.

Suppose, next, that the sensor MTF is either unity in the y direction or that the image is so long in the y vertical that it can be considered to be unity. In the x direction, let the MTF be $|R_o(N_h)|$. Then Eq. IV-57 is revised to read

$$SNR_{D/A} = \left[\frac{t/\alpha}{N_v \cdot N_h}\right]^{\frac{1}{2}} \frac{0.75\, C\, |R_o(N_h)|\, i_{s\,max}}{\left[0.75\,(2-C)\, |R_o(N_h)|\, e\, i_{s\,max}\right]^{\frac{1}{2}}} \qquad \text{(IV-58)}$$

The use of $|R_o(N_h)|$ in this form is somewhat unusual. It stems from the following reasoning. If the input image to a linear filter (or optical aperture) is a one-dimensional train of sine or cosine waves, then the output waveform will be a train of sine or cosine waves of identical spatial frequency but of reduced amplitude. The image wave-shape weighting function g(x) remains unchanged. The effect of the aperture is then only one of decreasing the signal and mean square noise equally in the sampling area. In other cases, however, the wave

shape is altered, as, for example, for square-wave (or bar-pattern) image inputs.

For the case of a square-wave input, suppose that the sensor MTF is unity once again. Also, let g(y) be given by Eq. IV-50 as before, but g(x) is

$$g(x) = \begin{cases} 0 & -\infty < x < -x_o/2 \\ 1 & -x_o/2 < x < x_o/2 \\ 0 & x_o/2 < x < \infty \end{cases} \qquad \text{(IV-59)}$$

Proceeding as before, we find that

$$a = x_o y_o = Y^2/N_h \times N_v \qquad \text{(IV-60)}$$

and

$$SNR_{D/A} = \left[\frac{t/\alpha}{N_v \cdot N_h}\right]^{\frac{1}{2}} \frac{C\, i_{s\,max}}{\left[(2-C)\, e\, i_{s\,max}\right]^{\frac{1}{2}}} \qquad \text{(IV-61)}$$

(for square-wave image inputs)

Thus, for a photoelectron-noise-limited sensor, the area form of the display signal-to-noise ratio is larger for a unit amplitude square-wave image than for a unit amplitude sine-wave image by a factor of $1/(0.75)^{\frac{1}{2}}$, or 1.15, presuming both to be of equal spatial frequency. Intuitively, we would expect square waves to be more detectable.

To consider the effects of the MTF on a periodic square wave, we will first decompose the square-wave input image to a series of sine waves, using the Fourier series representation

$$sq(x) = \frac{4}{\pi} \sum_k \frac{\sin(\pi k N_{h\ell} x)}{k} \qquad \text{(IV-62)}$$

$$k = 1, -3, 5, -7, 9, \ldots$$

where $N_{h\ell}$ is the spatial frequency of the square wave in half-cycles per picture height and is equal to

$$N_{h\ell} = 1/x_o \qquad \text{(IV-63)}$$

for x_o measured in units of picture height. If the sine-wave response or MTF is given by $|R_o(N_h)|$, the square-wave amplitude response may be written as

$$R_{SQ}(N_h) = \frac{4}{\pi} \sum_k R_o(N_h)/k \qquad \text{(IV-64)}$$

$$k = 1, -3, 5, -7, 9, \ldots$$

The MTF of a typical television sensor is plotted in Fig. IV-15. Also, the square-wave amplitude response, or MTF, is plotted for a typical television sensor, which here happens to be an I-SEBIR camera tube with a 25-mm target. The assumed MTF curve is seen to go to 0 at 900 TV lines. Thus, at $N_h > N_{hc}/3$, where N_{hc} is the cutoff frequency, the displayed image is a sine-wave input. At higher frequencies, the square-wave amplitude is $4/\pi$ times the value of MTF for a unit amplitude square-wave input. Indeed, this result holds with fair accuracy down to frequencies of $N_{hc}/4$ or $N_{hc}/5$. At lower frequencies, the square-wave amplitude response approaches unity. However, the energy keeps increasing, being 4/3 that of a unit amplitude sine wave at zero frequency. This effect is shown as the dashed curve in Fig. IV-15. We see the following interesting result. At frequencies above $N_{hc}/3$, a square-wave input yields a sine-wave output of amplitude $4/\pi$ times the input amplitude. Thus, one could treat it as a sine wave, using Eq. IV-58. The 3/4 factor of Eq. IV-58 becomes $3/4 \times 4/\pi = 0.955 \simeq 1.0$. At lower spatial frequencies, the energy relation must be used, but the only effect will be that $4/\pi$ becomes 4/3 at zero frequency. Thus, to a good approximation, we can write

$$SNR_{D/A} = \left[\frac{t/\alpha}{N_v \cdot N_h}\right]^{\frac{1}{2}} \frac{C \mid R_o(N_h) \mid i_{s\,max}}{\left[(2-C) \mid R_o(N_h) \mid e\, i_{s\,max}\right]^{\frac{1}{2}}} \qquad \text{(IV-65)}$$

(for square-wave image inputs)

where $|R_o(N_h)|$ is the sine-wave response or MTF, as before. Similarly, the square-wave amplitude response times 0.75 is a reasonable approximation for spatial frequencies from cutoff down to $N_{hc}/4$ or $N_{hc}/5$. Alternatively, the threshold value of $SNR_{D/A}$ can be adjusted when making limiting resolution predictions. Equation IV-65 is recommended for general calculations of SNR_D.

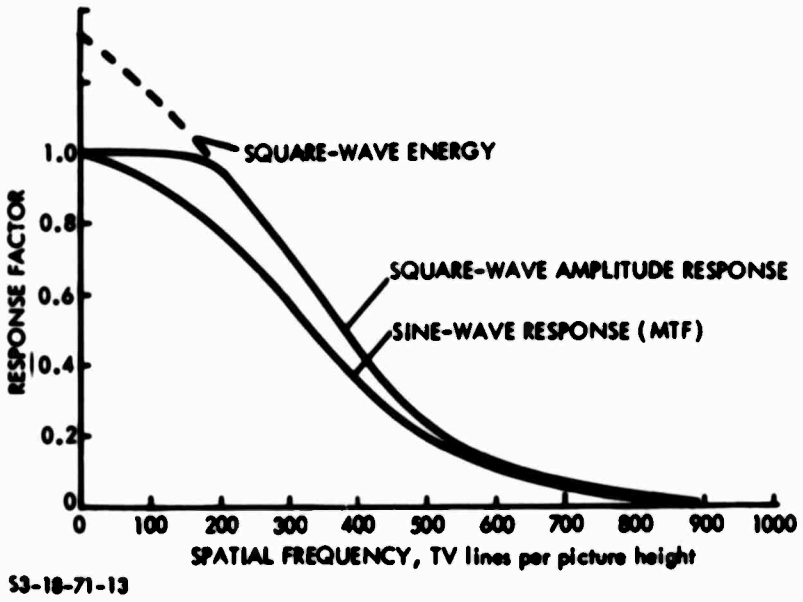

FIGURE IV-15. MTF and Square-Wave Response for an I-SEBIR TV Camera

SECTION IV. REFERENCES

1. A. Rose, "The Sensitivity Performance of the Human Eye on an Absolute Scale," J. Opt. Soc. Am., Vol. 38, No. 2, pp. 196-208, February 1948.

2. H. de Vries, "The Quantum Character of Light and its Bearing upon the Threshold of Vision, Differential Sensitivity and Visual Acuity of the Eye," Physica, Vol. 10, p. 553, 1943.

3. J. W. Coltman and A. E. Anderson, "Noise Limitations to Resolving Power in Electronic Imaging," Proc. IRE, Vol. 48, p. 858, May 1960.

4. R. Legault, "Visual Detection Process for Electrooptical Images: Man--the Final Stage of an Electrooptical Imaging System," Chapter 4 in L. M. Biberman and S. Nudelman, eds., Photoelectronic Imaging Devices, Vol. I, Plenum Press, New York, 1971.

5. Y. W. Lee, Statistical Theory of Communication, John Wiley and Sons, New York, 1961.

6. M. Goodman, Introduction to Fourier Optics, McGraw-Hill, New York, 1968.

7. M. Schwartz, Information Transmission, Modulation, and Noise, McGraw-Hill, New York, 1959.

8. I. Limansky, "A New Resolution Chart for Imaging Systems," The Electronic Engineer, June 1958.

9. J. W. Coltman, "The Specification of Imaging Properties by Response to a Sine Wave Input," J. Opt. Soc. Am., Vol. 44, No. 6, p. 468, June 1954.

10. J. S. Parton and J. C. Moody, "Performance of Image Orthicon Type Intensifier Tubes," in National Aeronautics and Space Administration, Proc. Image Intensifier Symposium, Ft. Belvoir, Va., 24-26 October 1961, NASA SP 2.

11. O. H. Schade, Sr., "Optical and Photoelectric Analog of the Eye," J. Opt. Soc. Am., Vol. 46, No. 9, pp. 721-739, September 1956.

12. General Electric Company, Schenectady, N.Y., Present and Future Performance of Photoconductive Camera Tubes, Research Report 58-RL-1990, R. W. Damon, J. R. Eshback, and R. W. Redington, July 1958.

V. IMAGE REPRODUCTION BY A LINE RASTER PROCESS

by Otto H. Schade, Sr.

A. THE SAMPLING PROCESS OF A LINE RASTER

The intensity function $I(\rho,\theta)$ of images formed by optical or electron lens systems is continuous in any radial direction (ρ,θ) of the format area. The modulation transfer functions $MTF(\theta,\rho)$ are generally isotropic for small radial distances (ρ) but may become anisotropic for larger radial distances because of point-image distortion by astigmatism or coma. Isotropy requires a point-image or sampling "aperture" of circular symmetry.

The conversion of continuous intensity functions $I(\rho,\theta)$ into one-dimensional time functions $I(t)$ and reconversion into continuous two-dimensional intensity functions in a television system involves scanning of the format area with an "aperture" along uniformly spaced parallel lines termed a "line raster." The raster process yields a set of continuous intensity functions $I(x)$ along the lines, whereas intensity functions $I(y)$ are transmitted as discrete amplitude samples taken at intervals Δy determined by the raster line spacing. It follows at once that continuity in the displayed image requires a display aperture having a particular spread $S(y)$ to fill the interline spaces of the raster and establish continuity in y, whereas the aperture spread $S(x)$ could be very much smaller, making the resolution in the image anisotropic. Similarly, the effective spread $S(y)$ of the sampling aperture in the camera must have a particular value to prevent loss of information contained in the interline spaces of the raster, indicating a "flat field" requirement* in the camera.

---

*The "flat field" requirement refers to a structure-free reproduction of a continuous field of uniform intensity by a line raster process. It specifies a uniform charge readout in the camera, leaving no interline charges on the storage surface, and is satisfied when the sum of the effective line image cross sections of the scanning aperture spaced at raster line distances yields a constant intensity function $I(y)$.

An isotropic image requires apertures of circular symmetry. Continuity in y can be obtained by selecting a raster line density to provide a large overlap of aperture positions in successive line scans. A high raster line density, however, is wasteful in terms of the electrical frequency channel and raises two questions: Is a flat, i.e., uniform, field necessary? What is the optimum aperture size and shape to achieve uniformity?

Most television displays have a visible line structure on the screen, and increased viewing distances are required to effect integration by the eye into a flat or structureless field. An image containing a visible line structure may appear to be sharper, but more detail becomes visible when the line structure is removed. This can be demonstrated convincingly by modulating a CRT with wide-band noise. It will be observed that the noise is much more visible when the interfering line structure is removed by defocusing the CRT spot or by increasing the viewing distance. The line structure is an interfering signal which, like noise, prevents detection of small detail.

Various other effects occur when the effective sampling apertures of the camera and display are too small relative to the raster line spacing. Diagonal lines become staircases, spurious diamond-shaped patterns appear in horizontal line wedges, low-frequency beat patterns occur in "vertical" resolution charts of parallel lines at higher frequencies, and the reproduction of significant detail depends on position relative to the raster lines.

Quantitative specifications can be derived by convolution of intensity functions in the space and time domains. An analysis in the frequency domain, however, is more convenient.

The discontinuous intensity function I(y) obtained by the raster process in the camera represents a pulse carrier wave with infinitesimal pulse width of spatial frequency f_r, amplitude modulated by the spatial frequencies f_m contained in the image, which are limited by the MTF_c of the camera aperture δ_c. The fundamental frequency f_r of the spatial carrier wave is equal to the number of raster lines per unit length.

The spatial intensity functions I(y) are converted by the sequential scanning process into time functions $I_y(t)$ contained in the video signal, which can be displayed with an electrical sampling circuit on an oscilloscope. The time signals are converted back into spatial modulated carrier waves in the display system by a synchronized scanning process. The pulse carrier must now be demodulated by a low-pass filter, the MTF of the display aperture δ_d, to restore a continuous undistorted modulation envelope from the transmitted samples. The solution for optimum low-pass MTF's is known from modulation theory and states that the MTF of both input and output filters must be limited to frequencies $f_m \leq 0.5\ f_r$ to eliminate all raster carrier components and unwanted modulation products. The MTF's should be constant for maximum utilization of the frequency channel. This optimum solution may not be realizable in a practical system. We therefore examine the general expression for the intensity function I(y) resulting from a carrier modulation by a frequency f_m, given by the following equation:

$$I(y) = \bar{I}\,(1 + 2\sum \tilde{r}_{d,kf_r} \cos(k \cdot 2\pi f_r y) \qquad (C)$$

$$+ \hat{I}_{f_m} \tilde{r}_c \tilde{r}_d \cos(2\pi f_m y + \theta) \qquad (f_m)$$

$$+ \hat{I}_{f_m} \tilde{r}_c \cdot \sum^{k} \left[\tilde{r}_{d,(kf_r+f_m)} \cos(2\pi(kf_r + f_m)y + \theta)\right] \qquad (S)$$

$$+ \hat{I}_{f_m} \tilde{r}_c \cdot \sum^{k} \left[\tilde{r}_{d,(kf_r-f_m)} \cos(2\pi(kf_r - f_m)y + \theta)\right] \qquad (D) \qquad \text{(V-1)}$$

where

$k = 1, 2, 3, \ldots$

f_m = modulation frequency, cycles/unit length

f_r = raster frequency, number of sampling points/unit length

y = distance along y-coordinate

$\bar{I}$ = mean intensity of test object wave form

$\hat{I}_{f_m}$ = crest intensity of sine-wave test object

$\tilde{r}_c$ = sine-wave response factor of camera at f_m

$\tilde{r}_d$ = sine-wave response factor of display system at f_m

$\tilde{r}_{d,(index)}$ = sine-wave response factor of display at index frequency

θ = phase displacement between $\hat{I}_{f_m}$ and raster lines

The first term (C) contains the dc level ($\bar{I}$) and an infinite number of steady carrier frequency components k f_r (k is an integer) with amplitudes $2\bar{I}\ \tilde{r}_d$ depending only on the MTF_d of the display system. The second term (f_m) is the normal MTF product ($\tilde{r}_c\ \tilde{r}_d$) of the system as obtained without raster process at any modulation frequency.

The third and fourth terms (S) and (D) are modulation products (sidebands) generated by sum and difference frequencies with the carrier components.

The entire frequency transfer characteristic for the y-coordinate of the television process is shown by the graphic representation in Fig. V-1. The MTF_c under the input frequency scale of the raster characteristic is the product of the MTF's of all two-dimensional aperture processes preceding the raster process and including the scanning beam in the camera.

The MTF of the video system is unity for the y-samples and need not be shown. The transfer functions of the raster itself are a network of diagonal lines with constant transfer factors ($\tilde{r} = 1$) for the frequency f_m and the sum and difference frequencies (D,S). The carrier frequencies (C_1, C_2, ...) are represented by horizontal lines because their existence depends only on the dc term and on the attenuation by the output filter.

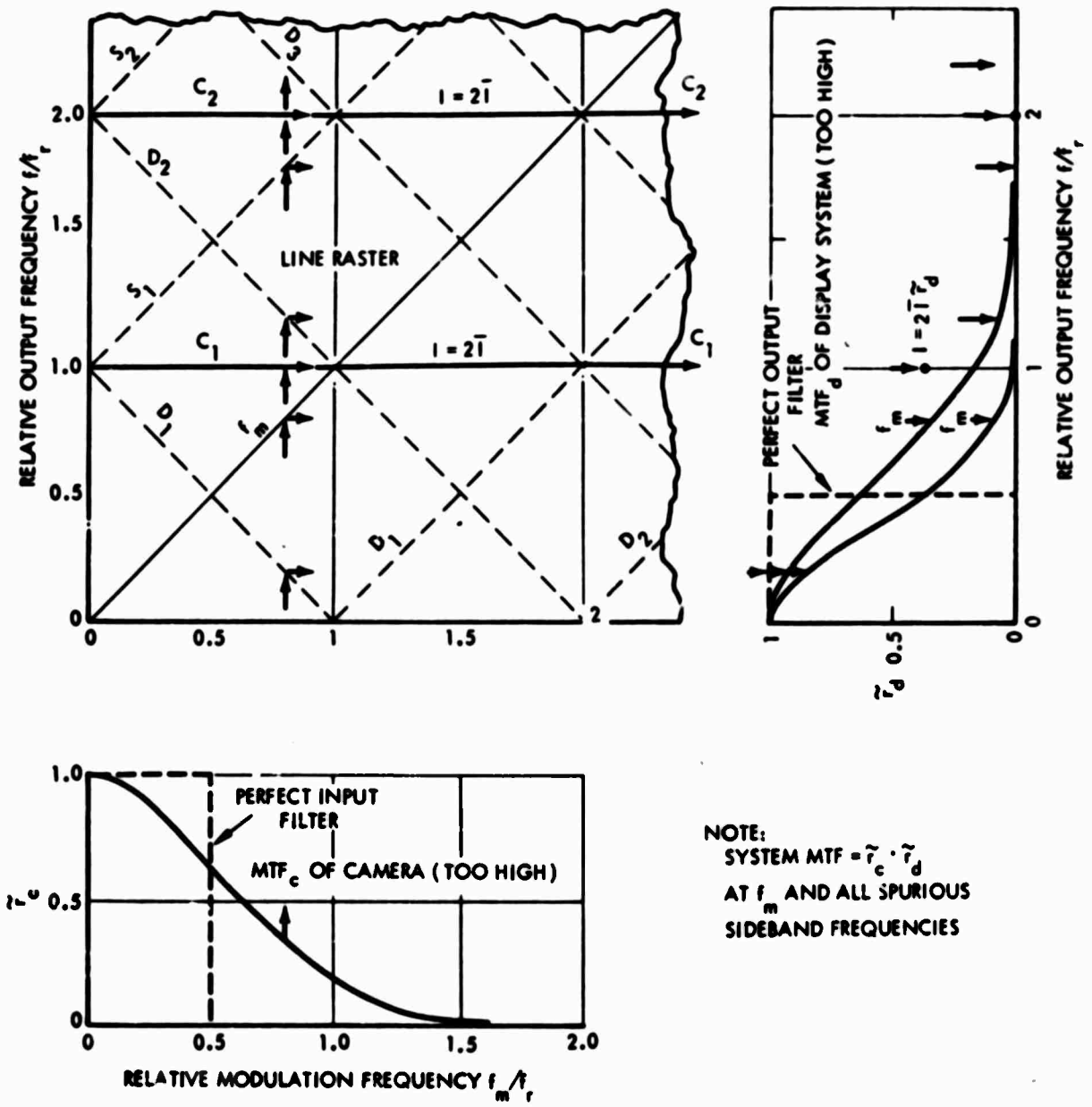

FIGURE V-1. Frequency and Modulation Transfer Characteristic in y-Coordinate of Television Systems with Line Raster Process

The MTF_d of the display system is drawn parallel to the output frequency scale of the raster characteristic. It is the product of the MTF's of all two-dimensional aperture processes following the raster process and includes, therefore, the MTF's of copying systems and the eye. Unless eliminated by adequate magnification, the MTF of the eye must obviously be considered in MTF specifications of display systems designed for a specific viewing distance.

The use of the diagram is simple. A vertical projection of an input frequency f_m (see arrows) locates the output frequencies of the raster process at the intersections with the various transfer lines. Horizontal projections from these points onto the output MTF_d indicate the attenuation ($2\bar{I}\ \tilde{r}_d$) of the carrier frequency components and the response factors $\tilde{r}_c$ for determining the relative amplitudes ($\tilde{r}_c\tilde{r}_d$) of the modulation products. The example illustrates that the higher MTF_d reproduces the carrier C, with a modulation amplitude of 36 percent, representing a 72 percent peak-to-peak variation in a uniform field ($\bar{I}$). The lower MTF_d reproduces a substantially flat field, but the raster generates a low difference frequency $f_D = 0.2\ f_r$ of amplitude $\tilde{r}_c\tilde{r}_d = 0.27$ from a modulation frequency $f_m = 0.8\ f_r$ of 32 percent amplitude because the input MTF_c exceeds the value $f_m = 0.5\ f_r$. It is seen at a glance that a complete elimination of all spurious modulation frequencies restricts the MTF's to the spatial frequency bands indicated by the broken line rectangle; i.e., to frequencies $f_m \leq 0.5\ f_r$. In other words, a minimum of one sample per half cycle is necessary to transmit a continuous sine wave by a sampling process.

B. RASTER LINE FREQUENCIES AND MTF COMBINATIONS FOR LOW SPURIOUS RESPONSE

The inverse transform of a rectangular frequency spectrum is a (sin x)/x impulse function or line image which can be realized with the coherent light of laser-beam image reproducers by using a rectangular lens stop. Similar functions can be synthesized from the Gaussian-type impulses by vertical aperture correction with tapped delay lines for noninterlaced or interlaced scanning (Ref. 1). Such

corrections may not be feasible in many cases that are then restricted to the MTF's of normal cameras and display systems, which are approximated in the illustrations by Gaussian functions.

A substantially flat field is obtained when the MTF_d at f_r is 2.5 percent or less. The carrier amplitude for the upper limit is $2\bar{I}r_d = 0.05\ \bar{I}$, producing a peak-to-peak ripple of 10 percent. The numerical evaluation of cross products is illustrated by Fig. V-2. Curves 1 through 5 represent the MTF_c of various cameras. The MTF of the display system repeats for the sum and difference frequencies of the side bands MTF_D and MTF_S, as shown in Fig. V-2. The spurious modulation products $\tilde{r}_c\ \tilde{r}_{D1}$ and $\tilde{r}_c\tilde{r}_{s1}$ are easily evaluated* and shown by curves 1 through 5 in Fig. V-3a for the five camera MTF's of Fig. V-2. Note that the zero frequency of the cross products occurs at the modulation frequency $f_m = f_r$ and that the modulation frequencies generate higher spurious frequencies for $f_m < 0.5\ f_r$ and lower frequencies for $f_m > 0.5\ f_r$. The maximum values of the spurious response are plotted in Fig. V-3b as a function of the camera response ($\tilde{r}_c$) at the theoretical frequency limit $f_m = 0.5\ f_r$. The straight line shows the overall MTF ($\tilde{r}_c\tilde{r}_d$) of the system.

A spurious response $\tilde{r}_{sp}$ of 10 percent may be considered an upper limit for good system design. This value is a worst case and occurs occasionally for 100 percent contrast in the scene. Spurious frequencies occur in the range indicated by a curve intermediate for curves 2 and 3 in Fig. V-3a and do not include low-frequency beats, which are most visible. It follows that the raster frequency (number of raster lines) should be

$$f_r \geq 2\ f_{m(0.26)} \qquad \text{(V-2)}$$

where $f_{m(0.26)}$ is the spatial frequency at which the camera has a sine-wave response factor $\tilde{r}_c = 0.26$. An overall system response $\tilde{r}_c\tilde{r}_d = 0.10$ is then obtained with a flat field display system having a sine-wave response $\tilde{r}_d = 0.38$ at the theoretical frequency limit $f_m = f_r/2$.

*The remaining products are very small or zero and can be neglected.

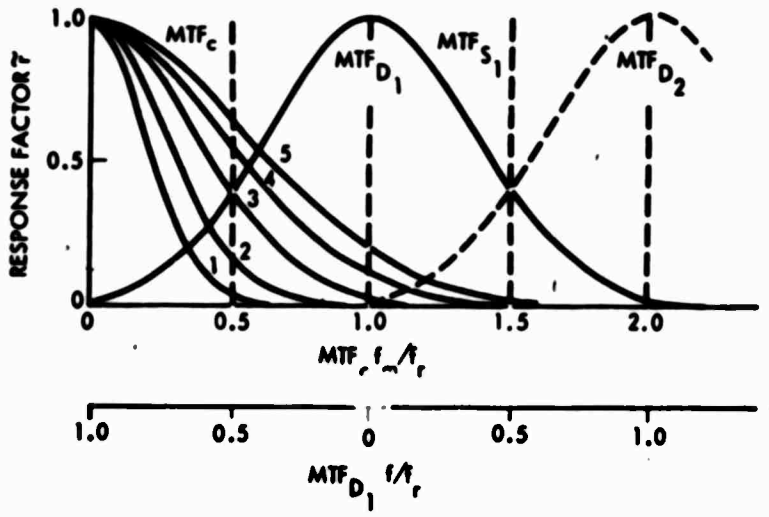

FIGURE V-2. Evaluation of Cross Products for an MTF_D Producing a Flat Field

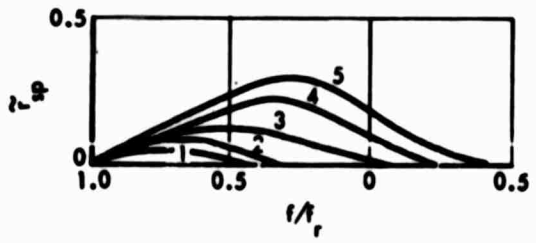

FIGURE V-3a. Cross Products $\tilde{r}_{sp}$ for MTF_S = MTF No. 3 and Various MTF_c Curves 1 → 5

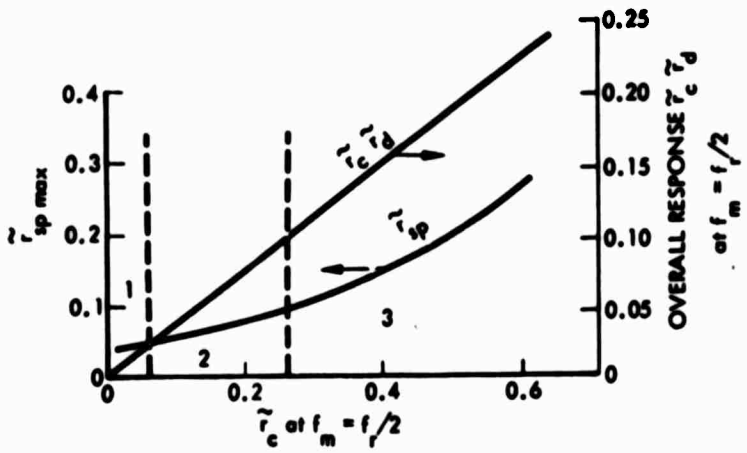

FIGURE V-3b. Maximum Spurious Response $\tilde{r}_{sp}$ and Overall Response $\tilde{r}_c r_d$ for MTF_d = MTF No. 3 and Various Camera MTF's at $f_m = f_r/2$

There is, of course, an upper limit for the raster frequency f_r because a frequency $f_m = f_r/2$ with negligible amplitude need not be sampled as expressed by

$$2f_{m(0.05)} \geq f_r \geq 2\, f_{m(0.26)}. \qquad \text{(V-3)}$$

The index numbers specify the camera response ($\tilde{r}_c$) at f_m. The upper limit $f_r = 2\, f_{m(0.05)}$ provides a very low level of spurious signals but requires a wide video passband.

C. SYSTEM DESIGN

The MTF_c of the camera determines the constants of the television system or vice versa. Equation V-3 states that the raster frequency should be in the range $f_r = 2\, f_{0.26}$ to $2\, f_{0.05}$, where $f_{0.05}$ and $f_{0.26}$ are the spatial frequencies at which the camera response is 26 percent and 5 percent, respectively. A design for best utilization of the electrical frequency channel would select the lower raster frequency ($2f_{0.26}$) whereas a design for maximum resolving power requires the upper limit. In terms of television line numbers (N) and the raster line number (n_r), Eq. V-3 specifies the range $n_r = N_{0.25}$ to $N_{0.05}$. A commercial 525 line system, for example, has an active raster line number $n_r = 490$ lines and the vertical camera response at this line number (N) is generally less than 26 percent.

A flat field and low spurious response dictate a display system designed for an MTF_d of 2.5 percent or less at the raster frequency (f_r). The MTF of a <u>good</u> commercial CRT is in the order of 27 percent at $f_r = 490$ <u>cycles</u> and, at a luminance B = 40 ft-L, the MTF of the eye (Ref. 2) is 5 percent for a relative viewing distance d/V = 4 and about 0 percent for d/V = 6. The MTF_d of the display system is thus 1.35 to 0 percent. The peak-to-peak ripple is 4 times higher and still visible at the shorter viewing distance. The line structure is very pronounced at close viewing distances and should be eliminated by vertical "spot wobble." The spot-wobble frequency should be outside the frequency spectrum of the system; about 20 MHz for standard

CRT's, 50 MHz for a 20-MHz video system and 140 MHz for 100-MHz systems and very high-resolution CRT's. Spot wobble is particularly recommended when the CRT image is magnified by overscanning the normal format. A laser-beam image recorder designed for a substantially rectangular frequency spectrum and a flat field increases the MTF_d and overall MTF of the system. It does, however, increase also the amplitude of the spurious response products. Figures V-1 and V-2 illustrate by rectangular broken lines that portions of the sidebands (D) are reproduced with unity response by a rectangular MTF_d. The modulation products shown in Fig. V-2a are zero for $f/f_r > 0.5$ and have amplitudes equal to r_c for $f/f_r < 0.5$, which are the portions of curves 1 to 5 in Fig. V-2 inside the rectangular first sideband. This condition recommends the use of higher raster frequencies $f_r \approx 2\, f_{m(0.10)}$ to reduce spurious low frequencies. The MTF's of the camera and display system are products of a number of components. It may thus occur that the MTF of the scanning aperture (beam) in the camera is much higher than the product, for example, when a high-resolution beam is used in combination with a light intensifier and a high-aperture lens. Calculation of the raster frequency with Eq. V-3 may indicate a relatively low raster frequency at which the scanning beam leaves unscanned interline spaces. Although sufficient integration of the image flux occurs in the stages preceding scanning, the efficiency of signal conversion is reduced by interline charges not contacted by the beam and can result in undesirable secondary effects recommending the use of a larger beam or a higher raster frequency. A similar situation may occur in a display system containing several "copying" stages which "diffuse" the image of the actual scanning spot to provide a flat field. The current or light density in the scanning spot may then become excessive, which can result in saturation effects.

A "perfect" television system having equal rectangular MTF's in x and y, producing a structureless field, is anisotropic because the effective apertures δ_c and δ_d have a square base, causing an increase of the spatial frequency spectrum by $\sqrt{2}$ in the diagonal directions.

The same anisotropy occurs in optical images formed with monochromatic light by a lens having a square lens stop. A practical television system in which the MTF is bandwidth limited in x by the video system is similarly anisotropic, as is readily confirmed by observation. The system becomes isotropic when the raster frequency has twice the value at which the camera response is 5 percent, the MTF of the display system is 2 percent or less at the raster frequency, and the video system has unity response up to the resolution limit of the overall MTF product because the MTF of the system is then limited in all radial directions by the isotropic response of its two-dimensional circular apertures. This is the preferred system design for high resolving power. It should be pointed out that the MTF of a charge storage camera can become anisotropic because of "self-sharpening" of a low-velocity beam in x or y, which depends on a low or excessively high raster line density, respectively. The MTF_c in the y-direction is readily measured with a horizontal pulse gating circuit, and isotropy in the reproduced image can be tested visually by comparing the contrast of vertical and horizontal resolution bars in a standard Air Force test object, which can be made equal by adjusting the MTF of the video system by aperture correction circuits.

SECTION V. REFERENCES

1. Otto H. Schade, Sr., Patent 3,030,440, Vertical Aperture Correction.

2. Otto H. Schade, Sr., "Optical and Photoelectric Analog of the Eye," J. Opt. Soc. Am., Vol. 46, No. 9, p. 721, 1956.

VI. THE GRAIN STRUCTURE OF TELEVISION IMAGES*

by

Otto H. Schade, Sr.

*Reprinted from "Image Gradation, Graininess and Sharpness in Television and Motion Picture Systems," Journal of Motion Picture and Television Engineers, Pt. III, Vol. 61, No. 2, pp. 97-164, August 1953.

Image Gradation, Graininess and Sharpness in Television and Motion-Picture Systems

Part III: The Grain Structure of Television Images

By OTTO H. SCHADE

CONTENTS

Presented by Otto H. Schade, Tube Dept., Radio Corporation of America, Harrison, N.J., in part on October 15, 1951, at the Society's Convention at Hollywood, Calif., and on April 28, 1953, at the Society's Convention at Los Angeles.

Note: Part I of this paper, "Image structure and transfer characteristics," was published in this *Journal* in February 1951, pp. 137-171; and Part II, "The grain structure of motion picture images — an analysis of deviations and fluctuations of the sample number," in March 1952, pp. 181-222.

(This paper was received first on March 3, 1953, and in revised form on June 5, 1953.)

SYMBOLS

Note: Peak values are designated by a peak sign over a symbol $\hat{f}$; and average or mean values by a horizontal bar, $\bar{f}$. When used with $\mathfrak{N}_c$-values, the bar indicates the geometric mean for two coordinates.

a Area of sampling aperture
a_e Equivalent sampling aperture
A Frame area
b Blanking factor (See Eqs. (61) and (72))
B Luminance
c A constant
C Capacitance
d Viewing distance
$\mathfrak{d}$ Noise voltage
E_t Exposure (unit: meter candle seconds)
E Signal voltage
$[E]$ Rms noise voltage
f Frequency: $f(x,y)$ a function of x and y
Δf Theoretical rectangular frequency channel (Eq. (63))
Δf_e Noise-equivalent passband of electrical elements or systems
h Horizontal dimension of equivalent sampling aperture or index for horizontal coordinate
H Horizontal dimension of picture frame
I Noise current
I Intensity or current
K A constant
l Unit of length
m Horizontal bandwidth factor of electrical circuits (Eq. (79))
N Line number — number of half-wavelengths of line- or sine-wave patterns per length unit
N_e Limiting resolution, $N_{e(0)}$ limiting resolution of aperture system following raster process
N_e Equivalent passband (Eqs. (22) to (28) Part II)
$\mathfrak{N}_e$ Equivalent passband of an asymmetric aperture (Eq. (23) Part II)
$N_{e(a)}$ Equivalent passband of all apertures preceding and including analyzing aperture of raster process
$N_{e(s)}$ Equivalent passband of all apertures following and including synthesizing aperture of raster process
$\mathfrak{N}_{e(T)} = (N_{e(A)}n_r)$ Equivalent passband of theoretical television channel (Eq. (64))
$\mathfrak{N}_{e(m)} = (N_{e(A)}N_{e(s)})$ Equivalent optical passband of measuring aperture δ_m
$\mathfrak{N}_{e(s)} = (N_{e(A)}N_{e(s)})_\delta$ Equivalent optical passband of system between origin of deviations and point of observation
n Number of particles or samples inside of sampling area
n_r Raster constant, number of points or lines in length unit
n_r Number of scanning lines including vertical blanking period (Eq. (62))
q_e Electron charge
Q_f Frame charge (Eq. (71))
r_ϕ Sine-wave response factor of an aperture (Eq. (18))
r_η Electrical sine-wave response factor (Eq. (65))
$r_{\phi a}$ Response factor of analyzing aperture (including preceding apertures)
$r_{\phi s}$ Response factor of synthesizing aperture (including following apertures)
$[r_\phi]$ Rms response factor
R Resistance
$[R]$ Signal-to-rms-deviation ratio, static value in a single image frame (Eq. (13) Part II)
$[R]_m$ Reference signal-to-deviation ratio measured at the source with a known aperture δ_m
$[R]_e$ Signal-to-deviation ratio of system
s Length of side of square aperture, or storage factor
t Time interval
T_f Frame time
v Vertical dimension of equivalent sampling aperture or index for vertical coordinate
V Vertical frame dimension
x,y Coordinates, x = coordinate in the direction of scanning
Y Amplitude
α $= (N_{e(a)}/N_e)_h$ Horizontal bandwidth factor (Eq. (66))
β $= N_{e(a)}/n_r$ Vertical bandwidth factor (Eq. (57))
$(\alpha\beta)_h = (\mathfrak{N}_{e(a)}/(N_{e(A)}n_r))$ Optical bandwidth factor (Eq. (68))
γ Constant gamma
$\dot{\gamma}$ Point gamma, definition in Part I, p. 145
$\dot{\gamma}_e$ Point gamma of system at a particular signal level between origin of deviations and point of observation
δ Characteristic aperture diameter
δ_f Equivalent optical aperture of theoretical television channel (Fig. 80)
ϵ Base of natural logarithm
τ Transmittance
σ Relative deviation (Eqs. (13) to (17) Part II)
θ Phase displacement between sample amplitude and crest intensity $\hat{I}_M$ (Fig. 69)
Φ Flux
$[\phi]$ Rms value of variational (a-c) flux (see Eq. (20))

SUMMARY OF PART III

The analysis of grain structures in imaging systems containing a point- or line-raster process requires evaluation of the sine-wave response in two coordinates. The characteristics of the raster process are developed by a Fourier analysis of the optical image. The sine-wave response perpendicular to the raster lines (for example the vertical sine-wave response of a television system) is shown to contain in general a carrier wave, the normal aperture response to sine-wave test signals, and a series of sum-and-difference components with magnitudes depending on the aperture response products of the analyzing and synthesizing apertures preceding and following the raster process (camera tube and kinescope in television systems). A graphic representation of the raster equation (Fig. 70) shows at a glance the number and magnitude of the sine-wave components for any combination of apertures used with the raster process. The application of the aperture theory developed in Part II yields an equivalent optical aperture (Fig. 80) and equivalent passband (Eq. (64)) for the theoretical television channel. The evaluation of the horizontal sine-wave response of electro-optical systems containing electrical and optical elements is simplified by establishing normalized characteristics for the sine-wave response, equivalent passband, aperture cross section, and edge transition of a variety of electrical response characteristics (including aperture correction) in cascade with optical apertures. Because of their general character and use in the evaluation and design of television systems, the range of parameters has been extended beyond the cases used in examples.

In normalized units equivalent passbands (horizontal and vertical) of electrooptical systems are specified by bandwidth factors (α and β), which are ratios of the equivalent passband of the system to the theoretical passbands N_{ch} and n, of the television channel (section D_1). These bandwidth factors emerge as significant parameters specifying the characteristics of the system.

The translation of electrical noise levels into optical deviations in a television frame is now readily accomplished, permitting evaluation of granularity by the methods discussed in Part II. It is shown that the electrical signal-to-noise ratios usually quoted for television systems have by themselves little meaning when television grain structures are compared, because the transfer characteristics and apertures of the system cause pronounced changes in signal-to-deviation ratios and the amplitude of the sine-wave components contained in optical deviations of a television picture frame. It is concluded that an adequate description of granularity in television and motion-picture frames requires specification of the sine-wave spectrum and signal-to-deviation ratio in the retinal image as a function of luminance and for a specified viewing distance. An assessment of the perception of deviations throughout the luminance range of motion pictures and television images can be made by introducing the characteristic of threshold signal-to-deviation ratios as a reference level.

A. REVIEW OF PRINCIPLES

The principles and method developed in the analysis of motion-picture granularity in Part II of this paper can be applied to all imaging systems and will be summarized briefly. Random fluctuations of luminance in motion-picture or television images cause the appearance of a moving granular structure. In a single picture frame representing a constant light level the structure is stationary

Fig. 65. Block diagram of television process and sources of random deviations.

and the luminance variations are *static deviations* from the average luminance which is the *optical signal*.

Optical signals and deviations are measured by taking samples of the image flux with an aperture. The average value of the sample readings is the signal. The relative magnitude of the deviations is expressed by the *relative deviation* σ or its reciprocal, the *signal-to-rms deviation ratio* $[R]$. When the deviations are random (see Part II for definition) the value $[R]$ measured at the source of deviations is directly proportional to the one-half power of the effective area a_e of the sampling aperture as stated by

$$[R] = 1/\sigma = (\bar{n}_0 a_e)^{\frac{1}{2}}$$

where $\bar{n}_0$ specifies the mean "particle" density in the random structure at the source. The effective sampling area of practical image-forming devices or systems can be determined from the geometry of their point image (see Part II) or from the total sine-wave energy response of the point image, obtained by a Fourier analysis of a test image such as a single sharp line, a single-edge transition, a random grain structure, or from sine-wave test patterns. The last two methods mentioned, particularly the method using sine-wave test patterns with variable line number, are known from analogous electrical measurements to be most accurate because of the high energy level of the observed signals and the simplicity of evaluation. In sine-wave response measurements the point image is regarded as an "aperture" of unknown geometry which is made to scan a series of constant-energy sine-wave test patterns. The total relative sine-wave energy of the aperture response characteristic is specified by a single number N, interpreted as an *equivalent passband*. The reciprocal of this measure K/N, specifies the diameter of the desired *equivalent sampling aperture* (see Table VII, Part II). The point images of practical devices are often asymmetric. In this case the equivalent sampling aperture can be specified as a rectangle with dimensions h and v, which are the reciprocals of two equivalents:

$$a_e = hv = [N_{e(h)} N_{e(v)}]^{-1} \qquad (51)$$

The asymmetric point image is described by two sine-wave response characteristics in rectangular coordinates (H and V) and their corresponding equivalent passbands $N_{e(h)}$ and $N_{e(v)}$.

The signal-to-deviation ratio $[R]$ can now be stated in the forms

$$[R] = \bar{n}_0^{\frac{1}{2}} / [N_{e(h)} N_{e(v)}]^{\frac{1}{2}}$$

$$[R] = \bar{n}_0^{\frac{1}{2}} / \bar{N}_e \qquad (52)$$

where $\bar{N}_e$ is the geometric mean of the two equivalent passbands.

The particle density $\bar{n}_0$ *at the source* can be determined by a count of the number of particles (grains or electrons) in a unit area of the random structure in which the deviations originate. When this is impractical, $\bar{n}_0$ is obtained from a reference value $[R]_m$ measured or computed with an aperture of known area a_m or equivalent passband $\bar{N}_{e(m)}$.

The actual signal-to-deviation ratio $[R]_o$ at any one point in the imaging system can then be computed accurately from the aperture ratio (Eq. (37) in Part II) which, stated in terms of N_e-values, has the form

$$[R]_o = [R]_m (\bar{N}_{e(m)} / \bar{N}_{e(o)}) / \dot{\gamma}_o \qquad (53)$$

where

- $[R]_m$ = signal-to-deviation ratio at the origin of deviations, measured with an aperture of equivalent passband $\bar{N}_{e(m)}$
- $\bar{N}_{e(m)} = (N_{e(h)} N_{e(v)})_m^{\frac{1}{2}}$ = equivalent optical passband of measuring aperture
- $\bar{N}_{e(o)} = (N_{e(h)} N_{e(v)})_o^{\frac{1}{2}}$ = equivalent optical passband of system aperture between origin of deviations and point of observation
- $\dot{\gamma}_o$ = overall transfer ratio or "point gamma" of system elements at the particular signal intensity between origin of deviations and point of observation.

The analysis of optical deviations in television images requires a translation of

television system parameters and characteristics into equivalent optical units. A schematic representation of a television process is shown in Fig. 65. The light flux in the optical image A_0 formed by the camera lens is transduced into an electrical image A_1 in the television camera tube. The charge image A_1 is scanned by an aperture δ_1 along a system of parallel lines termed a *line raster*. The aperture δ_1 is the electron beam of the camera tube which transduces the electrical aperture flux into video signals. The electrical signals are amplified, limited by electrical filters, transmitted and again transduced into light-flux variations by the aperture δ_2 of an electro-optical transducer (kinescope) scanning the frame area A_2. The two scanning apertures δ_1 and δ_2 are moved with uniform velocity and in synchronism over the respective frame areas. Like optical apertures, these scanning apertures have two dimensions, and their response is readily described by normal sine-wave response characteristics and equivalent passbands. New elements in the imaging system requiring evaluation in terms of optical response characteristics are the *line raster* and the electrical system of amplifiers and low-pass filters.

Luminance deviations in a television frame may be caused by a number of sources located at different points in the system (see Fig. 65). When the deviations originate in a preceding photographic process, the television system is an aperture process transferring a two-dimensional granular structure. Deviations originating in electrical elements, however, may not be associated with the transferred image. Electron sources such as the cathodes of electron guns or amplifier tubes continually produce random fluctuations in the flow of electrons, which are arranged and displayed artificially in two dimensions by the scanning process. The resulting luminance deviations in the frame area may, however, be regarded as the image of a random particle structure scanned with a hypothetical camera and measured with a theoretical sampling aperture $\delta_{(r)}$ which will be found to have a specific value given by the system constants. With this concept all cases can be treated by one method.

B. RASTER PROCESSES

1. The Raster Constant (n_r)

The formation of images by lenses or optical systems is continuous in both coordinates of the image area. It is, therefore, permissible to determine signals and deviations from a limited number of sample readings, because every point in the image area undergoes an aperture process. The aperture shape becomes indistinguishable in areas of constant luminance. In the presence of deviations, the steady "signal" flux can be considered as a "carrier" flux of constant intensity I "modulated" by random deviations.

Printing, facsimile and television are sampling processes in which the number of aperture positions is finite in one or both coordinates of the image frame. The image flux is no longer continuous in two coordinates but contains periodic components. An arrangement limiting aperture positions to a fixed number of uniformly spaced points in the image frame is termed a *point raster;* an arrangement providing continuous aperture positions along uniformly spaced parallel lines is termed a *line raster. The "raster" constant n_r specifies the number of aperture positions in the length unit of a geometric arrangement of points or lines;* it does not specify the dimensions of the "points" or "lines" themselves which are determined by the geometry of the sampling apertures used with the raster process.

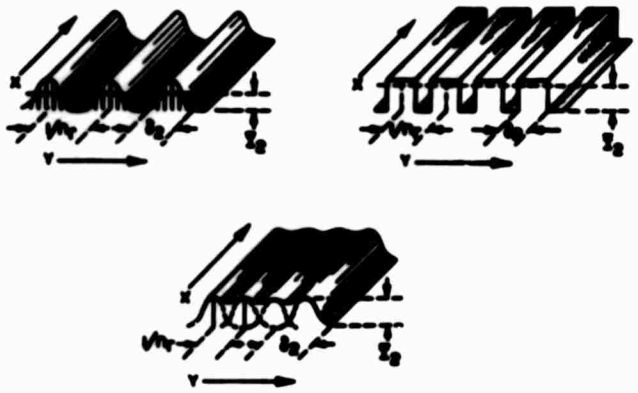

Fig. 66. Intensity distribution and "carrier" waves in the y-coordinate of line-rasters.

2. Carrier Wave and Line Structure

A line raster limits the number of aperture positions perpendicular to the raster lines. Areas of constant luminance are reproduced by the aperture δ_2 as a flux pattern in which the intensity is constant in the direction x parallel to the raster lines but contains a more or less pronounced periodic component in the y-coordinate defined as the coordinate perpendicular to the raster lines (Fig. 66). The following analysis of conditions in the y-coordinate of a line raster applies to optical as well as television processes† and also to point rasters which cause periodic components in both x- and y-coordinates. (In television images the coordinate Y is identical with the vertical coordinate V of the image frame.)

The periodic component can be regarded as a constant *carrier wave* added by the raster to the continuous carrier flux of a normal aperture process. The signal flux from the analyzing aperture δ_1 determines the average intensity level I, i.e., the scale factor of the image flux. It is seen by inspection of Fig. 66 that the length of the carrier wave is the reciprocal of the raster constant: $\Delta y = 1/n_r$, while waveform and relative amplitude of the carrier wave are determined by the geometry of the synthesizing aperture δ_2.

A Fourier analysis of this "pulse carrier wave" shows that the intensity distribution $I_{(y)} = f(y)$ contains the constant signal term $\bar{I}$ and a series of harmonic cosine waves:

$$I_y = \bar{I}\left[1 + \sum_{\rho} 2r_{\rho}\delta_{(\rho n_r)} \cos \rho r y n_r\right] \quad (54)$$

$(\rho = 2, 4, 6, \ldots)$

The cosine terms specify the harmonic components of the carrier wave, which have (television) line numbers $N_{r1} = 2n_r$, $N_{r2} = 4n_r$, $N_{r3} = 6n_r$, ... Their relative intensities are specified by coefficients which are the *sine-wave response factors* $r_{\rho 1}, \ldots$) in the y-coordinate of the particular aperture δ_2 at the line numbers of corresponding carrier harmonics. The cosine-wave components are in phase at the aperture center (on the raster line) when the aperture has axial symmetry† and its response decreases asymptotically to zero. When the response characteristic has an oscillatory form (compare Figs. 41 and 42 of Part II), the phase may reverse at each zero re-

† A two-dimensional Fourier analysis of the television picture was presented in an early paper by Roberts and Gray.[1]

† Apertures with asymmetric cross sections introduce phase shifts between cosine terms and will be discussed in Part IV.

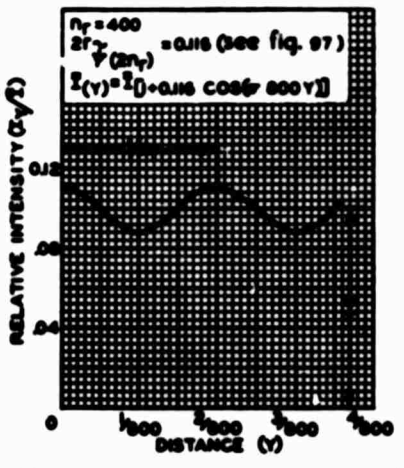

Fig. 67. Intensity distribution in y-coordinate of raster process with kinescope aperture $\delta_2 > 1/n_r$, passing only one cosine term of the carrier wave.

sponse point. Examples illustrating a numerical synthesis of the intensity distribution expressed by Eq. (54) are shown in Figs. 67 and 68. Equation (54) establishes a direct relation between the geometry of the *line image* and the sine-wave response characteristic of the line-generating point image. For the purpose of reconstructing an aperture cross section (i.e. an isolated line) from its sine-wave spectrum the fundamental component $N_{r1} = 2n_r$ in Eq. (54) is given a low value for which the bracketed terms of Eq. (54) equal zero at the distance $y = \frac{1}{2}n_r$. This condition is obtained when

$$2(r_{\delta(2n_r)} - r_{\delta(4n_r)} + r_{\delta(6n_r)} - \ldots) = 1 \quad (55)$$

A fundamental component $N_r = 2n_r = 200$ lines was used for the aperture synthesis (Fig. 68) from the sine-wave response characteristic (Fig. 95).

The presence of a pronounced line structure in the image is highly undesirable. Perfect continuity is restored when none of the carrier-wave components are reproduced by the aperture δ_2, i.e., when the aperture response is zero at line numbers which are integral multiples of $2n_r$. Practical imaging devices usually have an aperiodic response characteristic. In some cases the response has non-integral zeros, but the response is usually low beyond the first zero. A substantially continuous or "flat" field is, therefore, obtained when

$$r_{\delta(2n_r)} \lesssim 0.005 \quad (56)$$

This response factor causes a ripple amplitude of 1%, i.e., a peak-to-peak intensity variation of 2%. The aperture process δ_2 in the reproducing device (kinescope) is followed by other imaging processes, for example by the process of vision or by a photographic process. It is, therefore, unnecessary to restrict the response of the aperture δ_2 alone by Eq. (56) but rather the overall sine-wave response r_{δ_0} of the aperture system following the raster process (indicated by the index δ).

The flat-field condition specified by Eq. (56) may be stated in the form

$$N_{c(\delta)} \lesssim 2n_r \quad (56a)$$

Assume for example that a standard 35-mm motion-picture process (Table IX (1 to 4), Part II) which has a limiting resolution N_c of approximately 1100 lines, is used for video recording. It follows from Eq. (56a) that a standard 525-line television raster which contains $n_r = 490$ active line traces is just resolved in the optical projection of the 35mm print. Even with a kinescope having 3000-line resolution and an aperture response $r_{\delta(2n_r)} = 0.62$ which causes a pronounced line structure on the kinescope screen, the response in the optical 35mm projection is only 1% at $N = 2n_r$.† The carrier "ripple" has then an amplitude of 2% and a peak-to-peak amplitude of 4%.

† Failure to interlace perfectly will introduce carrier components at one-half the line number, for which the overall response is 22%.

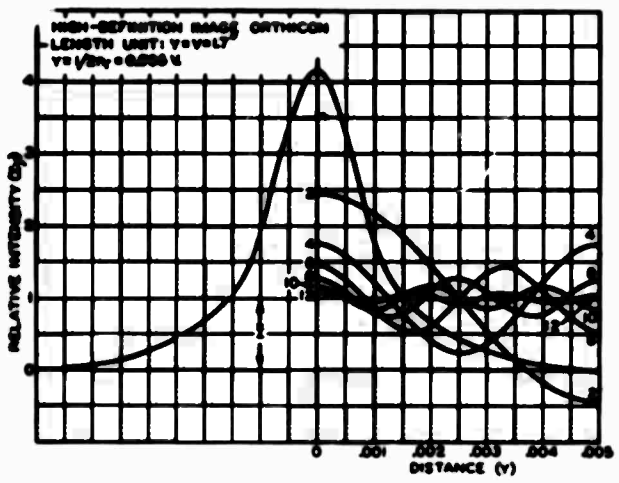

Fig. 68. Synthesis of line cross section formed by a camera-tube scanning beam for the condition $\delta \leq 1/n_r$ (nonoverlapping).

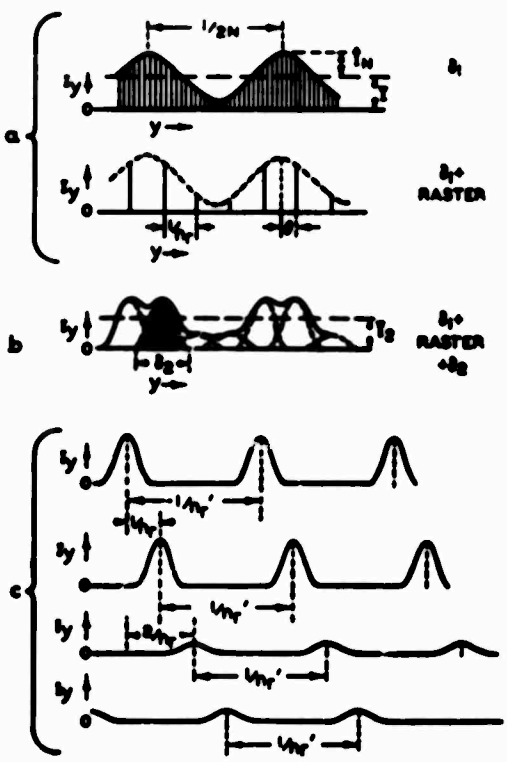

Fig. 69. Sampling and reproduction of sine-wave test pattern in the y-coordinate by a raster process and development of raster equation by regarding "modulated" carrier wave as the sum of interlaced carrier waves with different amplitudes.

3. Response to Sine-Wave Test Patterns and Equivalent Passband

A line raster has no effect on the sine-wave response of the apertures δ_1, and δ_2 in the x-coordinate (parallel to the raster lines), in which the aperture process is continuous. The discrete aperture positions in the y-coordinate affect the response of the two apertures in a different manner.

The analyzing aperture δ_1 "samples" the flux of a test pattern in the y-direction at the raster points only, all other aperture positions are "blocked" by the raster. What is left of the normally continuous aperture signal is a series of exact samples of its response at regularly spaced distances $\Delta y = 1/n_r$ as indicated by Fig. 69a. The reader may visualize the raster as an opaque plate with very fine slits (holes for a point raster) through which he, or a photoelectric device, views the test pattern from a fixed distance. He can control δ_1 by varying the spacing between the raster plate and the test object. When the test pattern line number N is varied, the sample amplitudes vary in direct proportion to the normal sine-wave response of δ_1. A further interpretation of these amplitudes cannot be given without considering the synthesizing aperture process.

For a linear system, the intensity of the light flux from the synthesizing aperture δ_2 is proportional to the signal amplitude delivered by δ_1 at corresponding raster points. The reproduced waveform, however, is only an artificial approximation of the test pattern wave, determined by the raster constant and the geometry of the aperture δ_2 as illustrated in Fig. 69b. The fundamental sine-wave response and the waveform distortion can be evaluated by a Fourier analysis. For this purpose the periodic wave may be regarded as the sum of a series of interlaced carrier waves, each having a constant amplitude and a wavelength $1/n_r'$ which is longer than the normal raster period (see Fig. 69c). These component carrier waves are displaced in phase by distances $1/n_r$, $2/n_r$ etc., with respect to one another and can be expressed by Fourier series (Eq. (54)) differing only in amplitude and phase of the terms. A vectorial addition of corresponding terms yields an expression for the waveform. For the conditions that the average intensity $\bar{I}_2$ in the image of the test pattern has the same numerical value as the test pattern intensity $\bar{I}$, and the transfer ratio of signals (gamma) is unity, the expression obtained for the intensity $I_{(y)}' = f(y)$ is the following Eq. (57):

$$I_{(y)2} = \bar{I}[1 + \Sigma_p 2r_{\delta_{(pn_r)}} \cos p\pi y n_r] \quad \text{(C)}$$

$$+ \bar{I}_N r_{\delta_1} r_{\delta_2} \cos[(N/n_r)\pi y n_r + \theta] \quad \text{(N)}$$

$$+ \bar{I}_N r_{\delta_1} \Sigma_p r_{\delta_{(pn_r+N)}} \cos[(p + N/n_r)\pi y n_r + \theta] \quad \text{(S)}$$

$$+ I_N r_{\delta_1} \Sigma_p r_{\delta_{(pn_r-N)}} \cos[(p - N/n_r)\pi y n_r - \theta] \quad \text{(D)}$$

where

- p = 2, 4, 6, . . .
- n_r = Raster constant (number of sampling positions per length unit)
- y = Distance along y-coordinate (same length units as $1/n_r$)
- $\bar{I}$ = Average intensity in y-coordinate
- $\bar{I}_N$ = Crest intensity of sine-wave flux in test pattern
- r_{δ_1} = Response factor of aperture δ_1 at the line number N
- r_{δ_2} = Response factor of aperture δ_2 at the line number N
- $r_{\delta_{(index)}}$ = Response factor of aperture δ_2 at line number indicated by index
- θ = Phase displacement between sample amplitude and crest $\bar{I}_N$ (Fig. 69).

The terms of Eq. (57) have been arranged in four products. The first product (C) contains only the *steady carrier components* as expressed by Eq. (54). The magnitude and numbers of the sine-wave terms depend on the aperture response of δ_2 only. The second product (N) is identified as the *normal sine-wave signal flux* ψ_{12} of the cascaded aperture δ_1 and δ_2 at the line number N. The third and fourth products (S) and (D) are harmonic components with line numbers which are the *sums and differences* of the

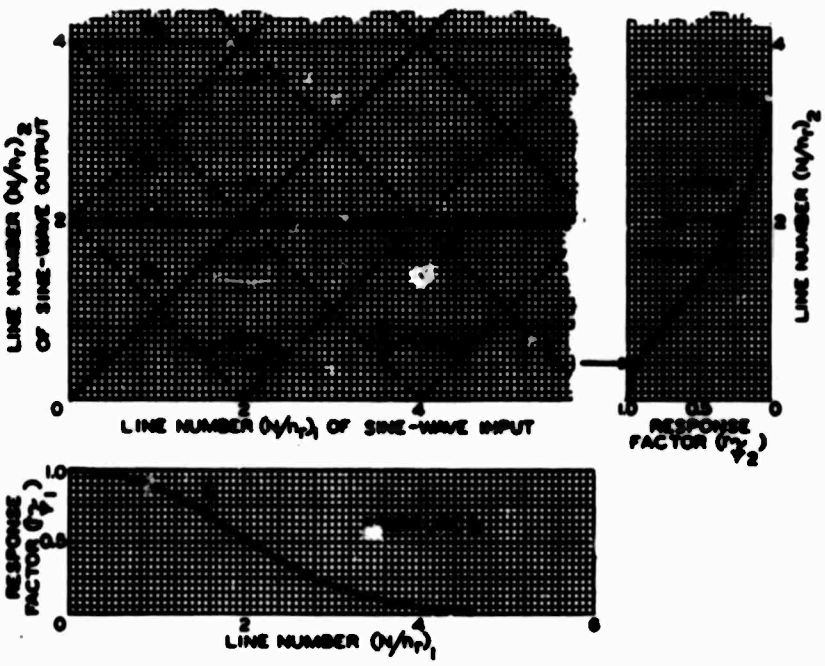

Fig. 70. Conversion characteristic of raster (Eq. (57)).

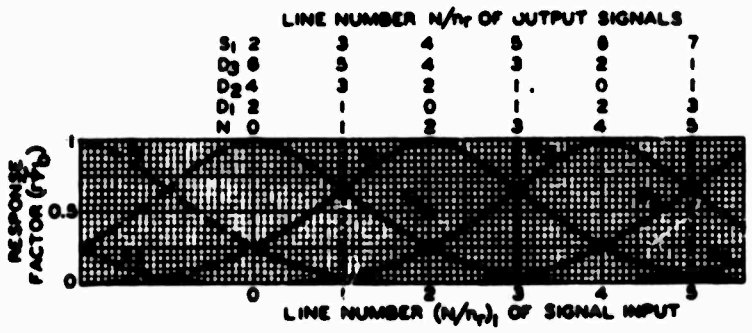

Fig. 71. Graphic representation of the combined sine-wave response of raster and synthesizing aperture δ_1 by normal aperture characteristic and "sidebands."

carrier components $2n_r$, $4n_r$, etc., and the "modulating" sine-wave signal N. Their magnitude and number depend on the response of both apertures δ_1 and δ_2.

The raster process introduces additional sine-wave components depending on the sine-wave response of the apertures δ_1 and δ_2. *The sine-wave response characteristic of the raster* itself can be represented graphically by a conversion characteristic (Fig. 70) with constant response factors $r_v = 1$ for all variable

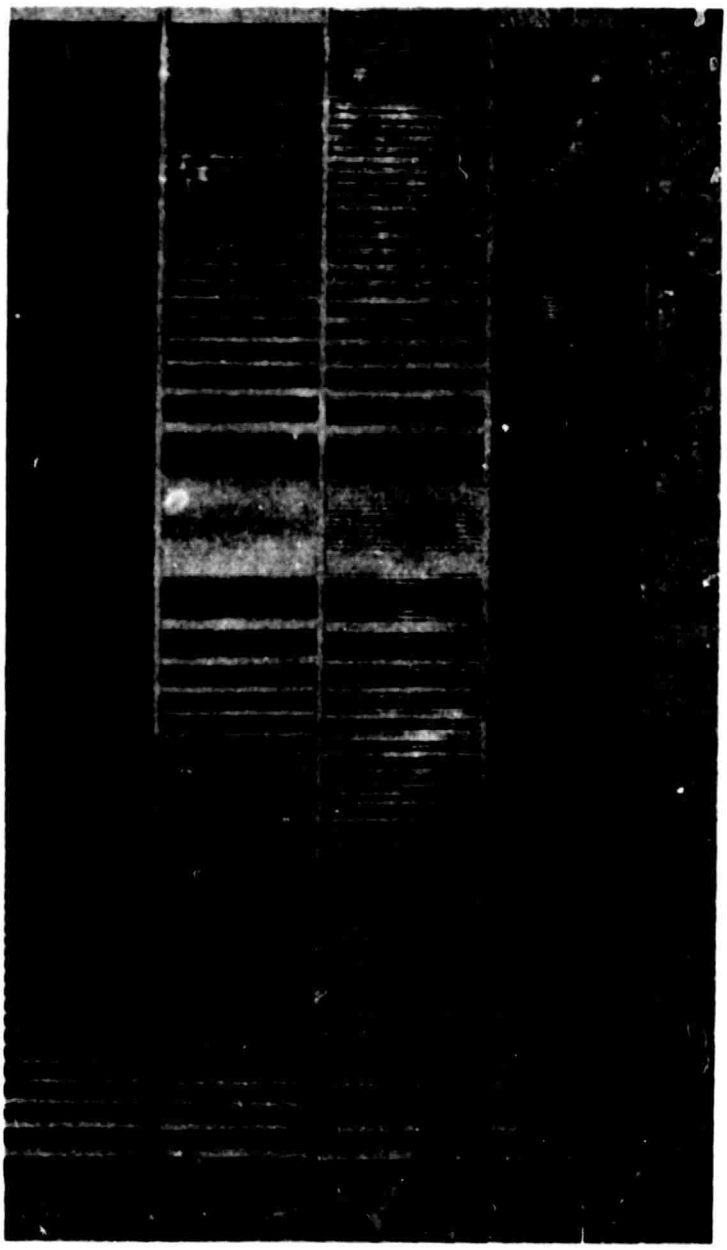

Fig. 72. Photographic proof of repeating line-number spectra ("sidebands") obtained by a line-raster process (see text).

Table XV. Sine-Wave Components $(N/n_r)_2$ and Response Factors (r_β) for $(N/n_r)_1 = 1.6$.

Component:	D_1	N	C_1	D_2	S_1	C_2
Line Number $(N/n_r)_2$	0.4	1.6	2	2.4	3.6	4
Response Factor r_{β_1}	0.675	0.675	0.675	0.675	0.675	0.675
Response Factor r_{β_2}	0.92	0.39	2×0.25	0.14	0.0	0.0
Overall Response Factor r_{β_2}	0.62	0.263	0.338	0.945	0.0	0.0

terms and the response $r_r = 2$ for the constant carrier components. The carrier components are represented by an infinite number of horizontal lines C_1, C_2 etc., because their existence is independent of the sine-wave signal input. The line number of the normal sine-wave components (line N) and the sum and difference terms (lines S_1, S_2, S_3. . . . and D_1, D_2, D_3. . . .), however, vary with the line number $(N/n_r)_1$ of the input-signal as shown by the network of diagonal raster characteristics. *The raster characteristic (Fig. 70) is a graphic representation of Eq. (57).* The use of the diagram is simple. A vertical projection of the input line number $(N/n_r)_1$ locates the output signal components at the intersections with the raster characteristics as illustrated for $(N/n_r)_1 = 1.6$. *The relative intensity of the sine-wave components* is the product of the aperture response factor r_{β_1} at the line number of the input-signal and the response factor r_{β_2} at the line number of the output-signal component. The sine-wave response characteristic of the "analyzing" aperture δ_1 is, therefore, drawn in Fig. 70 under the input coordinate of the raster characteristic, and the sine-wave response characteristic of the "synthesizing" aperture δ_2 is drawn with its line-number scale parallel to the output coordinate (both line-number scales must be in relative units N/n_r). The sine-wave response factors of the example are listed in Table XV for $(N/n_r)_1 = 1.6$.

To evaluate the total sine-wave spectrum of a raster process it is expedient to combine the raster response r_r with the response characteristic $r_{\beta_0} = r_{\beta_1} r_{\beta_2} \ldots r_{\beta_n}$ of succeeding apertures into one characteristic. The characteristic Fig. 71 represents the overall sine-wave response $r_{\beta_r 0}$ for constant amplitude sine-wave signals of the raster and a particular aperture process (δ_0) following the raster. Appropriate scales permit a direct reading of the line number and response factor r_{β_0} of all associated terms in the y-coordinate of the final image. The response factor $(2r_\beta)$ of the single constant carrier term C_1 is indicated. The normal response characteristic (N) of the aperture δ_0 appears symmetrically repeated† at each carrier line number $2n_r$, $4n_r$, etc. The response pattern between $N/n_r = 0$ and 1 repeats indefinitely. A large aperture for example has zero response at $N/n_r < 1$; its response nevertheless repeats up to infinity, periodically going to zero.

The fact that the passband of an aperture δ_0 is repeated by addition of a raster process, is demonstrated by Figs. 72a to 72d. Figure 72a is a photograph of a test pattern having a variable line number.[9] A sharp photograph (δ_0 small) of the pattern through a raster plate having very fine lines (δ_r small) is shown in Fig. 72b. A photograph made with a larger aperture δ_0 giving a flat field is shown in Fig. 72c which may be compared with the image Fig. 72d made without raster and the same aperture δ_0. In all practical cases the infinitely repetitive spectrum of the response $r_{\beta_r 0}$ is limited by the finite response r_{β_0} of apertures *preceding* the raster, because the overall

† Electrically known as "sidebands."

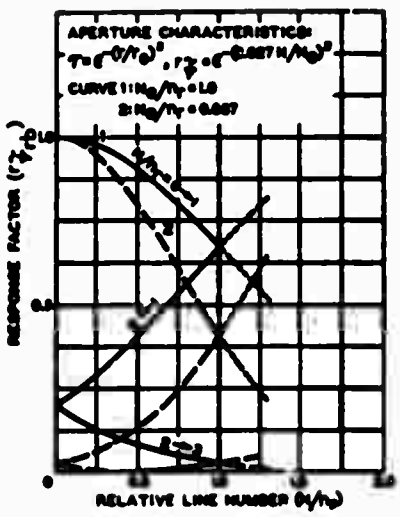

Fig. 73. Construction of repetitive spectrum by "folding" of response characteristic.

response of the entire imaging system $r\delta_{(p)} = r\delta_a r\delta_b r\delta_r$ becomes zero when the response factor $r\delta_a$ is zero.

4. Sine-Wave Spectrum and Equivalent Passband $N_{a(s)}$ for Random Deviations

For the analysis of deviations it is unnecessary to examine the waveform and phase distortion caused by the raster (to be discussed in Part IV of this paper), because the distribution of sine-wave components in a source of deviations is random. The sine-wave spectrum for deviations is, hence, obtained by arranging all sine-wave components in order of their line number, combining response factors at equal line numbers by a quadrature addition (square root of the sum of the squares). This process has been carried out for a variety of aperture combinations δ_a and δ_b having exponential cross sections $\tau = e^{-(x/r_a)^2}$ and a sine-wave response $r\delta = e^{-0.693(N/N_a)^2}$ (Fig. 44, Part II) which is a satisfactory equivalent for optical processes. The repetitive section of raster and aperture response characteristic $r\delta_{rb}$ can be constructed by "folding" the normal response characteristic into the range $N/n_r = 0$ to 1 as illustrated in Fig. 73 for two aperture sizes $N_a/n_r = 1$ and $N_a/n_r = 0.667$.

Overall sine-wave spectra computed for various combinations of aperture sizes are shown in Figs. 74a to 74c. When both apertures δ_a and δ_b are large, i.e., when N_a is smaller than the raster constant ($N_a/n_r = 0.5$ in Fig. 74a), the sine-wave spectrum is substantially the same as without raster; when $N_{a(b)}$ is increased, the high-"frequency" components increase considerably faster than without raster and show periodic maxima and minima. These variations decrease when $N_{a(a)}$ is increased (Fig. 74b), and disappear substantially for values $N_{a(a)} = 1$ (Fig. 74c). It is concluded that the addition of a raster process may increase the normal sine-wave response and extend the aperture passband to higher line numbers even for the "flat-field" condition $N_{a(a)} = N_{a(b)} = 0.67\ n_r$ (Fig. 74b) The raster can, therefore, have a substantial *negative aperture effect* which increases the intensity and edge sharpness of the reproduced grain structure in the y-coordinate.

The equivalent passband $N_{a(s)_e}$ of the raster process is the integral of squared response factors (Eq. (28), Part II) determined from the total sine-wave response of the system. The computation of the integral for various aperture combinations can be simplified by calculating the *rms response* of δ_b for the repetitive section $N/n_r = 0$ to 1. The rms response factor $[r\delta]_b$ at each input line number (Fig. 75) is obtained by a quadrature addition of associated sine-wave components (shown in Fig. 73). Because this response is repetitive, the integral

$$N_e = \int_0^\infty ([r\delta]_b r\delta_a)^2 d(N/n_r)$$

can be evaluated within the limits $N/n_r = 0$ and 1 from

$$N_{a(s)_e} = \int_0^{N/n_r=1} ([r\delta]_b [r\delta]_a)^2 d(N/n_r) \quad (58)$$

where $[r\delta]_a$ is the rms value of response factors of δ_a, coordinated by folding the

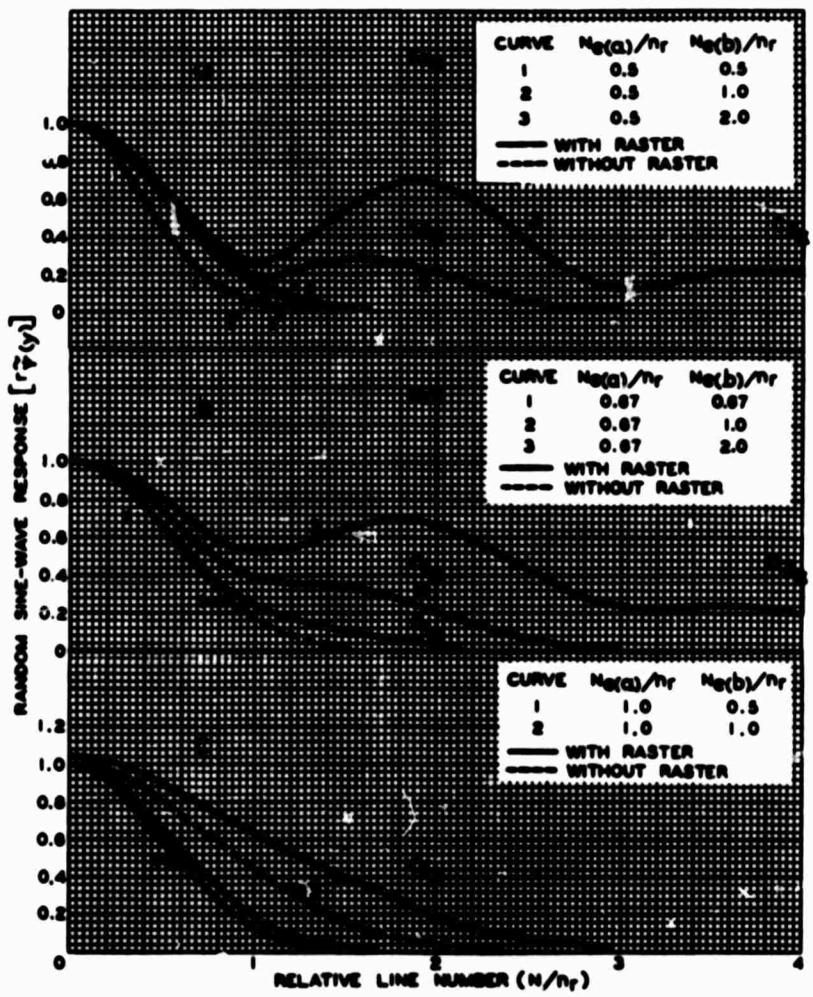

Fig. 74. Overall sine-wave spectra of raster processes for various aperture sizes δ_a and δ_b.

response characteristic $r\bar{\gamma}_a$ into the limits $N/n_r = 0$ to 1. The values $[r\bar{\gamma}]_a$ and $[r\bar{\gamma}]_b$ are identical when $\delta_a = \delta_b$. The products of various aperture combinations are, thus, easily computed from Fig. 75. The equivalent passbands $N_{e(a')}$ of the system are plotted in Fig. 76 as a function of the passband $N_{e(a)}/n_r$ of the analyzing aperture δ_a with $N_{e(b)}/n_r$ as a parameter. Examination of these functions reveals the following facts.

(a) *When both $N_{e(a)}$ and $N_{e(b)}$ are smaller than $0.7n_r$* the aperture flux at successive raster points is correlated sufficiently (overlapping) to eliminate the effect of the raster. The equivalent passband

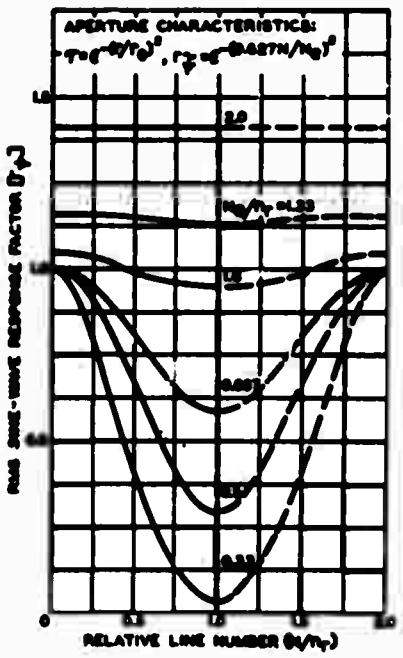

Fig. 75. Rms response of apertures and raster to sine-wave signals.

$N_{c(t)_0}$ of the process can then be computed from the normal aperture response without raster or may be approximated with good accuracy by the cascade formula:

$$1/N_{c(t)_0} = (1/N_{c(a)^2} + 1/N_{c(b)^2})^{\frac{1}{2}} \quad (59)$$

(*b*) *When one or both values* $N_{c(a)}$ *or* $N_{c(b)}$ *are greater than* n_r, the aperture flux is no longer correlated by at least one aperture, and the equivalent passband of the process can be computed with good accuracy from the product.

$$N_{c(t)_0} \simeq (N_{c(a)} N_{c(b)})/n_r \quad (60)$$

(*c*) *For all other values* the aperture flux is partially correlated and the value $N_{c(t)_0}$ should be computed as outlined above or may be approximated by the values computed for exponential aperture characteristics (Fig. 76). It should be mentioned that a square aperture presents a special case because of its strongly periodic aperture response and large number of terms which cause periodic deviations from the characteristics shown in Fig. 76. The square aperture is of interest as a mathematical equivalent, but its characteristics are in many cases undesirable for practical processes. The greatly enlarged reproduction of a photographic grain structure by point- and line-raster processes is illustrated in Fig. 77. The original grain structure is shown in Fig. 77a. The samples "seen" through a fine point raster plate (δ_0 small) are shown in Fig. 77b; their reproduction by a square aperture providing a "flat" field is shown in Fig. 77c. Reproduction of the same grain structure by a line-raster process using a square reproducing aperture is shown in Figs. 77d and e. The higher horizontal definition obtained with a vertical slit aperture is illustrated by Fig. 77f.

A comparison of a line-raster process (a) using a round $\cos^2$ aperture δ_0 with a continuous process (b) using the same apertures is shown with a lower magnification in Fig. 78. The slight increase in vertical sharpness by the raster process (a) observed in the originals will probably be lost in the printing process.

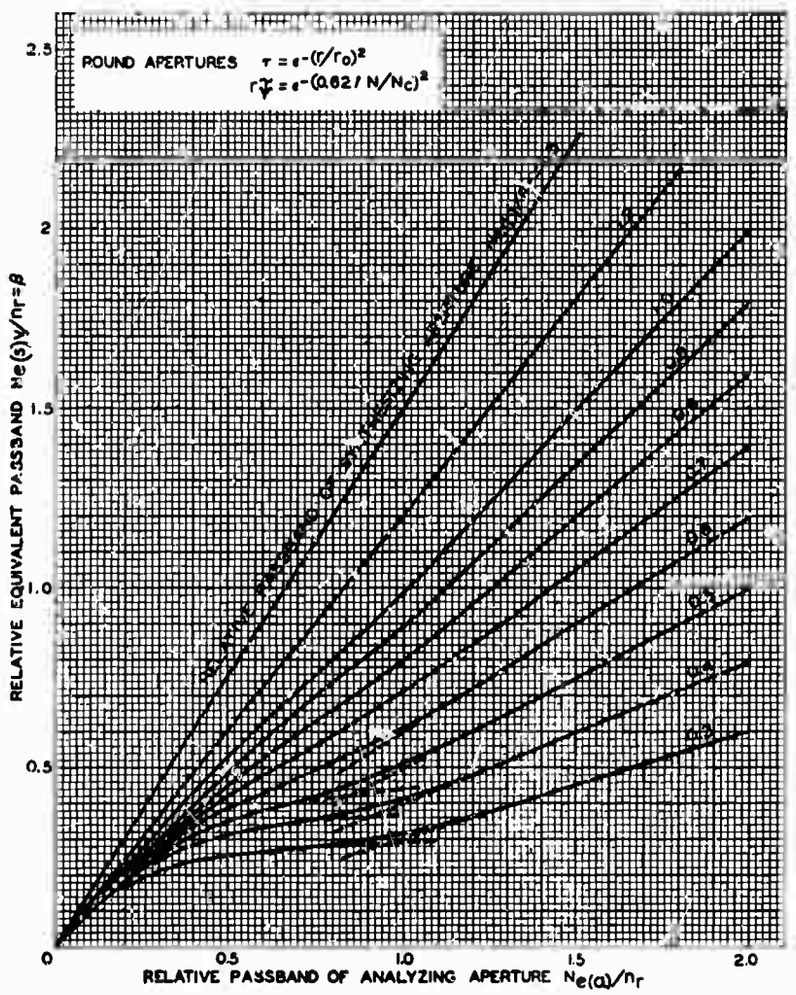

Fig. 76. Equivalent relative passband (β) of systems containing a raster process as a function of the relative passband $N_{e(a)}/n_r$ of the analyzing aperture δ_a for various relative passbands $N_{e(b)}/n_r$ of the synthesizing aperture δ_b.

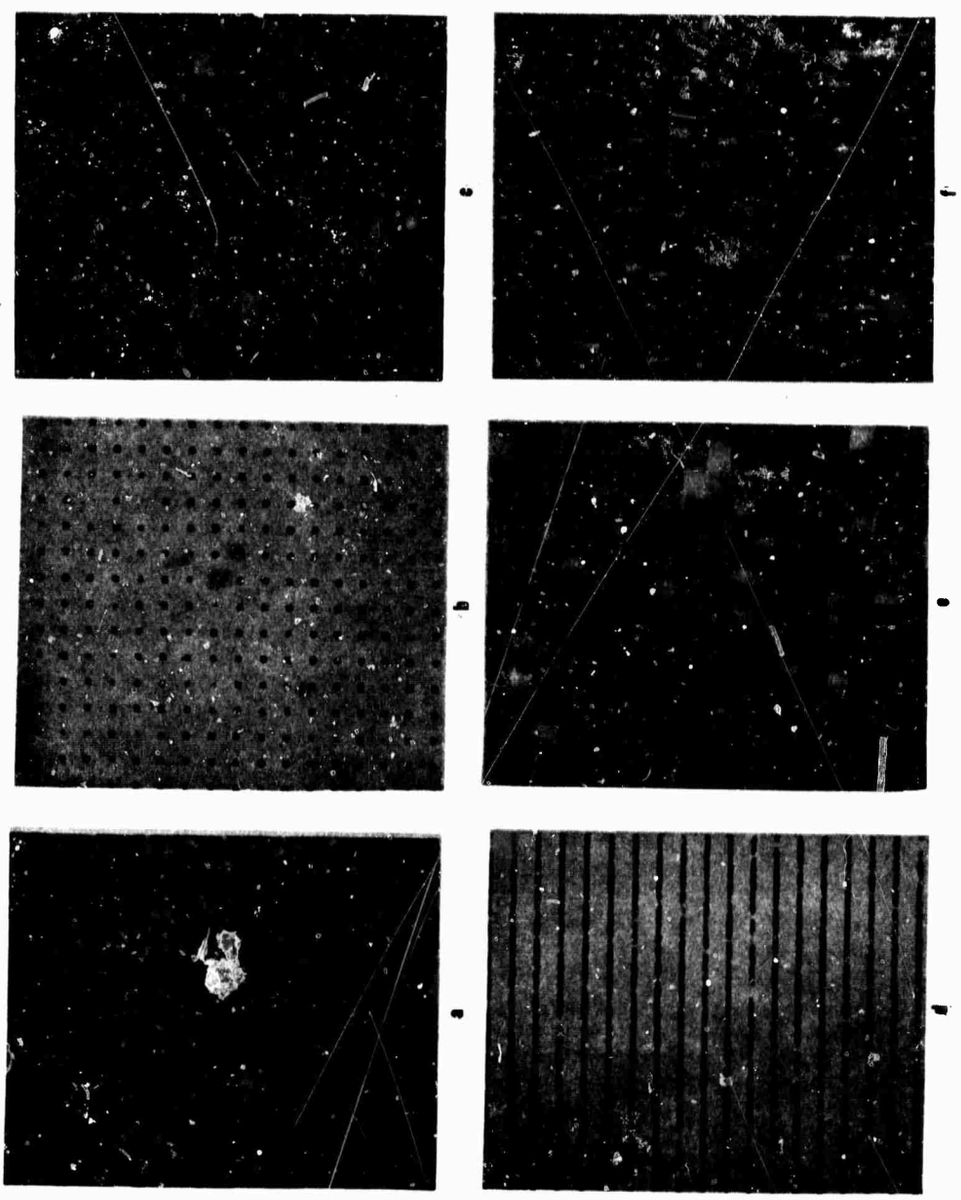

Fig. 77. Reproduction of photographic grain structure by point- and line-raster processes with rectangular apertures (highly magnified).

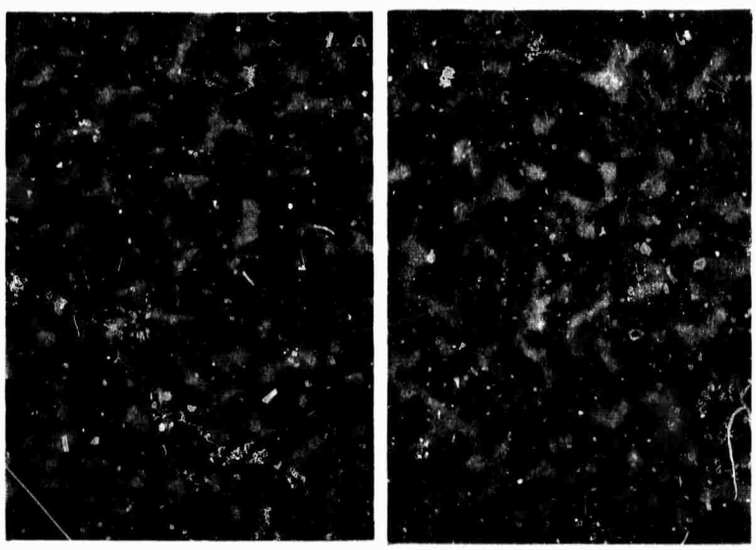

Fig. 78. Grain structure reproduced (a, at left) with, and (b, at right) without line-raster process by a round $\cos^2$ aperture.

NOTE: Figures 85 and 109 now follow on this coated paper insert. Figures 79, etc., are arranged below as best possible for nearness to pertinent text.

C. ELECTRICAL CONSTANTS AND APERTURES OF TELEVISION SYSTEMS

1. Frequency and Line Number

The transmission of two-dimensional images over an electrical frequency channel is based on a conversion of lengths into units of time. To effect this conversion, television systems make use of a horizontal-line raster scanned by a single aperture. The signals of all aperture positions in the raster are transmitted in sequence because of a time-proportional displacement of the aperture along the raster lines. The correlation of length and time units depend obviously on the dimensions of the raster, the order in which the raster lines are scanned, and the time T_f assigned for the transmission of one picture frame. The principal relations are illustrated in Fig. 79 for a raster constant $n_r = 12$ and the normal frame aspect ratio $H/V = 4/3$. A time allowance must be made for synchronizing signals and the finite return periods of the scanning apertures. These time percentages are the "blanking" periods t_{b_e} and t_{b_A} in Figs. 79b and c which correspond to the blanking margins b_A and b_e in Fig. 79a.

The length unit l is the vertical frame dimension V, as indicated in Fig. 79a. In the vertical coordinate the length l or any subdivision down to $\Delta l = 1/N_e = 1/n_r$ corresponds to relatively long time intervals, i.e., low electrical frequencies.

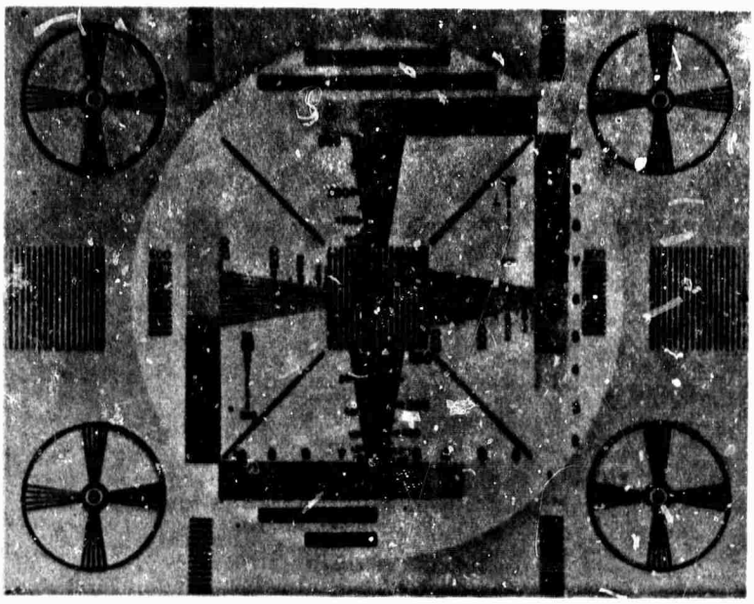

Fig. 85a. Composite print made by a photographic synthesis (Fig. 84).

Fig. 85b. Enlarged section of Fig. 85a showing edge "transients" in two coordinates.

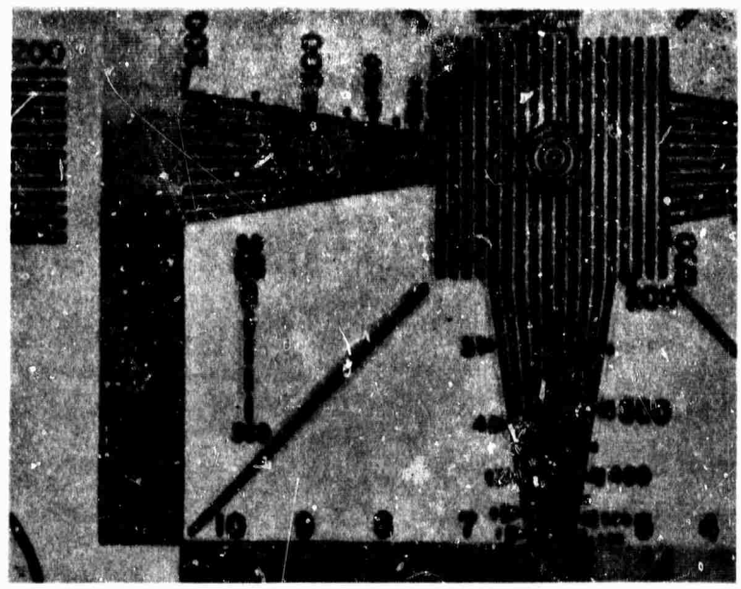

Fig. 85c. Addition of optical line-raster process to Fig. 85b.

A test pattern with $N_v = 2$ (right side of Fig. 79a) filling the entire frame area generates the video signal illustrated in Fig. 79b. The electrical frequencies f_v required for the reproduction of vertical sine-wave samples N_v are determined by the raster constant n_r. The highest electrical frequency $f_{v\,max}$ is generated when the signal amplitudes in *successively traced*† raster lines alternate between two values. One period is, therefore, completed in the time $2t_h = 2T_f/n_r$ (see Fig. 79b).

In all properly operating television systems the electrical sine-wave response is unity and is without phase error from the frame frequency $(1/T_f)$ on upwards to far beyond the frequencies occurring in the reproduction of vertical sine-wave samples. The sine-wave response, therefore, does not enter as a factor limiting the vertical sine-wave response of the television system. *The vertical response of the television system* is determined entirely by the raster constant n_r and the two-dimensional system apertures as described in the preceding section.

In the horizontal coordinate the length unit $l = V = 3/4H$ (see Fig. 79c) and the length of half-waves l/N_h in a sine-wave test pattern are scanned in very short time intervals t_{N_h} corresponding to high electrical frequencies. The spatial frequency of the optical test pattern wave has the value $0.5N_h/l$. The horizontal time unit is three fourths of the active line time, and the electrical frequency corresponding to a line number N_h is therefore:

† It is noted that successively traced raster lines in a 2 to 1 interlaced raster are either the even or the odd numbered raster lines which correspond to a test pattern line number $n_r/2$. Without interlacing, the frequency f_v max has the same value but the test pattern line number producing it is equal to n_r. With 2 to 1 interlace, a line number equal to n_r causes constant amplitude signals in one complete field and constant signals of different amplitude in the following field.

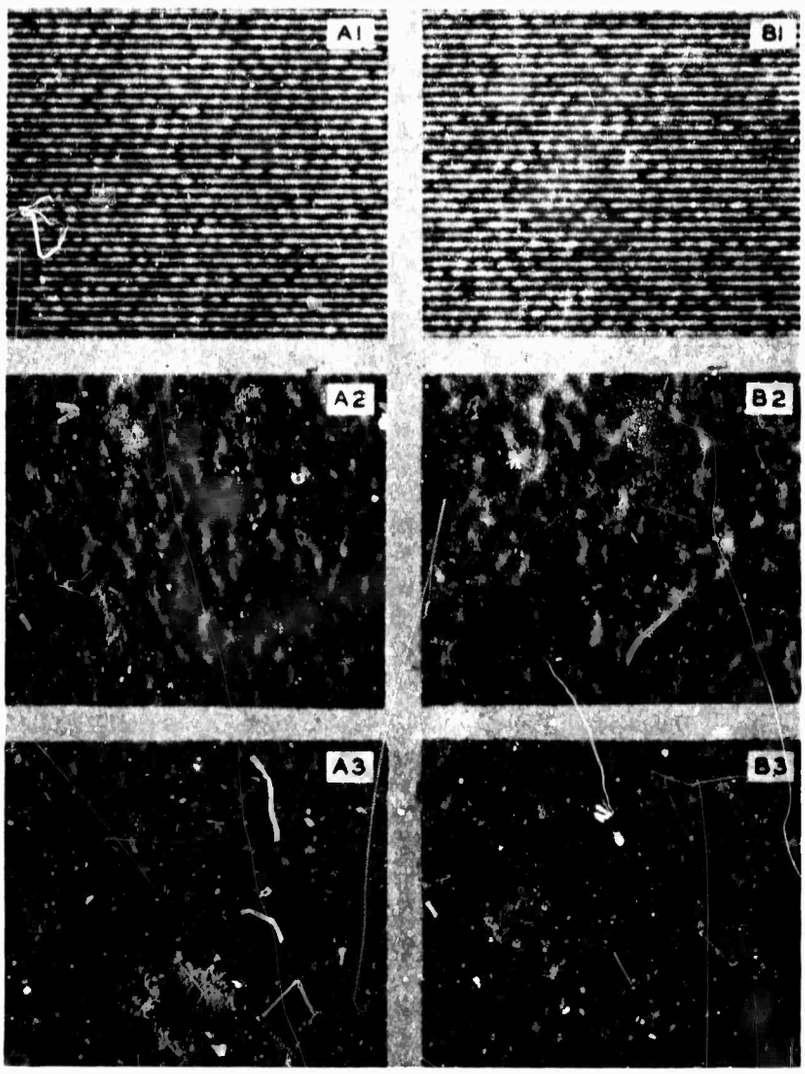

$$f_h = 0.5c\, N_h n_r / T_f \text{ cycles/sec} \quad (61)$$

where

T_f = Frame time in seconds ($\frac{1}{30}$ sec in standard television system)
n_r = Number of active raster lines in frame area
N_h = Horizontal line number
$c = (H/V)/(1 - b_h)(1 - b_v)$; the standard value is $c = (4/3)/(0.84 \times 0.935) = 1.7$

The total number of scanning lines including the inactive lines in the blanking margin b_v is usually stated as the scanning line number of the system, which is

$$n_s = n_r/(1 - b_v) = 1.07\, n_r \quad (62)$$

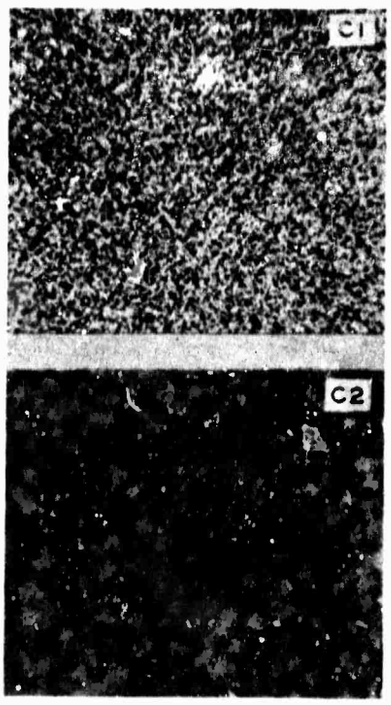

Fig. 109, A1–3 and B1–3 at left, and C1 and C2 above. Grain structures of television and motion-picture processes.

2. Theoretical Passband and Aperture (δ_f) of Television Systems

The video frequency channel of the television system is determined by the frame time T_f, the raster constant n_r, and the desired horizontal cutoff resolution $N_{e(h)}$ of the system; it is given for normal blanking percentages by the relation

$$\Delta f = 0.85\, N_{e(h)} n_r / T_f \text{ cycles/sec} \quad (63)$$

The product $(N_{e(h)} n_r)$ corresponds to the square of the equivalent passband $\bar{N}_e^2 = (N_{e(h)} N_{e(v)})$ of an optical aperture. The relation between the theoretical passband Δf of a television channel and its optical equivalent $\bar{N}_{e(f)}$ is, therefore:

$$\bar{N}_{e(f)} = (N_{e(h)} n_r)^{\frac{1}{2}} = K(\Delta f)^{\frac{1}{2}} \quad (64)$$

For normal blanking percentages the proportionality factor has the value $K = (T_f/0.85)^{\frac{1}{2}}$. The product $(N_{e(h)} n_r)$ has the dimension $(\text{length})^{-2}$, and its reciprocal represents a rectangular area of uniform transmittance which may be regarded as an *equivalent point image or sampling aperture of a theoretical television channel.* This equivalent sampling aperture is often referred to as a "picture-element." The term is misleading because the concept of an element implies an invariable intensity distribution in a small area of fixed size. A process which is continuous in one coordinate forms an infinite number of point images and its true "elemental" area is infinitesimal. Only a point raster process can produce an elemental area of finite size.

The concepts of a *two-dimensional aperture δ_f having the exact response characteristic of a theoretical television channel* is useful for an interpretation of electrical random fluctuations (noise) in terms of optical deviations.

Electrical signal-to-noise ratios are usually computed for a given passband Δf having a theoretically sharp cutoff. This evaluation is analogous to the process of sampling a two-dimensional grain structure with a measuring aperture $\delta_m = \delta_f$ of known geometry to determine a reference value $[R]_m$ for the particular random structure (see Part II D). The sources of electrical random fluctuations in a television system (see Fig. 65) can, therefore, be replaced by random particle structures scanned by a hypothetical television camera. The scanning aperture of this camera is infinitesimal and

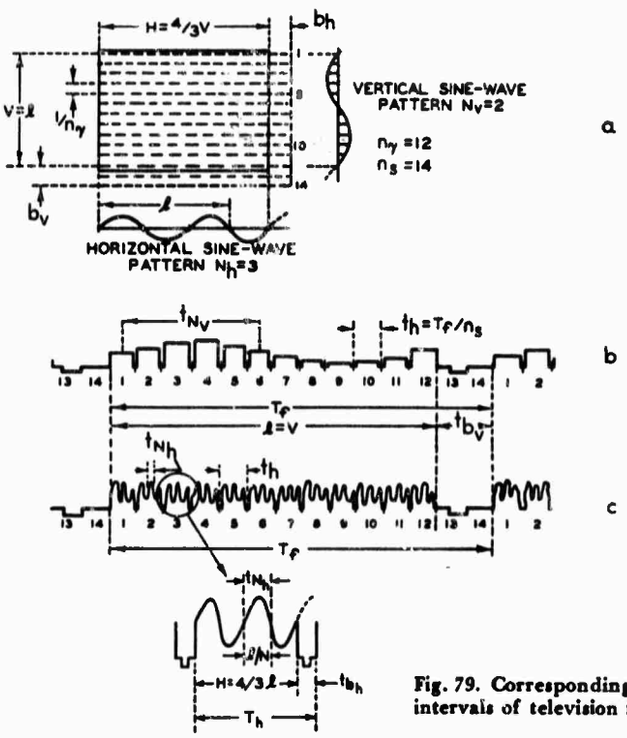

Fig. 79. Corresponding lengths and time intervals of television frame and signals.

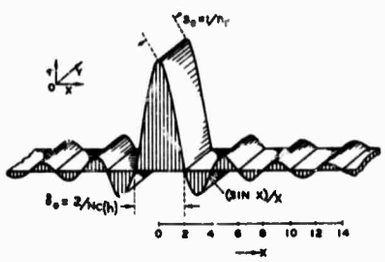

Fig. 80. Equivalent point image or sampling aperture of theoretical television channel.

its output signals are modified by the equivalent passband $\bar{N}_{e(e)}$ of the system elements following the "noise" source. The granularity (noise level) of the structure is computed by assuming that it is scanned with a measuring aperture δ_m = δ_f which must fill the requirements that its signals are indistinguishable from electrical fluctuations in the corresponding theoretical channel Δf. The horizontal sine-wave response of δ_f is, therefore, constant in the passband $N_{e(h)} = N_{e(h)}$, its equivalent vertical passband is $N_{e(v)} = n_r$, and the aperture signals in different raster lines are uncorrelated.

The frequency spectrum of δ_f in the vertical coordinate may be determined as follows: it is assumed for simplicity that no interlacing is used. A vertical cross section in the frame area corresponds to a series of amplitude samples taken from the electrical aperture signal at the line intervals t_h (see Fig. 79). The sampling of constant electrical sine-wave signals by the raster process results in a series of constant sample amplitudes ($N_r = 0$) for

all frequencies which are integral multiples of the line frequency $f_h = 1/t_h$. When the signal frequency is changed by an increment $\Delta' f = f_h/2$, the sample amplitudes alternate between two fixed values at a frequency corresponding to the line number $N_v = n_r$. Frequency increments $\Delta' f$ between $\Delta' f = 0$ and $\Delta' f = f_h/2$ as well as between $\Delta' f = f_h$ and $\Delta' f = f_h/2$ cause a sequence of sample amplitudes identical with those obtained with an aperture sampling optical sine-wave patterns with line numbers from $N_v = 0$ to $N_v = n_r$. The amplitudes of the electrically taken samples vary according to the phase relation between sampling points and sine-wave signal, just as aperture samples depend in magnitude on the relative phase between the raster lines and the optical sine-wave pattern. The electrical samples can, therefore, be attributed to a hypothetical aperture δ_f scanning sine-wave patterns with a line number range $N_v = 0$ to $N_v = n_r$. This range of line numbers is sampled repetitively throughout the video frequency band in every increment $\Delta' f = f_h/2$. Because the electrical response within any one of these small sections of the video passband is substantially constant, the rms values of the aperture signals at any one line number $N_v = 0$ to n_r from all sections $\Delta' f$ are alike. The vertical sine-wave response of δ_f is constant between $N = 0$ and $N = n_r$ and independent of the horizontal response characteristic of the video system.

The raster characteristic (Fig. 70) transforms this limited constant amplitude spectrum into an infinite frequency spectrum (see section B4) which is subsequently limited by the real aperture δ_h following the raster process, and results in an overall response identical with the response characteristic of δ_h. *An electrical "noise" source followed by a "flat" video channel Δf with theoretical rectangular cutoff can, therefore, be replaced by a random particle structure scanned by an aperture δ_f having constant sine-wave response in both x- and y-coordinates within the range of line numbers $N_{e(h)}$ and n_r respectively.* The equivalent passband of this hypothetical scanning aperture is $\bar{N}_{e(f)} = (N_{e(h)} n_r)^{\frac{1}{2}}$ as stated by Eq. (64).

It is of interest to determine the geometric characteristics of this aperture. A harmonic synthesis of the horizontal aperture cross section from its response characteristic (see Eq. 54) shows that the *transmittance* τ_h varies as a $(\sin x)/x$ function (Fig. 80) and has positive and negative portions decaying slowly to zero at infinity.† The central peak between the first zero points has a dimension $\delta_0 = 2/N_{e(h)}$. The aperture transmittance τ_v in the vertical coordinate (y) can be given a rectangular shape with constant transmittance $\tau_v = 1$ and a width $s_0 = 1/n_r$. This dimension meets the requirements $N_{e(v)} = n_r$ and that signals in different scanning lines be uncorrelated. The continuous sine-wave response (in y) of this rectangular aperture has a $(\sin x)/x$ form with a first zero at $N_v = 2n_r$. In conjunction with the raster characteristic, however, the $(\sin x)/x$ response produces a frequency spectrum identical with that from a constant aperture response in the range $N/n_r = 0$ to 1. The $(\sin x)/x$ response "folded" into this range results in unity rms response factors when the response factors of all input frequencies giving the same output frequency, are combined.

3. Horizontal Sine-Wave Response and Aperture Characteristics of Electrooptical Systems

(*a*) *General Formulation.* The principal elements determining the horizontal response characteristic of a television system are indicated in the block diagram Fig. 65. The horizontal sine-wave response of television systems can be made very dissimilar to that of optical systems by adjustment of the response

† An optical synthesis of images with apertures containing negative flux components is discussed in the following section.

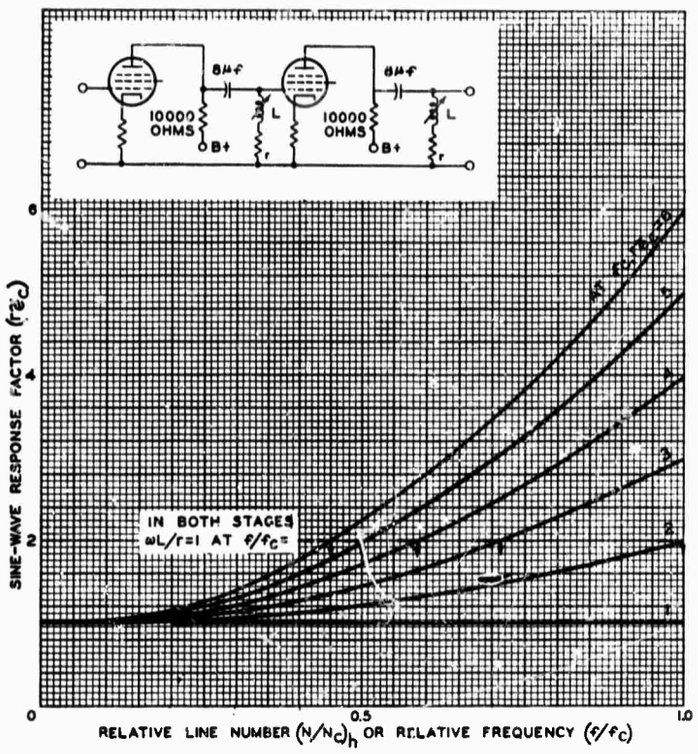

Fig. 81. Aperture correction circuit and response characteristics.

characteristic $r_{\bar{z}}$ of the video system. The response of amplifiers and filter circuits is normally constant within a substantial portion of their passband but can also be given a rising characteristic by corrective networks. The sine-wave response $r_{\bar{z}c}$ of a two-stage amplifier circuit for correcting the sine-wave response of camera tubes is shown in Fig. 81. A phase-correcting circuit is used in conjunction with the amplitude-correcting circuits. Electrical networks of this type are termed *aperture-correction circuits* because they can completely or partially compensate the decreasing horizontal response $r_{\Psi h}$ of two-dimensional apertures. The horizontal response of an electrooptical system is given in general by

$$r_{\Psi(v)h} = (r_{\bar{z}} r_{\Psi})_{(N/N_c)h} \qquad (65)$$

where

$r_{\bar{z}}$ = $(r_{\bar{z}12} r_{\bar{z}c} r_{\bar{z}f})_{(f/f_c)}$ = overall electrical response characteristics

$r_{\bar{z}12}$ = $r_{\bar{z}1} r_{\bar{z}2}$ = response of preamplifier ($r_{\bar{z}12} = 1$ for an equalized preamplifier, see discussion in 3(*c*)

$r_{\bar{z}c}$ = response factor of aperture correction circuits (Fig. 81)

$r_{\bar{z}f}$ = response factor of low-pass filter (Fig. 82)

$N_{c(h)}$ = horizontal cutoff resolution (Eq. 63))

r_{Ψ} = $(r_{\Psi(a)} r_{\Psi(b)})_{(N/N_c)h}$ = response characteristic of all two-dimensional system apertures.

(*b*) *Apertures and Aperture Effects of Electrical Elements.* An aperture correction $r_{\bar{z}c} = 1/r_{\Psi}$ results in a system response equal to that of the cutoff filter:

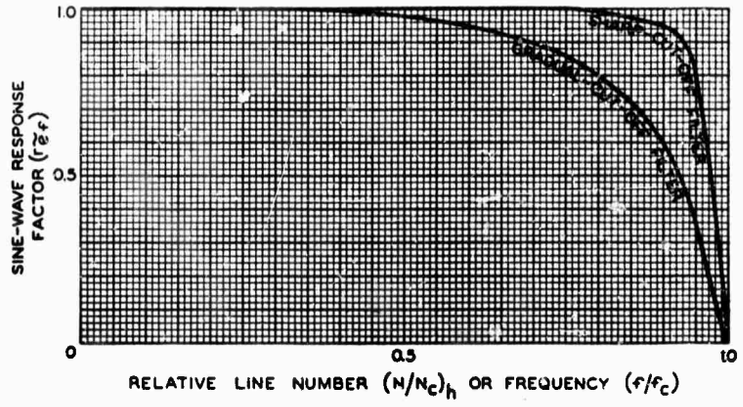

Fig. 82. Sine-wave response of electrical low-pass filters.

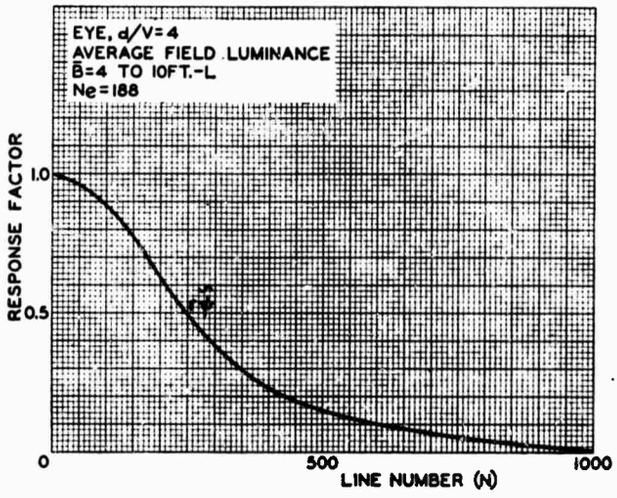

Fig. 83. Sine-wave response of the eye at moderate brightness levels and a viewing distance $d = 4V$.

$r_{\psi(e)} = r_{zf}$. The degree of aperture correction permissible in a particular case depends on the horizontal resolution $N_{e(h)}$ of the television system and the viewing distance which determines the relative aperture response of the eye. When the cascaded response characteristic $r_{\psi(e)}r_{\psi_{eye}}$, *including the visual system*, departs markedly from that of an optical aperture (excessive high-frequency response), the corresponding retinal point-image has abnormal characteristics because it has a transmittance (τ_a) with negative portions (compare Fig. 80). Such apertures cause edge transitions distorted by "transient" overshoots or oscillations, and result in a relief effect or multiple contour lines. It is not difficult

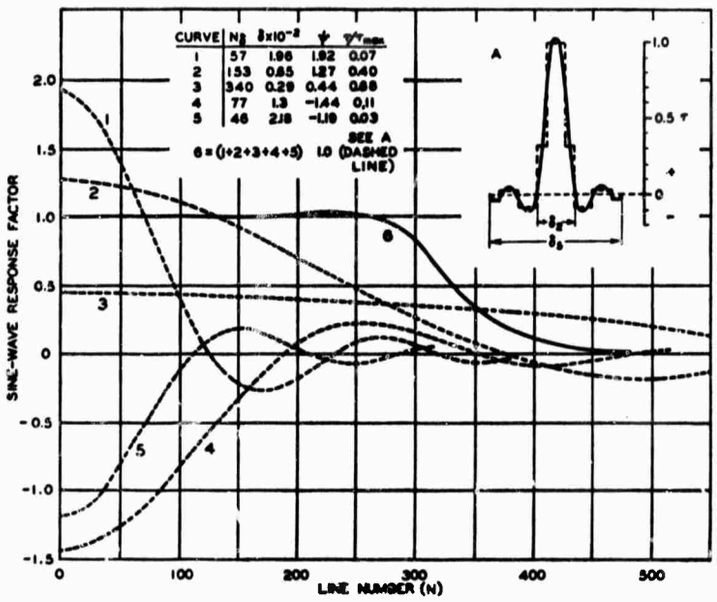

Fig. 84. Synthesis of a "flat"-response characteristic with sharp cutoff by addition of 3 positive- and 2 negative-response characteristics of round apertures with uniform transmittance.

to see that a system response $r\psi_{(s)}$ extending beyond two-thirds of the passband of the eye (see Fig. 83) can be given a constant value with sharp cutoff without causing an abnormal overall response in the retinal image. When the cutoff of the television system, however, occurs in the lower half of the visual passband, due to low system resolution or close viewing distances, aperture correction must be limited to a system response $r\psi_{(s)}$ having more gradual cutoff, to prevent abnormal optical conditions in the retinal image.†

The effects of apertures having negative transmittance can be demonstrated by a photographic correction process. The response characteristic (6) of the point image shown in Fig. 84, for example, can be synthesized by superimposition of three positive and two negative components. Images can be synthesized by two sets of out-of-focus projections with appropriate lens stops. The positive-aperture effects are combined in one plate by a triple exposure. The negative-aperture plate is made by a double exposure with positive apertures and reversed in polarity in a contact print. A composite print from the positive and negative plates in register is shown in Figs. 85a and b and illustrates the transients and sharp cutoff (in both image coordinates) produced by the response

† This subject will be discussed further in Part IV.

Figures 85a, 85b and 85c are on plate pages 116 and 117.

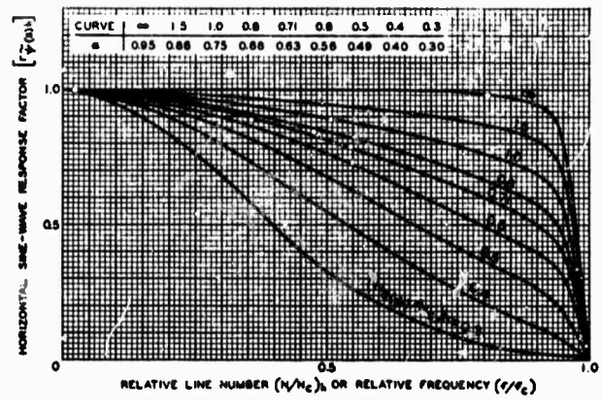

Fig. 86a. Normalized response characteristics for "flat" channel with sharp-cutoff filter (Fig. 82) in cascade with exponential apertures and 1× aperture correction (Fig. 81).

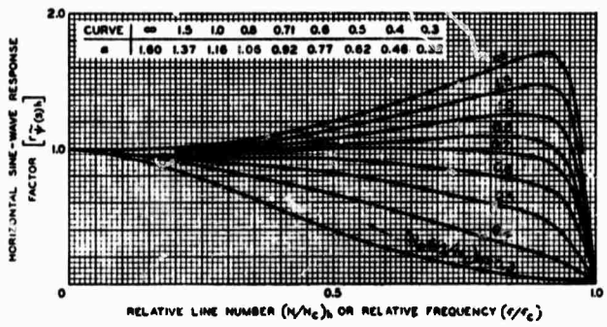

Fig. 86b. Normalized response characteristics for "flat" channel with sharp-cutoff filter (Fig. 82) in cascade with exponential apertures and 2× aperture correction (Fig. 81).

characteristics, Fig. 84. The similarity with an over-compensated television process can be increased by the addition of a raster process as shown in Fig. 85c. At increased viewing distances the undesirable transients disappear, because the overall response is then given a normal shape by the eye characteristic.

(*c*) *Generalized Response and Aperture Characteristics.* The sine-wave response characteristics of electrooptical systems have been computed in normalized units as a function of system parameters to simplify numerical evaluation. The curve families Figs. 86 and 87 are plots of Eq. (65) for an electrical response r_3 with four values of aperture correction and two different filter characteristics, in cascade with various optical apertures. The cascaded response of all two-dimensional apertures in the system under consideration is closely approximated by the response characteristic $r_{(\psi)}$ of one equivalent exponential aperture (Fig. 44 and Table VII, Part II). The parameter $(N_{a(\psi)}/N_c)_h$ specifies the equivalent pass-

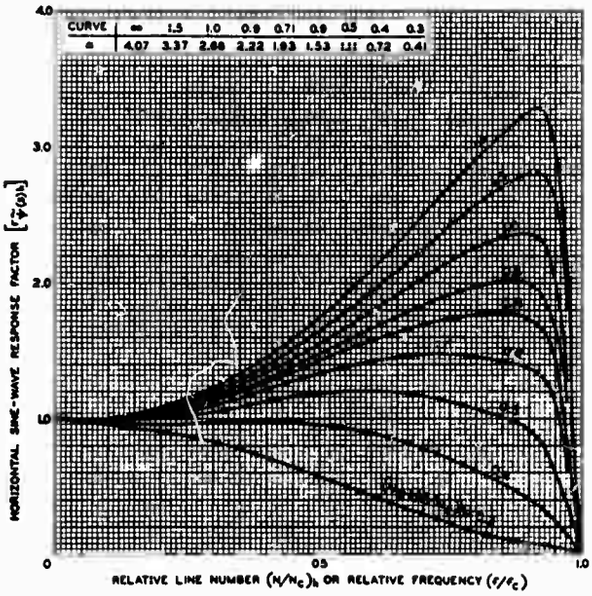

Fig. 86c. Normalized response characteristics for "flat" channel with sharp-cutoff filter (Fig. 82) in cascade with exponential apertures and 4× aperture correction (Fig. 81).

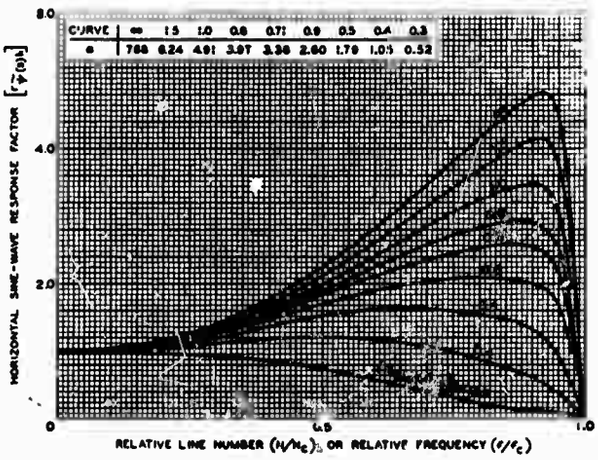

Fig. 86d. Normalized response characteristics for "flat" channel with sharp-cutoff filter (Fig. 82) in cascade with exponential apertures and 6× aperture correction (Fig. 81).

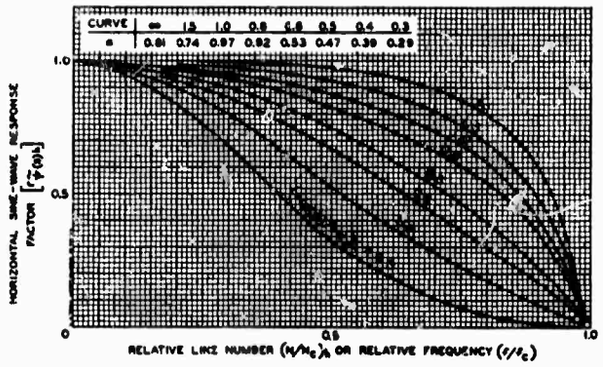

Fig. 87a. Normalized response characteristics for "flat" channel with gradual-cutoff filter (Fig. 82) in cascade with exponential apertures and 1× aperture correction (Fig. 81).

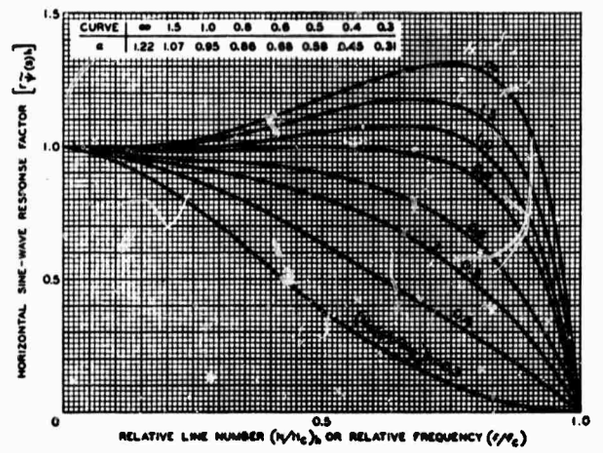

Fig. 87b. Normalized response characteristics for "flat" channel with gradual-cutoff filter (Fig. 82) in cascade with exponential apertures and 2× aperture correction (Fig. 81).

band of this aperture relative to the theoretical bandwidth $N_{c(h)}$ of the electrical system. The equivalent passband $N_{e(e)h}$ of the response characteristics is specified likewise in relative units by the ratio $\alpha = (N_{e(e)}/N_c)_h$ defined as the *bandwidth factor* in section D1.

If the system is considered as a purely electrical network, the *aperture transmittance* τ_h *of the system* is its response to a single impulse of infinitesimal duration. The optical equivalent is the response of the electrooptical system to isolated lines of infinitesimal width. The impulse shapes or aperture cross sections (transmittance τ_h) corresponding to the response characteristics Figs. 86 and 87 have been computed by a Fourier synthesis (Eq. (54)) which is valid for the condition of zero phase shift or a linear

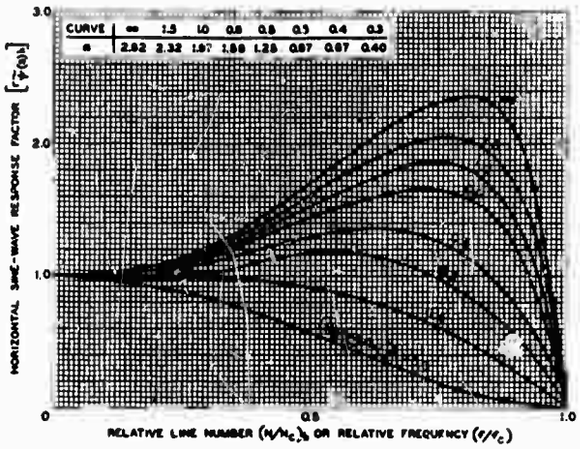

Fig. 87c. Normalized response characteristics for "flat" channel with gradual-cutoff filter (Fig. 82) in cascade with exponential apertures and 4× aperture correction (Fig. 81).

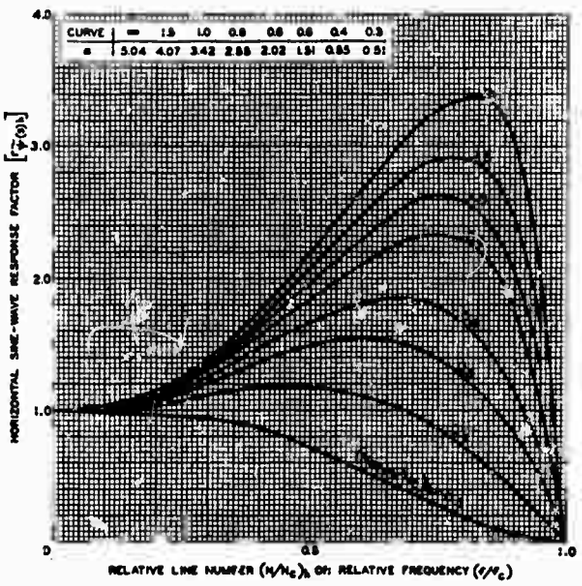

Fig. 87d. Normalized response characteristics for "flat" channel with gradual-cutoff filter (Fig. 82) in cascade with exponential apertures and 6× aperture correction (Fig. 81).

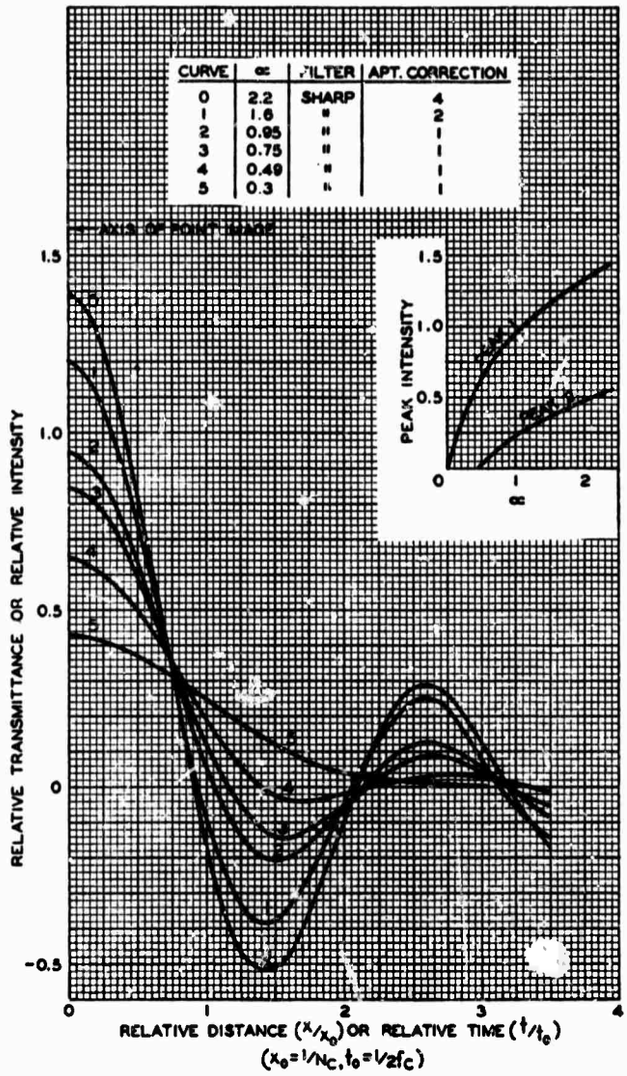

Fig. 88. Impulse forms or aperture transmittance obtained with response characteristics Figs. 86 and 87.

phase delay within the system passband. The aperture cross section (τ_A) depends, again, on the relative equivalent passband (α) as shown in Fig. 88.

Phase distortion between sine-wave components can occur in electrical and also in optical elements (lenses, etc.). In terms of aperture properties it is caused by an asymmetric aperture transmittance (coma for example) and results

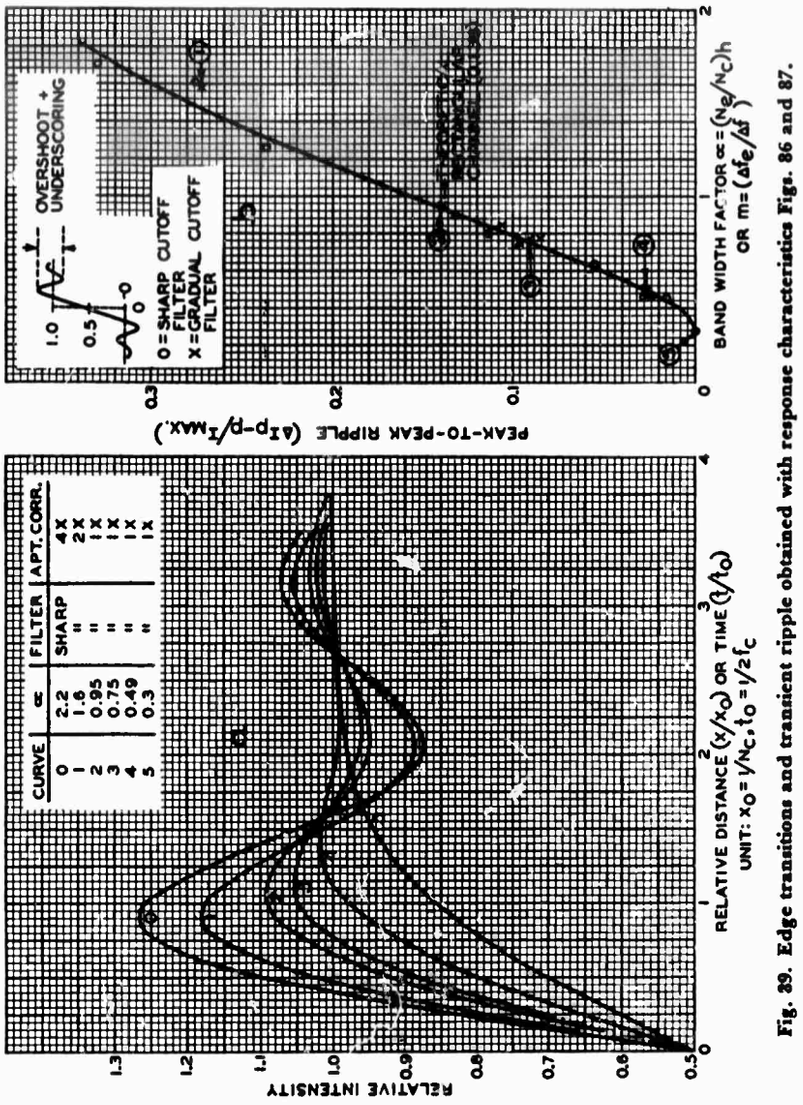

Fig. 39. Edge transitions and transient ripple obtained with response characteristics Figs. 86 and 87.

in asymmetric edge transitions. Phase distortion is of little importance in the transfer of random deviations, but it is an important aperture property determining waveform distortion. The measurement and effects of phase distortion will be discussed with the subjects of image sharpness and definition in Part IV of this paper.

The electrical response to a step function, or the corresponding electrooptical response to a sharp edge, is obtained by integration of

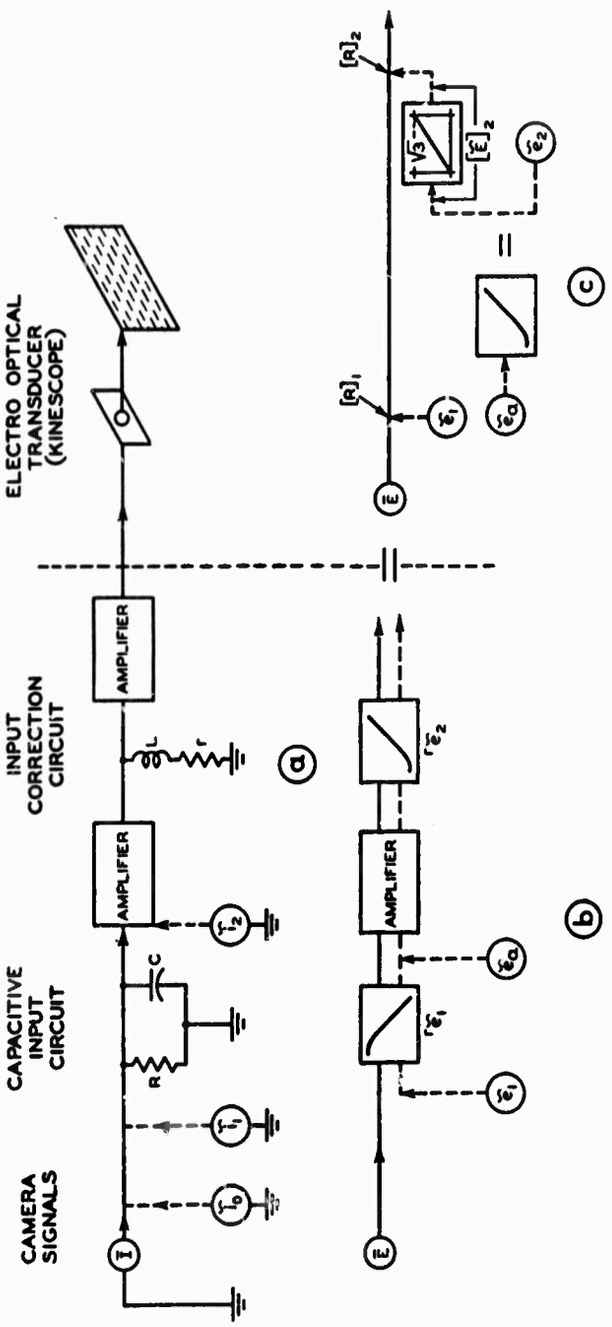

Fig. 90. Camera circuits and noise sources.

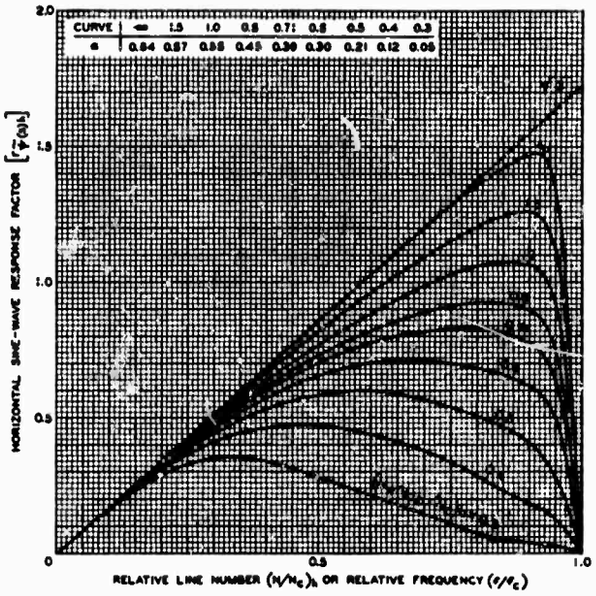

Fig. 91a. Normalized response characteristic for "peaked" channel with sharp-cutoff filter (Fig. 82) in cascade with exponential apertures and 1× aperture correction (Fig. 81).

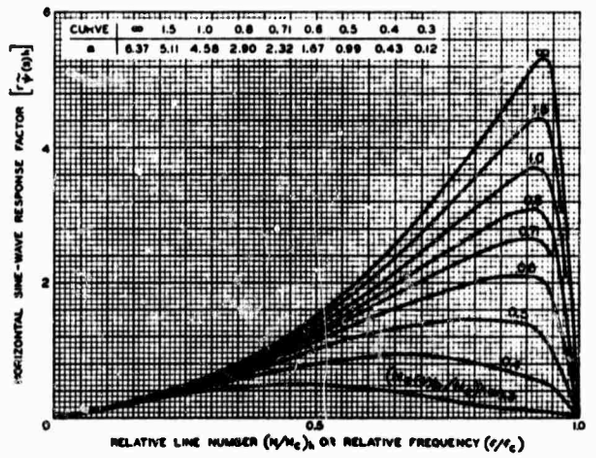

Fig. 91b. Normalized response characteristic for "peaked" channel with sharp-cutoff filter (Fig. 82) in cascade with exponential apertures and 4× aperture correction (Fig. 81).

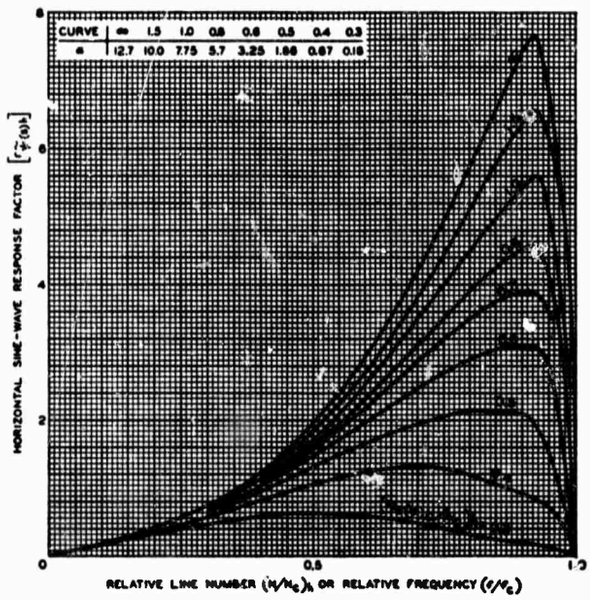

Fig. 91c. Normalized response characteristic for "peaked" channel with sharp-cutoff filter (Fig. 82) in cascade with exponential apertures and 6× aperture correction (Fig. 81).

the impulse function and shown in Fig. 89a for zero phase distortion. The normalizing or "filtering" effect of larger two-dimensional apertures (low α) in cascade with the "abnormal" electrical response characteristics is evident. *The peak-to-peak transient* ripple can be estimated from the α-value by the curve shown in Fig. 89b.

The response characteristics Figs. 86 and 87 include a complete video system and are required for calculation of signal-to-deviation ratios originating in electrical sources ahead of the video amplifier or in photographic grain patterns ahead of the television system. Fluctuations ($\bar{i}_0$) (see Fig. 65) in the photo-emission current of the camera tubes are usually of negligible magnitude compared to fluctuations ($\bar{i}_1$) originating in the camera tube beam-current or in the current of the first amplifier stage. (Fluctuations ($\bar{i}_t$) introduced later in the process of signal transmission (radio links, etc.) vary in magnitude according to distance and will be assumed negligible in this analysis.) The location of the dominating source $\bar{i}_1$ in the system is shown in more detail in Fig. 90a. The diagram Fig. 90b indicates the response characteristic $r_{\bar{z}1}$ of the capacitive input circuits in which the response decreases with frequency, and following the response characteristic $r_{\bar{z}2}$ (high-peaking circuit) by which the signal response is again corrected to a constant-amplitude response $r_{\bar{z}1}r_{\bar{z}2} = r_{\bar{z}12} = 1$. The equivalent diagram Fig. 90b illustrates that fluctuations $\bar{i}_1$ originating in a camera tube have a constant-amplitude frequency spectrum and are termed *flat channel noise*. Fluctuations $\bar{i}_a$ from the first video amplifier are modified in the input-correction circuit to have a sine-

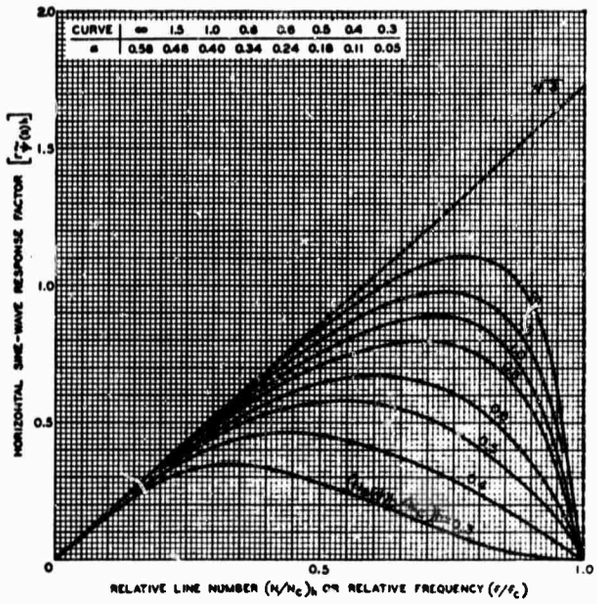

Fig. 92a. Normalized response characteristic for "peaked" channel with gradual-cutoff filter (Fig. 82) in cascade with exponential apertures and 1× aperture correction (Fig. 81).

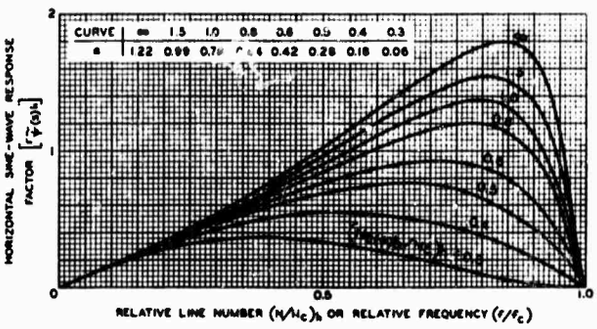

Fig. 92b. Normalized response characteristic for "peaked" channel with gradual-cutoff filter (Fig. 82) in cascade with exponential apertures and 2× aperture correction (Fig. 81).

wave spectrum with amplitudes proportional to frequency. *This type of fluctuation is termed peaked-channel noise.* The response factor of the theoretical triangular characteristic with sharp cutoff has been normalized to the value $r_{\mathcal{Y}1} = \sqrt{3}$ at $N = N_{c(h)}$ to obtain $N_{e1} = N_{e(h)}$ for the theoretical condition (see section D2.) In cascade with aperture correction circuits ($r_{\mathcal{Y}c}$), the cutoff filter ($r_{\mathcal{Y}f}$), and the apertures ($r_{\mathcal{Y}(b)}$) following the electrical system, the frequency spectrum

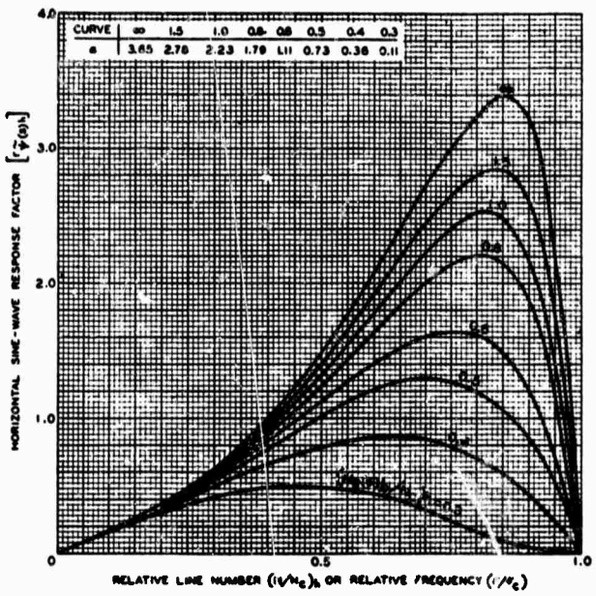

Fig. 92c. Normalized response characteristic for "peaked" channel with gradual-cutoff filter (Fig. 82) in cascade with exponential apertures and 4× aperture correction (Fig. 81).

for peaked channel noise is modified to the forms shown by the normalized response characteristics Figs. 91 and 92.

In the Fourier synthesis of the corresponding aperture transmittance (or impulse shape), the cosine terms are changed to negative sine terms because of a 90° phase shift in the reactive circuit (except for the lowest-frequency terms which can be neglected because of their small amplitude). The impulse waveform or horizontal-aperture transmittance of these characteristics is, therefore, a differentiated pulse as shown in Fig. 93 (obtained by differentiating the corresponding flat-channel pulse shapes (Fig. 88)).

4. Aperture Response of Camera Tubes and Kinescopes

The sine-wave response of *television camera tubes* is measured with the help of vertical and horizontal cross-section selector circuits[3] using sine-wave test patterns or a conversion from square-wave response characteristics. The sine-wave response is determined primarily by the aperture characteristic of an electron beam but is modified by a number of secondary aperture effects, such as image-plate granularity, out-of-focus conditions (particularly in iconoscope and image-iconoscope types which have inclined targets), or the aperture of electron-image sections.

The sine-wave response of camera tubes, decreases, therefore, more rapidly than that of a kinescope and the effective aperture is a composite of several exponential ($\epsilon^{-(r/r_0)^2}$) spot sizes. The sine-wave response of a typical camera tube is shown in Fig. 94. Although measured recently on image orthicons having 3-in. faceplates this characteristic may be regarded as typical of good commercial camera tubes in use at this time, includ-

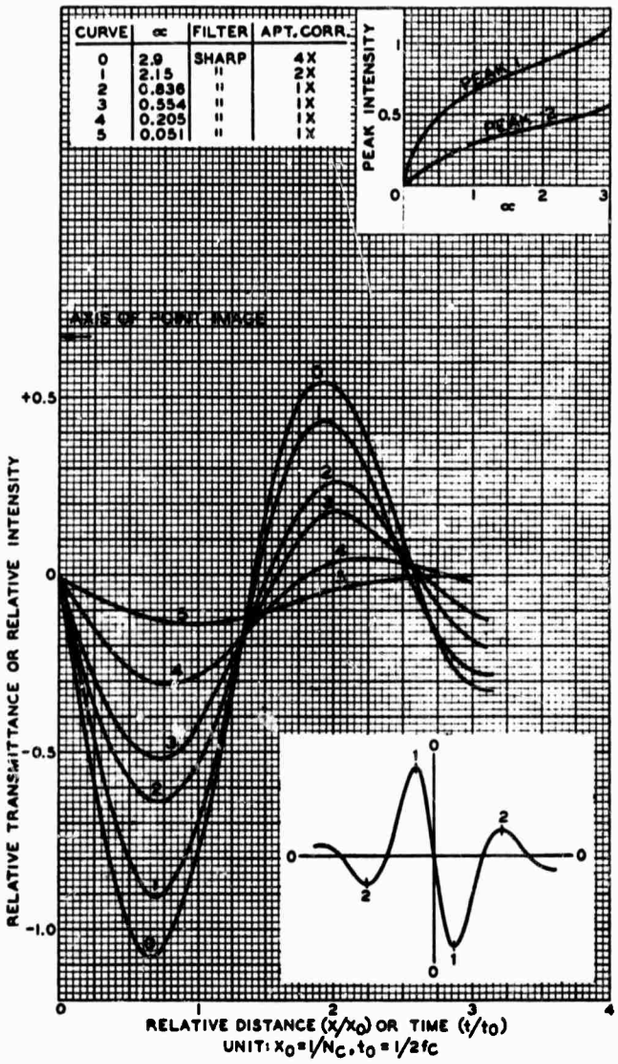

Fig. 93. Impulse forms or aperture transmittance obtained with response characteristics Figs. 91 and 92.

Table XVI. Equivalent Passband $\bar{N}_e$ and Approximate Limiting Resolution N_e of Television Components.

	$\bar{N}_e$	N_e^*	$r_\downarrow$
Square spot $\tau = 1$	$0.49\ N_e^*$		Part II, Fig. 41
Round spot $\tau = 1$	$0.45\ N_e^*$		" " " 42
Round spot $\tau = \cos^2 r$	$0.38\ N_e^*$		" " " 43
Exponential spot $\tau = e^{-(r/re)}$	$0.23\ N_e^*$		" " " 46a
Exponential spot $\tau = e^{-(r/re)^2}$	$0.32\ N_e^*$		" " " 44
	$0.20\ N_e^*$		(av. field luminosity $\bar{B} \simeq$ 4 to 10 ft-L)
Eye at viewing ratio: $d/V = 2$	376	1880	
4	188	940	Fig. 81
8	94	470	
Camera tubes	$\bar{N}_e$	N_e^*	$r_\downarrow$
Image iconoscope	200	800 (approx.)	
Image orthicon (type 5826)	200	800 "	Fig. 94
Image orthicon 4½-in. faceplate	250	1300 "	" 95
Vidicon (type 6198)	158	650 "	" 96
Kinescopes	265	920 "	" 97
	420	1500 "	
	500	1800 "	
	800	3000 "	

N_e^* at response $r_\downarrow \simeq 0.02$.

ing iconoscopes and European orthicon and image-iconoscope types.† According to the author's experience and measurements, there is no evidence supporting statements often found in the literature that high-velocity tubes, such as the iconoscope types, have higher resolution, i.e., a better response characteristic than low-velocity tubes. Theoretical advantages in one type are balanced by disadvantages imposed by tube geometry or auxiliary components in other types. The relative performance of different tubes is often thoughtlessly compared, disregarding large differences in the size of the storage surface and its capacitance. The response characteristics of an experimental high-definition image orthicon having a larger storage surface is shown in Fig. 95, and that of a small vidicon in Fig. 96 (both are low-velocity types).

The equivalent passband $\bar{N}_e$ of the characteristic in Fig. 94 is 200; this value may be regarded as representative of good commercial camera tube performance at the present time. Appropriate values for resolution (N_e) and equivalent passband $\bar{N}_e$ of camera tubes are listed in Table XVI.

The *sine-wave response characteristic of a kinescope* is shown in Fig. 97. The measured electrooptical response departs more or less from that of theoretical electron beams because of aberrations and the additional aperture effect of the particle structure of the screen phosphor. Uniformity of the response in the frame area and resolution depend on the design of the electron gun, electron lens, and the operating conditions. The resolution of kinescope types may vary from a few hundred to several thousand lines. The

† A recent publication[4] claims a resolution limit of 900 to 1000 lines for the center of a modern image iconoscope and about 700 lines at the edges. Low-velocity types have very little astigmatism and a substantially uniform spot diameter for correctly adjusted operating conditions.

response characteristic retains a shape similar to that in Fig. 97. Approximate values of the equivalent passband (N_e) and limiting resolution (N_e) for a variety of kinescopes are listed in Table XVI.

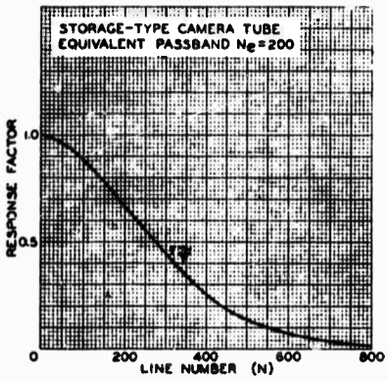

Fig. 94. Sine-wave response (r_ψ) of commercial camera tubes.

Fig. 95. Sine-wave response (r_ψ) of experimental high-definition camera tubes.

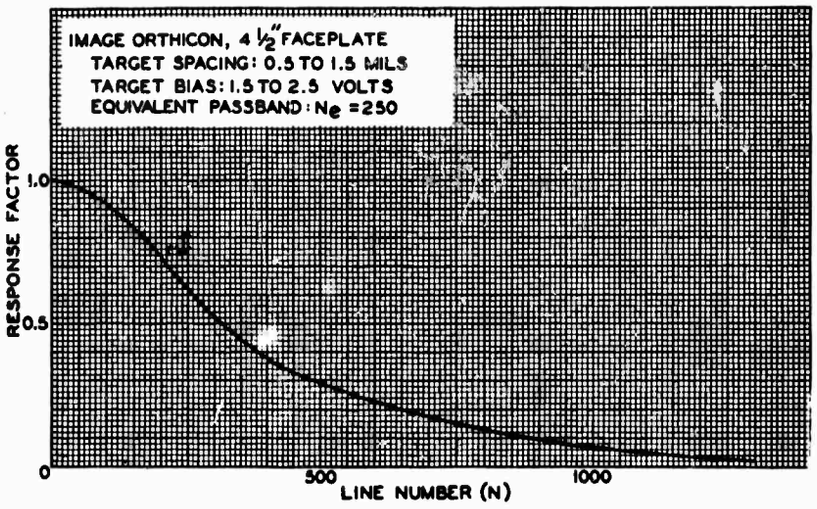

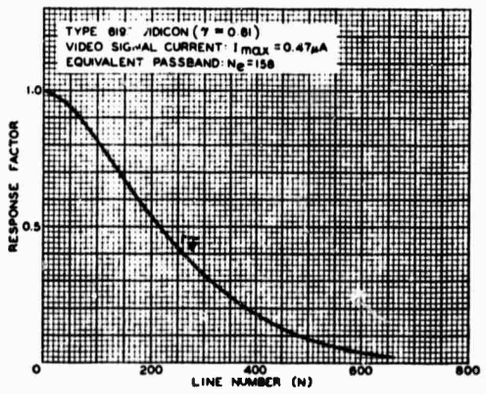

Fig. 96. Sine-wave response (r_ψ) of small camera tube (vidicon) with photoconductive target.

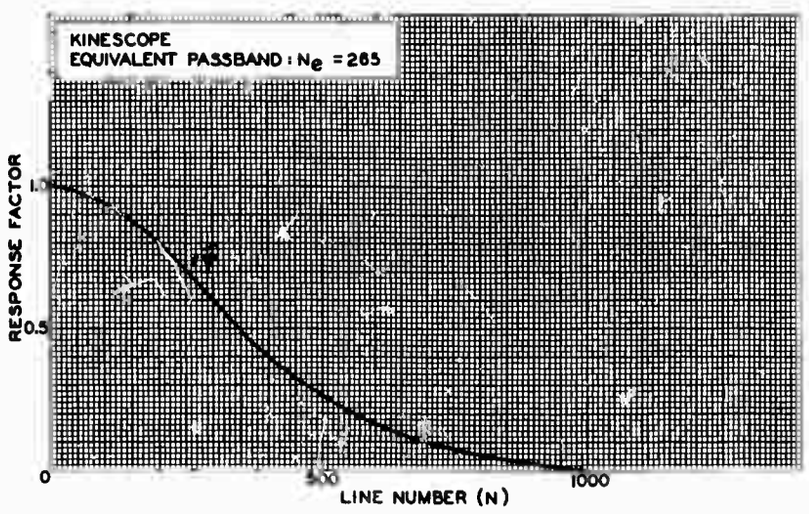

Fig. 97. Sine-wave response (r_ψ) of a kinescope.

D. EQUIVALENT PASSBANDS AND SIGNAL-TO-DEVIATION RATIOS

1. General Formulation

The passband of an electrooptical system, such as a television system, has a definite value defined by the electrical cutoff frequency f_c, or more adequately by the passband $N_{e(f)} = (N_{c(h)}n_r)^{\frac{1}{2}}$ of the theoretical measuring aperture. Because of the relation $f/f_c = N_{(h)}/N_{c(h)}$, frequencies and line numbers in the horizontal coordinate have been expressed in relative units $(N/N_c)_h$ permitting representation of the system response by generalized characteristics. *The equivalent horizontal passband $N_{e(e)h}$ of an electrooptical system* can hence be stated in the general form

$$N_{e(e)h} = \alpha N_{c(h)} \tag{66}$$

where

$\alpha = \int_0^1 (r_{\mathfrak{F}} r_\psi)^2_{(N/Nc)h}\, d(N/N_c)_h$ = relative equivalent passband

$r_{\mathfrak{F}_{(f/fc)}}$ = response characteristic of electrical system following source of deviations

$r_{\psi_{(N/Nc)h}}$ = response characteristic of aperture system following source of deviations.

The system response in the vertical coordinate is determined completely by the raster constant n_r and the two-dimensional apertures of the system, and has likewise been expressed in relative units N_v/n_r. *The equivalent vertical passband* $N_{e(e)v}$ of the system, can hence be stated in the general form.

$$N_{e(e)v} = \beta n_r \tag{67}$$

The relative equivalent passband $\beta = N_{e(e)v}/n_r$ is given by Eqs. (59), (60), or Fig. 76. For deviations of electrical origin, the analyzing aperture δ_a is the measuring aperture δ_f of the theoretical television system. (See section C2.) The equivalent vertical passband of $\delta_a = \delta_f$ is hence $N_{e(a)} = n_r$ and the vertical passband of the system is given exactly by Eq. (60), i.e., $N_{e(e)v} = N_{e(b)}$ and $\beta = N_{e(b)}/n_r$.

The factors α and β are defined by Eqs. (66) and (67) as ratios of the equivalent horizontal or vertical passband of the system to the corresponding theoretical passband of the television channel and are, therefore, termed *bandwidth factors*.

The equivalent symmetric passband $\bar{N}_{e(e)}$ of the system is the geometric mean of its equivalent horizontal and vertical passbands:

$$\bar{N}_{e(e)} = (\alpha\beta)^{\frac{1}{2}}(N_{e(h)}n_r)^{\frac{1}{2}} \quad (68)$$

The corresponding bandwidth factor $(\alpha\beta)^{\frac{1}{2}}$ of the system is the geometric mean of the horizontal and vertical bandwidth factors.

By combining Eq. (68) with Eq. (53), the signal-to-deviation ratio $[R]_e$ at any point in an electrooptical system can be stated in the convenient form:

$$[R]_e = [R]_m(\bar{N}_{e(m)}/\bar{N}_{e(f)})/(\alpha\beta)^{\frac{1}{2}}\dot{\gamma}_e \quad (69)$$

The meaning of the symbols is summarized for easy reference:

- $[R]_m$ = Signal-to-deviation or signal-to-noise ratio at origin of deviations
- $\bar{N}_{e(m)}$ = Equivalent passband of aperture with which $[R]_m$ is computed or measured
- $\bar{N}_{e(f)} = (N_{e(h)}n_r)^{\frac{1}{2}}$ = theoretical aperture of television channel
- α = Horizontal bandwidth factor (Eq. (66))
- β = Vertical bandwidth factor (Eq. (67))
- $\dot{\gamma}_e$ = product of all point gammas between origin of deviation and point of observation.

Deviations may originate at a number of points in the electrooptical system indicated in Fig. 65. The deviations from the various sources are computed separately (compare Part II) and combined by forming their rms sum. *Deviations (ψ) originating in the grain structure of a preceding motion-picture process* are transferred through the entire television system and observed in the final image. *Fluctuations originating in the electrical system* are displayed likewise as two-dimensional deviations in a picture frame, but they are also observed and measured as *signal-to-noise ratios* at various points of the electrical system. In all cases the signal-to-deviation ratio $[R]_e$ or signal-to-noise ratio $[R]$ may be computed with Eq. (69) by determining the proper reference values, bandwidth factors, and point gammas of the system elements involved in the transfer of signals and deviations.

2. The Reference Values $[R]_m$ and $\bar{N}_{e(m)}$

The signal-to-deviation ratio at the source is either computed or determined by measurements with an aperture of known equivalent passband $\bar{N}_{e(m)}$. *Optical deviations ψ* originate in a photographic system preceding the television process and appear in the projected film image (A_0 in Fig. 65) which can be regarded as the source of deviations. In a motion-picture transmission by a television system, the normal motion-picture projection lens δ_3 is replaced by the lens δ_0 of the television film camera (Fig. 65). When the lenses are of equal quality ($\delta_0 = \delta_3$), the measuring aperture is simply $\bar{N}_{e(m)} = \bar{N}_{e(p)}$, and the reference signal-to-deviation ratio is $[R]_m = [R]_p$, where $\bar{N}_{e(p)}$ and $[R]_p$ are the equivalent passband and signal-to-deviation ratio of the normal motion-picture process as computed in Part II. When the lenses are not identical, $\bar{N}_{e(m)}$ can be computed with $1/\bar{N}_{e(m)}^2 = (1/\bar{N}_{e(p)}^2) - (1/\bar{N}_{e(3)}^2) + (1/\bar{N}_{e(0)}^2)$ and

$$[R]_m = [R]_p(\bar{N}_{e(m)}/\bar{N}_{e(p)})\dot{\gamma}_2/\dot{\gamma}_0 \quad (70)$$

Electrical fluctuations $\bar{i}_0$ in photoelectric currents are normally computed from the number of electrons emitted in a time unit. The signal-to-noise ratio $[R]_0 = [R]_m$ can be obtained by the equivalent two-dimensional formulation given by Eq. (52) where $\bar{n}_0$ is the number of electrons, i.e., the total charge $Q_f/(H/V)$ in the unit area divided by the charge (q_e) of one electron:

$$[R]_m = [R]_0 = \left(\frac{Q_f}{q_e(H/V)}\right)^{\frac{1}{2}}/N_{e(m)} \quad (71)$$

with the frame charge $Q_f = I_0T_fb$ amp sec the electron charge $q_e = 1.6 \times 10^{-19}$ amp sec and the measuring aperture $\bar{N}_{e(m)} = \bar{N}_{e(f)}$ of the theoretical television channel:

$$[R]_0 = \left(\frac{I_0 T_f b\ 10^{10}}{1.6(H/V)}\right)^{\frac{1}{2}} / \bar{N}_{e(f)} \qquad (72)$$

where

I_0 = photo current (amp)
T_f = frame time ($\frac{1}{30}$ sec)
b = $(1 - b_h)(1 - b_v)$ = blanking factor ($b = 0.785$)
H/V = aspect ratio ($H/V = 4/3$)
$\bar{N}_{e(f)} = (N_{e(h)} n_r)^{\frac{1}{2}}$ (see Eq. (64)).

Fluctuations $\bar{i}_1$ *in the beam current of television camera tubes* can be computed similarly from the values of beam current and storage capacitance of the tube.[3] A reference signal-to-noise ratio $[R]$ is usually given by the manufacturer for a specified frequency channel Δf_c. The reference values for a frequency channel Δf are therefore:

$$[R]_m = [R]_1 = [R](\Delta f_c/\Delta f)^{\frac{1}{2}} \qquad (73)$$

and

$$\bar{N}_{e(m)} = \bar{N}_{e(f)}$$

Camera tubes not having an electron multiplier, such as iconoscopes, image iconoscopes, orthicons (C.P.S. Emitron) and vidicons, require the use of high-gain camera amplifiers. *The current fluctuations* $\bar{i}_2$ *in the first amplifier tube* become the dominant noise source. All high-gain camera amplifiers have a capacitive input circuit (Fig. 90a) which causes the signal-input voltage on the first amplifier tube to decrease with frequency as indicated in the voltage diagram Fig. 90b. The decreasing sine-wave response $r_{\bar{z}1}$ is, therefore, compensated by a corrective network ($r_{\bar{z}2}$) to a constant signal response $r_{\bar{z}1} r_{\bar{z}2} = 1$. The noise voltage $\bar{e}_a$ generated by the first amplifier current $\bar{i}_2$ is inserted between the input and correction circuits, and its normal "flat" spectrum is modified by the response $r_{\bar{z}2}$ to a spectrum with rising amplitude response termed a "peaked" channel. The amplifier circuit can, therefore, be represented as a flat (compensated) signal channel ($r_{\bar{z}12} = 1$) into which a noise voltage $\bar{e}_a$ is introduced over a peaked channel as indicated by the equivalent voltage diagram Fig. 90c. The rms-value $[\bar{E}]_a$ of the flat-channel noise voltage $\bar{e}_a$ can be computed in first approximation from the "equivalent noise resistance" R_{eq} of the amplifier tube[4] and has the value

$$[\bar{E}]_a = 1.3 \times 10^{-10}(R_{eq}\Delta f)^{\frac{1}{2}} \qquad (74)$$

The corrective network $r_{\bar{z}2}$ changes this value by the factor

$$a_2 = [\bar{E}]_2/[\bar{E}]_a = [\int_0^1 (g/g_0)^2 (f/f_c) d(f/f_c)]^{\frac{1}{2}} \qquad (75)$$

which is the *rms value* of the gain ratio (g/g_0) in the network. In terms of circuit constants the gain ratio is equal to the impedance ratio $\omega L/r$, which in turn must equal the time constant ωCR of the input circuit to obtain a complete compensation $r_{\bar{z}1} r_{\bar{z}2} = 1$. Integration furnishes the value

$$a_2 = (\omega_c CR/\sqrt{3}) = 2\pi\Delta f CR/\sqrt{3} \qquad (76)$$

where

C = effective capacitance of input circuit in farads
R = shunt resistance of input circuit in ohms.

For a general formulation it is expedient to replace the actual noise source $\bar{e}_a$ and the correcting circuit by a noise source $\bar{e}_2$ generating the rms voltage $[\bar{E}]_2$ in a flat channel Δf and to change the spectrum to a "peaked" frequency spectrum by a correction network having a normalized response characteristic and the response factor $r_{\bar{z}2} = \sqrt{3}$ at $f = f_c$. *The normalized characteristic* $r_{\bar{z}2}$ (see broken-line curve in Fig. 91a) does not change the rms value $[\bar{E}]_2$, because for $r_{\bar{z}2} = \sqrt{3}$ at f_c, the rms voltage ratio of the normalized correction network has the value

$$[\bar{E}]_2/[\bar{E}]_a = [\int_0^1 (r_{\bar{z}2})^2 (f/f_c) d(f/f_c)]^{\frac{1}{2}} = 1 \qquad (77)$$

The signal-to-noise ratio $[R]_2$ for amplifier noise (equivalent circuit Fig. 90c) is computed as follows:

The signal is the voltage $\bar{I} R$ developed

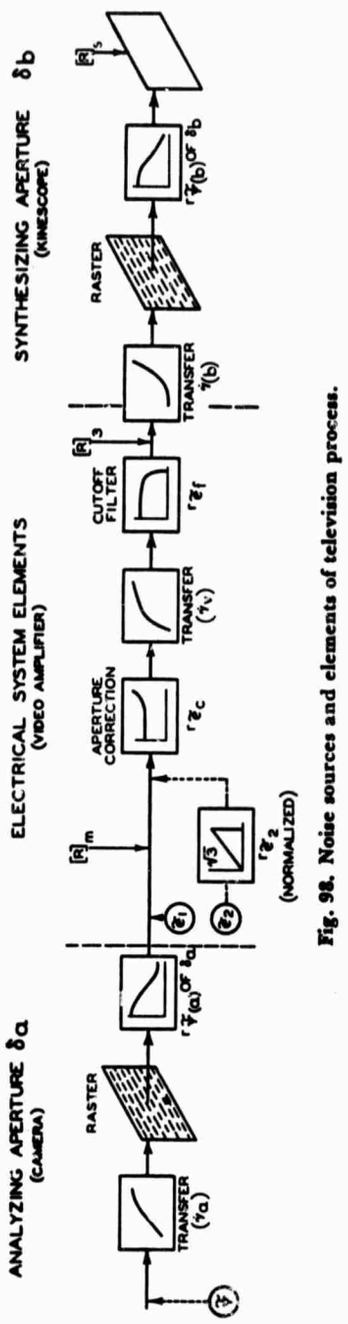

Fig. 98. Noise sources and elements of television process.

by the camera-tube signal current $\bar{I}$ in the input resistance R (Fig. 90a), because the effect of the shunt capacitance C has been compensated by a corrective network. The noise source is considered as a flat-channel noise source having an rms voltage $[\bar{E}]_2 = a_2[\bar{E}]_a$. Because of Eq. (77) the noise voltage after the peaking circuit has the same rms value. The measuring aperture for the normalized circuit has the equivalent passband $\bar{N}_{e(m)} = \bar{N}_{e(f)}$ and the signal-to-noise ratio is $[R]_2 = \bar{I}R/a_2[\bar{E}]_a$. With the values of Eqs. (74) and (76):

$$[R]_2 = 2.13\bar{I} \times 10^9/C(R_{eq})^{\frac{1}{2}}(\Delta f)^{\frac{1}{2}} \qquad (78)$$

The signal-to-noise ratio $[R]_2$ of practical amplifier circuits may have a lower value than the one computed with Eq. (78) which neglects noise contributed by circuit resistances, subsequent amplifier stages, and the effects of feedback. These contributions are usually small for circuits using a pentode input stage (type 6AC7). They are appreciable for a normal triode input stage but may be minimized by the use of special circuits and tubes having low grid-plate capacitance. A typical input stage used in older camera amplifiers uses a type 6AC7 amplifier tube as a pentode with the following constants:

$$R_{eq} = 720 \text{ ohm}, \quad C = 30 \times 10^{-12} \text{ farad}, \quad R = 10^6 \text{ ohm}$$

The maximum signal current $\bar{I}_{(max)}$ from camera tubes not having an electron multiplier is of the same order: $\bar{I}_{(max)} \simeq 0.1 \times 10^{-6}$ amp. With these values Eq. (78) furnishes the value $[R]_{2\,max} = 30$ in a frequency channel $\Delta f = 4.25 \times 10^6$ cycles/sec.

Modern high-gain camera amplifiers use special high-transconductance triodes with a somewhat higher effective capacitance but a much lower equivalent noise resistance $R_{eq} \simeq 110$ ohm in a "cascode" circuit, resulting in an improved signal-to-noise ratio $[R]_{2\,max} \simeq 70$ for $\Delta f = 4.25 \times 10^6$ cycles/sec. The variation of $[R]_2$ as a function of signal current, fre-

quency channel or other parameters is readily computed with Eq. (78). Reference values for various camera-tube types are listed in Table XVII.

3. Bandwidth Factors

The ratios of the equivalent passbands of an electrooptical system to the theoretical equivalents $N_{e(h)}$ and n_r of its electrical system (Eqs. (66), (67), (68)) have been termed bandwidth factors. A system containing two-dimensional apertures has horizontal and vertical bandwidth factors α and β and its equivalent symmetric aperture has a bandwidth factor $(\alpha\beta)^{\frac{1}{2}}$ which is their geometric mean. *The horizontal bandwidth factor* α includes the response $r\psi$ of two-dimensional apertures as stated by Eq. (66). It is used to compute the signal-to-deviation ratio in the final image frame for deviations originating (1) in a photographic process ahead of the television system or (2) in electrical noise sources. In case 1 the two-dimensional aperture response is $r\psi = (r\psi_{(a)}r\psi_{(b)})$. In case 2, $r\psi = r\psi_{(b)}$, because only apertures following the electrical network are in the system ($r\psi_{(b)}$ may include the response of the eye). Integration of the squared normalized response characteristics Figs. 86 and 87 furnishes electrooptical bandwidth factors α for case 1 and for case 2 with electrical flat channel noise sources $\bar{e}_1$. For convenience in plotting, the corresponding square roots $\alpha^{\frac{1}{2}}$ are shown in Fig. 99. The bandwidth factors for peaked channel noise sources $\bar{e}_2$ have been computed similarly for the characteristics Figs. 91 and 92, and their square roots are shown in Fig. 100.

For deviations ψ of optical origin, the vertical bandwidth factor β may be obtained from Fig. 76 or computed with Eqs. (59) or (60). For deviations of electrical origin ($\bar{e}_1$ or $\bar{e}_2$) the exact value of the vertical bandwidth factor of the system is given by

$$\beta = (N_{e(b)}/n_r) \qquad (81)$$

It has been shown that the electrical circuit response of a television system has no effect on the vertical aperture response of the system. The vertical bandwidth factor β of electrical elements is, therefore, $\beta = 1$. The bandwidth fac-

Table XVII. Maximum Signal-to-Noise Ratios $[R]_{m\ (max)}$ of Various Camera-Tube Types for Theoretical Channel $\Delta f = 4.25$ Mc.

Tube type	Use	Approx. target capacitance ($\mu\mu f$)	$\bar{I}(\mu a)$	$[R]_{m\ max}$	Noise** source	Spectrum
Iconoscope	Film Pickup	10000	0.1	70	$\bar{e}_2$	peaked
Vidicon type 6198	Film "	2200	0.45	315	$\bar{e}_2$	peaked
Image iconoscope	Live "	6000	0.1	70	$\bar{e}_2$	peaked
Orthicon* (without multiplier)	Live "	700	0.1	70	$\bar{e}_2$	peaked
Image orthicon						
Type 5820	Live "	100	10	34	$\bar{e}_1$	flat
5826	Live "	375	10	66	$\bar{e}_1$	flat
High-definition (4½-in. faceplate) image orthicon	Live "	1100	20–40	120	$\bar{e}_1$	flat

* Similar to C.P.S. Emitron.
** See Fig. 98.
Note: $[R]_{m\ max}$ for $\bar{e}_2$ is obtained only with modern cascode input circuits (see text).

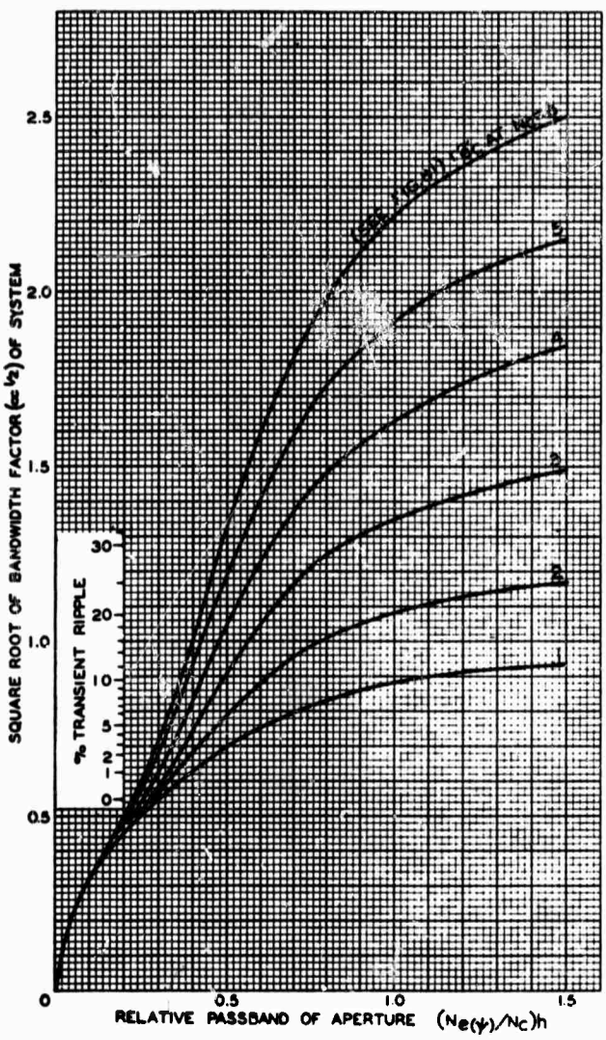

Fig. 99a. Bandwidth factors for "flat" channel noise sources with sharp-cutoff filter (Fig. 82) and aperture correction (Fig. 81) in cascade with exponential aperture.

tor $(\alpha\beta)^{\frac{1}{2}}$ of the equivalent aperture of electrical networks in an electrooptical system (excluding optical elements) has, therefore, a value $m^{\frac{1}{2}} = \alpha^{\frac{1}{2}}$, i.e., it is equal to the square root of its horizontal bandwidth factor m. The new symbol m is introduced to avoid confusion and indicate that this factor is reserved for purely electrical systems. According to Eq. (66), *electrical bandwidth factors* m are defined by

$$m = (\Delta f_e/\Delta f) = \int_0^1 (r_7)^2 (f/f_c) d(f/f_c) \quad (79)$$

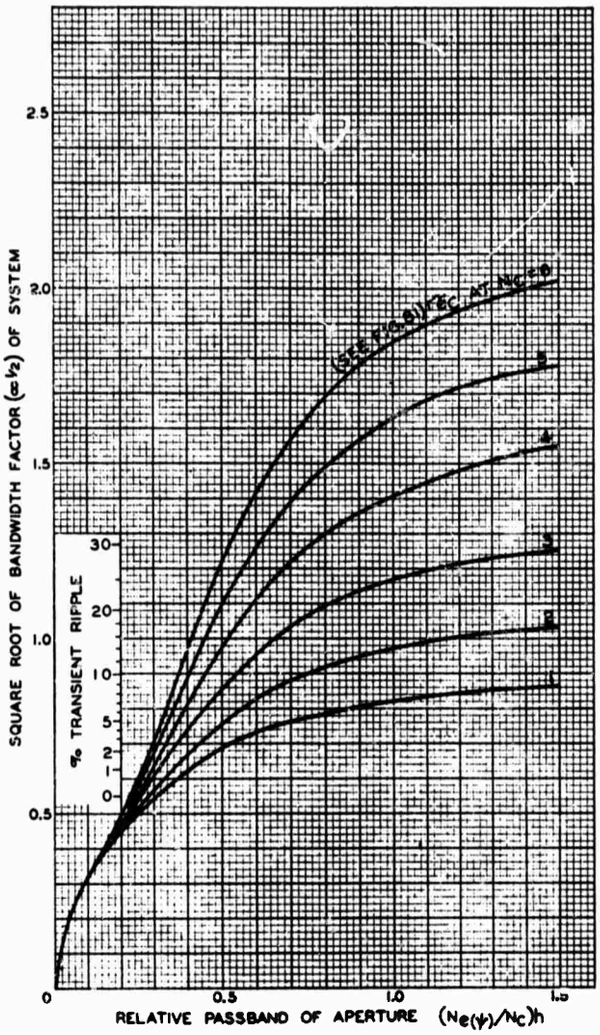

Fig. 99h. Bandwidth factors for "flat" channel noise sources with gradual-cutoff filter (Fig. 82) and aperture-correction circuits (Fig. 81) in cascade with exponential apertures.

where

Δf_e = noise-equivalent passband of the electrical system
Δf = theoretical (rectangular) passband of electrical system
r_s = sine-wave response factor of electrical system.

4. Signal-to-Noise Ratios in the Electrical System

The signal-to-noise ratio $[R]$ at different points in the electrical system (compare Eq. 69) reduces to

$$[R] = [R]_m/m^{\frac{1}{2}}\gamma_v \qquad (80)$$

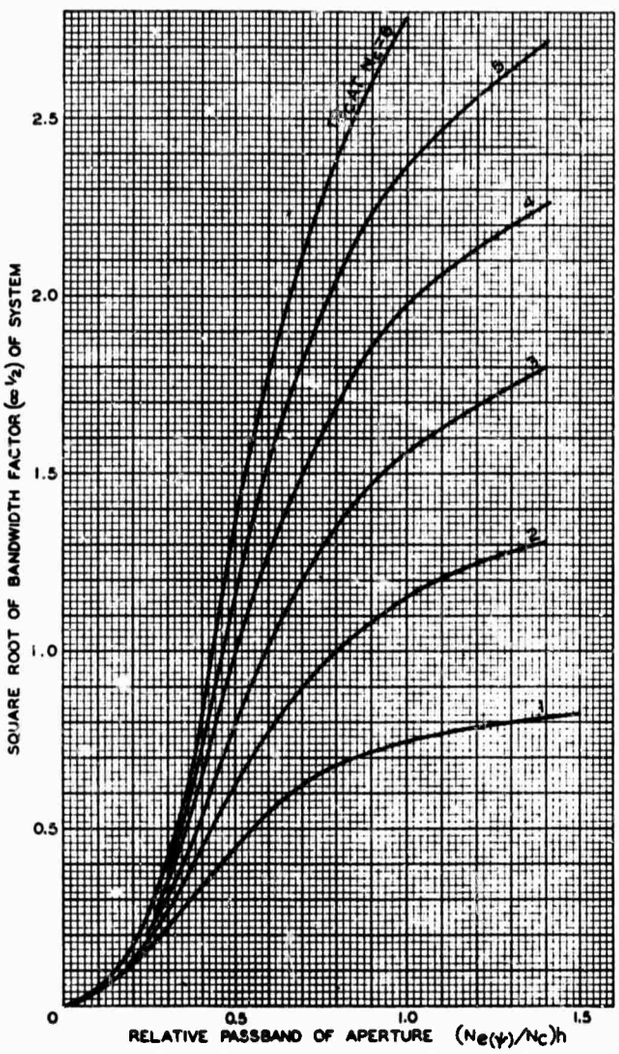

Fig. 100a. Bandwidth factors for "peaked" channel noise sources with sharp-cutoff filter (Fig. 82) and aperture correction (Fig. 81) in cascade with exponential apertures.

where

$[R]_m$ = signal-to-noise ratio computed for the theoretical passband Δf at the point of noise insertion (see preceding section)

m = electrical bandwidth factor computed for the frequency response r_z between the noise source and the point of observation (Eq. (79))

$\dot{\gamma}_v$ = point gamma of video amplifier between noise source and point of observation.

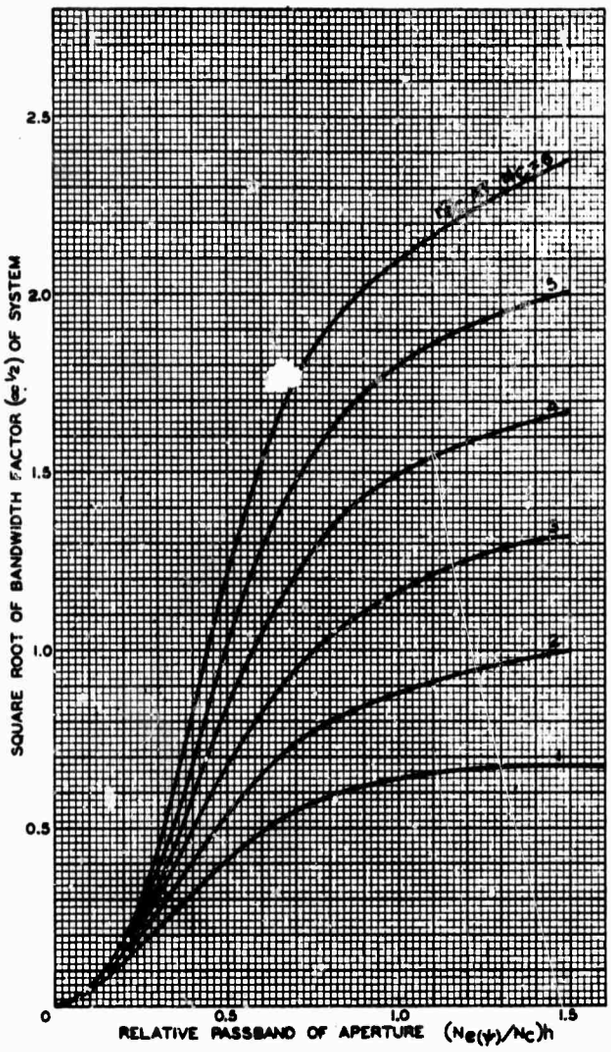

Fig. 100b. Bandwidth factors for "peaked" channel noise sources with gradual-cutoff filter (Fig. 82) and aperture correction (Fig. 81) in cascade with exponential apertures.

Actual measurements of the electrical signal-to-noise ratio are necessarily made at points following a cutoff filter, indicated in Fig. 98 by the index number 3. Figure 98 indicates all important electrical sources, the characteristics of the electrical system and the succeeding aperture system δ_4. The square roots $m^{\frac{1}{2}}$ of the bandwidth factors for circuit elements between the noise sources δ_1 (camera tube noise) or δ_2 (amplifier noise) have been computed for two filter

Table XVIII. Square Roots of Electrical Bandwidth Factors $m^{\frac{1}{2}}$.

Cutoff filter (Fig. 82)	Aperture correction at N_e (Fig. 81)	Noise source $\bar{i}_1$ (flat spectrum) $m_{12}^{\frac{1}{2}}$	Noise source $\bar{i}_2$ (peaked spectrum) $m_{22}^{\frac{1}{2}}$
Sharp	1 ×	0.98	0.914
"	2 ×	1.26	1.47
"	3 ×	1.63	2.0
"	4 ×	2.02	2.52
"	5 ×	2.4	3.04
"	6 ×	2.76	3.57
Gradual	1 ×	0.90	0.76
"	2 ×	1.09	1.10
"	3 ×	1.36	1.50
"	4 ×	1.68	1.91
"	5 ×	1.99	2.31
"	6 ×	2.24	2.70

characteristics (r_{zf}) and four values of aperture correction (r_{z_e}), and are listed in Table XVIII.

The calculation of signal-to-noise ratios $[R]$ in the electrical system and signal-to-deviation ratios $[R]_s$ in the final image by means of Eqs. (80) and (69) respectively, is now a simple operation because the bandwidth factors m, α, and β or their square roots have been tabulated or plotted. The values $[R]_s$ change with signal level and point gamma ($\dot{\gamma}$) as in photographic systems. A comparison requires, therefore, evaluation of the *signal-to-deviation characteristic* $[R]_s$ as a function of screen luminance.

E. THE SIGNAL-TO-DEVIATION CHARACTERISTIC $[R]_s = f(B)$ OF TELEVISION PICTURE FRAMES

Television-signal generators and camera tubes may be divided into two groups. One group, including light-spot scanners (flying-spot scanner) and image-dissector tubes, has no charge-storing elements and operates without auxiliary currents. The photoelectric signals are amplified by built-in electron multipliers and have a sufficiently large magnitude to make the noise contribution by amplifier tubes negligible. The signal-to-noise ratio $[R]_m$ is therefore a function of the *photocurrent* only (Eq. 72) and varies as the half power of the signal current:

$$[R]_m = [R]_0 = [R]_{0\,max}(I/\hat{I})^{\frac{1}{2}} \quad (82)$$

The second group of camera tubes has charge-storing elements (mosaics or targets), and employs electron beams for signal development. This group includes camera tubes having photo-emissive surfaces such as are used in the iconoscope, image iconoscope, orthicon and image orthicon, or photoconductive layers as used in the vidicon. The image orthicon is the only type in use having a built-in electron multiplier. It can, therefore, develop large signals and has a "flat" noise spectrum like that of multiplier phototubes. The signal-to-noise ratio $[R]_m = [R]_1$, however, varies in direct proportion to the signal current, because the dominant noise source is the *constant-beam current*

$$[R]_m = [R]_1 = [R]_{1\,max}(I/\hat{I}) \quad (83a)$$

The camera tubes not having electron multipliers (iconoscope and orthicon and vidicon types) have a relatively small signal-current output. Their signal-to-noise ratio $[R]_m = [R]_2$ is controlled by the constant *amplifier noise* (Eq. (78))

which has a "peaked" frequency spectrum and $[R]_2$ varies in proportion to the signal current:

$$[R]_m = [R]_2 = [R]_{2\,max}\,(I/\hat{I}) \quad (83b)$$

The optical signal-to-deviation ratio $[R]_e$ *in one picture frame* is computed with Eq. (69). With the substitutions from Eqs. (82) or (83) for $[R]_m$, and with $\bar{N}_{s(m)} = \bar{N}_{s(f)}$, the optical signal-to-deviation ratio for the first group of signal sources may be written:

$$[R]_e = [R]_{0\,max}\,(I/\hat{I})/(\alpha\beta)^{\frac{1}{2}}\dot{\gamma}_v\dot{\gamma}_b \quad (84)$$

and for the second group of storage tubes:

$$[R]_e = [R]_{1\,max}\,(I/\hat{I})/(\alpha\beta)^{\frac{1}{2}}\dot{\gamma}_v\dot{\gamma}_b \quad (85a)$$

and

$$[R]_e = [R]_{2\,max}\,(I/\hat{I})/(\alpha\beta)^{\frac{1}{2}}\dot{\gamma}_v\dot{\gamma}_b \quad (85b)$$

where

- $\dot{\gamma}_v$ = point gamma of video amplifier system
- $\dot{\gamma}_b$ = point gamma of succeeding aperture processes including kinescope ($\dot{\gamma}_2$)
- $[R]_0$ and $[R]_1$ = signal-to-noise ratios with "flat" noise spectrum
- $[R]_2$ = signal-to-noise ratio with "peaked" noise spectrum

1. Effect of Transfer Characteristics and Point Gamma on $[R]_e$

The relation of luminance (B) in a picture frame to the signal current I and scene luminance or camera-tube exposure (E_1) is determined by the transfer characteristics of the system elements. A valid comparison of the signal-to-deviation ratios obtained with different television-camera types requires that the overall transfer characteristic (tone scale) of the system be identical. This requirement is met when the point gammas $\dot{\gamma}_T = \dot{\gamma}_1\dot{\gamma}_v\dot{\gamma}_b$ of the television systems are alike at the same luminance values. It is of interest to examine first the general effect of the camera-tube gamma ($\dot{\gamma}_1$) on the shape of the signal-to-deviation characteristic $[R]_e = f(B)$, which determines the relative visibility of deviations in the luminance range.

The $[R]_e$-characteristic can have different shapes depending on the camera-tube gamma ($\dot{\gamma}_1$), even though the overall gamma of the television system has fixed values $\dot{\gamma}_T$.

(*a*) *The Relative Signal-to-Deviation Ratios* $[R]_e/[R]_{max}$ *of Constant Gamma Systems With Camera Tubes Having Constant Gamma.* It is assumed that the system gamma γ_T as well as the camera-tube gamma $\dot{\gamma}_1$ have constant values. The relative-signal current of the camera tube is then simply $I/\hat{I} = (E_1/\hat{E}_1)^{\gamma_1}$, where $(E_1/\hat{E}_1)$ is the relative exposure. With this relation and the substitutions $\dot{\gamma}_v\dot{\gamma}_b = \gamma_T/\gamma_1$ Eq. (85a) takes the form:

$$[R]_e = [R]_{1\,max}\,(E_1/\hat{E}_1)^{\gamma_1}/(\alpha\beta)^{\frac{1}{2}}$$

In terms of screen luminance $(B/\hat{B}) = (E_1/\hat{E}_1)^{\gamma_T}$, this expression may be written

$$[R]_e = [R]_{1\,max}\,(B/\hat{B})^{\gamma_1/\gamma_T}(\gamma_1/\gamma_T)/(\alpha\beta)^{\frac{1}{2}} \quad (86)$$

Inspection of Eq. (86) shows that the slope of the $[R]_e$-characteristic is controlled by the exponent (γ_1/γ_T) of the relative screen luminance $(B/\hat{B})$. A plot of Eq. (86) furnishes straight-line characteristics in log coordinates with a maximum value $[R]_e/[R]_{1\,max} = (\gamma_1/\gamma_T)/(\alpha\beta)^{\frac{1}{2}}$ at $(B/\hat{B}) = 1$ and the constant slope (γ_1/γ_T) as shown in Fig. 101 for $(\alpha\beta) = 1$ and an overall constant gamma $\gamma_T = 1.2$. It is seen from Fig. 101 that only a minor improvement of $[R]_e$ is obtained in the shadow tones $B/\hat{B} = 0.01$ to 0.04 by decreasing γ_1 below the value $\gamma_1 = 0.6$ at the expense of a larger reduction of $[R]_e$ in the highlight values $B/\hat{B} = 0.2$ to 1. The preferred camera-tube gamma for a constant-system gamma $\gamma_T = 1.2$ is therefore γ_1 optimum $\simeq 0.6$.

(*b*) *The relative signal-to-deviation ratios* $[R]_e/[R]_{max}$ *of systems with variable gamma.* It is impractical and actually undesirable to provide a constant overall gamma for the television system because of the finite limits imposed on the tone range by all practical imaging devices. According to photographic experience

Table XIX. Relative Signal-to-Deviation Ratios $[R]_s/[R]_{1\,max}$ for Image Orthicon (Also Iconoscope Film Pickup)* With Linear Amplifier ($\gamma_v = 1$), Kinescope Bias $E_0/\hat{E} = 0.13$ (Fig. 21, Part I) and $\alpha\beta = 1$.

$E_1/\hat{E}_1$	$I/\hat{I}$	$B/\hat{B}$	$\dot{\gamma}_v\dot{\gamma}_2$	$[R]_s/[R]_{1\,max}$	$\dot{\gamma}_1$	$\dot{\gamma}_T$
0.01	0.026	0.015	0.17	0 153	1.15	0.20
0.02	0.057	0.0185	0.40	0.142	1.15	0.46
0.04	0.125	0.031	0.95	0.132	1.10	1.045
0.07	0.22	0.06	1.45	0.152	0.85	1.23
0.10	0.295	0.095	1.70	0.174	0.75	1.275
0.20	0.47	0.22	1.90	0.247	0.58	1.10
0.40	0.69	0.46	2.00	0.345	0.49	0.98
0.70	0.88	0.77	2.05	0.429	0.39	0.80
1.00	1.00	1.00	2.10	0.476	0.31	0.65
(1)	(1)(2)	(2)	(3)	(4)	(5)	

Notes: (1) From Fig. 6, Part I. (2) From Fig. 21, Part I, ($I/\hat{I} = E/\hat{E}$). (3) $\dot{\gamma}_v = 1$. (4) Eq. (83a). (5) From Fig. 7, Part I.

* Transfer characteristic for $E_1 \simeq 15$, Fig. 11, Part I.

Table XX. Relative Signal-to-Deviation Ratios $[R]_s/[R]_{2\,max}$ for Image Iconoscope, and Orthicon ($\gamma_1 = 1$).

Image iconoscope*					Orthicon, linear vidicon, $\gamma_1 = 1$			
$E_1/\hat{E}_1$	$I/\hat{I}$	$\dot{\gamma}_1$	$\dot{\gamma}_v\dot{\gamma}_2$	$[R]_s/[R]_{1\,max}$	$I/\hat{I}$	$\dot{\gamma}_v\dot{\gamma}_2$	$[R]_s/[R]_{2\,max}$
0.01	0.0035	3.3	0.06	0.058	0.01	0.2	0.051
0.02	0.019	1.9	0.242	0.079	0.02	0.46	0.045
0.04	0.06	1.45	0.72	0.084	0.04	1 045	0.038
0.07	0.12	1.15	1.07	0.112	0.07	1.23	0.057
0.10	0.18	1.0	1.275	0.141	0.10	1.275	0.079
0.20	0.33	0.85	1.3	0.254	0.20	1.10	0.182
0.40	0.58	0.70	1.40	0.414	0.40	0.98	0.41
0.70	0.82	0.56	1.43	0.573	0.70	0.80	0.875
1.00	1.00	0.50	1.30	0.77	1.00	0.65	1.54

*Transfer characteristic similar to iconoscope for $E_1 \simeq 4$, Fig. II, Part I.

Table XXI. Relative Signal-to-Deviation Ratios $[R]_s/[R]_{max}$ for Vidicon ($\gamma_1 = 0.6$) and Light-Spot Scanner ($\gamma_1 = 1$).

Vidicon, $\gamma_1 = 0.6$				Light-spot scanner, $\gamma_1 = 1$			
$E_1/\hat{E}_1$	$I/\hat{I}$	$\dot{\gamma}_v\dot{\gamma}_2$	$[R]_s/[R]_{1\,max}$	$I/\hat{I}$	$(I/\hat{I})^{\frac{1}{2}}$	$\dot{\gamma}_v\dot{\gamma}_2$	$[R]_s/[R]_{0\,max}$
0.01	0.064	0.33	0.194	0.01	0.10	0.20	0.51
0.02	0.097	0.77	0.126	0.02	0.141	0.46	0.308
0.04	0.148	1.74	0.085	0.04	0.20	1.045	0.191
0.07	0.205	2.05	0.10	0.07	0.264	1.23	0.215
0.10	0.255	2.12	0.12	0.10	0.316	1.275	0.248
0.20	0.385	1.84	0.21	0.20	0.447	1.10	0.406
0.40	0.57	1.64	0.348	0.40	0.631	0.98	0.645
0.70	0.80	1.34	0.596	0.70	0.835	0.80	1.045
1.00	1.00	1.08	0.93	1.00	1.00	0.65	1.54

the most pleasing transfer characteristics are s-shaped as shown by Fig. 102 with a center-range gamma in the order of 1.2. The transfer characteristics obtained with linear amplifiers ($\gamma_a = 1$) from *iconoscopes used for motion-picture film pickup* or from *image orthicons* (studio pickups) are similar to that of a motion-picture process and will therefore be used as a representative standard.† For comparison the amplifier gamma ($\dot{\gamma}_a$) for all other camera-tube types will be adjusted to result in a system gamma (γ_T) and a transfer characteristic equal to curve 1 in Fig. 102.

Because the video amplifier is linear ($\gamma_a = 1$), the relative-signal voltage $E/\hat{E}$ at the kinescope grid is directly equal to the relative-signal current $I/\hat{I}$ from the camera tube. Corresponding values of screen luminance $B/\hat{B}$ and $\dot{\gamma}_2$ for the signals $E/\hat{E} = I/\hat{I}$ obtained from a representative kinescope characteristic (Fig. 21, Part I) are listed in columns 3 and 4 of Table XIX. The relative signal-to-deviation ratio $[R]_a/[R]_{1\ max}$ computed with Eq. (85a) for $\alpha\beta = 1$, $\gamma_a = 1$ and $\dot{\gamma}_b = \dot{\gamma}_2$ is tabulated in column 5, and shown by curve 1 in Fig. 103. Columns 6 and 7 of Table XIX list the point-gamma values of the image orthicon (Fig. 7, Part I) and the point gamma ($\dot{\gamma}_T$) of the overall system characteristic curve 1 in Fig. 102.

The signal-to-deviation characteristic for an *image-iconoscope* camera chain giving an identical overall transfer characteristic is readily computed by tabulating its signal-current ratio $I/\hat{I}$ and $\dot{\gamma}_1$ for the same relative exposure values $E_1/\hat{E}_1$ as listed in Table XX. The product $\dot{\gamma}_a\dot{\gamma}_2 = \gamma_T/\gamma_1$ is then computed for the desired values $\dot{\gamma}_T$ of Table XIX. The corresponding signal-to-deviation ratios are shown as curve 3 in Fig. 103. Table XX also lists the values obtained similarly for an *orthicon* or a *linear vidicon* camera ($\gamma_1 = 1$). The relative signal-to-deviation ratios for a *vidicon with low constant gamma* ($\gamma_1 = 0.6$) and *a light-spot scanner* ($\gamma_1 = 1$) are given in Table XXI. The values for the light-spot scanner phototube signals require calculation of $(I/\hat{I})^{\frac{1}{2}}$ because of Eq. (84). The preferred characteristic for camera tubes (curves 1 to 5 in Fig. 103) is that of the image orthicon and iconoscope (curves 1 and 2) which is a close approach to the characteristic obtained from a theoretical constant-gamma system with a camera-tube gamma $\gamma_1 = 0.6$. The previous conclusion that a $\gamma_1 = 0.6$ is optimum does, therefore, not apply to a system with variable gamma as seen by comparison of curve 5 of Fig. 103 with curve 0.6 of Fig. 101.

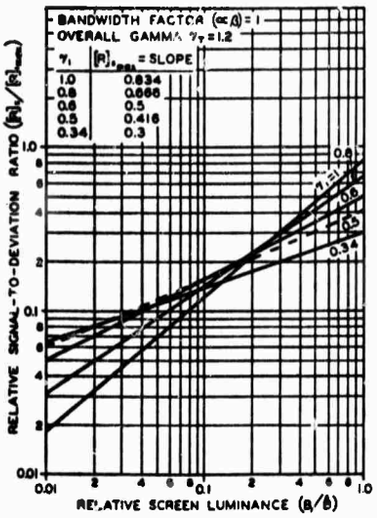

Fig. 101. Relative signal-to-deviation ratio of television systems having the same constant overall gamma and constant "flat" channel noise-level, but camera tubes with different constant gamma values.

† A different reference characteristic would not change relative performance values between television-camera tubes.

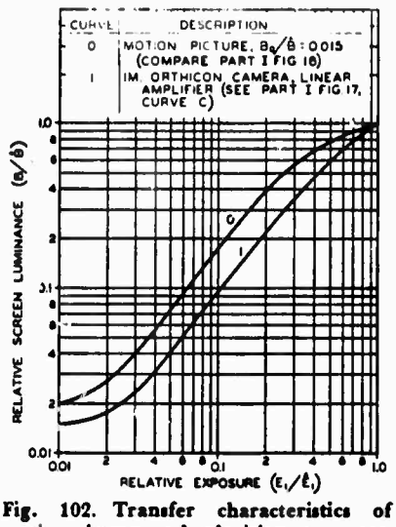

Fig. 102. Transfer characteristics of motion-picture and television processes.

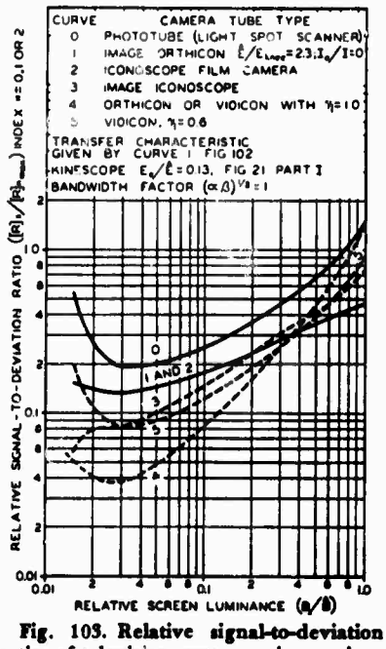

Fig. 103. Relative signal-to-deviation ratios of television systems using various camera-tube types having equal signal-to-noise ratios $[R]_m$ at the source and gamma correction to obtain the transfer characteristic 1, Fig. 102.

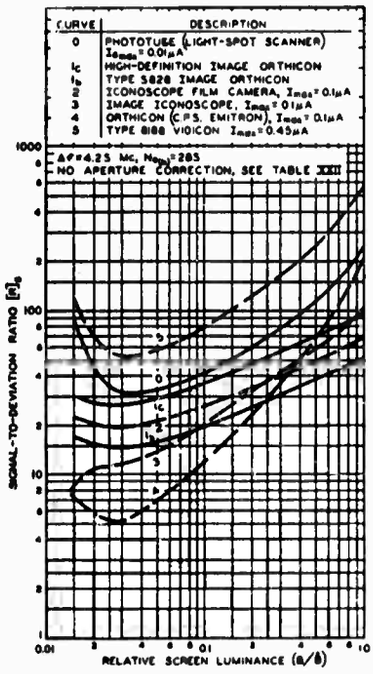

Fig. 104a. Signal-to-deviation ratios at the screen of standard 525-line USA television systems using an average kinescope ($N_{s(b)}$ = 265), no aperture correction, but gamma correction to obtain the transfer characteristic 1, Fig. 102.

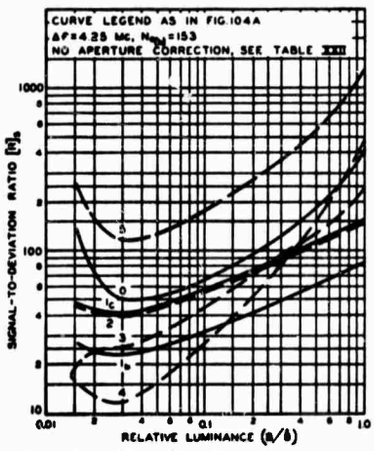

Fig. 104b. Signal-to-deviation ratios in the retinal image for the conditions of Fig. 104a modified by a viewing distance $d = 4V$, which changes $N_{s(b)}$ to 153.

2. Signal-to-Deviation Characteristics of Image Frames on the Kinescope Screen and at the Retina of the Eye

The signal-to-deviation characteristics in Fig. 103 are relative characteristics computed for identical transfer characteristics (curve 1, Fig. 102), identical signal-to-noise ratios at the source, and bandwidth factors $(\alpha\beta)^{\frac{1}{2}} = 1$. A numerical comparison of image granularity requires adjustment of the $[R]_e$-scale according to actually obtained signal-to-noise ratios $[R]_m$ and bandwidth factors $(\alpha\beta)^{\frac{1}{2}}$ for representative electrical systems and succeeding optical apertures $(N_{e(b)})$. The characteristics $[R]_e = f(B/\dot{B})$ are obtained according to Eqs. (84) and (85) by multiplication of the relative characteristics in Fig. 103 with appropriate scale factors $[R]_{m\ max}/(\alpha\beta)^{\frac{1}{2}}$. Electrical aperture correction and variation of the optical aperture passband $N_{e(b)}$ have a considerable effect on the numerical values $[R]_e$, which differ substantially for flat- and peaked-channel noise sources. The relative magnitude and appearance of deviations in the retinal image vary with viewing distance and can be computed by including the aperture process of the eye in the value $N_{e(b)}$ as shown in the following examples.

Without aperture correction ($r_{\eta_e} = 1$ at N_e) the factors $m^{\frac{1}{2}}$ and $\alpha^{\frac{1}{2}}$ of the system are determined by the type of noise source (flat or peaked), the cutoff filter, and the equivalent passband $N_{e(b)}$ of the optical apertures following the point of noise insertion, while $\beta^{\frac{1}{2}}$ is determined by n_r and $N_{e(b)}$ only. The values computed for a standard (U.S.A.) monochrome television channel and a typical kinescope are given in Table XXII and Figs. 104a and 104b. When the passband $N_{e(b)}$ of the optical-system apertures is changed, the $[R]_e$-characteristics for all camera chains with flat-channel noise sources are shifted as a group with respect to the group of $[R]_e$-characteristics for camera chains with peaked-channel noise sources because the difference in the horizontal frequency spectra causes $\alpha^{\frac{1}{2}}$ to change by different factors (see Figs. 99 to 100). *The visual appearance of grain structures* depends on the granularity of the retinal image which can be computed as follows. For direct-viewing conditions the equivalent passband $N_{e(b)}$ is the cascaded value for the kinescope (N_{e2}) and the eye $(N_{e(eye)})$, which varies as a function of viewing distance, and may be obtained for an average field luminance of 4 to 10 ft-L from:

$$N_{e(eye)} = 752\,(V/d) \qquad (87)$$

The characteristics in Fig. 104a represent, therefore, a close viewing distance where $N_{e(b)}$ is substantially equal to the equivalent passband of the kinescope: $N_{e(b)} \simeq N_{e2} = 265$. An increase of the viewing ratio to $d/V = 4$ changes $N_{e(eye)}$ to 188 and the cascaded value (Eq. (30b), Part II) of kinescope and eye to $N_{e(b)} = 153$, resulting in the characteristics given in Fig. 104b. Before conclusions can be drawn, it is advisable to consider the effects of aperture correction.

Aperture correction ($r_{\eta_e} > 1$ at N_e) is used to increase the high-frequency sine-wave signals from the camera tube in order to obtain better definition. The magnitude of the correction depends on the response of the camera tube and varies, therefore, for different tube types. A change of the high-frequency response of the video amplifier, however, alters its relative passband and the bandwidth factors m and α. A proper comparison of $[R]_e$-characteristics from different camera tubes should therefore be based on the additional condition that the horizontal sine-wave response $r_{\psi_1} r_{\eta}$ of camera tube, aperture-correcting circuit, and electrical filter is adjusted to be substantially alike. The correction required for each case can be determined as follows. Assume that it is desired to obtain a response $r_{\psi_1} r_e$ equal to that of the sharp-cutoff filter shown in Fig. 82. This filter has a factor $m^{\frac{1}{2}} = 0.975$. It is only necessary to determine the bandwidth factor $\alpha_1 = (N_{e1}/N_e)_A$ of the camera tube, locate it

Table XXII. Maximum Signal-to-Deviation Ratios $[R]_{s\ max}$ of 525-line Television System With $\Delta f = 4.25$ Mc, Transfer Characteristic Curve 1, Fig. 103, No Aperture Correction ($r_{\bar{z}_e} = 1$ at N_e).

Curve No.	Type of signal source	$[R]_{m\ max}$	$m\frac{1}{2}$	$\dot{\gamma}_v$	$[R]_{s\ max}$	$N_{c(b)} = 265$ (Kinescope) $\beta\frac{1}{2}$	$\alpha\frac{1}{2}$	$\dot{\gamma}_e$	$[R]_{e\ max}$	$\bar{N}_{e(a)}$	$N_{c(b)} = 153$ (Kine. + eye for $d/V = 4$) $\beta\frac{1}{2}$	$\alpha\frac{1}{2}$	$[R]_{e\ max}$	$\bar{N}_{e(a)}$
0	Light-spot scanner, $I_{max} \simeq 0.01\mu$	100	0.98	0.31	330	0.735	0.825	0.65	254	247	0.56	0.665	414	152
1a	Image orthicon, 5820	34	0.98	1.0	37.7	0.735	0.825	2.1	26.8	247	0.56	0.665	43.5	152
1b	Image orthicon, 5826	66	0.98	1.0	67.4	0.735	0.825	2.1	52	247	0.56	0.665	84.5	152
1c	Image orthicon, high-definition	120	0.98	1.0	122.5	0.735	0.825	2.1	94.6	247	0.56	0.665	153.5	152
2	Iconoscope (film pick-up), $I_{max} = 0.1\ \mu a$	70	0.914	1.0	76.5	0.735	0.66	2.1	69.0	201	0.56	0.4	149	91.6
3	Im. iconoscope, $I_{max} = 0.1\ \mu a$	70	0.914	0.62	123.5	0.735	0.66	1.3	111.0	201	0.56	0.4	240	91.6
4	Orthicon [C.P.S. Emitron), $I_{max} = 0.1\ \mu a$	70	0.914	0.31	247	0.735	0.66	0.65	222	201	0.56	0.4	482	91.6
5	Vidicon, 6198, $I_{max} = 0.45\ \mu a$	315	0.914	0.515	668	0.735	0.66	1.08	600	201	0.56	0.4	1300	91.6
		(1)	(2)	(3)	(4)	(5)	(6)	(7)	(8)	(9)	(5)	(6)	(8)	(9)

Notes:
(1) From Table XVII.
(2) From Table XVII sharp filter, aperture correction 1 ×.
(3) $\dot{\gamma}_v = \dot{\gamma}_s\dot{\gamma}_2/2.1$ value at $\hat{B}$ from Tables XIX to XXII.
(4) Signal-to-noise ratio after filter, Eq. (80).
(5) Eq. (81) for $n_r = 490$.
(6) From Figs. 99a or 100a for $N_{c(b)} = 340$, curve 1.
(7) From Tables XIX to XXII at $\hat{B}$.
(8) Eq. (69).
(9) Eq. (68).

Table XXIII. Maximum Signal-to-Deviation Ratios $[R]_{s\ max}$ of 525-line Television System With $\Delta f = 4.25$ Mc, Transfer Characteristic Curve 1, Fig. 103, and Maximum Aperture Correction.

Curve no.	Type of signal curve	$[R]_{m\ max}$	N_{el}	Apt. corr. at N_s	$N_{e(b)} = 265$ $\alpha^{\frac{1}{2}}$	$\beta^{\frac{1}{2}}$	γ_s	$[R]_{s\ max}$	$\bar{N}_{e(s)}$	$N_{e(b)} = 153$ (Kinc. + eye for $d/V = 4$) $\alpha^{\frac{1}{2}}$	$\beta^{\frac{1}{2}}$	$[R]_{s\ max}$	$\bar{N}_{e(s)}$
0	Light spot scanner, $I_{max} = 0.01\ \mu a$	100	250	2	1.0	0.735	0.65	210	300	0.74	0.56	372	169
1a	Image orthicon, 5820	34	200	2.5	1.12	0.735	2.1	19.7	336	0.79	0.56	37	180
1b	Image orthicon, 5826	66	200	2.5	1.12	0.735	2.1	38.2	336	0.79	0.56	71	180
1c	Image orthicon, high-definition	120	250	2	1.0	0.735	2.1	78	300	0.74	0.56	138	170
2	Iconoscope (film pickup), $I_{max} = 0.01\ \mu a$	70	200	2.5	1.15	0.735	2.1	39	346	0.61	0.56	98	140
3	Image iconoscope, $I_{max} = 0.1\ \mu a$	70	200	2.5	1.15	0.735	1.3	64	346	0.61	0.56	158	140
4	Orthicon (C.P.S. emitron), $I_{max} = 0.1\ \mu a$	70	200	2.5	1.15	0.735	0.65	127	346	0.61	0.56	315	140
5	Vidicon, 6198, $I_{max} = 0.45\ \mu a$	315	158	4	1.66	0.735	1.08	239	500	0.84	0.56	620	192
		(1)	(2)	(3)	(4)		(5)	(6)	(7)	(4)		(6)	(7)

Notes:
(1) From Table XXII.
(2) Equivalent passband of camera tubes (approximate values).
(3) Obtained from Fig. 99a for $(N_{e(\psi)}/N_s)_h = N_{el}/340$ and $\alpha^{\frac{1}{2}} = 0.975$ (to obtain $r_{\psi\psi'g} = r_{gf}$).
(4) From Fig. 99a or 100a for $N_{e(h)} = 340$ and $N_{e(\psi)} = N_{e(b)}$.
(5) From Table XXII, value at $\bar{B}$.
(6) Eq. (69).
(7) Eq. (68).

Table XXIV. Maximum Signal-to-Deviation Ratios $[R]_{s\ max}$ of 625-line Theater Television System With $\Delta f = 8$ Mc, Transfer Characteristic Curve 1, Fig. 103, and Maximum Aperture Correction.

Curve no.	Type of signal source	$[R]_{m\ max}$	Apt. corr. at N_e	$m^{\frac{1}{2}}$	$\dot{\gamma}_v$	$[R]_{i\ max}$	$N_{e(b)} = 400$, (at screen) $\alpha^{\frac{1}{2}}$	$\beta^{\frac{1}{2}}$	$\dot{\gamma}_v$	$[R]_{s\ max}$	$\bar{N}_{e(s)}$	$N_{e(b)} = 240$, $(d/V = 2.5)$ $\alpha^{\frac{1}{2}}$	$\beta^{\frac{1}{2}}$	$[R]_{s\ max}$	$\bar{N}_{e(s)}$
0	Light-spot scanner, $I_{max} \simeq 0.01\ \mu$	73	4	2.02	0.31	116.5	1.43	0.83	0.65	94.7	665	0.94	0.642	186	338
1b	Image orthicon, 5826	48.1	6	2.76	1.0	17.4	1.9	0.83	2.1	14.5	884	1.18	0.642	30	425
1c	Image orthicon, high-definition	87.5	4	2.02	1.0	43.3	1.43	0.83	2.1	35.1	665	0.94	0.642	69	338
3	Image iconoscope, $I_{max} = 0.1\ \mu a$	27.1	6	3.57	0.62	12.2	2.26	0.83	1.3	11.1	1050	1.08	0.642	30	388
4	Orthicon (C.P.S. emitron), $I_{max} = 0.1\ \mu a$	27.1	6	3.57	0.31	24.5	2.26	0.83	0.65	22.2	1050	1.08	0.642	60	388
5	Vidicon, 6198, $I_{max} = 0.45\ \mu a$	122 (1)	6 (2)	3.57	0.515 (3)	66.5 (4)	2.26 (5)	0.83 (6)	1.08 (3)	60.2	1050 (7)	1.08 (5)	0.642 (6)	163	388 (7)

Notes:
(1) Values from Table XXII multiplied by $(4.25/8)^{\frac{1}{2}}$ for curves 0, 1b and 1c; and by $(4.25/8)^{\frac{1}{2}}$ for curves 3, 4 and 5.
(2) Curves 0 and 1c corrected to $\alpha^{\frac{1}{2}} = 0.975$; curves 1b, 3 and 4 corrected to $\alpha^{\frac{1}{2}} = 0.95$; curves 3, 4 and 5 corrected to $\alpha^{\frac{1}{2}} = 0.71$
(3) From Table XXII.
(4) Electrical signal-to-noise ratio after filter, Eq. (80).
(5) From Figure 99a or 100a for $N_{e(b)} = 537$.
(6) Eq. (81) for $n_r = 584$.
(7) Eq. (68) for $(N_{e(b)} n_r)^{\frac{1}{2}} = 560$.

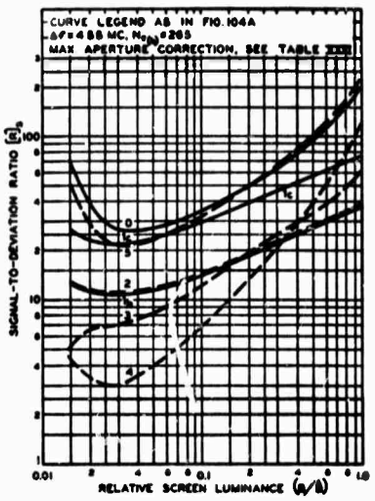

Fig. 105a. Signal-to-deviation ratios at the screen of standard 525-line USA television systems using an average kinescope ($N_{a(b)} = 265$), aperture correction for equal horizontal sine-wave response, and gamma correction to obtain the transfer characteristic 1, Fig. 102.

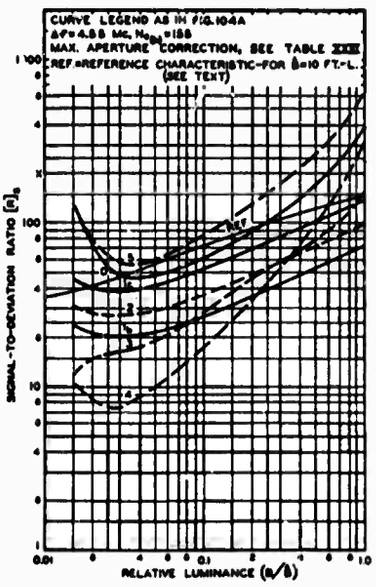

Fig. 105b. Signal-to-deviation ratios in the retinal image for the conditions of Fig. 105a modified by a viewing distance $d = 4V$.

on the abscissa of Fig. 99a and read off the aperture correction required for the desired value $\alpha^{\frac{1}{2}} = m^{\frac{1}{2}} = 0.975$. A tabulation of the values obtained for a standard television channel ($N_{a(A)} = 340$) is given in column 3 of Table XXIII. The various degrees of aperture correction alter the factors $\alpha^{\frac{1}{2}}$ of the system following the point of "noise" insertion as listed in column 4 for the previously used apertures $N_{a(b)} = 265$ and $N_{a(b)} = 158$ following the electrical system. The corresponding $[R]_e$-characteristics shown in Figs. 105a and 105b are based on equal transfer characteristics and equal horizontal response in a standard television channel with $n_r = 490$ and $N_{a(A)} = 340$.

A comparison of the signal-to-deviation characteristics of a standard 35mm motion-picture projection (Fig. 57b, Part II) and television images of similar quality is given in Table XXIV and Figs. 106a, 106b, and 106c. It will be shown in Part IV that a 30-frame television system having $n_r = 625$ lines and a video passband $\Delta f = 8$ mc is adequate to duplicate 35mm motion-picture performance. This performance can be obtained only with high-quality signal sources, maximum aperture correction and high quality reproducers ($N_{a2} = 400$). The performance of all camera-tube types, however, has been computed for comparison. The $[R]_e$-characteristics Fig. 106a represent conditions at the screen and Figs. 106b and 106c at the retina of the eye for the viewing distances $d = 2.5V$ and $4V$ respectively. The motion-picture characteristic in Fig. 106a is the $[R]_p$-characteristic shown in Fig. 57b of Part II. At a viewing distance $d = 2.5V$ the equivalent passband of the eye is $N_{a(eye)} = 300$ (Eq. (87)). In cascade with the equivalent passband $N_{a(p)} = 370$ of the motion picture, the overall system passband be-

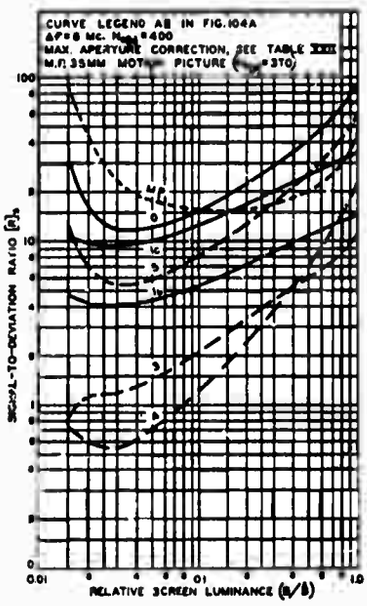

Fig. 106a. Signal-to-deviation ratios at the screens of 35mm motion-picture and 625-line theater-television systems (Δf = 8 mc) having the transfer characteristics in Fig. 102, a television projector with $\bar{N}_{s(b)}$ = 400 and high aperture correction to provide equivalent sharpness (see text).

comes $\bar{N}_{s(s)}$ = 233. The motion-picture characteristic in Fig. 106b is obtained with $[R]_s = [R]_p$ (370/233) and in Fig. 106c with $[R]_s = [R]_p$ (370/188) because in these cases the relative amplitude distribution in the deviation spectrum and the products $[R]_p\bar{N}_{s(s)}$ remain substantially constant (see p. 22, Part II). The characteristics in Fig. 106 show that in the medium and light tone range the motion-picture frames have larger deviations (lower $[R]_s$) than the television systems curves 0, 1*c* and 5, but that the granularity of the motion picture is lower in the shadow tones.

With increasing viewing distance, the signal-to-deviation characteristic of the aperture-corrected television systems im-

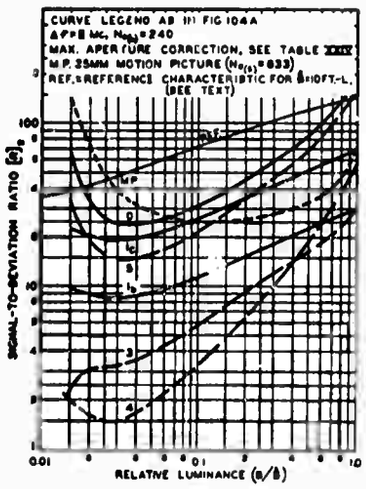

Fig. 106b. Signal-to-deviation ratios in the retinal image for the conditions of Fig. 106a modified by a viewing distance $d = 2.5V$.

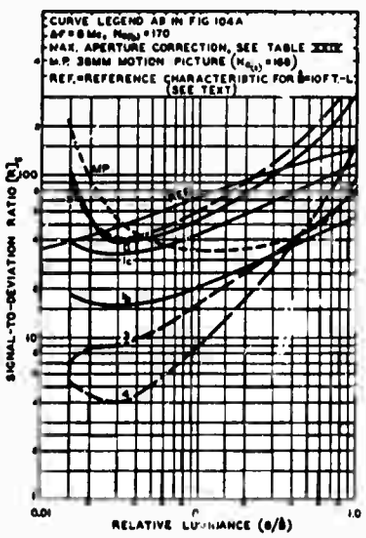

Fig. 106c. Signal-to-deviation ratios in the retinal image for the conditions of Fig. 106a modified by a viewing distance $d = 4V$.

proves more rapidly than that of the motion picture. It must also be borne in mind that the signal-to-deviation ratios evaluated for the motion picture are values that neglect all defects and scratches which noticeably increase the deviation level in the film projection above the ideal values after relatively few runs, as borne out by measurements of the noise level from the sound track of motion-picture film. There is no parallel degradation in live-television systems, because every showing is a "first" showing. The signal-to-deviation characteristics of the theater-television systems using the high-definition image orthicon (Fig. 95), light-spot scanners, or the type-6198 vidicon are, therefore, satisfactory in comparison with motion pictures. The definition obtained with the type-6198 vidicon, however, is not equivalent to 35mm motion pictures.

3. Equivalent Passband ($\bar{N}_{e(o)}$) and Sine-Wave Amplitudes

Amplitude distribution and N_e-values for the sine-wave spectrum of the deviations in a television frame can be computed accurately from the products of corresponding response factors for the system elements following the noise source.

The sine-wave response of a particular combination of elements can be approximated with good accuracy by one of the normalized characteristics given in this paper. The analysis of the intensity distribution in the vertical coordinate (Eq. (57) and Fig. 70) has shown that the television raster may produce a carrier wave containing a series of sine-wave components with fixed amplitudes. These constant carrier components are not included in the total energy of the deviations. When the deviations originate in electrical elements, the vertical-frequency spectrum is in all cases that of the aperture δ_h following the electrical elements (see section C2). The sine-wave response of theater-television systems (not including camera) is illustrated in Fig. 107. The response factors are by definition the amplitudes obtained with a normalized sine-wave energy input into the theoretical television channel, i.e., for an rms noise input voltage $[\bar{E}]_m = 1$. The equivalent passbands in the horizontal and vertical coordinates have been related to the theoretical passband by bandwidth factors; $N_{e(h)} = \alpha N_e$ and $N_{e(v)} = \beta n_r$ to permit evaluation by normalized characteristics. The equivalent passband ($\bar{N}_{e(o)}$) of the system is computed with Eq. (68) (see Tables XXII to XXIV).† While the response factors in the horizontal and vertical coordinates are independent of one another, the actual amplitudes of the sine-wave flux components of the deviation flux are not, because the total sine-wave deviation energy $P_0 = c^2\bar{N}_e$ is independent of direction. For a normalized deviation "output" energy $P_0 = 1$, the amplitude scale factor is therefore $c = \bar{N}_e^{-\frac{1}{2}}$ for symmetrical apertures, and the amplitude distribution $Y_{(N)} = f(N)$ is obtained by multiplying the response factors r_ψ by the scale factor:

$$Y_{(N)} = r_\psi c = r_\psi(\bar{N}_e)^{-\frac{1}{2}} \qquad (89)$$

Similarly for television systems:

$$\left.\begin{aligned} &Y_{(N)h} = r_{\psi(h)} \qquad c_{(h)} = r_{\psi(h)}(\alpha N_e)^{-\frac{1}{2}} \\ &\text{and} \\ &Y_{(N)v} = r_{\psi(v)}c_{(v)} = r_{\psi(r)}(\beta n_r)^{-\frac{1}{2}} \end{aligned}\right\} \qquad (90)$$

The *relative* amplitude characteristics corresponding to Fig. 107 are shown in Fig. 108. The characteristic of the 35mm

† Because of aperture correction the value $\bar{N}_{e(o)}$ does exceed the theoretical value $\bar{N}_{e(m)}$ considerably for the condition $N_{e(h)} = 400$ in Table XXIV. This abnormal condition exists for deviations only and it should be remembered that an equivalent passband is by definition a "flat" passband which would contain the same total deviation energy. The system response to sine-wave components in picture signals is normal, because it includes the decreasing response of the camera tube.

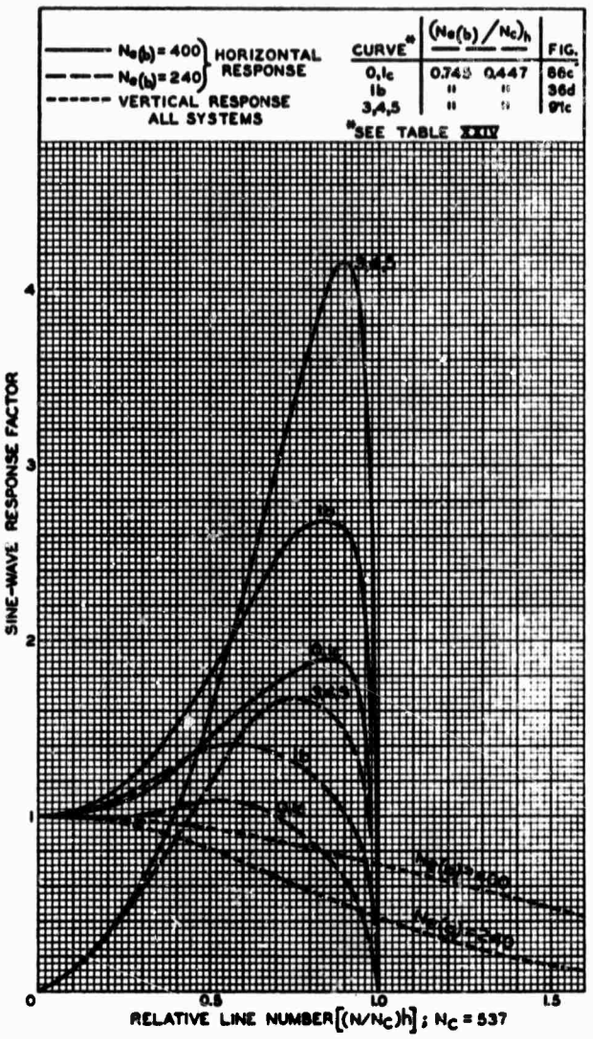

Fig. 107. Sine-wave response factors of theater-television and motion-picture systems for the conditions of Figs. 106a and 106b.

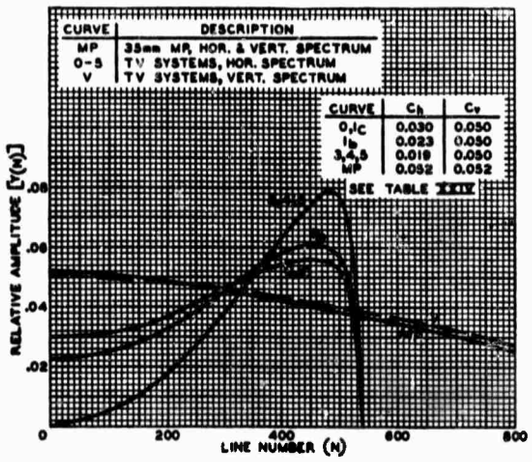

Fig. 108a. Relative amplitudes of sine-wave spectra for equal-energy signals and deviations at the screen of theater-television and motion-picture systems.

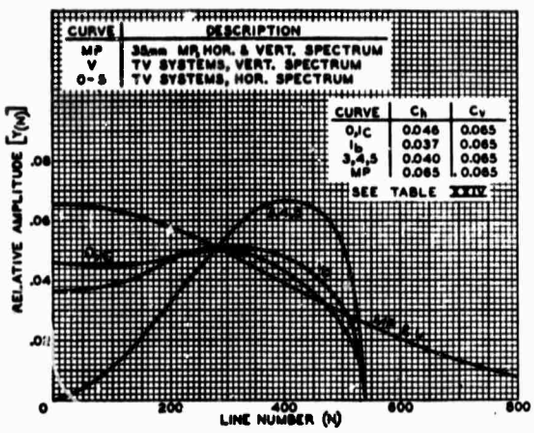

Fig. 108b. Relative amplitudes of sine-wave spectra for equal-energy signals and deviations at a viewing distance $d = 2.5V$ from the screen of theater-television and motion-picture systems.

motion picture in Fig. 108a is that of Fig. 59, Part II, normalized for $P_0 = 1$ by multiplication with $c = 370^{-\frac{1}{2}} = 0.0518$, and by $c = 233^{-\frac{1}{2}} = 0.0653$ for Fig. 108b, which represents conditions at the retina for a viewing distance $d = 2.5V$.

The visual appearance of the grain structures in motion-picture and television frames is indicated by the amplitude spectra (Fig. 108) for equal signal-to-deviation ratios. The vertical spectra are substantially identical and the preponderance of low frequencies indicates a soft grain structure. The horizontal television spectra for "flat" channel deviations (0, 1*b*, 1*c*) have a somewhat smaller and sharper appearing grain size. The "peaked" channel deviations (3, 4, 5) containing no low frequencies and having maximum energy at a fairly high line number ($N = 400$ to 500), have a smaller and more uniform appearing grain size.

This interpretation of the amplitude spectra may be compared with the grain

Figure 109 is on plate pages 118 and 119.

structure photographs shown in Fig. 109 which were taken under somewhat similar conditions in a 4.5-mc system for the purpose of measuring the deviation ratio in an image frame by sampling with a physical aperture. The linear dimension of the samples in Fig. 109 is approximately one-fourteenth of a picture frame. The samples A, B and C are photographs of "peaked" channel, "flat" channel, and 35mm motion-picture grain structures respectively. In the top row (index 1) are single-frame grain structures obtained with small apertures δ_1 showing the raster line structure of the television samples A and B. The middle row (2) illustrates the condition for a larger aperture δ_2 for all 3 cases. This aperture was given a value to produce a "flat field" in the television frames and equal the spot size of the supercinephor lens for C2. Note the longer grain size in the vertical direction of A2 which is evidence of the flat-frequency spectrum across the raster even from a peaked "noise" source, which causes positive- and negative-grain doublets in the horizontal coordinate due to the absence of low frequencies and the differentiated pulse shape shown in Fig. 93. The samples A3 and B3 show the effect of superimposing the grain structures of six television frames by a photographic exposure of $\frac{1}{5}$ sec. The deviations were increased in magnitude to show more clearly that the grain doublets have practically disappeared in A3 due to random superposition.

4. Discussion of Results

Examination of the various signal-to-deviation characteristics shows clearly that the theoretical signal-to-noise ratios $[R]_{m\ max}$ (Table XVII) is not an adequate measure of camera-tube performance. It is evident from Tables XXII and XXIII that the electrical signal-to-noise ratios $[R]_{3\ max}$ which can be measured in the video-transmission link, may also differ substantially from the theoretical value $[R]_{m\ max}$, because for comparable definition the sine-wave response of the camera tube is reflected in the degree of aperture correction and alters the sine-wave amplitudes in the frequency spectrum of the deviations.

Aperture correction increases the noise level by a factor which is larger for peaked-channel noise than for flat-channel noise, as illustrated by the value of the electrical factor m^3 in Table XXIV for conditions 1b and 3, for example. The filtering action of succeeding apertures has an opposite effect, reducing the deviation level $(1/[R]_s)$ and granularity of the retinal image by a larger factor for peaked-channel noise than for flat-channel noise. These factors are given by the ratio of corresponding factors α^3 which, according to Table XXII, is 0.665/0.4 = 1.66 in favor of peaked-channel noise without aperture correction and at a viewing distance $d = 4V$ from a standard 525-line television image.† When moderate aperture correction is used the ratio decreases (see Table XXIII) and with high aperture correction it approaches unity (see Table XXIV) and may even reverse. *It therefore appears desirable to specify the entire signal-to-deviation characteristic in the retinal image for a given viewing distance.* To judge the entire characteristic it is necessary to establish a *reference characteristic based on the perception of random deviations* as a function of luminance.

Subjective observations as well as fun-

† This value is considerably lower than the ratio given in the author's earlier paper.[3] The earlier values are in error because they are ratios of bandwidth factors (α) rather than factors (α^3).

A camera tube with adequate signal output and definition such as the experimental high-definition image orthicon (curve 1*c* in Fig. 106, and Table XXII is required for a theater-television system having a granularity comparable to that of a 35mm motion picture using plus X) negative and fine-grain positive film (1302). The theoretical value $[R]_{m\ max}$ at the source for this type of camera tube corresponds to an electrical noise level of −38.8 db, or −41.3 db including synchronizing signals. The noise level in the video-transmission system (corresponding to $[R]_s = 43.4$) is −32.7 db, or −35.2 db including synchronizing signals. To prevent impairment of this performance, the noise level of the transmission system itself should be approximately 6 db better, or both the transmission system and the camera tube should have noise levels 3 db lower than stated above.

A more accurate statement can be made when the amplitude distribution in the frequency spectrum of the additive noise is known. Statistical tests of signal-to-deviation ratios by the sampling of television grain-structure photographs on 4 × 5-in. film have been in good agreement with computed values. The above method has also been applied to compute the noise levels reported by Pierre Mertz in two publications.[8,9] In view of the estimates which had to be made for a number of unspecified system constants the calculated values appeared to be in satisfactory agreement with the reported values.

Many relations between apertures and their sine-wave response characteristics as well as characteristics of vision have only been indicated and will be discussed in more detail in Part IV of this paper.

References

1. Pierre Mertz and T. Gray, "The theory of scanning and its relation to the characteristics of the transmitting signal in telephotography and Television," *Bell Sys. Tech. J., 13:* p. 464, 1934.
2. I. C. Gardner, "A new resolving power test chart," (abstract), *J. Opt. Soc. Am., 40:* 257, Apr. 1950.
3. O. H. Schade, "Electro-optical characteristics of television systems, Part III—Electro-optical characteristics of camera systems," *RCA Rev., 9:* 490–530, Sept. 1948.
4. P. Schagen, H. Bruining and J. C. Francken, "The image iconoscope—a camera tube for television," *Philips Tech. Rev., 13:* 119–133, May 1951 (abstracted in *Jour. SMPTE, 58:* 501–514, June 1952).
5. W. A. Harris, "Fluctuations in vacuum tube amplifiers," *RCA Rev., 5:* 505–525, Apr. 1941; *ibid., 6:* 114–124, July 1941.
6. O. H. Schade, "Electro-optical characteristics of television systems, Part IV—Correlation and evaluation of electro-optical characteristics of imaging systems," *RCA Rev., 9:* 653–686, Dec. 1948.
7. A. Rose, "Television pickup tubes and the problem of vision," *Advances in Electronics, I:* 133-166, Academic Press, New York, N.Y., 1948.
8. Pierre Mertz, "Perception of television random noise," *Jour. SMPTE, 54:* 8–34, Jan. 1950.
9. Pierre Mertz, "Data on random noise requirements for theater television," *Jour. SMPTE, 57:* 89–107. Aug. 1951.

VII. FACTORS AFFECTING IMAGE QUALITY IN A TWO-DIMENSIONAL IMAGING ARRAY

by Richard R. Legault

It is conventional to assess the performance of an imaging device in terms of its spatial frequency response. The spatial frequency response (optical response) reflects both the amplitude and the phase response of the optical system. The amplitude response is frequently called the modulation transfer function (MTF). So much has been written on this subject that it serves no purpose to repeat it here.* The optical response of a photographic system may be characterized as follows (Eq. VII-1):

$$O(r_1,r_2) = S(r_1,r_2)\ M(r_1,r_2)\ R(r_1,r_2) \qquad \text{(VII-1)}^{**}$$

where (r_1,r_2): spatial frequency coordinates

$O(r_1,r_2)$: spatial frequency representation of output image

$S(r_1,r_2)$: spatial frequency representation of the scene

$M(r_1,r_2)$: spatial frequency response of the optical system (aperture, lens, etc.)

$R(r_1,r_2)$: spatial frequency response of the recording film

I shall formulate the image quality as measured by $O(r_1,r_2)$ for an imaging device which consists of a two-dimensional array of point

---

* Instead, an extract from Summary of Mathematical Work Related to Infrared Radiation Data Processing, by W. Duane Montgomery, Paul C. Shields, and James L. Alward, is reproduced as an addendum.

** The reader should note that no scale changes between object and image plane are identified.

detectors. Such a system is illustrated in Fig. VII-1. There are obviously three new aspects of this imaging system which must be accounted for: (1) the detector spacing (sampling); (2) the detector size or, more generally, the area weighting function of the detectors; (3) the recording spot size or area weighting function.

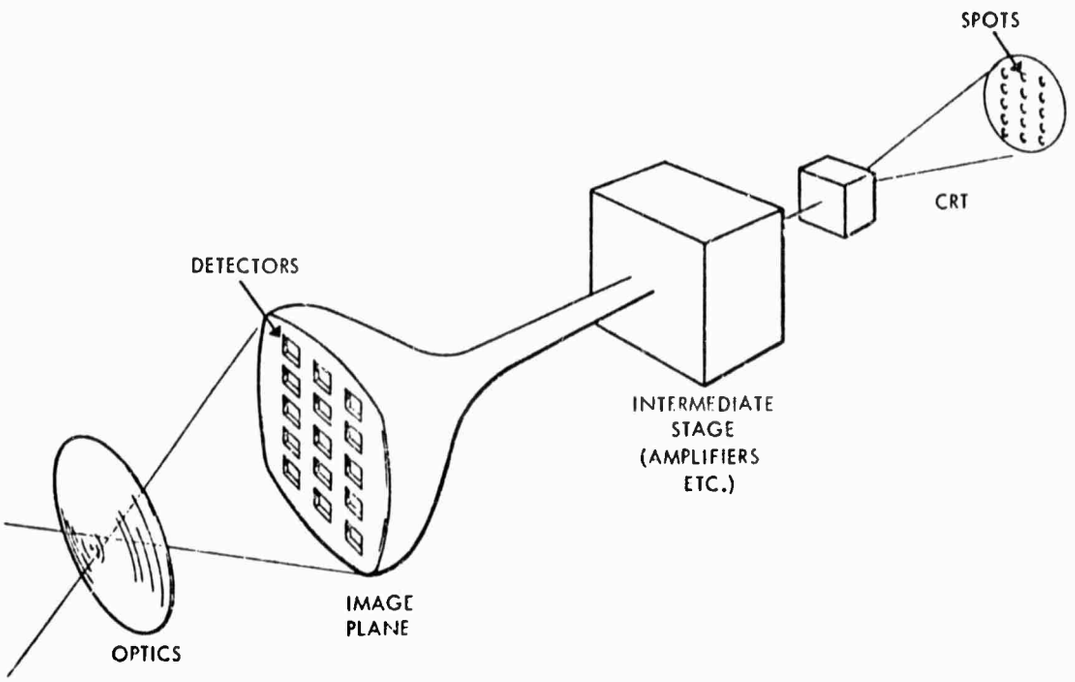

FIGURE VII-1. Schematic of Some Image Transmission Systems

Let us first turn our attention to the detector spacing or, as I shall call it, the sampling lattice. Most of us are familiar with one-dimensional sampling of a temporal signal. The Nyquist limit for signal reproducible is well known: the highest reproducible frequency for a sampled record where the samples are T seconds apart is $\frac{1}{2T}$. The same result holds if T is a spatial distance. Sampling theory for two dimensions is less well known. Although intuitively extending sampling theory to two dimensions by analogy with one dimension gives some insights, some rather important insights can be overlooked. Fortunately, the theory of two-dimensional sampling is well developed (Ref. 1).

The addendum is an application and extension of these results to the problem of sampling with detectors of finite areas.

The usual sampling lattice in one dimension has a uniformly spaced sampling interval. The most easily visualized two-dimensional sampling lattice is a rectangular grid with equal spacings in both the x and y directions. Figure VII-2 depicts a rectangular sampling array. We can generate such a periodic lattice by defining the primary vectors a_1 and a_2. The points of the lattice are given by the linear combinations (Eq. VII-2):

$$a_n = n_1 a_1 + n_2 a_2 \qquad n_1, n_2 = 0, \pm 1, \pm 2, \pm 3, \ldots . \tag{VII-2}$$

The corresponding lattice in the spatial frequency domain (reciprocal lattice) is generated by the vectors b_1, b_2 defined by the relations:

$$\left.\begin{aligned} a_1 \cdot b_2 &= 0 \\ a_2 \cdot b_1 &= 0 \end{aligned}\right\} \quad \text{primary and reciprocal lattice vectors perpendicular}$$

and

$$a_1 \cdot b_1 = 1$$

$$a_2 \cdot b_2 = 1$$

The square primary lattice of Fig. VII-2 has exactly the same lattice in the frequency (reciprocal) space but $a_1 = b_2$ and $a_2 = b_1$. The square lattice of Fig. VII-2 has some peculiar features.

With a spacing of $\frac{1}{2B}$ in the x and y directions we have a spatial frequency limit of B in the x and y directions. The spatial frequency limit in the 45-deg direction (Fig. VII-2) is $\sqrt{2}$ B. It has been observed that resolution and TV displays in direction 45 deg to the scan

directions are better than in the horizontal and vertical directions. This effect is even more evident in two-dimensional sampling arrays. The number of detectable line pairs is a factor of $\sqrt{2}$ greater in the 45-deg direction. This must appear strange to those familiar with photographic systems. The resolution in photographic systems is the same (or nearly so) in all directions, since the optical frequency response of the system is symmetric. Of course, the frequency response of the optical system for the two-dimensional sampling array is symmetric. The square sampling array introduces the asymmetry. There is no justification for this asymmetry in a reconnaissance system. In fact, we pay for it by using more detectors than necessary.

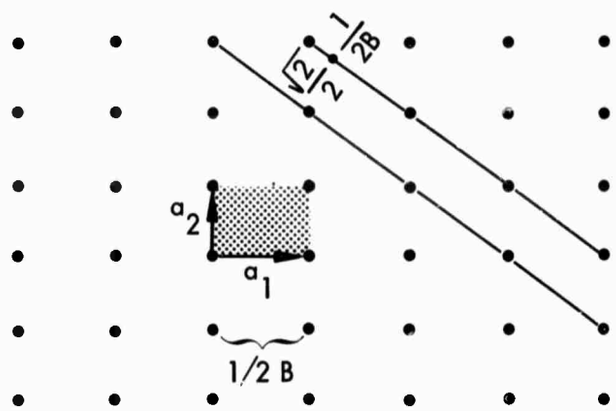

FIGURE VII-2. Rectangular Sampling Lattice

The attachment to the square array is a product of our one-dimensional intuition. We can, in fact, select any noncollinear lattice vectors a_1 and a_2. We should select a_1 and a_2 so that we achieve a resolution of B line pairs in all directions and minimize the number of detectors required in the array. This can be accomplished by making the sampling array a 120-deg rhombic (Fig. VII-3). The number of resolvable line pairs in all directions is B for the array of Fig. VII-3. Suppose we have an m·n square array as represented in Fig. VII-2, with spacing $\frac{1}{2B}$, and consequently B resolvable line pairs in

the x and y directions. The 120-deg rhombic array of equivalent area would use $\frac{nm\sqrt{3}}{2}$ detectors. This represents more than 13 percent fewer detectors in the sampling array. This is a considerable saving in the detector array.

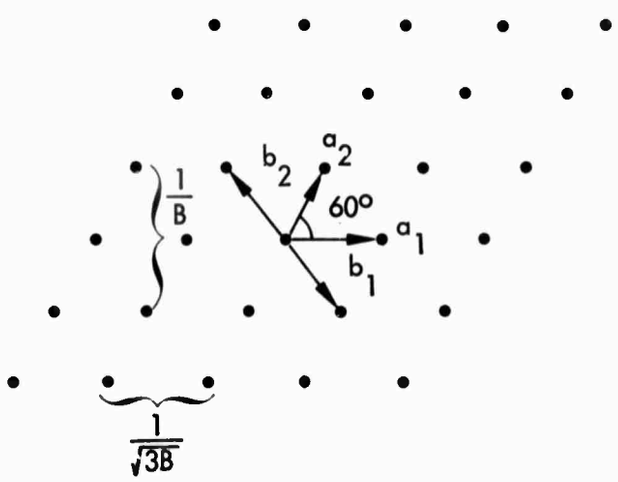

FIGURE VII-3. Best Symmetric Array

We will now turn our attention to the detector size and weighting. Let a(x,y) be the area weighting response of the detectors (Fig. VII-1). The output from each detector is $\int s(x,y)\ a(x-a,\ y-a_2)\ dx\ dy$. Let b(x,y) be the display spot weighting (Fig. VII-1). The output display is given in Eq. VII-3. The spatial frequency representation is given in Eq. VII-4. The difference between a photographic and two-dimensional sampling system is seen by comparing Eqs. VII-1 and VII-4. The film $R(r_1,\ r_2)$ is replaced by the point detector $A(r_1,\ r_2)$ and the spot reproduces $B(r_1,\ r_2)$. There are some very significant differences.

$$o(x,y) = \sum_{n_1=-\infty}^{\infty} \sum_{n_2=-\infty}^{\infty} \int f(x,y)\ a(x-a_1n_1,\ y-a_2n_2)\ dx\ dy \qquad \text{(VII-3)}$$

$$\times\ b(x-a_1n_1,\ y-a_2n_2)\ f(x,y) = \int s(u,v)\ m(u-x,\ v-y)\ du\ dv$$

$$O(r_1,r_2) = \frac{B(r_1,r_2)}{A} \sum_{n_1=-\infty}^{\infty} \sum_{n_2=-\infty}^{\infty} A^*(r_1 + b_1n_1,\ r_2 + b_2n_2)$$

$$\times\ S(r_1 + b_1n_1,\ r_2 + b_2n_2)\ M(r_1 + b_1n_1,\ r_2 + b_2n_2) \qquad \text{(VII-4)}$$

NOTE: Capital letters denote Fourier transforms.

We can see that, given a reasonable spot size and weighting, $B(r_1,r_2)$ is non-zero and significant only on the parallelogram defined by b_1 and b_2, and $O(r_1,r_2)$ is periodic with periodicity defined by b_1 and b_2. Consequently, the "faithful" reproduction of frequencies is confined to the parallelogram defined by b_1 and b_2. The "peculiar" summations in Eq. VII-4 are significant. An image output frequency of (r_1,r_2) contains not only the scene frequency (r_1,r_2) but all frequencies $(r_1+n_1b_1,\ r_2+n_2b_2)$ $n_1,\ n_2 = 0\pm1,\ \pm2,\ \pm3\ldots$ in the scene. This unhappy consequence of the two-dimensional sampling array is called aliasing.

In scenes with high-amplitude periodic components, aliasing can produce rather confusing moiré patterns. However, the vast majority of natural scenes do not contain periodic patterns, and the consequences of aliasing are rather difficult to determine. We see from Eq. VII-4 that the detector size and weighting $A(r_1,r_2)$ takes the role of a prefilter on the frequency content of the scene, $S(r_1,r_2)$. This offers us the possibility of filtering aliased frequencies by the appropriate selection of detector geometry. A square detector of size 2d will be represented by Eq. VII-5.

$$a(x,y) = 1 \quad \begin{matrix} -d \le x \le d \\ -d \le y \le d \end{matrix} \qquad \text{(VII-5)}$$

$$= 0 \quad \text{elsewhere}$$

$$A(r_1,r_2) = \frac{\sin 2\pi\, dr_1\ \sin 2\pi\, dr_2}{\pi^2\ r_1 r_2}$$

The first zero contour in the frequency plane (r_1, r_2) occurs when r_1 or r_2 equals $\frac{1}{2d}$ and to a rough approximation we may consider the square of side $\frac{1}{2d}$ the bandpass of a square detector of size 2d. The detector size which matches the detector bandpass to the Nyquist limits of a sampling lattice of spacing $\frac{1}{2B}$ has $\frac{1}{2d} = B$ or $2d = \frac{1}{B}$. Thus, the "matched" detector is twice as large as the spacing between sampling centers, and the edge of one dececter would touch the edge of the center of the adjacent detector. This construction cannot be realized in a mosaic but can be realized in a scanning system by over scan. The usual mosaic has adjacent detectors touching. The detector size is $\frac{1}{2B}$ and the detector bandpass is 2B. The aliased frequencies would then lie in the band B to 2B. It should be noted that the frequency response of the optical system can be used to filter the aliased frequencies.

Objects smaller than the sample spacing will be detected by a detector mosaic. The detection of such small objects is improved by passing the aliased frequencies unattenuated. As we make the detectors smaller, more of the aliased frequencies are passed. However, making the detector smaller reduces the radiant flux sensed by the detector. The detectivity is proportional to the linear dimension of the detector. Considering both the detector's detectivity and the spatial frequency response, the response to a frequency (r_1, r_2) is given by $\frac{2d \sin 2\pi\, dr_1 \sin 2\pi\, dr_2}{r_1 r_2}$. The detector should not be bigger than $\frac{1}{B}$. Maximizing the response with respect to the detector dimension d can result in a detector smaller than $\frac{1}{B}$. If the detector is smaller than $\frac{1}{2B}$ we may miss the target completely.

The fundamental problem remains. What are the consequencies of aliasing in a normal nonperiodic scene? We do not have an answer. A quick experiment was conducted to yield some intuition. The experimental setup is depicted in Fig. VII-4. This was a coherent optical setup. The sample space D was 0.3 mm and the sampling aperture d was 0.075 mm. One would like d much smaller. Then the integration role played by the detector is represented solely by the first Fourier plane

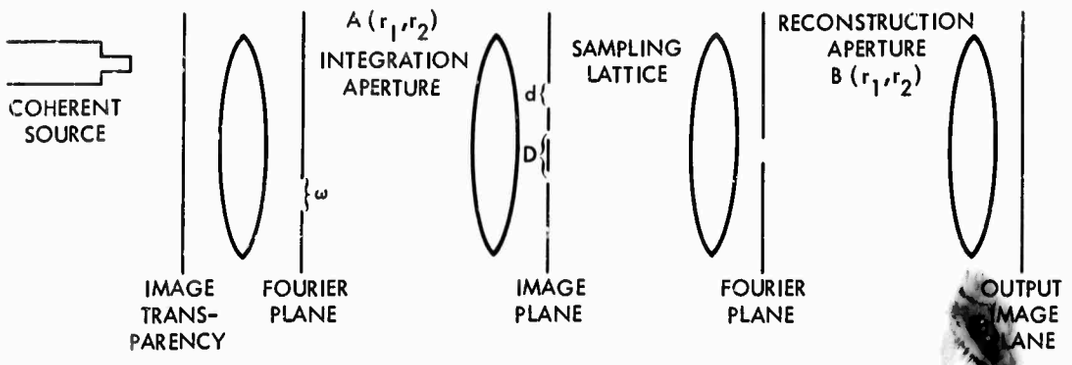

FIGURE VII-4. Experimental Setup

aperture. The integration aperture $A(r_1,r_2)$ was a rectangular hole rather than the desired sinc function. Consequently, the integration function $a(x,y)$ is $\frac{\sin 2\pi\omega x \sin 2\pi\omega y}{\pi^2 xy}$ rather than the usual detector integration function $a(x,y) = 1$ for $\frac{1}{-2\omega} \leq x \leq \frac{1}{-2\omega}$ and $\frac{1}{-2\omega} \leq y \leq \frac{1}{-2\omega}$ and zero elsewhere. High-contrast scene elements can produce an irrelevant ringing in this simulation, but for most portions of the usual scene the sinc function will fall off fast enough. This effect decreases as we make the aperture larger. In short, as we simulate more and more aliasing the approximation of the sinc function integration is less disturbing. Figure VII-5 is the original scene. Figure VII-6 is an image taken in the first image plane of the optical setup without sampling. This is the image seen by the sampling grid. The aperture $A(r_1,r_2)$ was set to pass the Nyquist limit for the sampling grid 1.7 cycles/mm. Both positive and negative frequencies were passed. This corresponds to a detector of size 2D or 0.6 mm.

Figure VII-7 is an image of the aliased frequencies in the band $-\omega$ to -2ω and ω to 2ω. This corresponds to the aliased frequencies for the usual adjoining detectors of size 0.3 mm. Some ringing in Fig. VII-6 can be seen due to the sinc function approximation. Figure VII-8 is a sampled image taken in the final image plane. The reconstruction aperture $B(r_1,r_2)$ was set to pass 1.7 cycles/mm the appropriate reconstruction function for the sampling grids used. This setting was used for the images of Figs. VII-8 and VII-9. Figures

FIGURE VII-5. The Original Scene

NOT REPRODUCIBLE

FIGURE VII-6. Image in the First Image Plane of the Optical Setup Without Sampling. The Image Seen by the Sampling Grid.

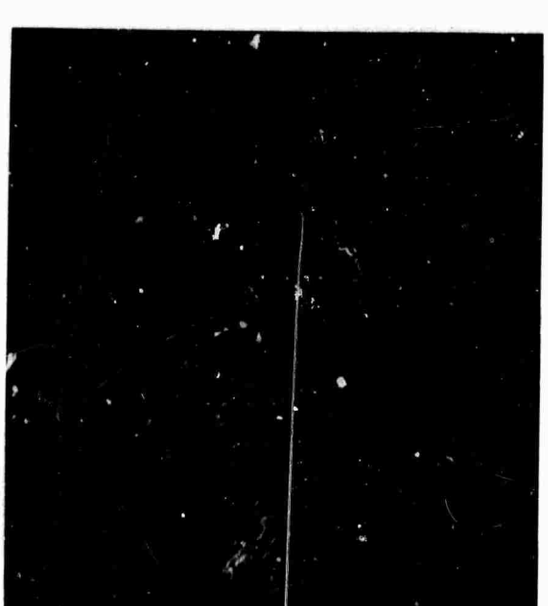

FIGURE VII-7. Image of the Aliased Frequencies in the Band $-\omega$ to -2ω and ω to 2ω.

FIGURE VII-8. Sampled Image $|\omega| \leq 1.7$ cycles/min

FIGURE VII-9. Sampled Image $|\omega| \leq 3.4$ cycles/mm

VII-8 and VII-9 are negatives of the original scene due to the optical setup. Further, the circular ringing in some portions of both scenes are experimental defects, dust spots on the lens.

Figure VII-8 used a setting of $A(r_1,r_2)$, the integration aperture of $|\omega| \leq 1.7$ cycles/mm which simulates the overlapping detectors or an optical transfer function $M(r_1,r_2)$ which cuts off at the Nyquist limit. Figure VII-9 used a setting of $A(r_1,r_2)$, where $|\omega| \leq 3.4$ cycles/mm. This corresponds to the case of adjoining detectors where we have aliased the components of Fig. VII-7. The aliased image of Fig. VII-9 has less contrast than the unaliased image of Fig. VII-8. The reader may see this by examining some of the brighter objects in the scene. The approximations involved make this contrast reduction less apparent than it would have been had we been able to make (1) $A(r_1,r_2)$ a sinc function and (2) d, the sampling aperture, very small. This suggests that the aliased frequencies in a general nonperiodic scene might be considered as noise reducing the contrast.

These aspects of two-dimensional sampled imaging systems are really unresolved. The results presented only suggest that the aliased frequencies reduce the performance significantly. The problem deserves further attention.

SECTION VII. REFERENCE

1. D.P. Peterson and D. Middleton, "Sampling and Reconstruction of Wave-Number Limited Functions in N-Dimensional Spaces," Information and Control, Vol. 5, p. 279, 1962.

ADDENDUM

EXTRACT FROM

SUMMARY OF MATHEMATICAL WORK RELATED TO INFRARED RADIATION DATA PROCESSING*

by

W. Duane Montgomery
Paul C. Shields
James L. Alward

*Infrared and Optical Sensor Laboratory, Willow Run Laboratories, the Institute of Science and Technology, the University of Michigan, Report 6054-4-T, March 1966.

ADDENDUM

EXTRACT FROM SUMMARY OF MATHEMATICAL WORK RELATED TO INFRARED RADIATION DATA PROCESSING

by W. Duane Montgomery, Paul C. Shields, and James L. Alward

1.2. REVIEW OF ONE- AND TWO-DIMENSIONAL SAMPLING THEORY

This review can be best introduced by presenting a heuristic discussion of one-dimensional sampling theory.

1.2.1. ONE-DIMENSIONAL SAMPLING THEORY. A one-dimensional function f(t) is given whose Fourier transform F(r) is given by

$$F(r) = \int_{-\infty}^{\infty} f(t)e^{-j2\pi rt}dt \tag{1}$$

The function f(t) is assumed to be band limited so that F(r) is zero for $|r| > B$. An example of what F(r) might look like is given in Fig. 2. Sampling is done at intervals spaced by T so that the sampled function becomes f(kT), $k = 0, \pm 1, \pm 2, \ldots$. It is necessary to find a weighting function g(t) [also assumed to be Fourier transformable] which can be used to weight the discrete function f(kT) so that the original f(t) can be perfectly reconstructed according to the following weighting formula:

$$f(t) = \sum_{k=-\infty}^{\infty} f(kT)g(t - kT) \tag{2}$$

The function of this formula is to shift the weighting function to center at each of the sample points and multiply its amplitude by the sample value at that point. By using the well known "sifting" property of the Dirac delta function, the values f(kT) in Eq. 2 can be represented as the integral of the product of f(t) and the delta function with its argument evaluated at the sample points:

$$f(t) = \sum_{k=-\infty}^{\infty} g(t - kT) \int_{-\infty}^{\infty} f(\tau)\delta(\tau - kT)d\tau \tag{3}$$

Reversing the order of summation and integration yields

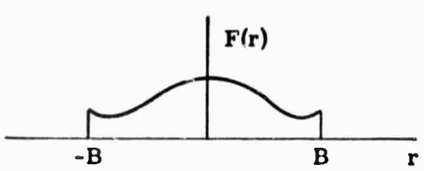

FIGURE 2. REPRESENTATION OF F(r)

$$f(t) = \int_{-\infty}^{\infty} f(\tau)g(t - \tau) \sum_{k=-\infty}^{\infty} \delta(\tau - kT)\,d\tau \qquad (4)$$

The summation of delta functions is a periodic function and can be expanded in a Fourier series. The coefficients are all equal to 1/T:

$$\sum_{k=-\infty}^{\infty} \delta(\tau - kT) = \frac{1}{T} \sum_{k=-\infty}^{\infty} e^{-2\pi jk\tau/T} \qquad (5)$$

Equation 4 is now seen to be a sum of convolutions of the following two functions:

$$\overbrace{\frac{g(t)}{T}} \quad \text{and} \quad \overbrace{f(t)e^{-2\pi jkt/T}}$$

It is well known that the Fourier transform of the convolution of two functions is the product of the Fourier transforms of the functions. Thus, the Fourier transform of Eq. 4 becomes

$$F(r) = \frac{G(r)}{T} \sum_{k=-\infty}^{\infty} F\left(r + \frac{k}{T}\right) \qquad (6)$$

(The shifting of the original F(r) to center at intervals spaced by 1/T results from the exponential term in Function 2 above.)

There are three special cases to consider, depending on whether (a) $T < 1/2B$, (b) $T = 1/2B$, (c) $T > 1/2B$. These situations are illustrated, respectively, in Fig. 3(a), 3(b), and 3(c).

In Fig. 3(a) and 3(b), the center portion (between -B and B) is precisely the Fourier transform F(r) of the desired function. Therefore the purpose of G(r)/T in Eq. 6 must be to select only that center portion. The value of G(r)/T must be unity between -B and B for Fig. 3(a) and 3(b); it must be zero everywhere else for Fig. 3(b); and, for Fig. 3(a), it must be zero everywhere where $\sum_{\substack{k=-\infty \\ \neq 0}}^{\infty} F\left(r + \frac{k}{T}\right)$ is not zero. In the spaces of Fig. 3(a) where the summation function is itself equal to zero, G(r)/T is arbitrary. Figures 4(a) and 4(b) show G(r) for the situations corresponding to those in Fig. 3(a) and 3(b). For the situation illustrated in Fig. 3(c), there is no reconstruction function G(r) which can separate the overlap of the repetitive spectra. The confusion of frequencies resulting from this overlap is sometimes called "aliasing."

Thus it is seen that, in order to permit reconstruction of the sampled function, the sampling period T must be less than or equal to 1/2B. In other words, the sampling must be done at

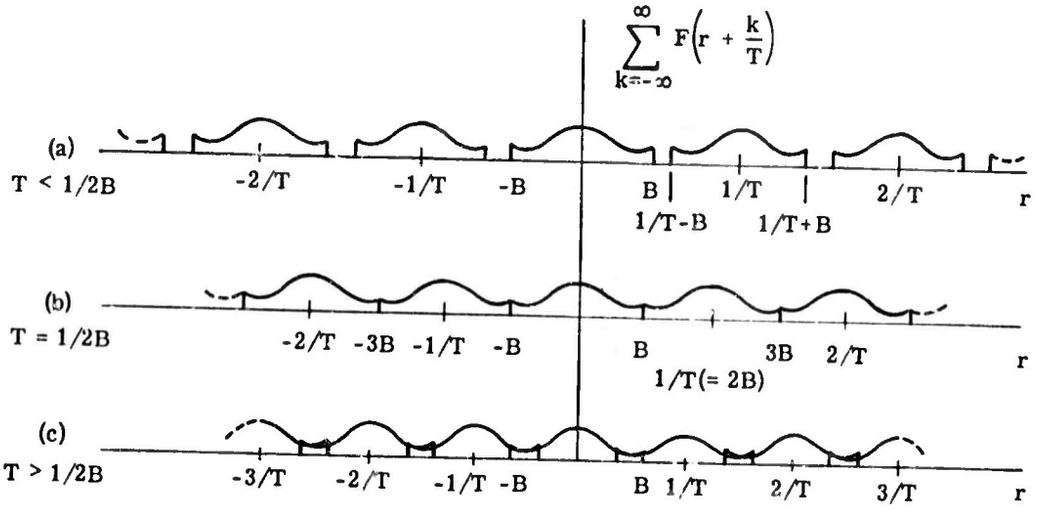

FIGURE 3. ILLUSTRATION OF REPETITIVE SPECTRA

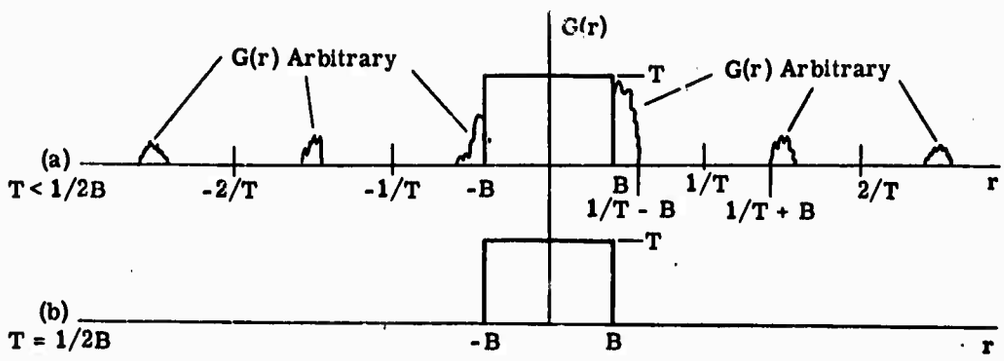

FIGURE 4. RECONSTRUCTION FUNCTION G(r)

least as often as twice every cycle of the highest frequency present in the function. However, as seen from Fig. 3 and 4 and Eq. 6, there is no need to sample more often than T = 1/2B. There is no information about the sampled function to be gained by sampling more often. Thus, the optimum (most efficient) reconstruction function G(r) is the rectangular pulse shown in Fig. 4(b). The corresponding weighting function g(t) is of the familiar $\frac{\sin x}{x}$ form, shown in Fig. 5.

Equation 2, the reconstruction equation for the case of most efficient sampling [T = 1/2B], is depicted in Fig. 6. At each sample point, all weighting functions are zero except the one centered at that sample point. The summation of weighting functions precisely fills in f(t) between the sample points.

It can also be shown that, if the first derivative f'(kT) is sampled, as well as f(kT), then the sample points can be spaced twice as far. In other words, knowledge of the first derivative at each sample point is equivalent to knowledge of the function value halfway between points.

1.2.2. TWO-DIMENSIONAL SAMPLING THEORY. The sampling theory of Petersen and Middleton is multidimensional; that is, functions of arbitrarily high dimension are treated. However, the following discussion is limited to the two-dimensional case because it is of most interest to this contract. The concepts discussed can readily be extended to higher orders of dimensionality.

The function to be sampled is $f(\underline{t})$ where $\underline{t}$ is a two-dimensional variable vector (t_1, t_2), and $f(\underline{t})$ is assumed to have a Fourier transform $F(\underline{r})$ defined by

$$F(\underline{r}) = \int_{R^2} f(\underline{t}) e^{-j2\pi \underline{r}\cdot\underline{t}} \, d\underline{t} = \int_{-\infty}^{\infty} \iint f(t_1, t_2) e^{-j2\pi(r_1 t_1 + r_2 t_2)} \, dt_1 \, dt_2 \qquad (7)$$

(R^2 refers to the two-dimensional Euclidean vector space.) Further, $f(\underline{t})$ is also assumed to be band limited or "wave-number" limited. This means that $F(\underline{r})$ is nonzero only in a finite region of the (r_1, r_2) plane. This finite region is called the "support" of $F(\underline{r})$. The support may be just a single region, or it may be disconnected as shown in Fig. 7.

The function $f(\underline{t})$ is sampled at points on a periodic lattice. This lattice is generated from "basis vectors" $\underline{a}_1$ and $\underline{a}_2$. The collection of vectors $\underline{a}_n$ defining the periodic lattice is generated by the following equation:

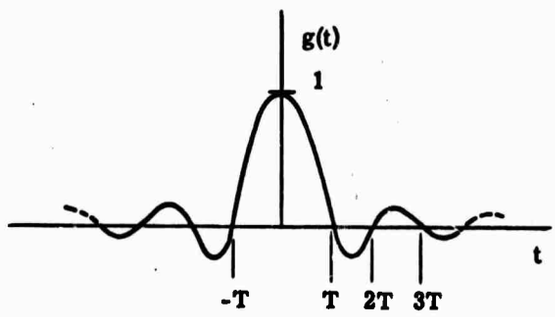

FIGURE 5. OPTIMUM WEIGHTING FUNCTION

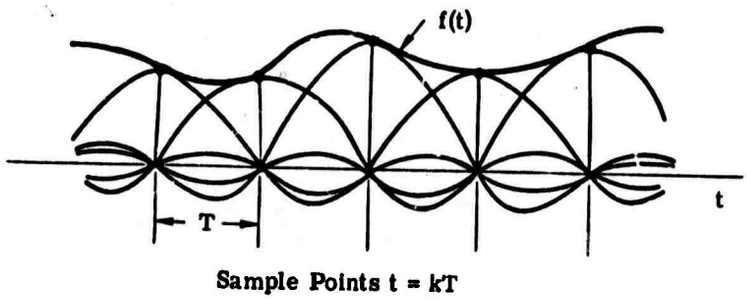

FIGURE 6. RECONSTRUCTION OF SAMPLED FUNCTION

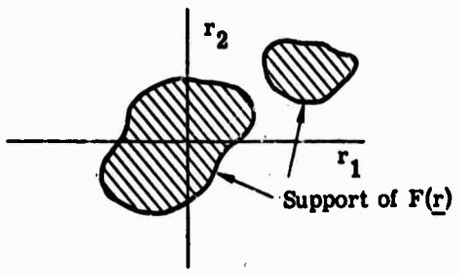

FIGURE 7. EXAMPLE OF WAVE-NUMBER LIMITING

$$\underline{a}_{\underline{n}} = n_1\underline{a}_1 + n_2\underline{a}_2$$

where

$$n_1 \text{ and } n_2 = 0, \pm 1, \pm 2, \ldots$$

This array of lattice points is illustrated in Fig. 8. The sample values of the function are $f(\underline{a}_{\underline{n}})$. The reconstruction, as in the one-dimensional case, is done with a weighting function $g(\underline{t})$, as in Eq. 8:

$$f(\underline{t}) = \sum_{\underline{n}} f(\underline{a}_{\underline{n}})g(\underline{t} - \underline{a}_{\underline{n}}) \tag{8}$$

The problem is to find $g(\underline{t})$ and the best sampling lattice.

The solution is directly analogous to the one-dimensional case. The resulting reconstruction formula, in frequency space $\underline{r}$, is

$$F(\underline{r}) = \frac{G(\underline{r})}{A} \sum_{\underline{n}} F(\underline{r} + \underline{b}_{\underline{n}}) \tag{9}$$

where A is the area of the basis parallelogram. This result is directly comparable to Eq. 6 for the one-dimensional case, in which the spacing of the samples was T, and the spacing of the shifted spectra was 1/T. In Eq. 9, the samples are spaced according to the lattice $\underline{a}_{\underline{n}}$, and the spectra (supports) are shifted according to a reciprocal lattice $\underline{b}_{\underline{n}}$. This reciprocal lattice has basis vectors $\underline{b}_1$ and $\underline{b}_2$ defined so that $\underline{a}_1 \cdot \underline{b}_1 = 1$, $\underline{a}_2 \cdot \underline{b}_2 = 1$, $\underline{a}_1 \cdot \underline{b}_2 = 0$, $\underline{a}_2 \cdot \underline{b}_1 = 0$. This definition results in the geometry shown in Fig. 9, where $\underline{b}_1$ is perpendicular to $\underline{a}_2$ and $|\underline{b}_1| = \frac{1}{|\underline{a}_1| \sin\theta}$, and $\underline{b}_2$ is perpendicular to $\underline{a}_1$ and $|\underline{b}_2| = \frac{1}{|\underline{a}_2| \sin\theta}$. The area of the basis parallelogram B is equal to 1/A. Assume that the support of $F(\underline{r})$ appears as in Fig. 10. The array of these supports on the lattice $\underline{b}_{\underline{n}}$ corresponding to Eq. 9 is shown in Fig. 11.

There is a basic difference between the results of two-dimensional and one-dimensional sampling theory. In the one-dimensional case, one could always choose T = 1/2B and thus eliminate the regions in which G(r) could be arbitrary. In general, this cannot be done for the two-dimensional case because, depending on the shape of the support, there will be regions between the supports in which $G(\underline{r})$ will be arbitrary, no matter how closely packed the supports may be. Overlapping, of course, is not permitted. The problem, given $F(\underline{r})$, is to select a lattice $\underline{b}_{\underline{n}}$ such that the fraction of the basis parallelogram B covered by the array of supports is a maximum. This is equivalent to minimizing the $\underline{b}_{\underline{n}}$ lattice spacings (and thus the area B) to that degree which is still consistent with the avoidance of overlap. This fraction is called the

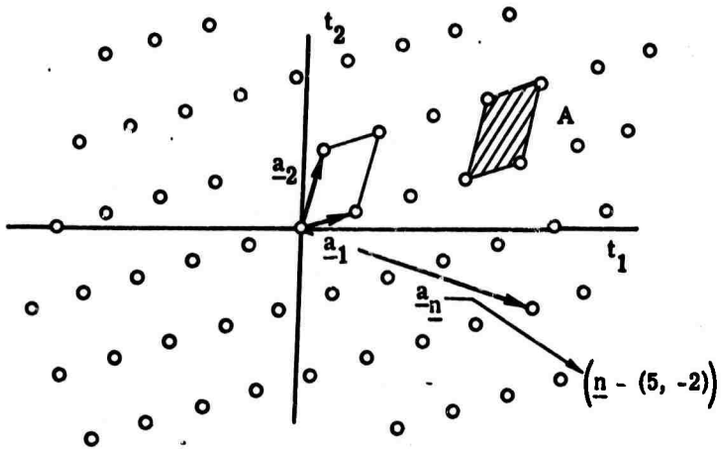

FIGURE 8. GENERATION OF SAMPLING LATTICE

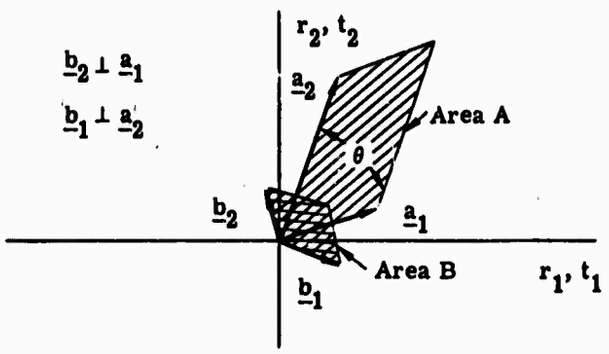

FIGURE 9. GEOMETRY OF BASIS VECTOR $\underline{b}$

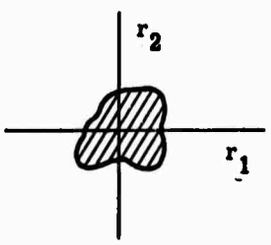

FIGURE 10. REPRESENTATIVE SUPPORT FOR F(r)

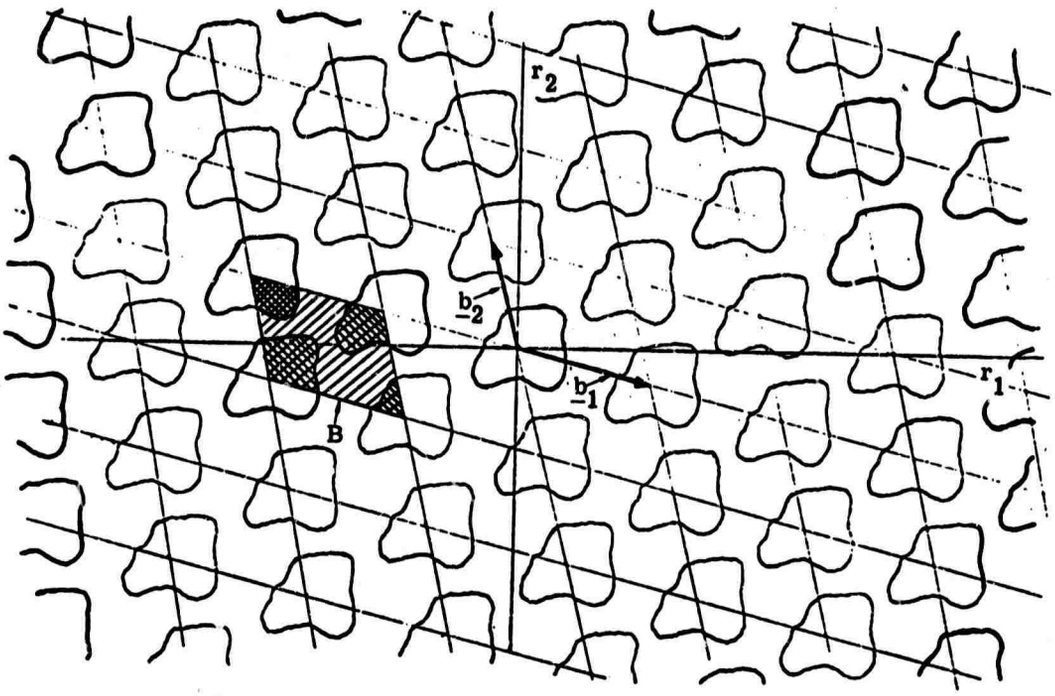

FIGURE 11. ARRAY OF SUPPORTS

sampling efficiency. Maximizing the sampling efficiency will in general be a cut-and-try process. In certain special cases, the lattice for maximum efficiency is known. For example, if the support is circular, the maximally efficient lattice is a 120^0 rhombic lattice. There are also examples of supports for which the sampling efficiency can be 100%. A few of these are shown in Fig. 12.

Once the sampling lattice efficiency has been maximized, thus determining $\underline{b}_n$ and therefore $\underline{a}_n$, $G(\underline{r})$ must be chosen equal to A over the support centered at the origin, and equal to zero over all other supports. For simplicity, it is probably best to choose $G(\underline{r})$ equal to zero over the interstitial spaces as well.

In most of the practical cases where $f(\underline{t})$ is real, the support of the spectrum of the sampled function is symmetrical about the origin. This is particularly true for situations in which the band limiting results from the resolution limitations of optical systems. When the support is symmetrical, it usually can be approximated by a simple symmetrical region such as a square, a rectangle, a circle, or an ellipse. It is much easier to select a sampling lattice based on these simple geometrical shapes, because the optimum packing density is already known; no cut-and-try process is needed.

1.3. SAMPLING OF VALUES WEIGHTED OVER A FINITE AREA

This section discusses the technique of sampling the integral of the function in a weighted region around each sample point; the investigation of this technique is presented in Appendix A. A sampling technique of this kind is often realized in such devices as mosaic detector arrays, reticles, and scanning apertures.

If the weighting function is represented by $\gamma(\underline{t})$, then the sample values $f(\underline{a}_n)$ in Eq. 8 must be replaced by the convolution of $f(\underline{a}_n)$ with the weighting function to yield the following reconstruction formula:

$$f(\underline{t}) = \sum_{\underline{n}} g(\underline{t} - \underline{a}_n) \int_{R^2} \gamma(\underline{a}_n - \underline{s}) f(\underline{s})\, d\underline{s} \qquad (10)$$

where $\underline{s}$ is a dummy variable. The size of the support of $\gamma(\underline{t})$ is limited by the support of $F(\underline{r})$: $\gamma(\underline{t})$ is physically restricted to have nonzero values only over a finite region of space. In most applications (such as reticle bars or mosaic detector arrays), the response of the weighting function $\gamma(\underline{t})$ is sharply defined spatially. This means its Fourier transform $\Gamma(\underline{r})$ will have an oscillatory behavior, taking on a value of zero on several closed curves in the $\underline{r}$ plane. To permit reconstruction of $f(\underline{t})$, the support of $F(\underline{r})$ cannot cross a zero curve of $\Gamma(\underline{r})$. If the support

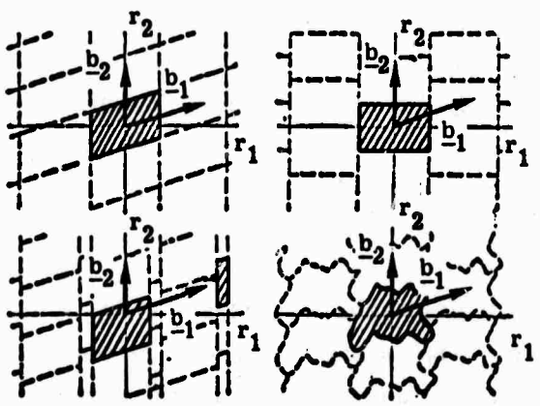

FIGURE 12. EXAMPLES OF SUPPORTS PERMITTING 100% SAMPLING EFFICIENCY

of $F(\underline{r})$ is simply connected, it must be entirely contained within the innermost zero curve of $\Gamma(\underline{r})$. This is illustrated in Fig. 13. There results a minimum size for the first zero curve of $\Gamma(\underline{r})$ and therefore a maximum size for $\gamma(\underline{t})$. [For a circular uniform weighting function, the diameter of the circle can be no larger than the spatial wavelength of the highest space frequency present in $F(\underline{r})$.] Thus, the support of $F(\underline{r})$ determines both the maximum spacing of the sampling lattice $\underline{a}_n$ and the maximum extent of the weighting function. When both the sample spacing and the extent of the weighting function are maximized with respect to a given support, the weighting function and the lattice are said to be "matched."

1.4. SAMPLING OF DERIVATIVES AND GRADIENTS

Three of the extensions of the basic Petersen-Middleton work are concerned with the sampling of gradients or derivatives of the multidimensional function as well as values of the function itself. The results of these extensions are summarized here.

A common form of sampling is line-scanning in which discrete points are sampled by a point aperture as it scans along a raster of parallel lines. The directional derivative along the scan line can also be sampled. Such a sampling is a special case of sampling the function and its gradient.

Appendix B presents an N-dimensional discussion of sampling, not only of sampling the function $f(\underline{a}_n)$ at the sample points, but the gradient $\nabla f(\underline{a}_n)$ as well. The gradient is, of course, a vector quantity. Thus, the sample lattice would have gradient vectors for each sample point, as shown in Fig. 14. The effect of sampling the gradient is similar to that of sampling the derivative of one-dimensional functions. It provides information about the behavior of the function between the sample points. Thus, there is a certain amount of overlap of supports permitted on the $\underline{b}_n$ lattice. In Appendix B, general conditions on the nature of the overlap are derived, and specific examples are worked out for a rectangular support and for a disconnected three-region support. For these cases, the reconstruction function $G(\underline{r})$ is not a constant over the central support, but consists of sloping planar surfaces.

Appendix C presents a two-dimensional treatment of a line-scan-sampling procedure in which the scan lines are equally spaced and pass through the sample points. At each sample point, the value of the function $f(\underline{a}_n)$ is read, and the projection of the gradient along the scan line $[\underline{\mu} \cdot \nabla f(\underline{a}_n)]$ is read; $\underline{\mu}$ is the unit vector in the direction of scan. The optimization procedure is the same as before; that is, to minimize the number of sample points per unit area (maximize basis area A, minimize basis area B). The scan direction is chosen to be that of the basis vector $\underline{a}_1$. The results show that there can be several different optimum lattices

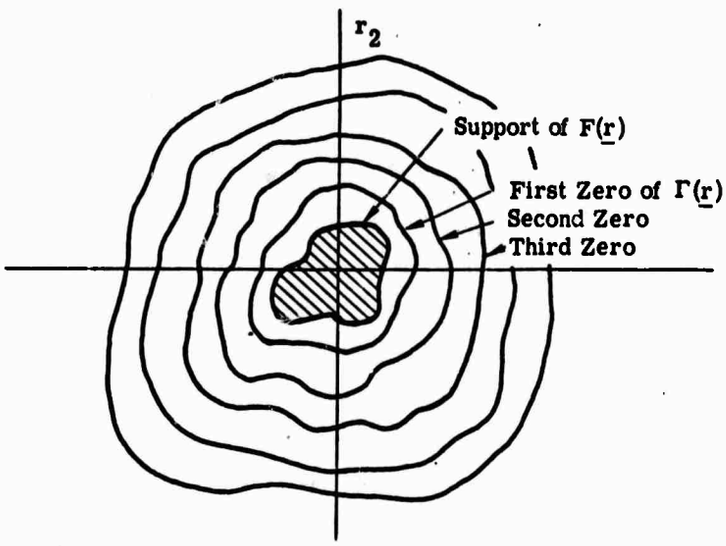

FIGURE 13. LIMITATION ON $\Gamma(\underline{r})$

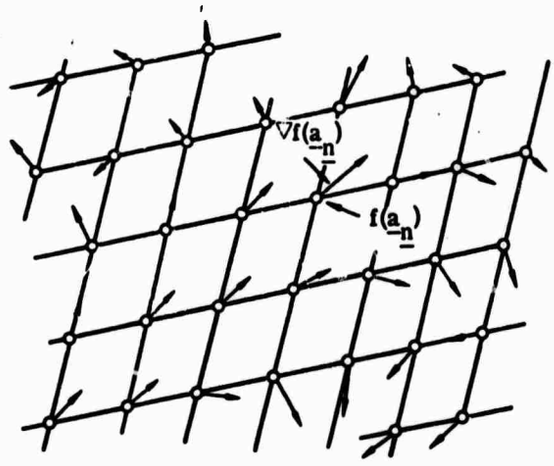

FIGURE 14. ILLUSTRATION OF GRADIENT SAMPLES

with the same maximum basis area A, each of which can be scanned in an infinite number of ways. The "infinite number of ways" arises because the function and its gradient component can be sampled less times per unit distance along the scan lines, while the lines themselves become more closely spaced. An example is worked out assuming an isotropic support.

Appendix D is an extension of the gradient analysis of Appendix A to include sampling of k-order derivatives of the function. For example, if $k = 2$, the following quantities would be determined for each sample point ($\underline{a}_{\underline{n}}$): $f, \frac{\partial f}{\partial t_1}, \frac{\partial f}{\partial t_2}, \frac{\partial^2 f}{\partial t_1^2}, \frac{\partial^2 f}{\partial t_2^2}$, and $\frac{\partial^2 f}{\partial t_1 \partial t_2}$. Needless to say, the sampling of six quantities of information tells a great deal about the behavior of the function between the sample points. It is shown that, for a given support, the optimum basis area B will be less for a higher order k than for a lower order.

Appendix A
SYNTHESIS OF FUNCTIONS FROM SAMPLED WEIGHTINGS

A.1. INTRODUCTION

Consider a class of real valued transformable functions $f(\underline{t})$, $\underline{t} = (t_1, t_2)$, defined on the plane R^2 and characterized by the set $\mathcal{S}$ in reciprocal space over which they have nonzero spectra. For a given transducer function $\gamma(\underline{t})$, we seek a reconstruction function $g(\underline{t})$ universal with respect to the class of functions $f(\underline{t})$ such that

$$f(\underline{t}) = \sum_{\underline{n}} g(\underline{t} - \underline{a}_{\underline{n}}) \int_X \gamma(\underline{s} - \underline{a}_{\underline{n}}) f(\underline{s})\, d\underline{s} \tag{11}$$

The vectors $\underline{a}_{\underline{n}} = n_1\underline{a}_1 + n_2\underline{a}_2$, $\underline{n} = (n_1, n_2)$ terminate on the sampling lattice generated by the basis vectors $\underline{a}_1$, $\underline{a}_2$. The form of reconstruction in Eq. 11 is from Middleton [3] and stems from classical work on sampling theory.

Some notational conventions are the following:

$$f(\underline{t}) = \int_{\mathcal{S}} F(\underline{r}) e^{2\pi i \underline{t}\cdot\underline{r}}\, d\underline{r}, \quad \underline{r} = (r_1, r_2) \tag{12}$$

where $\mathcal{S}$ is all of reciprocal space R^2, and

$$F(\underline{r}) = \int_X f(\underline{t}) e^{-2\pi i \underline{t}\cdot\underline{r}}\, d\underline{t}, \quad \underline{t} = (t_1, t_2) \tag{13}$$

where X is all of the original space R^2.

If $h(\underline{t})$ is periodic on the sampling lattice $(\underline{a}_1, \underline{a}_2)$, then

$$h(\underline{t}) = \sum_{\underline{n}} c_{\underline{n}} e^{2\pi i \underline{t}\cdot\underline{b}_{\underline{n}}}, \quad \underline{b}_{\underline{n}} = n_1\underline{b}_1 + n_2\underline{b}_2 \tag{14}$$

where the reciprocal lattice $(\underline{b}_1, \underline{b}_2)$ has the usual properties

$$\underline{a}_i \cdot \underline{b}_j = \delta_{ij} \text{ for } i, j = 1, 2 \tag{15}$$

and

$$c_{\underline{n}} = \frac{1}{A} \int_{\mathcal{A}} h(\underline{t}) e^{-2\pi i \underline{t}\cdot\underline{b}_{\underline{n}}}\, d\underline{t} \tag{16}$$

Here, ω is the subset of X which is contained in the parallelogram generated by the two vectors $\underline{a}_1$, $\underline{a}_2$; A is the area of the set ω; and, similarly, B is the "area" of the subset $\mathcal{B}$ of $\mathcal{M}$ which is contained in the parallelogram generated by $\underline{b}_1$, $\underline{b}_2$. Clearly, $A = |\underline{a}_1 \times \underline{a}_2|$, $B = |\underline{b}_1 \times \underline{b}_2|$, and $A = 1/B$.

Two cases are considered: In the first, all the functions are assumed to be Lebesgue transformable on R^2, and equality means that the functions differ only on a set of Lebesgue measure zero. Here, the transducer function is restricted to one whose spectrum is nonzero almost everywhere on $\mathcal{S}$. For this case, a rectangular, uniformly-weighted transducer is investigated. In the second, much more restrictive conditions are imposed in order to get reconstruction of $f(\underline{t})$ for all $\underline{t}$. Here, we assume that f, γ, and g are Riemann transformable, which implies continuity almost everywhere. The transducer function $\gamma(\underline{t})$ is, in addition, assumed to be nonzero on the set $\mathcal{S}$. Recall that $\mathcal{S}$ is the set on which the class of functions $f(\underline{t})$ have a nonzero spectrum.

A.2. THE CASE OF LEBESGUE TRANSFORMABLE FUNCTIONS ON R^2

Taking the Fourier transform of both sides of Eq. 11, we obtain interchanging integrations and summations,

$$F(\underline{r}) = G(\underline{r}) \sum_{\underline{n}} e^{-2\pi i \underline{a}_{\underline{n}} \cdot \underline{r}} \int_{\mathcal{M}} \Gamma(\underline{q}) F(\underline{q}) e^{2\pi i \underline{a}_{\underline{n}} \cdot \underline{q}} d\underline{q}$$

where we note that $\Gamma(\underline{q}) = \Gamma(-\underline{q})$ for real γ.

If we define

$$c_{\underline{n}} = \frac{1}{B} \int_{\mathcal{M}} \Gamma(\underline{q}) F^*(\underline{q}) e^{-2\pi i \underline{a}_{\underline{n}} \cdot \underline{q}} d\underline{q} \tag{17}$$

we have

$$F^*(\underline{r}) = \frac{G^*(\underline{r})}{A} \sum_{\underline{n}} c_{\underline{n}} e^{2\pi i \underline{a}_{\underline{n}} \cdot \underline{r}} \tag{18}$$

If we define $\mathcal{B} + \underline{b}_{\underline{k}} = \{\underline{r} + \underline{b}_{\underline{k}} \mid \underline{r} \in \beta\}$, we can write Eq. 17 is

$$c_{\underline{n}} = \frac{1}{B} \sum_{\underline{k}} \int_{\mathcal{B}+\underline{b}_{\underline{k}}} \Gamma(\underline{q}) F^*(\underline{q}) e^{-2\pi i \underline{a}_{\underline{n}} \cdot \underline{q}} d\underline{q}$$

By changing variables $\underline{q} - \underline{b}_{\underline{k}} = \underline{r}$ and interchanging summation and integration, we obtain

$$c_{\underline{n}} = \frac{1}{B}\int_{\mathcal{B}} \sum_{\underline{k}} \Gamma(\underline{r} + \underline{b}_{\underline{k}})F^*(\underline{r} + \underline{b}_{\underline{k}})e^{-2\pi i \underline{a}_{\underline{n}}\cdot\underline{r}}\, d\underline{r} \tag{19}$$

Comparing Eq. 18 and 19 with Eq. 14 and 16, respectively, we have,

$$F(\underline{r}) = \frac{G(\underline{r})}{A}\sum_{\underline{k}} \Gamma^*(\underline{r} + \underline{b}_{\underline{k}})F(\underline{r} + \underline{b}_{\underline{k}}) \tag{20}$$

We will here define some useful concepts in connection with Eq. 20. For a given set $\mathcal{S}$ and reciprocal lattice $(\underline{b}_1, \underline{b}_2)$, let $\mathcal{S}_p = \left\{\underline{r} + \underline{b}_{\underline{n}} \,|\, \underline{r} \in \mathcal{S}, n_i \text{ integers}\right\}$ be called the periodic extension of $\mathcal{S}$ by $(\underline{b}_1, \underline{b}_2)$. We will say that $\mathcal{S}_p$ has overlap if for an arbitrary but fixed $\Gamma(\underline{r})$, an $F(\underline{r})$ can be found such that $\sum_{\underline{k}\neq\underline{0}} \Gamma(\underline{r} + \underline{b}_{\underline{k}})F(\underline{r} + \underline{b}_{\underline{k}})$ is unequal to zero on a set $\mathcal{P} \subset \mathcal{S}$ of positive measure. If $\mathcal{S}_p$ has overlap for all choices of $(\underline{b}_1, \underline{b}_2)$, we will call $\mathcal{S}$ unextendable. If $\mathcal{S}$ is bounded except for a set of measure zero, then it is clear that $\mathcal{S}$ is extendable. Equation 20 shows that for an extendable $\mathcal{S}$ and appropriate $(\underline{b}_1, \underline{b}_2)$, we have

$$F(\underline{r}) = \frac{G(\underline{r})}{A}\Gamma^*(\underline{r})F(\underline{r}) \qquad \text{for } \underline{r} \in \mathcal{S} \tag{21}$$

which can be satisfied by letting $G = A/\Gamma^*$. Although G is not uniquely determined for $\underline{r} \notin \mathcal{S}$, we can let it equal zero so that Eq. 20 will be satisfied for all $\underline{r}$. Thus we see that an extendable $\mathcal{S}$ is a sufficient condition for the existence of $g(\underline{t})$, providing that $1/\Gamma^*$ is transformable on $\mathcal{S}$.

Let us here consider a rectangular transducer which weights uniformly over its surface. If $\gamma(\underline{t}) = 1$ for $\underline{t}$ in the rectangle $-\epsilon \leq t_1 \leq \epsilon$, $-\delta \leq t_2 \leq \delta$ with $\epsilon, \delta > 0$, we can easily derive

$$\Gamma(\underline{r}) = 4\epsilon\delta \frac{\sin 2\pi r_1\epsilon}{2\pi r_1\epsilon}\,\frac{\sin 2\pi r_2\delta}{2\pi r_2\delta} \tag{22}$$

If $\mathcal{S}$ contains a neighborhood of a point on the boundary of the rectangle $-1/2\epsilon \leq r_1 \leq 1/2\epsilon$, $-1/2\delta \leq r_2 \leq \delta/2$, we can show that $1/\Gamma^*$ is not transformable on $\mathcal{S}$. If $\mathcal{S}$ contains a neighborhood of a point $\underline{t}$ for which $t_1 = 1/2\epsilon$ then a β is chosen such that $0 < \beta < 1/2\epsilon$ and $(1/2\epsilon - \beta, t_2) \in \mathcal{S}$. We now consider the limit

$$\lim_{\substack{\alpha\to 0\\ \beta>\alpha>0}} \int_{\frac{1}{2\epsilon}-\beta}^{\frac{1}{2\epsilon}-\alpha} \left| \frac{2\pi r_1 \epsilon e^{2\pi i \underline{r}\cdot\underline{t}}}{\sin 2\pi r_1 \epsilon} \right| dr_1 \tag{23}$$

Thus we have

$$\int_{\frac{1}{2\epsilon}-\beta}^{\frac{1}{2\epsilon}-\alpha} \frac{2\pi r_1 \epsilon}{\sin 2\pi r_1 \epsilon} dr_1 > \int_{1/2\epsilon-\beta}^{1/2\epsilon-\alpha} \frac{2\pi\epsilon(1/2\epsilon-\beta)}{\sin 2\pi r_1 \epsilon} dr_1$$

Now consider the substitution $r_1 + 1/2\epsilon = q$,

$$\int_{\frac{1}{2\epsilon}-\beta}^{\frac{1}{2\epsilon}-\alpha} \frac{K}{\sin 2\pi r_1 \epsilon} dr_1 = K\int_{\alpha}^{\beta} \frac{dq}{\sin 2\pi q\epsilon} > K\int_{\alpha}^{\beta} \frac{dq}{2\pi q\epsilon} = \frac{K}{2\pi\epsilon} \log q \Big|_{\alpha}^{\beta} \qquad +\infty \text{ as } \alpha \qquad 0+$$

Therefore, if $\mathcal{A}$ is an open, simply connected set containing the origin, it must lie within the rectangle $1/2\epsilon \le r_1 \le 1/2\epsilon$, $1/2\delta \le r_2 \le 1/2\delta$, if we are to solve a universal $g(\underline{t})$. If ϵ and δ are small, such an $\mathcal{A}$ might cover a large "area" in $\mathcal{N}$, and we would then say that the transducer has a high "frequency" response.

Notice that for the usual simply connected spectrum [domain to $F(\underline{r})$] which contains the origin, the previous work implies that it must lie within the rectangle $K = \{(r_1, r_2) | 1/2\epsilon < r_1 < 1/2\epsilon, 1/2\delta \le r_2 < 1/2\delta\}$ for the case of a uniform, rectangular transducer. When we speak of reconstruction of $f(\underline{t})$, we main via the summation form of Middleton [3], so that what we have here is a frequency cutoff of $r_0 = 1/2\epsilon$ in the t_1 direction. This says that the smallest spatial wavelength λ_t to which the transducer can respond in the t_1 direction is equal to its dimension 2ϵ in that direction. (If the rectangular transducer were replaced by a uniform, circular one of radius ρ, our results would be similar with a Bessel function as the transform of $\lambda(t)$ having its first zero at $r_0 = 1/2p$.) This is a very interesting result for if we restrict our sampling, for the moment, to a rectangular lattice, we already know that the cutoff frequency due to the lattice spacing ξ in the t_1 direction is 2ξ. That is, the smallest spatial wavelength λ_s to which the sampling lattice can respond in the t_1 direction is equal to half the spacing 2ξ in that direction. If the transducer and lattice are "matched," we should have $\lambda_s = \lambda_t$. For the unmatched condition $\lambda_s < \lambda_t$, we see that the transducer is the limiting factor. In such a case, we should either make the transducers smaller, if higher frequencies are desired, or, if we do not want to raise the frequency response, sample less often. Similar considerations hold for $\lambda_t < \lambda_s$.

When the above results are applied to electron beam scanning, assuming a uniform weighting over the beam spot, we see that a matched condition in the vertical direction (the scanning

is assumed to be horizontal) is one in which the radius of the spot is equal to the vertical spacing between lines. In the horizontal direction, we are limited by the spot size so that nothing is gained by reading the output voltage continuously. If it is convenient, we need only sample the voltage at times corresponding to a horizontal distance equal to the spot radius.

A.3. THE CASE OF RIEMANN TRANSFORMABLE FUNCTIONS

We can proceed exactly as in the previous case to arrive at Eq. 20. Here we define $\mathcal{S}_p$ just as before, but we redefine the concept of overlap in a way more appropriate to the present case. For a given $\mathcal{S}$ and lattice $(\underline{b}_1, \underline{b}_2)$, we say that $\mathcal{S}_p$ has overlap if there exists a $\underline{r}_0 \in \mathcal{S}$ such that $\underline{r}_0 + \underline{b}_{\underline{n}} \in \mathcal{S}$ for some $\underline{n} \neq \underline{0}$. As before, we say that $\mathcal{S}$ is unextendable if $\mathcal{S}_p$ has overlap for all choices of $(\underline{b}_1, \underline{b}_2)$. It can easily be seen from the following, that the necessary and sufficient condition for a solution of $G(\underline{r})$ is that $\mathcal{S}$ be extendable. As before, bounded sets are clearly extendable.

If $\mathcal{S}$ is unextendable, then for any lattice $(\underline{b}_1, \underline{b}_2)$ there exists a point $\underline{r}_0 \in \mathcal{S}$ such that $\underline{r}_0 + \underline{b}_{\underline{n}} \in \mathcal{S}$ for $\underline{n} \neq \underline{0}$, so we write (note that $G \neq 0$ for $F \neq 0$ is necessary)

$$F(\underline{r}_0)\left[\frac{A}{G(\underline{r}_0)} - \Gamma^*(\underline{r}_0)\right] = \sum_{\underline{k}\neq\underline{0}} \Gamma^*(\underline{r}_0 + \underline{b}_{\underline{k}})F(\underline{r}_0 + \underline{b}_{\underline{k}}) \tag{24}$$

With at least one nonzero term on the right side of Eq. 24, it is clear that different F's can be chosen so that the left side is constant but so that the right side has different values. Thus a necessary condition for the solution of $G(\underline{r})$ is that the $\mathcal{S}$ be extendable. This condition is clearly sufficient because, for an appropriate reciprocal lattice, the right side of Eq. 24 will be zero for all $\underline{r} \in \mathcal{S}$. In such a case, we may choose $G = A/\Gamma^*$ for all $\underline{r} \in \mathcal{S}$. For $\underline{r} \in \mathcal{S}_p - \mathcal{S}$ for which the right side of Eq. 24 is nonzero, we must choose $G = 0$. For $\underline{r} \in \mathcal{N} - \mathcal{S}_p$, the choice of G is arbitrary.

The necessity of choosing $\Gamma \neq 0$ on $\mathcal{S}$ is clearly seen from Eq. 24. Thus the result for a rectangular, uniform transducer is much the same as in the previous case.

An open question that appears here is whether unbounded, nontrivial, extendable sets $\mathcal{S}$ exist. It seems that there should be none, but a rigorous proof is needed.

Appendix B
THE GRADIENT IN THE SAMPLING OF N-DIMENSIONAL BAND-LIMITED FUNCTIONS

B.1. INTRODUCTION

The use of sampled data is well known in control-engineering problems. The Whittaker-Shannon formulation is the one usually used when it is desirable to linearly interpolate the data exactly for band-limited functions. Since the publication of their work, generalizations in several directions have continued to shed additional light on the reconstruction problem. In the work of Fogel [4] and Jagerman and Fogel [5], the periodic sampling of the values of a function is extended to include the first derivative as well. This is carried out in essentially one dimension for band-limited functions, with the result that one need only sample half as often because each sample contains two pieces of information instead of one. These results are generalized by Linden and Abramson [6] to the case of an arbitrary number of derivatives. On the other hand, Petersen and Middleton [1] have extended the original form of Whittaker-Shannon to the case of sampled values on periodic lattices for functions defined on N-dimensional Euclidean space. The purpose of this appendix is to apply a reconstruction formula, similar to the one used by Middleton [3], to the problem of using the sampled values of the function and its gradient on a periodic lattice in N dimensions.

To state the problem more precisely, our universal set of functions consists of the complex valued functions of L_2 defined on N-dimensional space R^N. The particular set of functions of interest is that which contains those functions whose Fourier transforms (which always exist) have a fixed bounded support of positive measure in reciprocal space.[1] We have generalized the use of the one-dimensional term "band-limited" to designate this bounding of the support S for the N-dimensional case. Both the original space, upon which the functions $f(\underline{t})$ are defined, and the reciprocal space, upon which their transforms $F(\underline{r})$ are defined, are denoted by R^N, since no physical dimensions such as time or distance enter the formulation. For any given basis $\left\{\underline{a}_i; i = p, \ldots, N\right\}$ of the space R^N, we have an associated lattice $\left\{\underline{a}_{\underline{n}} = \sum_{i=1}^{N} n_i \underline{a}_i; \underline{n} = (n_1, n2, \ldots, n_N), n_i \text{ integers}\right\}$. This lattice, consisting of the points or vectors, has a reciprocal lattice counterpart $\left\{\underline{b}_{\underline{n}} = \sum_{i=1}^{N} n_i \underline{b}_i; \underline{n} = (n_1, n_2, \ldots, n_N), n_i \text{ integers}\right\}$ generated by

[1] The support of a function is that subset of its domain of definition on which it assumes nonzero values.

Appendix C
RECONSTRUCTION OF PICTURES FROM SCANNED RECORDS

C.1. INTRODUCTION

In a paper by Petersen and Middleton [1], there appears a generalization of the Whittaker-Shannon sampling theorem which enables one to proceed to higher dimensions while sampling on periodic lattices other than those of rectangular form. These results have been generalized (Appendix D) to the sampling of partial derivatives of arbitrary order in N dimensions. The present discussion presents an adaptation of these general methods to the specific problem of reconstructing a two-dimensional picture from a scanned record. It is assumed that the picture is typical of those non-negative intensity patterns which appear in the image plane of an optical system. These are band-limited (i.e., their two-dimensional Fourier transforms have a bounded support), because of the finite aperture of the system. Aside from this actual band-limiting, there may be practical reasons, such as resolution requirements, for considering the picture to be more severely band-limited. In addition to the band-limiting, the picture, except for minor diffraction effects, is essentially spatially limited.

The following argument assumes that such a picture is scanned by a "beam" which moves along a set of parallel equally spaced lines as shown in Fig. 20. The intensity and its rate of change with distance along the direction of scan are sampled periodically in such a way that the sampled points lie on a two-dimensional lattice $\{\underline{a}_{\underline{n}}\}$. Such a lattice is generated by taking integral linear combinations $n_1\underline{a}_1 + n_2\underline{a}_2 = \underline{a}_{\underline{n}}$ of any two basis vectors $\{\underline{a}_1, \underline{a}_2\}$, where $\underline{n} = (n_1, n_2)$ gives the integers involved. Each sampling lattice has a corresponding reciprocal lattice $\{\underline{b}_{\underline{n}}\}$ generated by basis vectors $(\underline{b}_1, \underline{b}_2)$ which are defined by the relations $\underline{a}_i \cdot \underline{b}_j = \delta_{ij}$. The picture is described by an intensity function $f(\underline{t})$, with $\underline{t}$ in R^2, and its Fourier transform $F(\underline{r})$ is defined on the reciprocal space (sometimes called wave-number space) of R^2. This latter space is designated as R^2 also, although with the components of $\underline{t}$ having the dimensions of distance, the components of $\underline{r}$ must have the dimensions of reciprocal distance. The reciprocal lattice clearly lies in the reciprocal space.

For purposes of mathematical convenience, we assume that our class of functions $f(\underline{t})$ are all L_2 functions on R^2 whose transforms $F(\underline{r})$ all have the same fixed bounded support S of positive measure, Fig. 21. It is clear that the scanning procedure just outlined is not one which will give the gradient of the intensity at each sample point, but rather the projection of it along the direction of scan. In Appendix B, the reconstruction formula is

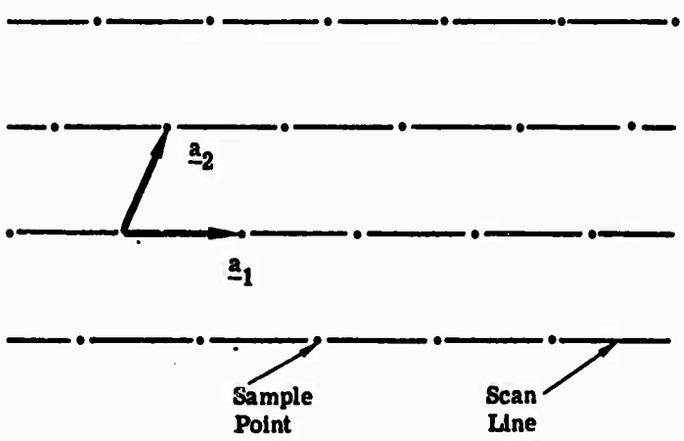

FIGURE 20. ILLUSTRATION OF SCAN LINES

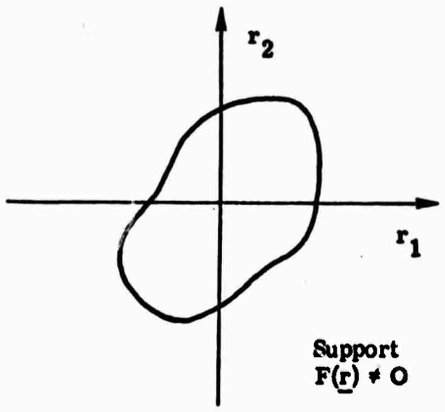

FIGURE 21. EXAMPLE OF SUPPORT

$$f(\underline{t}) = \sum_{\underline{n}} \left\{ [1 + (\underline{t} - \underline{a}_{\underline{n}}) \cdot \nabla] f(\underline{a}_{\underline{n}}) \right\} g(\underline{t} - \underline{a}_{\underline{n}}) \tag{49}$$

where the problem becomes one of finding the relations that must exist between the reciprocal lattice $\{\underline{b}_{\underline{n}}\}$ and the support S in order that such a reconstruction function $g(\underline{t})$ can be found which is universal with respect to the given class of functions $f(\underline{t})$. An adaptation of Eq. 49 to the use of the directional derivative $\underline{u} \cdot \nabla f(\underline{a}_{\underline{n}})$, where $\underline{u}$ is a unit vector in the direction of scan, is

$$f(\underline{t}) = \sum_{\underline{n}} \left\{ [1 - (\underline{t} - \underline{a}_{\underline{n}}) \cdot \underline{u}\underline{u} \cdot \nabla] f(\underline{a}_{\underline{n}}) \right\} g(\underline{t} - \underline{a}_{\underline{n}}) \tag{50}$$

Other similar forms of reconstruction, which do not have a coefficient of the directional derivative which is dependent on $\underline{t} - \underline{a}_{\underline{n}}$, impose conditions on the transform $G(\underline{r})$ of $g(\underline{t})$ which cannot be satisfied in general. In what follows, we obtain the general conditions for the existence of a $g(\underline{t})$ in Eq. 50.

C.2. THE DIRECTIONAL DERIVATIVE

To take the Fourier transform of both sides of Eq. 50, we substitute $\underline{t}$ for $\underline{t} - \underline{a}_{\underline{n}}$ on the right side and obtain, writing $\underline{w} = 2\pi\underline{r}$,

$$F(\underline{r}) = \sum_{\underline{n}} e^{-i\underline{w}\cdot\underline{a}_{\underline{n}}} \left\{ f(\underline{a}_{\underline{n}}) G(\underline{r}) + [\underline{u} \cdot \nabla f(\underline{a}_{\underline{n}})] \underline{u} \cdot \int_{R^2} \underline{t}\, g(\underline{t}) e^{-i\underline{w}\cdot\underline{t}}\, d\underline{t} \right\}$$

Since the integral above can be written as the gradient of $G(\underline{r})$, we obtain

$$F(\underline{r}) = \sum_{\underline{n}} e^{-i\underline{w}\cdot\underline{a}_{\underline{n}}} \left[f(\underline{a}_{\underline{n}}) + (\underline{u} \cdot \nabla f(\underline{a}_{\underline{n}})) \frac{i}{2\pi} \underline{u} \cdot \nabla \right] G(\underline{r}) \tag{51}$$

The lattice $\{\underline{b}_{\underline{n}}\}$ induces a natural periodic extension of $F(\underline{r})$ so that it possesses a Fourier series expansion,

$$F_p(\underline{r}) = \sum_{\underline{k}} F(\underline{r} - \underline{b}_{\underline{k}}) = \sum_{\underline{n}} c_{\underline{n}} e^{i\underline{w}\cdot\underline{a}_{\underline{n}}}$$

If we let C denote any of the reciprocal lattice cells of volume B, the above coefficients can be written as

$$c_{\underline{n}} = \frac{1}{B}\int_C F_p(\underline{r})e^{-i\underline{w}\cdot\underline{a}_{\underline{n}}}d\underline{r} = \frac{1}{B}\int_C \sum_{\underline{k}} F(\underline{r} - \underline{b}_{\underline{k}})e^{-i\underline{w}\cdot\underline{a}_{\underline{n}}}d\underline{r}$$

Interchanging the two operations, we obtain

$$\sum_{\underline{k}}\int_{C+\underline{b}_{\underline{k}}} F(\underline{r})e^{-i\underline{w}\cdot\underline{a}_{\underline{n}}}d\underline{r} = \int_{R^2} F(\underline{r})e^{-i\underline{w}\cdot\underline{a}_{\underline{n}}}d\underline{r} = f(-\underline{a}_{\underline{n}})$$

Therefore, the first sum in Eq. 51 becomes

$$\sum_{\underline{n}} f(-\underline{a}_{\underline{n}})e^{-i\underline{w}\cdot\underline{a}_{\underline{n}}} = B\sum_{\underline{n}} c_{\underline{n}}e^{i\underline{w}\cdot\underline{a}_{\underline{n}}} = B\sum_{\underline{k}} F(\underline{r} - \underline{b}_{\underline{k}}) \tag{52}$$

Similarly, the components of the second sum in Eq. 51 become, with $\underline{u} = (u_1, u_2)$

$$\sum_{\underline{n}} \frac{i}{2\pi}u_j \frac{\partial}{\partial t_j} f(\underline{a}_{\underline{n}})e^{-i\underline{w}\cdot\underline{a}_{\underline{n}}} = -B\sum_{\underline{k}} F(\underline{r} - \underline{b}_{\underline{k}})u_j(\underline{r} - \underline{b}_{\underline{k}})_j \tag{53}$$

so that the substitution of Eq. 52 and (53) into (51) gives (54):

$$F(\underline{r}) = B\sum_{\underline{n}} \left\{[1 - (\underline{r} - \underline{b}_{\underline{n}})\cdot\underline{u}\,\underline{u}\cdot\nabla]G(\underline{r})\right\}F(\underline{r} - \underline{b}_{\underline{n}}) \tag{54}$$

where B is the "area" of the parallelogram generaged by $(\underline{b}_1, \underline{b}_2)$ and A is the area of the one corresponding to $(\underline{a}_1, \underline{a}_2)$, so that $A = 1/B$. Keeping in mind the fact that equations involving functions of L_2 can not hold on sets of zero measure, we see that Eq. 54 is satisfied if the coefficient of $F(\underline{r} - \underline{b}_{\underline{n}})$ is equal to A for $\underline{n} = \underline{0}$ and $\underline{r} \in S$, and equal to 0 for any $\underline{n} \neq \underline{0}$ such that $\underline{r} - \underline{b}_{\underline{n}} \in S$ on a set of positive measure. Because of the flexibility of the functions F having the same support S, these conditions are also necessary. There is generally a non-uniqueness in defining the coefficient term of S, but for simplicity we will assume G to be zero there.

For any scan pattern of the type already mentioned, it is evident from Fig. 20 that we can always choose $\underline{a}_1$ to be along the direction of scan. Thus, with $\underline{u} = \underline{a}_1/|\underline{a}_1|$, the coefficient term in Eq. 54 must satisfy the following conditions:

$$(1 - \underline{r}\cdot\underline{u}\,\underline{u}\cdot\nabla)G(\underline{r}) = A \quad \text{for all } \underline{r} \in S \tag{55}$$

$$[1 - (\underline{r} - \underline{b}_{\underline{n}})\cdot\underline{u}\,\underline{u}\cdot\nabla]G(\underline{r}) = 0 \quad \text{for all } n \neq \underline{0} \text{ and all } \underline{r} \in E_{\underline{n}} \tag{56}$$

such that $E_{\underline{n}} = \left\{\underline{r} \in S;\ \underline{r} - \underline{b}_{\underline{n}} \in S\right\}$ has positive measure. Subtracting Eq. 55 from (56), with $\underline{u}\cdot\underline{b}_{\underline{n}} = n_1/|\underline{a}_1|$, we obtain

$$\frac{n_1}{|\underline{a}_1|}\underline{u}\cdot\nabla G(\underline{r}) + A = 0 \quad \text{for all } \underline{n} \neq \underline{0} \text{ and all } \underline{r} \in E_{\underline{n}} \tag{57}$$

such that $E_{\underline{n}}$ has positive measure. Two necessary conditions follow immediately from Eq. 57. One is that n_1 cannot be zero, and the other is that there must not be a subset E of S of positive measure for which $\underline{r} - \underline{b}_{\underline{n}} \in S$ for all $\underline{r} \in E$ for more than one value of $n_1 \neq 0$. Geometrically, this means that if we construct an image of the support at each reciprocal lattice point, those images at points lying on the straight line through the points $\underline{0}$ and $\underline{b}_2$ must not overlap the support, and no two images at points having different n_1 coordinates can have an intersection intersecting the support. These conditions are also sufficient, for we then choose $G(\underline{r}) = A$ on that subset of S where no overlap occurs and choose $G(\underline{r}) = A\left(1 - \frac{|\underline{a}_1|}{n_1}\underline{u}\cdot\underline{r}\right)$ on that subset of S which intersects images at points having n_1 as their first coordinate.

To illustrate these conditions, consider an arbitrary bounded support S and assume it is desirable to minimize the number of sample points per unit area (i.e., $1/A = B$) subject to the overlap conditions as constraints. Now there is a one-to-one correspondence between each sampling lattice and its reciprocal lattice, while there are in general an infinite number of different basis vector sets which will generate the same lattice. Because of the unrestrictive condition that $\underline{a}_1$ be the direction of scan, our constraint conditions are in terms of a basis set. Thus it is conceivable that the mininization of B may lead to more than one reciprocal lattice, with each of these having an infinite number of distinct basis sets which satisfy the overlap conditions. In the sampling space, this means that several different lattices may arise, all with the same value of A, each of which can be scanned in an infinite number of different ways. This infinite number of different ways comes about as we sample value and derivative less times per unit distance along the scan lines, while the lines themselves become more closely spaced. If the permitted directions of scan are found to be undesirable for some reason, it is always possible to choose a sampling lattice with more points per unit area which will permit scanning along the desired direction.

As an example, consider an isotropic support. The reciprocal lattice shown in Fig. 22 can be proven to be the single lattice with a minimum value of B, which can be generated by basis sets satisfying the overlap conditions. Only two of these basis sets, primed and unprimed, are shown. One singular difference in the isotropic case is that the direction of scan can be

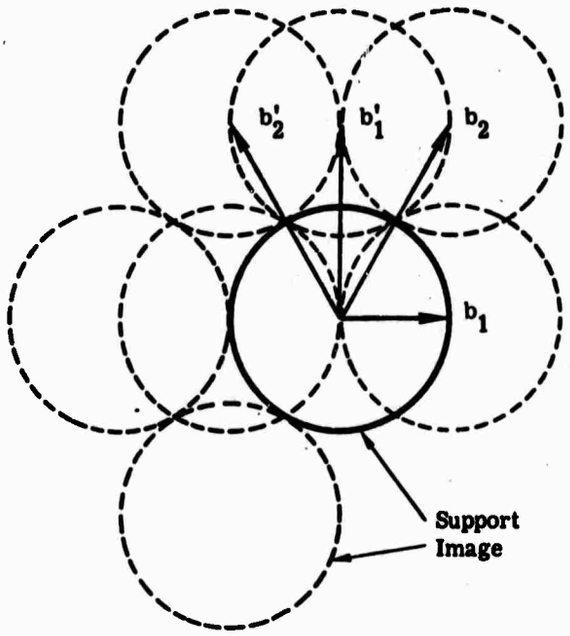

FIGURE 22. EXAMPLE USING ISOTROPIC SUPPORT

chosen arbitrarily first. With the direction of $\underline{a}_1$ fixed, that of $\underline{b}_2$ is determined by rotating the configuration of Fig. 22 until a permitted basis set has its $\underline{b}_2$ vector in the scan direction. Consequently, the sampling lattice is then rotated so that the corresponding $\underline{a}_1$ is along the scan direction.

C.3. SUMMARY

It has been shown that for two-dimensional band-limited functions, such as those imaged by an optical system, there are in general an infinite number of different optimum scan patterns that yield data sufficient for the reconstruction of the original picture. The scan patterns involve the sampling of the intensity and its directional derivative at equally spaced points along the direction of scan, with the scan lines themselves parallel and equally spaced. The word "optimum" here means that the area density of points sampled is a minimum. Finding the scan directions involves a minimization in reciprocal space subject to constraints that relate the support of the Fourier transform of the original intensity function to a basis set of vectors generating the reciprocal lattice. The different optimum scan patterns not only vary with different scan directions, but they also vary with the number of samples per unit distance with a corresponding variation in scan-line spacing. Thus the approach we have followed has been one of sequential optimization in which the first priority has been given to the minimization of the area sampling density. Clearly, other requirements may have greater preference in some applications.